UNIVERSIDADE FEDERAL DE SANTA CATARINA
CENTRO TECNOLÓGICO
PROGRAMA DE PÓS-GRADUAÇÃO EM ENGENHARIA QUÍMICA

Patricia Viera de Oliveira

Formation of naringin and naringenin particles in supercritical medium and evaluation of biological activities *in vitro* and *in vivo*

FLORIANÓPOLIS, SC
2024

Patricia Viera de Oliveira

Formation of naringin and naringenin particles in supercritical medium and evaluation of biological activities *in vitro* and *in vivo*

Tese submetida ao Programa de Pós-Graduação em Engenharia Química da Universidade Federal de Santa Catarina como requisito para a obtenção do título de Doutora em Engenharia Química.

Orientador: Prof. Dr. José Vladimir de Oliveira
Coorientadores: Dr. Gean Pablo Silva Aguiar
Profa. Dr[a]. Anna Maria Siebel

FLORIANÓPOLIS

2024

Ficha catalográfica gerada por meio de sistema automatizado gerenciado pela BU/UFSC.
Dados inseridos pelo próprio autor.

de Oliveira, Patricia Viera de
Formation of naringin and naringenin particles in supercritical medium and evaluation of biological activities in vitro and in vivo / Patricia Viera de de Oliveira ; orientador, José Vladimir de Oliveira, coorientador, Anna Maria Siebel, coorientador, Gean Pablo Silva Aguiar, 2024.
180 p.

Tese (doutorado) - Universidade Federal de Santa Catarina, Centro Tecnológico, Programa de Pós-Graduação em Engenharia Química, Florianópolis, 2024.

Inclui referências.

1. Engenharia Química. 2. Cocristalização. 3. Micronização. 4. Fluido supercrítico. 5. Compostos bioativos. I. de Oliveira, José Vladimir . II. Siebel, Anna Maria. III. Aguiar, Gean Pablo Silva IV. Universidade Federal de Santa Catarina. Programa de Pós Graduação em Engenharia Química. V. Título.

Patricia Viera de Oliveira

Formation of naringin and naringenin particles in supercritical medium and evaluation of biological activities *in vitro* and *in vivo*

O presente trabalho em nível de Doutorado foi avaliado e aprovado, em 23 de fevereiro de 2024, pela banca examinadora composta pelos seguintes membros:

Prof.ª Dr.ª Claudia Sayer.
Universidade Federal de Santa Catarina

Dr.ª Thayli Ramires Araujo
Universidade Federal de Santa Catarina

Prof.ª Dr.ª Liz Girardi Müller
Universidade Comunitária da Região de Chapecó

Certificamos que esta é a versão original e final do trabalho de conclusão que foi julgado adequado para obtenção do título de Doutora em Engenharia Química

GOV.BR
Documento assinado digitalmente
DEBORA DE OLIVEIRA
Data: 04/03/2024 17:06:57-0300
CPF: ***.453.929-**
Verifique as assinaturas em https://v.ufsc.br

Coordenação do Programa de Pós-Graduação

ICP-Edu
Documento assinado digitalmente
Jose Vladimir de Oliveira
Data: 04/03/2024 13:17:59-0300
CPF: ***.858.198-**
Verifique as assinaturas em https://v.ufsc.br

Prof. José Vladimir de Oliveira Dr.
Orientador

ACKNOWLEDGMENTS

I would like to thank God and my family for their constant support and encouragement.

Professor José Vladimir de Oliveira, Anna Maria Siebel, and Gean Pablo S. Aguiar for their guidance, dedication, and encouragement. I would like to thank Professor Liz Girardi Müller at Community University of the Chapecó Region for their collaboration in carrying out the *in vivo* tests and for the many teachings. Professor Adailton Bortoluzzi for his collaboration and teachings.

Professor Claudio Trapella, from the Università degli Studi di Ferrara (UNIFE), for his supervision during the sandwich doctoral period Lindomar Lerin, Giada Botti, Anna Bianchi, Valentina Gentili, Roberta Rizzo, Barbara Pavan, Alessandro Dalpiaz, and Giulia Turrin for teaching and collaboration on this thesis. I thank all my friends and colleagues at LATESC for their interaction, learning, and support during this journey.

I would also like to thank Federal University of Santa Catarina professors for sharing knowledge, collaboration, questions, and discussions that were fundamental to my professional development. To the technicians and staff at UFSC, especially the analytical center of the Department of Chemical and Food Engineering, Lindem, LCP, Chemical Analysis Center, and LCME.

I want to thank CAPES for the financial support and CNPq for the opportunity to conduct the sandwich doctorate.

Finally, I would like to thank everyone who contributed in any way to make this work a reality!

"The mind that opens to a new idea will never return to its original size."

Albert Einstein

RESUMO

Os flavonoides naringina e seu derivado naringenina apresentam várias propriedades biológicas notáveis, destacando-se por suas atividades anti-inflamatórias, antioxidantes, neuroprotetoras, antiapoptóticas e potencial antipsicótico. Porém, possuem baixa solubilidade e biodisponibilidade, o que dificulta a sua aplicação farmacológica. Sabe-se que a cocristalização e a micronização de substâncias podem alterar propriedades físico-químicas como solubilidade, dissolução, biodisponibilidade, estabilidade, podendo ocasionar a redução de efeitos colaterais. Além disso, o uso de fluidos supercríticos no processamento destas partículas apresenta como vantagens a redução do estresse térmico e mecânico; utilização de temperaturas moderadas e atmosfera inerte que evita a degradação dos produtos; eliminação ou redução no uso de solventes orgânicos em comparação aos métodos tradicionais. Diante disso, o objetivo deste trabalho é micronizar os compostos bioativos naringina e naringenina e cocristalizar naringenina utilizando fluidos supercríticos, e avaliar a sua atividade *in vitro* e *in vivo*. A micronização de naringenina e naringina pela técnica GAS (gás antissolvente) foi realizada com sucesso obtendo partículas com menor tamanho e aumento na área superficial e taxa de dissolução comparada às formas comerciais. Além disso, as formas micronizadas de naringina e naringenina, quando testadas *in vivo*, mostraram potencial antipsicótico contra sintomas positivos de esquizofrenia utilizando o modelo de hiperlocomoção induzida por cetamina em camundongos. A cocristalização naringenina:betaína (NRG:BTN) utilizando a técnica GAS apresentou melhor taxa de dissolução da naringenina, se comparada com a forma comercial e mistura física. O teste *in vitro* de permeabilidade através de células intestinais (IEC-6) mostraram que o cocristal NRG:BTN deve seguir administração oral com baixas doses e doses frequentemente administradas. A permeação do cocristal em células da barreira hematoencefálica (ECV 304) sugerem um efeito sinérgico de NRG e BTN para o cocristal e a mistura física que possibilitam um aumento da permeação de NRG através do BBB. Portanto, este trabalho abre um potencial para a aplicação de naringenina e naringina micronizada e cocristal NRG:BTN na área farmacêutica, bem como outras aplicações a serem exploradas.

Palavras-chaves: GAS, CO_2 supercrítico, micronização, cocristalização, flavonoides

RESUMO EXPANDIDO

Introdução

Os flavonoides, naringina e seu metabólito naringenina, apresentam diversas propriedades biológicas, destacando-se como antioxidantes, anti-inflamatórios, antidepressivos, antiapoptóticos, neuroprotetores e com potencial antipsicótico. Apesar de apresentarem atividades biológicas promissoras, estas moléculas encontraram barreiras de cunho farmacocinético que dificultam a aplicação farmacêutica. A naringenina é pouco solúvel em água (46 $\mu g.mL^{-1}$) e, consequentemente, possui biodisponibilidade oral insatisfatória (5,81%), além de instabilidade no meio fisiológico. A naringina também apresenta baixa solubilidade em água (0,6502 $mg.mL^{-1}$), baixa biodisponibilidade oral. Assim, estas características são um limitante para aplicações medicinais e em alimentos, fazendo com que seja necessário o desenvolvimento de sistemas de entrega e/ou formulações alternativas. Neste sentido, diferentes técnicas são utilizadas para incrementar a baixa taxa de dissolução, solubilidade e biodisponibilidade de fármacos. A técnica de micronização consiste em reduzir o tamanho de partículas, na qual, proporcionam-se mudanças nas propriedades estruturais, físico-químicas e funcionais como taxa de dissolução e biodisponibilidade. Além disso, estas características tornam possível a redução da dose de medicamentos ingeridos, diminuindo efeitos colaterais, promovendo uma liberação controlada dos princípios ativos, aumentando o tempo de circulação do fármaco no organismo. A técnica de cocristalização possibilita modificar propriedades físico-químicas do composto ativo como solubilidade, dissolução, biodisponibilidade, estabilidade, capacidade de fabricação (fluxo, compactação e processabilidade), higroscopicidade, mantendo e/ou melhorando as atividades terapêuticas. Dentre as vantagens de usar estes métodos para produção de partículas a utilização de fluidos supercríticos, como o CO_2 destacam-se devido a redução do estresse térmico e mecânico; utilização de temperaturas moderadas e atmosfera inerte que evita a degradação dos produtos; eliminação ou redução no uso de solventes orgânicos em comparação aos métodos tradicionais.

Objetivos

O objetivo desta tese foi investigar a síntese de cocristais e micronização dos compostos bioativos naringina e naringenina em meio supercrítico e avaliar o uso dessas partículas através de testes *in vitro* e *in vivo* no tratamento dos sintomas da esquizofrenia. Os objetivos específicos foram: micronizar naringenina e naringina; sintetizar cocristais de naringenina utilizando a técnica gás antissolvente (GAS); avaliar a influência das variáveis do processo GAS (pressão, temperatura, concentração e fluxo de CO_2) no tamanho de partícula para micronização de naringina; realizar testes de dissolução *in vitro* para partículas comerciais, micronizadas e cocristalizadas; avaliar a atividade antipsicótica de partículas micronizadas processadas em meio supercrítico *in vivo*: camundongos (*Mus musculus*), para tratamento de sintomas de esquizofrenia; avaliar a permeação de cocristal, mistura física e composto comercial em membranas fisiológicas por meio de ensaios *in vitro*.

Metodologia

As partículas de naringina e naringenina foram micronizadas e cocristal de naringenina:betaína foram sintetizados utilizando CO_2 supercrítico como antisolvente por meio da técnica gás antissolvente (GAS). Em seguida as partículas produzidas foram caracterizadas pelas técnicas: espectroscopia no infravermelho com transformada de Fourier (FTIR), calorimetria diferencial de varredura (DSC), difração de raio X (DRX) e microscópio eletrônico de varredura (SEM). Após, foi avaliado a taxa de dissolução das partículas produzidas comparando-as com as formas comercialmente disponíveis e a mistura-física no caso do cocristal. Para as partículas

micronizadas de naringina e naringenina foram realizados testes *in vivo* utilizando camundongos por meio do modelo de hiperlocomoção induzida por cetamina. O cocristal naringenina:betaína (NRG:BTN) foi realizado ensaios de permeação em barreiras fisiológicas por meio de modelos *in vitro* em células intestinais (IEC-6) e células que simulam a barreira hematoencefálica (ECV304).

Resultados e discussão

Micropartículas de naringenina foram obtidas com sucesso pela técnica GAS (P= 8 MPa, T=308 K, C=17,5 mg·mL^{-1}, fluxo de CO_2=10 mL.min^{-1}). As análises FTIR, DSC e XRD indicam que não ocorrem alterações significativas na estrutura química do cristal de naringenina durante o processamento. Ensaios de taxa de dissolução confirmaram que a naringenina micronizada exibiu uma taxa de dissolução significativamente maior em comparação à naringenina comercial em todos os meios estudados (água destilada; solução de HCl 0,1 M e solução tampão fosfato - PBS, pH 6,8). A melhor taxa de dissolução é devida à redução do tamanho das partículas (aproximadamente 2,6 vezes) e ao aumento da área superficial (11 vezes) da naringenina micronizada em comparação com a naringenina comercial. Os dados *in vivo* sugerem o potencial antipsicótico da naringenina micronizada, que está relacionado ao aumento da taxa de dissolução e, provavelmente, ao aumento da biodisponibilidade.

A naringina foi produzida por meio da técnica GAS e realizado o Delineamento Composto Central 2^4. Os resultados do *Run 11* com C= 5 mg·mL^{-1}, P= 12 MPa, T= 308 K, fluxo de CO_2= 15 mL.min^{-1}, diâmetro de partícula= 0.835± 1.252 µm mostraram partículas amorfas enquanto do *Run 14* com C= 10 mg.mL^{-1}, P= 8 MPa, T= 318 K, vazão de CO_2= 15 mL.min^{-1} , diâmetro de partícula=8.997±2.771 µm, mantiveram a estrutura cristalina da naringina. Ensaios *in vivo* utilizando camundongos por meio do modelo de hiperlocomoção induzida por cetamina mostraram resultados promissores com partículas cristalinas (*Run 14*), provavelmente devido ao aumento da biodisponibilidade, e partículas amorfas (*Run 11*) tiveram efeitos semelhantes à naringina comercial devido à recristalização quando em contato com o meio aquoso.

Para os cocristais naringenina:betaine (1:1) produzidos pela técnica GAS (P= 9 MPa, T=318 K, fluxo de CO_2=10 mL.min^{-1}). As caracterizações pelas técnicas DRX, FTIR, DSC confirmam a formação do cocristal. O diâmetro médio das partículas foi de 65,78 µm para naringenina e 76,65 µm para betaína ambas comerciais. Para o cocristal e a mistura física (naringenina-betaína) o diâmetro médio das partículas foi de 9,05 e 110,93 µm, respectivamente. O cocristal NRG:BTN processado com GAS resultou em um aumento de 6 vezes na área superficial específica em comparação com a mistura física (NRG-BTN) e 10 vezes em comparação com a naringenina comercial. Os ensaios de permeabilidade *in vitro*, conduzidos em células intestinais (IEC-6) demonstratam que o cocristal NRG:BTN revelou-se potencialmente útil para aprimorar a permeação através da barreira intestinal, devido à melhora na cinética de permeação. A permeação do cocristal em células da barreira hematoencefálica (ECV 304) sugerem um efeito sinérgico de NRG e BTN no cocristal e a mistura física, proporcionando um aumento da permeação de NRG através do BBB.

Considerações finais

A micronização de naringenina e naringina e cocristalização de naringenina:betaína por meio da técnica gás antisolvente foi realizada com sucesso. Foi observado uma redução no tamanho de partícula e consequente aumento da área superficial das partículas processadas pela técnica GAS se comparadas com a forma comercial. Além disso, os dados *in vivo* sugerem que o potencial antipsicótico da naringenina e naringina (*Run 14*) micronizadas, está relacionado ao aumento da taxa de dissolução e, provavelmente, ao aumento da biodisponibilidade.

O cocristal naringenina:betaína apresentou uma melhora na taxa de dissolução se comparado a naringenina comercial o que provavelmente causa uma melhora na biodisponibilidade da naringenina. Os ensaios de permeabilidade em células intestinais e da barreira hematoencefálica indicam que o cocristal NRG:BTN é potencialmente útil após sua administração oral com baixas doses de cocristal, e doses frequentemente administradas são necessárias para uma absorção intestinal segura. Portanto, a micronização da naringenina e naringina e cocristalização da naringenina:betaína pela técnica GAS é uma abordagem promissora para a aplicação farmacêutica destes compostos.

Palavras-chaves: GAS, CO_2 supercrítico, micronização, cocristalização, flavonoide

ABSTRACT

The flavonoids naringin and its derivative naringenin have several notable biological properties, standing out for their anti-inflammatory, antioxidant, neuroprotective, anti-apoptotic, and antipsychotic potential activities. However, they have low solubility and bioavailability, which makes their pharmacological application difficult. It is known that cocrystallization and micronization of substances can alter physical-chemical properties such as solubility, dissolution, bioavailability, and stability, which can reduce side effects. Furthermore, the use of supercritical fluids in processing these particles has the advantages of reducing thermal and mechanical stress, use of moderate temperatures, and an inert atmosphere that prevents product degradation, elimination, or reduction in the use of organic solvents compared to traditional methods. Therefore, this work aims to micronize the bioactive compounds naringin and naringenin, and cocrystallize naringenin using supercritical fluids and evaluate its activity *in vitro* and *in vivo*. The micronization of naringenin and naringin using the GAS (anti-solvent gas) technique was successfully carried out, obtaining particles with smaller sizes and increased surface area and dissolution rate compared to commercial forms.

Furthermore, micronized forms of naringin and naringenin, when tested *in vivo*, showed antipsychotic potential against positive symptoms of schizophrenia using the ketamine-induced hyperlocomotion model in mice. Naringenin: betaine (NRG:BTN) cocrystallization using the GAS technique showed a better naringenin dissolution rate than the commercial form and physical mixture. The *in vitro* permeability test through intestinal cells (IEC-6) showed that the NRG:BTN cocrystal should follow oral administration with low doses and frequently administered doses. Cocrystal permeation in blood-brain barrier cells (ECV 304) suggests a synergistic effect of NRG and BTN for the cocrystal and the physical mixture that increases NRG permeation across the BBB. Therefore, this work opens up the potential for the application of naringenin and micronized naringin, and NRG:BTN cocrystal in the pharmaceutical area, as well as other applications to be explored.

Keywords: GAS, supercritical CO_2, micronization, cocrystallization, flavonoids

LIST OF FIGURES

LIST OF TABLES

LIST OF ABBREVIATIONS AND ACRONYMS

ANVISA- Brazilian Health Regulatory Agency

ASES- Aerosol solvent extraction system

API-Active Pharmaceutical Ingredient

ATCC-American Type Culture Collection

ATR-Attenuated Total Reflectance

ANOVA-Analysis of Variance

BBB-blood-brain barrier

BCS- Biopharmaceutics Classification System

BTN-Betaine

BET-Brunauer–Emmett–Teller

CEUA-Ethics Committee on the Use of Animals

COC-Cocrystal

CONCEA- National Council for the Control of Animal Experimentation

CPCSP-Powder coating spraying process

CAN-BD-Carbon dioxide assisted nebulization with bubble dryer

CSD -Cambridge Structural Database

CAF-Caffeine

CBZ-Carbamazepine

CNS- Central Nervous System

DOX-Doxorubicin HCl

DSC- Differential scanning calorimetry

DELOS- Depressurization of an expanded liquid organic solution

DPBS-Dulbecco's phosphate buffer saline

DMEM-Dulbecco’s modified Eagle’s medium

D_2R- Dopamine Receptor

DCC- Design Central Composite

ECACC-European Collection of Authenticated Cell Cultures

EMA-European Medicines Agency

EPS- Extrapyramidal effects

ESI-Electrospray Interface

FTIR- Fourier transform infrared spectroscopy

FBS-Fetal Bovine Serum

FDA -Food and Drug Administration

FEB-Free Energy of Binding

FSC- Supercritical fluids

GAS-Gas antisolvent

GC-FID- Gas Chromatography-Flame Ionization Detector

GA- Gallic acid

GRAS- Generally Recognized as Safe

HPLC- High-Performance Liquid Chromatography

INM-Isonicotinamide

ICH -International Conference on Harmonisation

Ki, Inhibition Constant

LPROL- L-proline

LAG- Liquid-assisted grinding

SEM- Scanning electron microscopy

MS -Mass spectrometry

MTT-3-(4,5-dimethylthiazol-2-yl)-2,5-diphenyltetrazolium bromide

MIX-Physical mixture

MICRO-Microparticles

NMDA-N-metil-D-aspartate

NAC- N-acetylcysteine

NAFDL- Non-alcoholic fatty liver disease

NIC-Nicotinamide

NITRO- Nitrofurantoin

NAR-Naringin

NRG-Naringenin

OLN-Olanzapine

OXA-Oxaliplatin

PBS-Phosphate Buffer Solution

PDB-Protein Data Bank

PET-Polyethylene terephthalate

PCA- Picolinic acid

P_E-Permeability coefficients

Papp-apparent permeability

PGSS - Particles from Gas Saturated Solutions

P_C-Critical pressure

PTFE- Polytetrafluoroethylene

QUE-Quercetin

R.M.S.D-Root-Mean-Square-Derivation

RESS - Rapid Expansion of *Supercritical* Solution

RSD-Relative standard deviation

$ScCO_{2-}$ Supercritical carbon dioxide

SAS- Supercritical Antisolvent

SEDS- Solution Enhanced Dispersion by *Supercritical* Fluids

SAA-*Supercritical*-assisted atomization

SPA- Sinapic acid

T_C- Critical temperature

TEER-Transepithelial electrical resistance

UPLC-Ultra-high-performance liquid chromatography

XRD- Powder-X-ray diffraction

5-HT_{2A}-Serotonin Receptor

SUMMARY

1.INTRODUCTION

Naringenin is the aglycone and metabolite of naringin, belonging to flavonoids called flavonones (HSIU et al., 2002). Abundantly present in citrus fruits, oranges, lemons, grapes, beans, cherries, cocoa, and oregano (PASAM et al., 2017; YUSOF; GHAZALI; KING, 1990; ZAIDUN; THENT; LATIFF, 2018). Recently, naringin and naringenin have attracted significant scientific interest due to their versatility in promoting health effects and exerting important biological activities. They were demonstrating anti-inflammatory properties (INÊS AMARO et al., 2009; SPAGNUOLO; MOCCIA; RUSSO, 2018), and antioxidant capabilities (CAVIA-SAIZ et al., 2010; RAJADURAI; STANELY MAINZEN PRINCE, 2006), which co contribute to neuroprotective effects (ATOKI et al., 2023; BEN-AZU et al., 2019; EMRAN et al., 2022; RAZA et al., 2013; WANG et al., 2021), and antiapoptotic properties (MOGHADDAM et al., 2020). Furthermore, it has the ability to cross the blood-brain barrier ((MUSCATELLO; ZOCCALI; BRUNO, 2018), not only contributes to cognitive enhancement (KUMAR; DOGRA; PRAKASH, 2010; YANG et al., 2014), but also multitarget agents with multicomponent therapeutic potential (GROSSO et al., 2013). These attributes hold particular relevance in the context of mental disorders (BHANDARI; PALIWAL; KUHAD, 2018; SWAMY et al., 2023; ZHANG et al., 2023), highlighting the properties of antipsychotics (GEORGE et al., 2021; MUSCATELLO; ZOCCALI; BRUNO, 2018), naringin exhibited effe effectiveness in mitigation adverse effects, particularly when added to treatment with the antipsychotic clozapine (GEORGE et al., 2020).

Despite presenting promising biological activities, these molecules have encountered pharmacokinetic barriers that make pharmaceutical application impossible. Naringenin is poorly soluble in water (46 $\mu g.mL^{-1}$) and, consequently, has unsatisfactory oral bioavailability (5,81%), in addition to instability in a physiological environment (KANAZE et al., 2007; KHAN et al., 2015). Naringin also has low water solubility. (0.6502 $mg.mL^{-1}$), low oral bioavailability and undesirable bitter taste (LEE et al., 1999). Therefore, these characteristics are a limitation for medicinal and food applications, making developing alternative delivery systems and formulations necessary.

In this sense, different techniques are used to change drug dissolution rate, solubility, and bioavailability (KHADKA et al., 2014). For example, amorphous solid dispersions can be used (VAN DEN MOOTER, 2012), inclusion with cyclodextrins (DOS SANTOS LIMA et al., 2019), nanoparticles (CASTRO; COSTA; CAMPOS, 2020; TIRUWA, 2016), formation of salt,

solvates, hydrates (GUPTA et al., 2018; HEALY et al., 2017), chemical modifications (JAIN; CHELLA, 2021), self-emulsifying formulations (AGUBATA, 2020), among others. Among the processes, micronization and cocrystallization in supercritical media stand out as innovative processes (MACEACHERN; KERMANSHAHI-POUR; MIRMEHRABI, 2020; MARTÍN; COCERO, 2008).

The micronization technique reduces particles' size, which changes structural, physicochemical, and functional properties. Properties are improved on a micrometer scale due to the increase in surface area, enhancing the bioavailability of drugs that are poorly soluble in water due to better dissolution of substances on a nanometer or micrometer scale (CEREA et al., 2016; CHEN et al., 2018; RASENACK; MÜLLER, 2004). Furthermore, these characteristics make it possible to reduce the medication ingested dose and side effects promote an increase in the drug's circulation time in the body (YORK; KOMPELLA; SHEKUNOV, 2004).

The cocrystallization technique is based on the interaction between two or more chemically different molecules that are generally in the stoichiometric ratio (AITIPAMULA et al., 2012; DUNITZ, 2003; FRIŠČIČ; JONES, 2009). This gives rise to a pharmaceutical cocrystal, generally formed by an API (active pharmaceutical ingredient) and a conformer; molecules usually included in the list of substances GRAS (Generally Recognized as Safe) (GADADE; PEKAMWAR, 2016; SHAIKH et al., 2018). Furthermore, the components of cocrystals are predominantly non-ionized and interact through non-ionic interactions such as hydrogen bonds, electrostatic π-π interactions, or van der Waals forces. (STEED, 2013). The main objective in producing a cocrystal is to increase the solubility of an API, which is usually poorly soluble in water. The use of cocrystals in the pharmaceutical area and the development of new drugs stand out due to their ability to modify physicochemical properties of the API such as dissolution, bioavailability, stability, manufacturability (flow, compaction, and processability), hygroscopicity, maintaining and improving therapeutic activities (GADADE; PEKAMWAR, 2016; KAVANAGH et al., 2019; LI; MATZGER, 2016; PESSOA et al., 2019; RIBAS et al., 2019a, 2019b; SHAIKH et al., 2018; SOKAL; PINDELSKA, 2017).

Among the advantages of using these innovative particle production methods using supercritical fluids, the following stand out the reduction of thermal and mechanical stress; use of moderate temperatures and an inert atmosphere that prevents product degradation; elimination or decrease in the use of organic solvents compared to traditional methods (PANDO; CABAÑAS; CUADRA, 2016). Furthermore, the use of supercritical fluids

considered "green solvents for the future" has been gaining prominence, with the most used being supercritical carbon dioxide ($scCO_2$) due to its mild critical conditions (Tc= 31.1°C and Pc = 73.9 bar). In the vicinity of its critical point, carbon dioxide, in addition to having a density similar to a liquid, its viscosity and diffusivity remain advantageously between the values of the liquid and gaseous states (BRUNER, 1994; MATOS et al., 2019). It was using SCF, small changes in pressure and temperature result in changes in the density and solvation power of CO_2 in the vicinity of the critical point (BRUNER, 1994). Furthermore, using $scCO_2$ has the advantages of being non-toxic, non-flammable, thermodynamically stable, and relatively low cost (KNEZ et al., 2019; LOZOWSKI, 2010).

This study aims to investigate the micronization of naringin and naringenin and the cocrystallization of naringenin using supercritical media through the gas antisolvent (GAS) technique. Additionally, these particles will be evaluated through *in vitro* and *in vivo* tests.

1.1.OBJECTIVES

1.1.1. General objectives

Investigate the synthesis of cocrystals and micronization of the bioactive compounds naringin and naringenin in supercritical media and evaluate the use of these particles through *in vitro* and *in vivo* tests.

1.1.2. Specific objectives

- Micronize naringenin and naringin using the gas antisolvent (GAS) technique;
- Synthesize naringenin cocrystals using the gas antisolvent (GAS) technique;
- Evaluate the influence of the GAS process variables (pressure, temperature, concentration, and CO_2 flow) on particle size for naringin micronized;
- Accomplish *in vitro* dissolution tests for commercial, micronized, cocrystallized, and physical mixture;
- To evaluate the antipsychotic activity of naringin and naringenin micronized in the supercritical medium using *in vivo* assays in mice (*Mus musculus*) for the treatment of schizophrenia symptoms;

- Evaluate the permeation of cocrystal, physical mixture, and commercial compound in physiological membranes using cell models *in vitro*.

2. LITERATURE REVIEW

2.1. FLAVONOIDS

Flavonoids are a large group of low molecular weight polyphenolic compounds (CAVIA-SAIZ et al., 2010). They are natural substances with variable phenolic structures found in fruits, vegetables, grains, peels, stems, roots, flowers, wines, and teas (PANCHE; DIWAN; CHANDRA, 2016). Notably, fruits and vegetables are the main dietary sources of flavonoids for humans (YAO et al., 2004). It is worth noting that the same flavonoid compound can present different concentrations depending on the plant organ in which it is found (SIMÕES et al., 2017). More than 9000 natural flavonoids have been described in the literature, and this number continues to grow (WANG; CHEN; YU, 2011).

The basic structure of flavonoids consists of a basic core with 15 carbon atoms, which are arranged in three aromatic rings, two substituted phenol rings (rings A and B) and a ring C (WOJDYŁO; OSZMIAŃSKI; CZEMERYS, 2007). Different flavonoid groups are formed depending on which carbon of the C ring the B ring is attached to and the degree of unsaturation and oxidation of the C ring. If the B ring is bound to position 3 of the C ring, they are called isoflavones. When the B ring is attached to position 4, they are called neoflavonoids, while those with the B ring attached to position 2 can be divided into subgroups based on the structural characteristics of the C ring. The flavonoid groups are flavones, flavonones, flavonoids, flavonols or catechins, anthocyanins and chalcones, according to Figure 1 (PANCHE; DIWAN; CHANDRA, 2016).

Figure 1- Basic structures of flavonoids and their classifications.

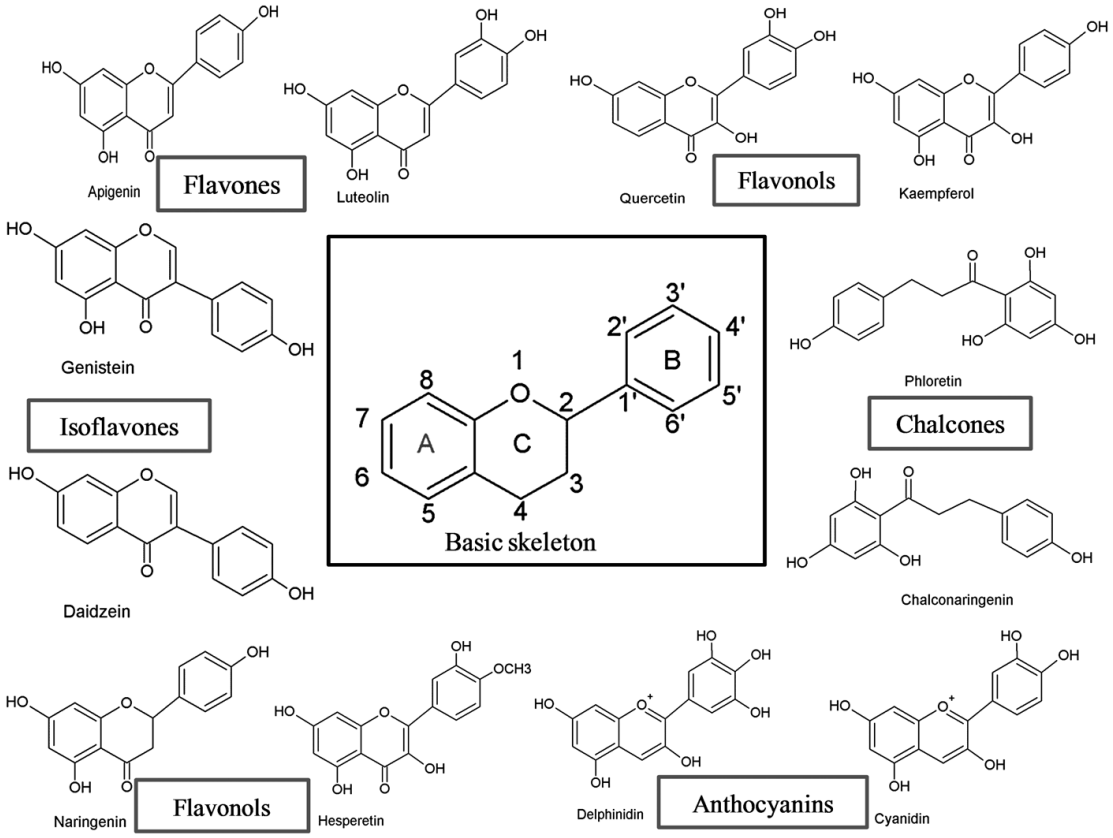

Source: (PANCHE; DIWAN; CHANDRA, 2016).

Flavonoids that exert biological activities are called bioflavonoids (WANG; LI; BI, 2018). They have several properties, such as antioxidants, anti-inflammatory, antiallergic, antiviral, and anticarcinogenic (BRODOWSKA; BRODOWSKA, 2017). Furthermore, recently, interest has arisen in the neuroprotective effect of flavonoids, as it is recognized that the majority of citrus polyphenols and flavonoids and their metabolites naringenin, hesperetin, and isorhamnetin, derived from naringin, hesperidin, and quercetin, are capable of crossing the blood-brain barrier (MUSCATELLO; ZOCCALI; BRUNO, 2018).

Flavonoids also act in the causes of disorders that affect the central nervous system due to their antioxidant activity, preventing oxidative stress, and having the ability to reduce enzymatic activities, modulate receptors, and inhibit inflammation and apoptosis and being beneficial to assist in the treatment of neurodegenerative diseases and mental disorders, such as Alzheimer's disease, Parkinson's disease, epilepsy, depression, and schizophrenia (GROSSO et al., 2013; NIJVELDT et al., 2001). It is noteworthy, therefore, that flavonoids behave as multi-target agents with multi-component therapeutic potential, which is an advantage for the

pharmaceutical industry as they can present beneficial effects for the treatment of various diseases in various ways (GROSSO et al., 2013).

2.1.1. Naringenin and Naringin

The naringin (4',5,7-trihydroxy-flavanone-7-rhamnoglucoside, $C_{27}H_{32}O_{14,}$ molecular weight 580.5 g/mol) and naringenin (4′,5,7-trihydroxy flavonone, $C_{15}H_{12}O_{5,}$ molecular weight 272.25 g/mol) are flavonoids classified as flavonones present in citrus fruits, grapes, beans, cherries, cocoa, oregano and tomatoes (YUSOF; GHAZALI; KING, 1990). The amount of naringin depends on the maturity of the fruit (GÜRSUL et al., 2016).

Commercial grapefruit juice (*Citrus paradisi*) is the richest source of naringin (43.5 mg per 100 mL), where this compound is significantly more concentrated than in the hand-squeezed juice equivalent (23.0 mg per 100 mL). Likewise, industrial bergamot juice (*Citrus bergamia*) represents another valuable source of this compound, with naringin levels around 26.1 mg per 100 mL (GATTUSO et al., 2007). Notably, naringin is the main compound causing bitterness in some citrus juices (CAVIA-SAIZ et al., 2010).

In humans, naringin is metabolized to the aglycone naringenin by naringinase found in the liver. Naringin can be hydrolyzed by the α-L-rhamnosidase activity of naringinase to rhamnose and prunin, which can further be hydrolyzed to glucose and naringenin by the β-D-glucose component of naringinase, which is then absorbed from the intestine, according to the Figure 2 (RIBEIRO, 2011).

Figure 2- Naringin hydrolysis.

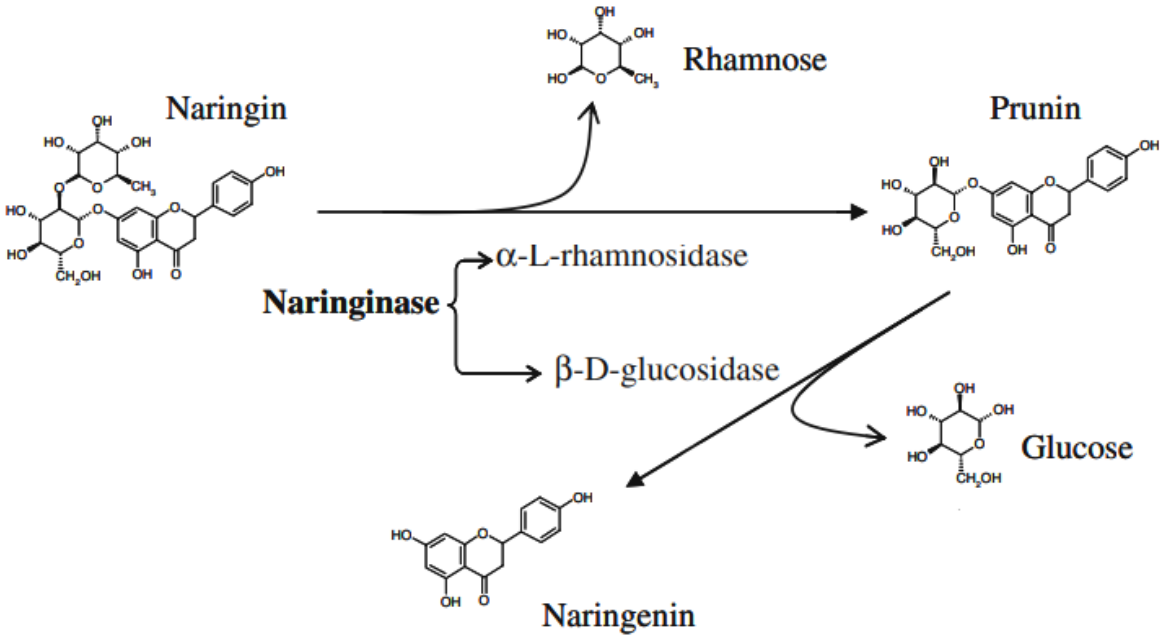

Source: (RIBEIRO, 2011)

Both naringin and naringenin compounds have been the subject of studies of their biological properties, which will be described below. Naringenin has antioxidant activity (CAVIA-SAIZ et al., 2010; HEO et al., 2004), anticancer (JIN et al., 2011; KRISHNAKUMAR et al., 2011), anti-inflammatory (LIN; LIN, 2011; SPAGNUOLO; MOCCIA; RUSSO, 2018; TSAI et al., 2012), anti-viral (GOLDWASSER et al., 2011), antidiabetic (AHMED et al., 2017), antimutagenic (LEE; YOON; MOON, 2004), antibacterial (AGUS; ACHMADI; MUBARIK, 2017; WANG et al., 2018a), neuroprotective (HEGAZY; ALI; SABRY, 2016), antiapoptotic (WANG et al., 2017) among others. Naringin has antiulcer, antioxidant activity (RAJADURAI; STANELY MAINZEN PRINCE, 2006), anti-inflammatory (INÊS AMARO et al., 2009), antiapoptotic and anti-autophagic (KANDEMIR et al., 2017), antihyperlipidemic (ROTIMI et al., 2018), anticancer (RAMESH; ALSHATWI, 2013), effects on bone regeneration and metabolic syndrome, (Chen *et al.*, 2016), in addition to being beneficial for the treatment of obesity, diabetes, hypertension (ALAM et al., 2014), among others.

Highlighting that naringin has antipsychotic potential reported in the work of Geroge et al. (2020) demonstrated that treatment with naringin and/or clozapine significantly attenuated the symptoms of schizophrenia induced by ketamine, as well as the central oxidative lesions caused by the administration of ketamine in rodents. Furthermore, ketamine provoked neuronal apoptosis by increasing Bax/Bcl2 expression, caspase-3 activity, and Cytochrome C and Akt

protein expression, whereas naringin/clozapine treatment significantly inhibited this apoptotic effect. Furthermore, naringin activated neurodevelopment through the wnt/β-catenin signaling pathway, evidenced by increased pGSK-3β expression and reduced pβ-catenin expression.

Additionally, George et al. (2021) reported that naringin was effective in reducing adverse effects when added to treatment with the antipsychotic clozapine. Naringin, showing protective effects in the model of schizophrenia symptoms induced by ketamine in Wistar rats, increased the animals' total leukocyte count, preventing agranulocytosis when administered alone or in combination with clozapine. Also, naringin treatment reduced serum levels of total cholesterol and triglycerides. Naringin prevented weight gain caused by clozapine and reduced serum glucose levels, preventing hyperglycemia associated with treatment with the antipsychotic. These findings may suggest that naringin has a potential benefit when used as an add-on therapy (along with clozapine) in the treatment of schizophrenia (GEORGE et al., 2021).

In the study of Wang et al. (2021), the neuroprotective potential of naringin was investigated against orofacial dyskinesia induced by haloperidol in rats, models of tardive dyskinesia. Naringin administration demonstrated significant prevention of the development of orofacial dyskinesia, suggesting its beneficial effects. Furthermore, naringin reduced haloperidol-induced oxidative stress and neural inflammation, indicating antioxidant and anti-inflammatory properties. These findings highlight the therapeutic potential of naringin in alleviating neuropsychiatric disorders such as tardive dyskinesia, highlighting its neuroprotective properties in clinical settings (WANG et al., 2021).

Wang et al. (2023) investigated the potential rapid antidepressant effects after a single dose of naringin using behavioral tests and classical depressive models. A single dose of naringin (20 mg/kg) exhibited significant antidepressant action after 2 hours in the tail suspension test and forced swim test. Furthermore, ketamine-like effects were observed in chronic mild stress models and learned helplessness, reversing all behavioral impairments. Naringin also improved the abnormal expressions of the NMDA receptor NR1 and the PKA/CREB/BDNF pathway in the hippocampus. Activation of NMDA receptors blocked the antidepressant effects of naringin, while inhibition promoted antidepressant effects similar to the effective dose. In summary, naringin demonstrates rapid antidepressant action, possibly by inhibiting NMDA receptors in the hippocampus (WANG et al., 2023)

Despite presenting promising biological activities, these molecules have encountered pharmacokinetic barriers that make pharmaceutical application impossible. Naringenin is poorly soluble in water (46 $\mu g.mL^{-1}$), and consequently, it has unsatisfactory oral

bioavailability (5.81%) in addition to instability in physiological environments (KANAZE et al., 2007; KHAN et al., 2015). Naringin also has low water solubility (0.6502 $mg.mL^{-1}$), low oral bioavailability, and undesirable bitter taste (LEE et al., 1999). According to the Biopharmaceutical Classification System (BCS), naringin is classified as class II (low solubility, high permeability), and naringenin is classified on the other hand as class II or class IV (low solubility, low permeability) depending on the formulation (SHARMA; BHARDWAJ; ARYA, 2021; STASIŁOWICZ-KRZEMIEŃ et al., 2022)These characteristics are a limitation for medicinal and food applications, making it necessary to developing delivery systems and alternative formulations.

2.2. CLASSIFICATION OF APIS

Active pharmaceutical ingredients can be classified as amorphous or crystalline (Figure 3). The amorphous state has a higher energy state and mobility than the crystalline form, in addition to increased solubility, dissolution rate and bioavailability. However, the amorphous material is physically unstable and tends to recrystallize over time, in addition to presenting physical and chemical instability compared to the crystalline state (CHIENG; RADES; AALTONEN, 2011; RODRIGUES et al., 2018; YAMAMOTO et al., 2016). The crystalline state represents more stable forms, which are easy to purify, but its main disadvantage is low solubility (CHIENG; RADES; AALTONEN, 2011; RODRIGUES et al., 2018; YAMAMOTO et al., 2016). Notably, crystalline forms can include polymorphs, hydrates, solvates, cocrystals, and salts (SHAIKH et al., 2018), which will be detailed below.

Figure 3 – Shapes of APIs.

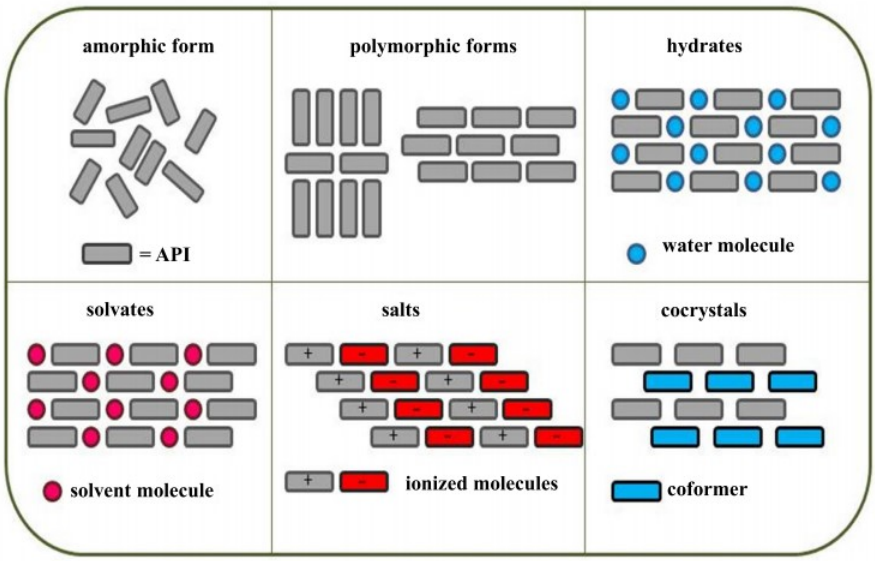

Source: (SOKAL; PINDELSKA, 2017)

Polymorphs are components that have the same chemical composition but different physicochemical properties. Molecules come together in space with different arrangements or conformations of the constituents in the crystal lattice. This form presents ease of compaction, resistance to thermal and mechanical stress, and solubility and dissolution rate, which affects absorption and bioavailability (KARAGIANNI; MALAMATARI; KACHRIMANIS, 2018; SHAIKH et al., 2018; TALACZYNSKA; DZITKO; CIELECKA-PIONTEK, 2016).

Hydrates are molecular compounds containing API and organic solvent water in their crystalline network. This is a viable form for medicinal use, as it does not present any safety problems (KARAGIANNI; MALAMATARI; KACHRIMANIS, 2018; SHAIKH et al., 2018).

Solvates are molecular compounds containing the API and organic solvents in the crystal lattice (HEALY et al., 2017). These are considered a problem in the pharmaceutical industry, as they are unstable; in addition, most solvents used are toxic and should not be included in the final dosage (RODRIGUES et al., 2018).

Salts are composed of ionized molecules in a stoichiometric ratio of API and counter ions (HEALY et al., 2017). Its advantage is that it is a simple and economical method to improve water solubility and bioavailability for ionizable drugs (ELDER; HOLM; DE DIEGO, 2013; KARAGIANNI; MALAMATARI; KACHRIMANIS, 2018; SERAJUDDIN, 2007). More than 50% of drugs are administered in salt form. However, salt is an inappropriate form for non-ionizable drugs (RODRIGUES et al., 2018). Notably, more than 50% of drug molecules

do not have ionizable groups for salt formation to occur, requiring the study of new formulations in the solid state (THAKURIA; SARMA, 2018).

The pharmaceutical cocrystal is generally formed by an API and a coformer, which are generally molecules in the list of substances generally recognized as safe (GADADE; PEKAMWAR, 2016; SHAIKH et al., 2018). Furthermore, the cocrystal components are predominantly non-ionized and interact through non-ionic interactions such as hydrogen bonds, electrostatic π-π interactions, or Van der Waals forces (STEED, 2013).

It is noteworthy that the main difference between salt and cocrystal is in relation to the value of Δ pKa: if it is less than zero, the cocrystal can be formed; if the value is greater than 3 it results in salt formation. If the value of Δ pKa is between 0-3, one can expect a salt or a cocrystal (AAKERÖY; FASULO; DESPER, 2007; YUAN; HUI; JIANJUN, 2010). Another difference is that the salt is formed by transferring a proton to the acidic base, and there must be a balance in the charge balance and a defined stoichiometry (BOND, 2011). In the cocrystal there is no proton transfer, and the substances present in the crystalline structure, the API and coformer, are neutral (CERREIA VIOGLIO; CHIEROTTI; GOBETTO, 2017; PINDELSKA; SOKAL; KOLODZIEJSKI, 2017). Both forms are widely used to increase the solubility and dissolution of pharmaceutical compounds with intermediate to low aqueous solubility (SATHISARAN; DALVI, 2018).

In addition to these previously mentioned forms, there may be combined forms of these APIs. The co-amorphous stands out, which is characterized by a combination of two or more forms, initially crystalline, with low molecular weight components (such as amino acids and small molecules such as nicotinamide) that form a single homogeneous phase of the amorphous system (LIU et al., 2021). The conformer physically stabilizes the amorphous form of the drug by interacting with the drug at a molecular level (such as salt formation, hydrogen bonding, π-π interaction, or molecular mixing). As advantage, the co-amorphous form increases the physical stability of the amorphous form (thermodynamically unstable) (LIU et al., 2021).

2.2.1 Cocrystals

The FDA (Food and Drug Administration) and EMA (European Medicines Agency) are two regulatory agencies, American and European, respectively, that address the quality control of pharmaceutical cocrystals. The definition of cocrystals, according to the FDA (2018) is ‘crystalline material composed of two or more different molecules, one of which is the API, in

a defined stoichiometric ratio within the same crystal lattice that is associated by non-ionic and non-covalent bonds' (FDA, 2019). According to the EMA (European Medicines Agency) (2015) the definition is 'homogeneous (single-phase) crystalline structures composed of two or more components in a defined stoichiometric ratio in which the arrangement in the crystal structure is not based on ionic bonds (how you leave us) (EUROPEAN MEDICINES AGENCY, 2014).

According to recent regulatory frameworks, the classification of cocrystals for the FDA (2018), are considered equal to polymorphs or API salts and the FDA reduces regulatory and financial burdens, encouraging innovation in the area and recent medicinal advances. (ALMANSA et al., 2019). For EMA (2015), cocrystals are considered in the same way as hydrates, solvates, salts, and polymorphs; in the case of a cocrystal of a previously licensed medicinal product, it is not classified as a new active substance unless it has a different efficacy and/or safety than the constituent APIs (ALMANSA et al., 2019). In Brazil, the agency that regulates the approval of cocrystals is ANVISA (2017) (National Health Surveillance Agency); it is aligned with the guidelines of the international agencies FDA and EMA.

It should be added that there are already some cocrystal products successfully commercialized on the market, such as ipragliflozin-proline (Suglat® from Astellas Pharma and Kotobuki Pharmaceutical), available for sale in Japan, Korea, and Thailand, used to treat type 2 diabetes mellitus (POOLE; DUNGO, 2014). Valsartan-sacubitril (Entresto^{TM}, Novartis) used to treat chronic heart failure, was approved by the FDA in 2015, reduces valsartan dosing frequency due to an increase in bioavailability after cocrystallization (KALE; ZODE; BANSAL, 2017). Depakote® cocrystal valproic acid -valproate sodium was approved by the FDA in 1983 for the treatment of epilepsy (KAVANAGH et al., 2019). Lexapro® (escitalopram oxalate) used to treat depression and generalized anxiety disorders, approved by the FDA in 2009; among other medicines that are in the clinical trial phase and have registered patents (KALE; ZODE; BANSAL, 2017; KUMAR; KUMAR; NANDA, 2018; PINDELSKA; SOKAL; KOLODZIEJSKI, 2017; SHAIKH et al., 2018).

2.2.2 Cocrystal engineering

The rational design of new solid-state crystalline materials, medicines with personalized biopharmaceutical properties, has led to the development of a new area called cocrystal

engineering; this is a relatively modern technology for modulating material properties (ALMARSSON; ZAWOROTKO, 2004; GAO et al., 2017; KAVANAGH et al., 2019).

The concept of cocrystal engineering in solid-state chemistry was introduced by Pepinsky R in 1955. Desiraju (2007) defined crystal engineering as "the understanding of intermolecular interactions in the context of crystal packing and the use of such understandings in design of new solids with physical and chemical properties"(DESIRAJU, 2007). Cocrystal engineering is seen as a form of supramolecular synthesis, chemistry beyond the molecule, and has already become capable of developing pharmaceutical and functional materials (CERREIA VIOGLIO; CHIEROTTI; GOBETTO, 2017; SUN et al., 2019).

Understanding intermolecular interactions is necessary to design promising cocrystals and assists in choosing a potential coformer from the synthesis of supramolecular synthons. Supramolecular synthons are classified into two groups. Supramolecular homosynthons exhibit intermolecular interactions between the same functional groups, for example, carboxylic acid-carboxylic acid and amide-amide. Supramolecular heterosynthons and intermolecular interactions are between two different functional groups. These intermolecular interactions are usually hydrogen bonds, e.g., carboxylic acid-amide, carboxylic acid-amide, and alcohol-pyridine (DOUROUMIS; ROSS; NOKHODCHI, 2017; NANGIA; DESIRAJU, 1998). According to the literature, heterosynthons have stronger interactions than homosynthons due to polarity differences (QIAO et al., 2011). Using computational tools such as CSD (Cambridge Structural Database) helps to isolate supramolecular synthons and evaluate the possibility of hydrogen bonding between crystal molecules (GROOM et al., 2016; SAVJANI, 2015).

2.3. PHYSICOCHEMICAL PROPERTIES OF COCRYSTAL

The physicochemical properties of cocrystals are a combination of individual properties of the cocrystal formers. The physicochemical properties are melting point, solubility, dissolution, stability, and bioavailability (SCHULTHEISS; NEWMAN, 2009).

2.3.1. Solubility

Solubility is the thermodynamics of solute equilibrium between solid and liquid (HILDEBRAND, 1924). For equilibrium to occur, the temperature, pressure, and free energy

of each species in each of the phases that make up the system must be equal (HIGUCHI; CONNORS, 1965; RODRÍGUEZ-HORNEDO, 2012).

The main objective of producing a cocrystal is to increase the solubility of a poorly soluble compound in water. This characteristic is essential in the case of drugs in classes II (low solubility and high permeability) and IV (low solubility and low permeability), according to the Biopharmaceutical Classification System (BCS) (BELL; KOTT; BELL, 2017; DRESSMAN; REPPAS, 2000). It is estimated that 60% of new drug molecules exhibit low aqueous solubility, which can be attributed to the size and high lipophilicity of the molecule (ALMEIDA E SOUSA et al., 2016).

Furthermore, solubility is an important characteristic as it affects the bioavailability of drugs (SCHULTHEISS; NEWMAN, 2009). The methods used to evaluate the solubility of a cocrystal are based on kinetic and thermodynamic approaches. Thermodynamic equilibrium methods provide measurement of solubility processes in cocrystals, while kinetic studies provide information on the time scale of dynamic processes and concentration fluctuations during crystal dissolution (SCHULTHEISS; NEWMAN, 2009; THAKURIA; SARMA, 2018).

Furthermore, the miscibility of cocrystal constituents can be predicted using solubility parameters, such as the Hansen solubility parameter, which aid in the formation of cocrystals (MARTIN, 1987; MOHAMMAD; ALHALAWEH; VELAGA, 2011). If the solubility difference between API and conformer is less than seven, it is considered miscible and will probably form a cocrystal (MARTIN, 1987).

The solubility of a cocrystal can vary considerably depending on the equilibrium condition, lack of purity of the cocrystal, and solution conditions such as pH and additives (SCHULTHEISS; NEWMAN, 2009; THAKURIA; SARMA, 2018). Therefore, solubility studies must be carried out with different dissolution media, such as water, simulated gastric fluids, simulated intestinal fluids, and buffered solutions, to evaluate the influence of pH on API solubility (SREENIVAS REDDY et al., 2009).

It is added that the polarity of the solvent, solubility of the API and coformer, temperature, pH, are important parameters to determine the cocrystal formation zone. For this, the phase solubility diagram, also called ternary phase diagram API-coformer-solvent can be constructed using this data that serves as a fundamental tool to identify the region of cocrystal formation, understand the chemistry of the solution and the solubility behavior of cocrystals (AINOUZ et al., 2009; LEE; KIM; ULRICH, 2015). In Figure 4, the ternary diagram can be seen, which is highly influenced by the relative solubilities of the two components. The ternary

diagram for two components of similar solubility in a given solvent (Figure 4(a)). The ternary phase diagram shown in Figure 4 (b) is more complicated, representing the components with very different solubilities. From these diagrams, it can be seen that slow evaporation of a 1:1 solution of two components, 1 and 2 can result in a single-component phase mixture or just the starting material, depending on whether the crystallization path passes through the mixed-phase region D or single-phase region E (BLAGDEN et al., 2008; STEED, 2013).

Figure 4-Schematic representation of the isothermal ternary phase diagram (a) similar solubility and (b) different solubilities between cocrystal-forming components (1 and 2) in a solvent S. The region A component 1 and solvent; B component 1+ cocrystal, C cocrystal, D component 2+cocrystal, E component 2 and solvent, F solution.

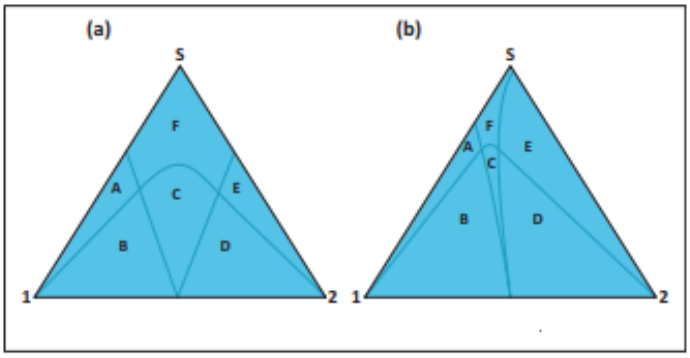

Source: (STEED, 2013)

2.3.2. Stability

The stability of a solution is the ability of the cocrystal components to remain in the solution and not crystallize spontaneously. Furthermore, stability is defined as the shelf life, which is considered normal under normal processing and storage conditions (SCHULTHEISS; NEWMAN, 2009)

Factors that affect stability may be coformer compatibility and the amount of water present, which may lead to product degradation (SCHULTHEISS; NEWMAN, 2009). Physical and chemical stability are obtained under accelerated stability conditions to determine developability and shelf life. Cocrystal stability tests include relative humidity, thermal stress, and chemical solution stability (MATHUR, 2011). Stress and relative humidity are used to identify the best storage conditions for the product (QIAO et al., 2011). Thermal and chemical stress are less studied properties. Solution stability tracks solubility or dissolution studies to

better understand the behavior of cocrystals in different release media (QIAO et al., 2011). In cocrystals, the stability of the solution is a determining factor due to the dissociation of the material, which results in the precipitation of the less soluble compound (MATHUR, 2011).

2.3.3. Melting point

The melting point determines the temperature at which the solid phase is in equilibrium with the liquid phase. Since the melting point is a thermodynamic process in which the transition free energy is zero (KARAGIANNI; MALAMATARI; KACHRIMANIS, 2018). The melting point value is calculated by the ratio of the total enthalpy of fusion to the phase change of the entropy of fusion (JAIN; YANG; YALKOWSKY, 2004). This property can be determined using the DSC (differential scanning calorimetry) technique to obtain thermal and fusion data such as fusion enthalpy (QIAO et al., 2011).

This is an important feature during the development of solid medicines. The factors that contribute to the melting of a crystalline solid are crystal structure, molecular symmetry, conformational degree of freedom of the molecule (BROWN; BROWN, 2000; KATRITZKY et al., 2001). Multicomponent systems become more complex as each component has characteristics that influence intermolecular interactions. High melting points are desirable but may contribute to low solubility (FLEISCHMAN et al., 2003). Low melting points can hamper processing, drying, and stability. It is possible to increase or decrease an API's melting point by selecting a coformer with a higher or lower melting point than the API. Furthermore, the melting point correlates with properties such as processability, solubility, and stability, and in multicomponent cocrystals, it will present a more complex analysis (QIAO et al., 2011).

2.3.4. Bioavailability

Bioavailability is the rate or measure at which the active compound reaches systemic circulation levels and is available at the site of action (CHIOU, 2001). The bioavailability of an API depends mainly on the dissolution rate (kinetic factor) and solubility (thermodynamic factor) (MANGIN; PUEL; VEESLER, 2009). Improving bioavailability means improving the pharmacokinetic properties and desired therapeutic effect (BOLLA; NANGIA, 2016).

The biopharmaceutical classification (BCS), proposed by Amidon and collaborators (1995), correlates the dissolution of drugs *in vitro* with bioavailability *in vivo* and categorizes

APIs from the orally administered group into four classes: class I (high solubility and high permeability), class II (low solubility and high permeability), class III (high solubility and low permeability) and class IV (low solubility and high permeability)(AMIDON et al., 1995).

It should be added that animal bioavailability is an important parameter to be analyzed for the development of new compounds (QIAO et al., 2011). *In vivo* studies are performed in rodents, rabbits, dogs, pigs, and primates to determine pharmacokinetics in initial compound development studies. To analyze the bioavailability parameter, the amount of medication in the blood after oral administration of the original drug and the drug in cocrystal form that reaches the systemic circulation is evaluated (EMAMI et al., 2018).

2.3.5. Dissolution

Dissolution is the rate or speed at which drug substance dissolves in the medium, providing information about the rate and extent of absorption within the human body (SHAIKH et al., 2018). It is desirable for a drug to dissolve when in the intestinal tract; long dissolution times may result in less absorption. Since the dissolution rate depends on particle size, the intrinsic dissolution rate better assesses this parameter (SCHULTHEISS; NEWMAN, 2009).

Intrinsic dissolution rate is a good indicator of *in vivo* performance of APIs (QIAO et al., 2011), This measures the dissolution rate independent of the particle size effect (SCHULTHEISS; NEWMAN, 2009). The intrinsic properties of the drug depend on the pH of the medium, ionic strength, and counterbalance ions; however, several parameters need to be considered and tested to obtain intrinsic dissolution data in cocrystals (QIAO et al., 2011).

2.4. CONVENTIONAL METHODS FOR PRODUCTION OF COCRYSTALS

Cocrystals can be synthesized by various conventional methods, such as solvent evaporation, solid grinding, liquid-assisted grinding, slurring, extrusion (twin screw extrusion, hot melt crystallization) (MUNDHE, 2013).

2.4.1. Solvent evaporation

In the solvent evaporation, API and coformer in a suitable stoichiometric ratio are dissolved in a common solvent until completely evaporated (KARAGIANNI;

MALAMATARI; KACHRIMANIS, 2018). The selection of an appropriate solvent is essential because if the solubility of the two components is not similar, then the component with lower solubility will precipitate (KARAGIANNI; MALAMATARI; KACHRIMANIS, 2018). During the evaporation process, the molecules in the solution change, such as creating hydrogen bonds between functional groups, forming a thermodynamically favourable product (KARAGIANNI; MALAMATARI; KACHRIMANIS, 2018).

The main advantages of this technique are that it does not require complex equipment and results in the formation of high quality and pure cocrystals. The disadvantage is using high amounts of solvents, which limits its scale-up (KARAGIANNI; MALAMATARI; KACHRIMANIS, 2018; MUNDHE, 2013). The solvent can also be incorporated into the crystalline network, enabling the formation of a solvate/hydrate (PADRELA et al., 2010). For screening cocrystals, this technique has the disadvantage that the less soluble component can crystallize instantly, leading to partial or no cocrystal formation (PADRELA et al., 2010).

2.4.2. Neat grinding

The solid-state grinding technique or neat grinding is a solvent-free crystallization method. The solid materials will be mixed stoichiometric, pressed, and crushed with a mortar and pestle, ball mill, or vibrator mill. Grinding duration varies from 30 to 60 minutes. Reducing particle size increases the specific surface area for interactions between materials to develop intermolecular bonds. However, manual grinding, with a mortar and pestle, has limitations regarding its reproducibility, as it is carried out in an open environment, it allows the solvent used in the synthesis to volatilize, in addition to not allowing control of the pressure applied in the grinding process (LI et al., 2016). Furthermore, several reports show an incomplete cocrystallization when dry milling is used (LI et al., 2016).

Mechanochemical grinding, on the other hand, acts on the behavior of materials when they are subjected to mechanical forces, providing reduction and homogeneity in particle size, increasing the covalent reactivity of materials due to the kinetic force that induces structural and chemical transformations (FRIIĆ et al., 2009). The advantage is that it is a quick technique to produce cocrystals (KARAGIANNI; MALAMATARI; KACHRIMANIS, 2018).

2.4.3. Liquid- assisted grinding (LAG)

The liquid-assisted grinding technique is a simple grinding modification in which a small amount of solvent (approximately a few tenths of a solvent equivalent per mole of component) is added during the grinding process (KARAGIANNI; MALAMATARI; KACHRIMANIS, 2018). Making it possible to increase the rate of cocrystal formation, increase reaction kinetics, and increase molecular collisions and orientationally and conformational degrees of freedom of the molecule at various interfaces (SHAN; TODA; JONES, 2002).

The advantages of the technique are increased performance, ability to control the production of polymorphs, and improved crystallinity; this method increases the rate of cocrystallization, produces cocrystals with high purity with a significant reduction in preparation time in addition to being the most efficient method for studying cocrystals, salts, and polymorphic forms of pharmaceutical compounds (KARAGIANNI; MALAMATARI; KACHRIMANIS, 2018). The advantage of LAG under milling includes high yield, increased crystallinity of the product formed, and the ability to control polymorph formation (FRIŠČIČ; JONES, 2009). The limitations of the technique are that production is small-scale, in addition to high energy consumption (KARAGIANNI; MALAMATARI; KACHRIMANIS, 2018).

2.4.4. Slurring technique

The slurring technique is a simple process in which the solid API dissolves in the solvent, forming a solution, and then the coformer is added, after which the resulting suspension is stirred, filtered, and dried (KARAGIANNI; MALAMATARI; KACHRIMANIS, 2018). The advantages of the process are that it uses a simple methodology and experimental apparatus and is efficient in screening on a laboratory scale. The main limitation of the process is its use on a large scale and the use of organic solvents, which may contain residuals in the final product. (RODRIGUES et al., 2018).

2.4.5. Extrusion

The hot melting extrusion method combines the melting and mixing of the drug and coformer simultaneously through the use of a heated screw extruder (KARIMI-JAFARI et al., 2018). It is a process in which obtaining an efficient mixture leads to better contact between the drug and coformer, facilitating the formation of cocrystals without using solvents (CHAVAN et al., 2018).

The advantages of this technique are the production of high-purity cocrystals, solvent-free method, continuous single-step process, and large-scale production, and fast operation time (GAJDA et al., 2019). Limitations include high energy, high shear forces, and high temperatures, which can cause degradation of the drug or polymer and/or change in the amorphous form of the API (HWANG; KANG; PARK, 2017).

Another technique for continuous production of cocrystals is twin screw extrusion, which operates at temperatures below the melting point of the starting material. Twin screw extruders are generally classified as co-rotating or counter-rotating, with counter-rotating extruders having high shear in the interlacing region, resulting in ineffective mixing and low speed and mass transfer rates. Co-rotating extruders offer a higher shear rate, making them ideal for industrial purposes (SHAIKH et al., 2018).

2.5. SCREENING OF COCRYSTAL

The screening aims to identify complementary coformers to form the cocrystal with API and improve the API's physical and mechanical properties. It is common for APIs to be poorly soluble in water and highly water-soluble coformers to be selected to produce stable cocrystals that allow greater supersaturation and dissolution in water and, therefore, greater bioavailability (MALAMATARI et al., 2017). In addition to identifying coformers with API with physical and chemical properties superior to API (MALAMATARI et al., 2017).

Milling methods are ideal for screening cocrystals, but a bit unrealistic for scale-up (PADRELA et al., 2010). The milling efficiency in screening cocrystals and stoichiometry variations is controlled by modifications in the composition of the reaction mixture; due to the absence of solvent (maceration) or a minimal amount of it as in the case of liquid-assisted milling, it is unlikely that preferential formation of the cocrystal occurs, not being a method limited by the difference in solubility of the crystalline components, as it is a characteristic of solvent-based methods (PADRELA et al., 2010).

It is added that understanding hydrogen bonds is often used for cocrystal design. For this Etter and Reutzel (1991) proposed 3 rules that state: (1) suitable proton donors and acceptors are used in hydrogen bonds, (2) intramolecular hydrogen bonds of six-membered rings preferentially form an intermolecular hydrogen bond, (3) the best proton donors and acceptors remaining after forming intramolecular hydrogen bond, form, intermolecular hydrogen bonds (ETTER; REUTZEL, 1991).

Furthermore, the CSD (Cambridge structural database) tool can be used for cocrystal secretion, as it helps to study and understand intermolecular interactions and the functional groups involved in synthon formation and cocrystal engineering and can help in selecting coformers for experimental screening (GROOM et al., 2016; SAVJANI, 2015).

2.6. MICRONIZATION

Micronization is a term to describe particle size reduction <10 μm (JOSHI, 2011). Micronization involves using hydrodynamic and mechanical methods to destroy internal bonds and cause the material to break down (CHEN et al., 2018). Changes in structural, physicochemical, and functional properties can accompany the reduction in particle size. Properties such as water absorption and flavor release are enhancing on a micro scale due to the increase in surface area, improving the bioavailability of poorly water-soluble drugs due to increased dissolution of substances on a nanometer or micrometer scale (CEREA et al., 2016; CHEN et al., 2018; RASENACK; MÜLLER, 2004). Furthermore, these characteristics make it possible to reduce the dose of medication ingested and side effects, promoting a controlled release of active ingredients and increasing the drug's circulation time in the body (YORK; KOMPELLA; SHEKUNOV, 2004).

These properties are enhanced through size reduction, increasing surface area. According to the Noyes-Whitney equation, the dissolution rate is directly proportional to the drug's surface area (HENG et al., 2008; NOYES; WHITNEY, 1897).

Mosharraf & Nystron (1995) studied the effects of particle size and shape on the dissolution rate. As a result, they observed that the dissolution rate of moderately soluble drugs is related to particle shape and size. The dissolution rate decreases for particles with the same size as the particle irregularity increases. This fact can be explained by the Prandtl boundary layer equation, in which the change in the average thickness of the hydrodynamic boundary layer leads to a change in the distance over which diffusion dominates, causing a change in the diffusion rate. Therefore, their studies concluded that small spherical particles have a higher dissolution rate than large and irregular particles (MOSHARRAF; NYSTRÖM, 1995). Furthermore, it is recommended to consider the specific area over particle size. Particle size may be obscure as particle aggregation significantly reduces the specific area (PERRUT; JUNG; LEBOEUF, 2005).

Work on micronization of active compounds was successfully carried out, showing interesting results. Aguiar et al. (2018), carried out the micronization of the nutraceutical compound trans-resveratrol using the SEDS technique. As a result, an increase in water solubility of approximately 2.8 times and an increase in the dissolution rate of approximately 1.8 times was observed. The authors conclude that the results obtained in the study can be used in the food, pharmaceutical, and chemical industries (AGUIAR et al., 2018).

Furthermore, another study carried out by Decui et al (2020), shows that resveratrol has been suggested for the treatment of epilepsy. Therefore, resveratrol was micronized, and its anticonvulsant effect was induced by pentylenetetrazol in zebrafish larvae (*Danio rerio*), comparing commercial and micronized resveratrol. In the analysis of locomotor activity carried out 24 hours after the crisis, it was observed that the occurrence of the tonic-clonic phase was prevented only with diazepam (positive control) and micronized resveratrol. Furthermore, micronized resveratrol prevented the deleterious effects of convulsions induced by pentylenetetrazol and did not cause impairment in the locomotor assessment and exploratory behavior of the animals. The data obtained demonstrate that the micronization process enhances the anticonvulsant effect of resveratrol. Therefore, micronized resveratrol obtained a similar effect to classic diazepam, with the benefit of being a safe candidate for use during the neurodevelopment stage (DECUI et al., 2020).

Aguiar et al (2017) studied the micronization of N-acetylcysteine (NAC), a promising molecule for treating psychiatric disorders. Micronization was performed using the SEDS technique, and *in vivo* and *in vitro* activities were evaluated. It was observed that micronization reduced the particle size by 245 times, and *in vitro* studies showed an increase in the dissolution rate and antioxidant activity and modification in the crystalline structure. *In vivo* tests to evaluate anxiolytic activity demonstrated that micronization reduced the minimum effective concentration of NAC and induced anxiolytic-like effects in zebrafish (AGUIAR et al., 2017).

2.6.1. Conventional particle micronization technique

There are different ways to obtain micronized particles, depending on the product. It can be reduced in size by applying pressure, friction, impact, or shear (RASENACK; MÜLLER, 2004). Conventional techniques such as jet grinding, ball mill grinding, or pearl milling are used. However, the micronization process using mills is inefficient, as the high energy input can alter surface properties and characteristics, such as mixing and flow properties, to the wide

particle size distribution obtained (RASENACK; MÜLLER, 2004). The high-pressure homogenization technique usually causes changes in the crystal structure and an increase in amorphous particles, affecting characteristics such as powder flow, agglomeration, and electrostatic behaviour, consequently affecting reactivity to chemical degradation (RASENACK; MÜLLER, 2004).

The freeze-drying technique, also called freeze-drying, requires a subsequent grinding step and produces particles with a wide particle size. The advantage of this technique is the improvement of the stability of labile drugs (ETZL; WINTER; ENGERT, 2014; TANG; PIKAL, 2004). The spray-drying technique makes it possible to control the particle size to be obtained, in addition to being a continuous processing operation method; however, the high temperatures of the process can affect thermolabile substances (RÉ, 1998; YOSHII et al., 2008).

Furthermore, there are nanoization technologies for processing compounds with low water solubility. In which APIs are generally stabilized using surfactants and/or polymeric stabilizers adsorbed on their surface. In which the average particle size typically varies from 100 to 1000 nm (MÖSCHWITZER, 2010).

Next, in section 2.8, methods that use supercritical fluids for micronization will be described in more detail.

2.7. SUPERCRITICAL FLUIDS

Supercritical fluids (FSC) are defined as fluids that are above a critical temperature and pressure (BRUNER, 1994; BRUNNER, 2005). In this region, thermophysical properties exhibit very high rates of change in temperature and pressure. These characteristics make FSC suitable for a wide variety of solutes, where any variation in pressure and temperature close to the critical point can alter the dissolution power and selectivity (BRUNER, 1994).

FSCs have gas-liquid transport properties. Figure 5 shows that FSCs have liquid-like density, but viscosity and diffusivity remain advantageous between liquids and gas (BRUNER, 1994). Furthermore, supercritical fluids are considered “green solvents for the future”. Supercritical carbon dioxide ($scCO_2$) is the supercritical fluid selected in most applications due to its mild critical conditions (Tc= 31.1°C and Pc= 73.9 bar) (MATOS et al., 2019). In addition to having the advantages of being non-toxic, non-flammable, thermodynamically stable, and relatively low cost (KNEZ et al., 2019; LOZOWSKI, 2010).

Furthermore, they exhibit almost zero surface tension; due to these transport properties, FSC is used in different applications such as extraction (DA SILVA; ROCHA-SANTOS; DUARTE, 2016; YOUSEFI et al., 2019), chromatography (BERNAL; MARTÍN; TORIBIO, 2013; WEST, 2018), particle generation (KNEZ et al., 2014b; MISHIMA, 2008; TAN; BORSADIA, 2001; YORK, 1999). The application of supercritical fluids in the pharmaceutical area stands out as an alternative to the use of organic solvents, as residual organic solvents in the final formulation of medicines can cause harmful effects on health (KNEZ et al., 2014a; PATTNAIK; ARUN; SWAIN, 2020). Therefore, the application of this technology is used in the cosmetic and therapeutic areas and the generation of products for food use, among others.

Figure 5- Phase diagram of a compound and the physicochemical properties of liquids, gases and FSC.

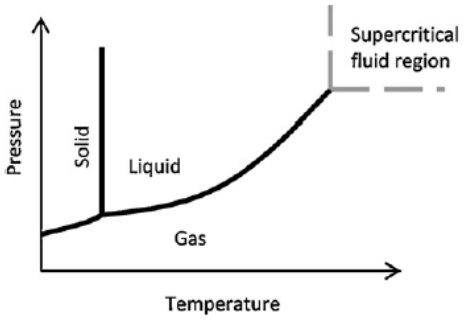

	Density ($kg \cdot m^{-3}$)	Viscosity ($mPa \cdot s$)	Diffusivity ($cm^2 \cdot s^{-1}$)
GAS	0.8-1.3	0.01-0.03	0.1-0.2
LIQUID	800-1200	0.4-1.1	0.00001-0.0001
SCF	300-1000	0.05-0.01	0.0001-0.001

Source:(TABERNERO; MARTÍN DEL VALLE; GALÁN, 2012)

2.8. MICRONIZATION AND COCRYSTALLIZATION USING FSC

The techniques used for micronization using supercritical fluid can be divided into supercritical fluid (FSC) acting (a) as a solvent: RESS (rapid expansion of the supercritical solution) (b) as a solution: PGSS (particles that form gas-saturated solutions) and (c) as anti-solvent: SAS (supercritical anti-solvent), GAS (anti-solvent gas), ASES (aerosol solvent extraction system), SEDS (supercritical fluid enhanced dispersion in solution) (FAHIM et al., 2014).

2.8.1. RESS- Rapid expansion of supercritical solutions

The technique began in 1984 when Kmkonis showed its potential to process a wide variety of difficult-to-grind solids and obtain small, uniform particles (DEBENEDETTI et al., 1993). Patented in 1986, it is being applied to products that have reasonable solubility in supercritical carbon dioxide, that is, low polarity compounds (ESFANDIARI, 2015; JUNG; PERRUT, 2001; SMITH, 1986).

The technique consists of dissolving the solute in the supercritical fluid, in which the solution containing the solute is rapidly expanded (reaching < 10^{-5}s) and depressurized; this solution undergoes throttling passing through a fine capillary nozzle, which leads to rapid supersaturation and the formation of small particles (Figure 6) (DEBENEDETTI et al., 1993; MISHIMA, 2008). During supercritical solution expansion, the density and strength of the solvent decrease, resulting in supersaturation of the solution and precipitation of free particles from a residual solvent (DEBENEDETTI et al., 1993; MISHIMA, 2008).

The main advantage of applying this technique is the need for a single-step reuse of FSC in a continuous process. It is added that as the solute is dissolved in a supercritical fluid, in most cases, it does not require the use of an organic solvent (FAHIM et al., 2014). Furthermore, using moderate temperatures (generally below 80°C), and obtaining fine particles with a narrow size distribution (FAHIM et al., 2014; JOSHI, 2011; MARTÍN; COCERO, 2008).

However, the technique has a limitation most materials are not soluble only in supercritical fluids. Furthermore, CO_2 is unsuitable solvent for polar and high molecular weight substances, such as polymeric materials (PADRELA et al., 2018). The technique allows the use of a co-solvent in the process as it is previously dissolved in CO_2, with preference given to the use of low-toxicity solvents such as acetone and ethanol; however, the advantage of not using any chemical solvent in the technique will be lost (Fages *et al.*, 2004). Furthermore, obtaining small particles makes it difficult to use them in the appropriate pharmaceutical form due to aggregation; in addition, large-scale production is complex, as there is the possibility of blocking the nozzles (TÜRK, 2009). Mishima (2008) proposed to overcome this limitation by using a high shear mixer in the expansion vessel to assist in the circulation of particles to improve the homogeneity of the process (MISHIMA, 2008). Another negative point of the technique is the high consumption of supercritical fluids and the high process pressures (YORK; KOMPELLA; SHEKUNOV, 2004).

Figure 6- Schematic diagram of the technique RESS.

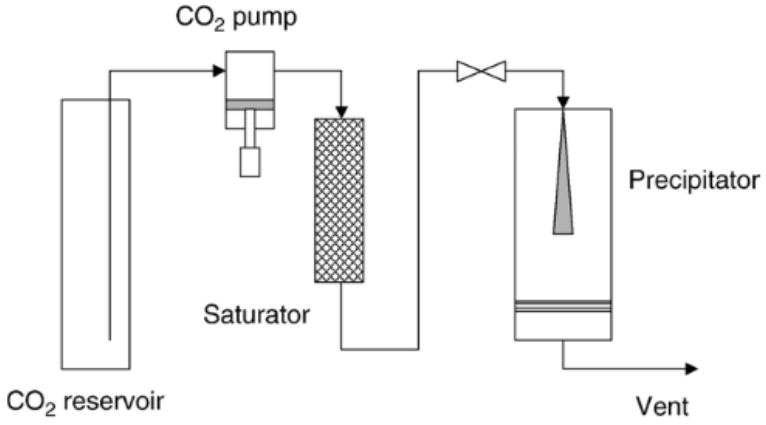

Source: (MARTÍN; COCERO, 2008)

2.8.2.GAS- Gas antisolvent

The anti-solvent gas technique induces particle formation by removing the solvent from a solution using FSC (PARIKH, 2016). The first method using pressurized antisolvent was described by Gallagher and collaborators (1989) and applied to solid compounds that are not soluble only in supercritical fluids. Gallagher proposes this process to overcome the limitations found in the RESS process; it is suggested to use supercritical fluids or gases close to vapor pressure as antisolvents. The use of CO_2 as an antisolvent allows the use of mild temperatures (CHARBIT; BADENS; BOUTIN, 2004; GALLAGHER et al., 1989).

The process consists of the solid material micronized or cocrystallized being dissolved in the organic solvent, then the FSC is injected into the solution, and with increasing pressure in the chamber, the particles precipitate (Figure 7). When the particle is precipitated, gas is added to remove residual solvent and produce a dry precipitate until depressurization (CHARBIT; BADENS; BOUTIN, 2004; DEHGHANI; FOSTER, 2003; GIROTRA; SINGH; NAGPAL, 2013).

In this methodology, the principle of the technique is solvent-induced phase separation (YEO; KIRAN, 2005). To use this technique, the solute must be miscible in the organic solvent but insoluble in the supercritical fluid (COCERO; MARTIN, 2008).

The advantage of the GAS technique is that the particle size distribution can be controlled by adjusting the pressure, temperature, and composition (MISHIMA, 2008). Furthermore, it allows obtaining particles with a reduced size (micrometric/submicrometric), in the range of 1 to 10μm (MARTÍN; COCERO, 2008). It adds the flexibility to choose the solvent

with fewer operational problems compared to other techniques; and also to being possible to recover the organic solvent by depressurization (FAHIM et al., 2014). The process is operated at moderate pressures (5-8 MPa) (MARTÍN; COCERO, 2008).

As a disadvantage, there is the possibility of low levels of remaining solvent (KŐRÖSI et al., 2017; MISHIMA, 2008; THIERING; DEHGHANI; FOSTER, 2001). In addition the production capacity is limited by the capacity of the precipitation vessel (MARTÍN; COCERO, 2008).

Figure 7-Schematic diagram of the GAS technique.

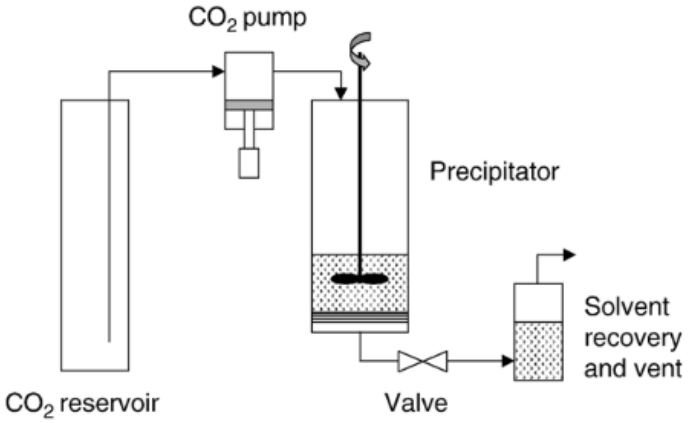

Source: (MARTÍN; COCERO, 2008)

2.8.3. SAS-Supercritical Antisolvent

It was developed to overcome the limitations of the GAS process (MARTÍN; COCERO, 2008). This technique can be used on any compound that is not soluble in supercritical CO_2 but is soluble in an organic solvent, in which the supercritical fluid acts as an antisolvent (JUNG; PERRUT, 2001). Firstly, the API is dissolved in a liquid solvent, and the solution is sprayed into a chamber in which there is already a pre-existing supercritical fluid (antisolvent); the rapid contact between the two media generates supersaturation, resulting in rapid nucleation, growth, and finally, the precipitation of microparticles (Figure 8) (GIL-RAMÍREZ; RODRIGUEZ-MEIZOSO, 2021; HAKUTA; HAYASHI; ARAI, 2003).

As advantages, this technique presents the ability to control nanoparticle and microparticle sizes; adaptability to large-scale production; in addition to the continuous recovery of CO_2 in the process (KALANI; YUNUS, 2011; YEO; KIRAN, 2005). As

advantages, this technique presents the ability to control nanoparticle and microparticle sizes, adaptability to large-scale production in addition to the continuous recovery of CO_2 in the process (CHAFIDZ, 2018; KALANI; YUNUS, 2011; YEO; KIRAN, 2005).

The main disadvantage is that particle aggregation occurs in the atomizing nozzle over time (CHAFIDZ, 2018). However, this problem can be alleviated through intensive mixing of the supercritical antisolvent and the solution, as it increases mass transfer and produces smaller particles. An alternative to this technique limitation is the use of ultrasonic nozzles to obtain a more intensive mixing (JIA et al., 2015; JUNG; FLUIDS; 2001; KALANI; YUNUS, 2011). Operating pressures are higher than the GAS process, in the range of 9 and 15 MPa; in this pressure range, CO_2 is completely miscible in organic solvents (MARTÍN; COCERO, 2008).

Figure 8- Schematic diagram of the SAS technique.

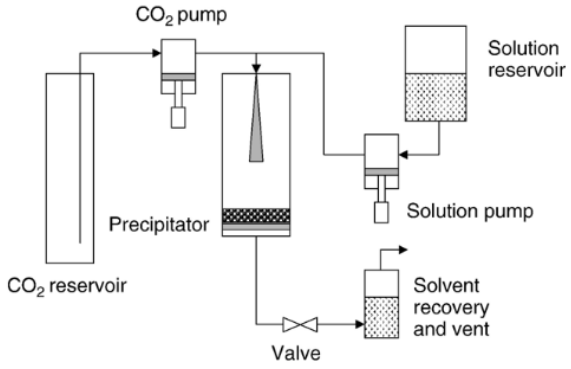

Source:(MARTÍN; COCERO, 2008)

2.8.4. PGSS- Particles from Gas-Saturated Solutions

The PGSS technique was patented by Weidner and collaborators in 1995. Used to micronize non-miscible solids in FSC; polycaprolactone encapsulation; micronization of liquids, suspensions, and emulsions (KNEZ et al., 2014b). Based on this PGSS process, others were also developed, such as CAN-BD (carbon dioxide-assisted nebulization with bubble dryer), SAA (*supercritical*-assisted atomization), DELOS (depressurization of an expanded liquid organic solution), and CPCSP (powder coating spraying process) (JOSHI, 2011).

They are designed to produce particles that absorb FSC in high concentrations. First, the FSC is dissolved in the molten polymer or liquid suspension solution; then, the high-pressure mixture is quickly depressurized through a nozzle that leads to precipitation and particle formation (YEO; KIRAN, 2005).

PGSS entails a reduction in melting point to create a solution. When the material to be treated is solid, the solid is first melted, and compressible gas is added to the molten material until saturation is reached (Figure 9). The temperature of the solution is adjusted above or below the melting point of the solid under atmospheric pressure. The mixture is discharged through a nozzle or expansion device; operating conditions are altered until the compressed fluid turns into a gas, facilitating particle separation. Evaporation or the Joule-Thomson effect results in cooling of the mixture, which causes the temperature to reduce below the melting point of the material and then precipitate. It is noticed that the melting point of the solid decreases due to pressurization with dense gases (YORK; KOMPELLA; SHEKUNOV, 2004).

The main advantage of the technique is that particle characteristics can be controlled by manipulating conditions such as initial solute concentration, temperature, expansion pressure, and nozzle geometry (SAMPAIO DE SOUSA et al., 2009). Furthermore, it does not require the use of additional solvent, making it attractive for the processing of pharmaceutical compounds as it can be operated in continuous mode and has a low processing cost (FAHIM et al., 2014; YORK; KOMPELLA; SHEKUNOV, 2004).

The limitation of using this technique is obtaining a wide distribution of particle sizes. Furthermore, for thermally labile compounds, the temperature required to melt the solid is so high that the material can be damaged (YORK; KOMPELLA; SHEKUNOV, 2004).

Figure 9-Schematic diagram of the PGSS technique.

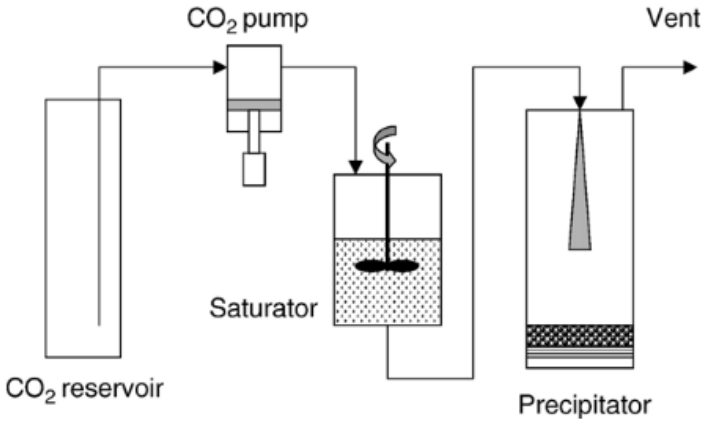

Source: (MARTÍN; COCERO, 2008)

2.8.5. SEDS-Solution enhanced dispersion by supercritical fluid

It is based on the same general principle as SAS; the difference between the techniques is how they introduce the phases, in which SEDS uses a coaxial nozzle. The liquid solution and FSC are sprayed together through a specially designed coaxial nozzle. FSC is used as an antisolvent and as a dispersion medium. Spontaneous contact of FSC and liquid solution in a high-velocity flow generates a finely dispersed mixture and rapid particle precipitation (YEO; KIRAN, 2005). Generally, it produces nanometer or micrometer-scale particles (YORK; KOMPELLA; SHEKUNOV, 2004).

Hanna and York (2000) designed a nozzle containing two or three coaxial passages to provide the simultaneous introduction of solution/suspension and different solvents, aiming to overcome solubility drawbacks (Figure 10 (a)) (HANNA, M.; YORK, 2000; TABERNERO; MARTÍN DEL VALLE; GALÁN, 2012). A two-pass coaxial nozzle with a mixer at the end of the nozzle is used to provide a premix between FSC and the solution (Figure 10 (b)). Initially, the solution is introduced along the inner surface, while FSC is pumped along the outer surface, allowing for effective contact and enhanced mass transfer. Particles of approximately 1 to 5 µm are obtained with this nozzle configuration (TABERNERO; MARTÍN DEL VALLE; GALÁN, 2012).

The advantage of the technique is the use of a coaxial nozzle that induces uniform particle formation (YORK; KOMPELLA; SHEKUNOV, 2004). Furthermore, the technique is suitable for polymers, as most of these materials are not soluble in FSC, and adaptation for continuous and large-scale operations (FAHIM et al., 2014).

Figure 10-Different nozzle schemes for the SEDS technique.

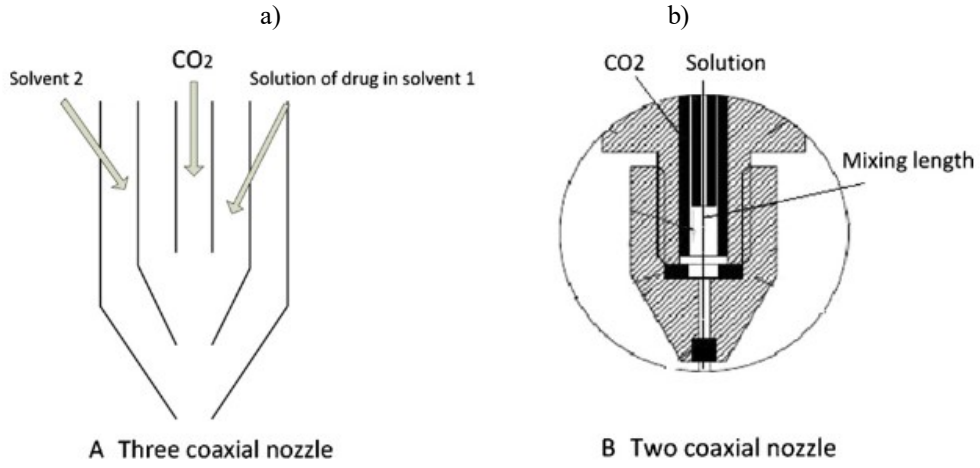

Source: (TABERNERO; MARTÍN DEL VALLE; GALÁN, 2012)

2.8.6.CSS- Cocrystallization with supercritical solvent

A special type of RESS is the CSS technique that allows control of supersaturation, nucleation and growth rates. CSS is induced by variations in temperature and concentration of solutes in systems without volatile organic solvents or in the presence of small amounts of a co-solvent (KNEZ; WEIDNER, 2003; LONG et al., 2021).

The application of this technique requires that the pure components have solubility ideally equal to CO_2 under supercritical conditions (PADRELA et al., 2009). The principle is based on the power of the solvent, supercritical CO_2 dissolved in a pure solid component; in some cases, a magnetic stirrer is used to assist in mixing the solid components. This solution is placed inside a stainless steel chamber; supersaturation is caused by depressurization, leading to precipitation and cocrystal formation (Figure 11)(RODRIGUES et al., 2018).

The advantage of the technique is the use of supercritical CO_2 to produce cocrystals, avoiding impurities from organic solvents or co-solvents in the particles generated (PADRELA et al., 2018). Furthermore, FSC facilitates intermolecular interactions, molecular association, nucleation, growth, and cocrystal formation (PADRELA et al., 2018). Another advantage is the high yield and the absence of drying steps in the final process (Fages *et al.*, 2004; Knez *et al.*, 2019).

The main disadvantages are that small amounts of solids can be processed over time, it requires relatively high pressures because the solute has low CO_2 solubility requires high investment costs for commercial production and presents difficulties in increasing production scale, which is generally carried out in batches (LONG; RYAN; PADRELA, 2019; PADRELA et al., 2018; PANDO; CABAÑAS; CUADRA, 2016).

Figure 11- Schematic diagram of the CSS technique.

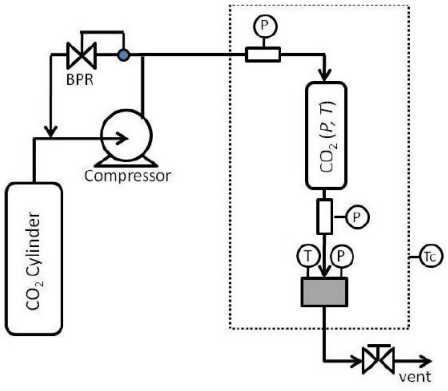

Source: Adapted (PADRELA et al., 2018)

2.9. CONSIDERATIONS ABOUT THE STATE OF THE ART

In recent years, interest in flavonoids as bioactive compounds for the prevention and possible treatment of diseases has grown exponentially due to their numerous biological properties (RUPASINGHE, 2020). However, flavonoid aglycones and glycosides are classified, according to the BCS biopharmaceutical classification system, as belonging to class II (low solubility and high permeability) and class IV (low solubility and low permeability), respectively (NAEEM et al., 2021). The resulting characteristics limit the potential for application, making it necessary to study approaches that aim to overcome such limitations. Next, some works involving naringin and naringenin, flavonoids targeted in this study, and the micronization and cocrystallization techniques reported in the literature will be detailed, highlighting the main results found and the gaps that require further investigation.

In the literature, the micronization of naringin, the work of Adami et al 2022, micronization of naringin using supercritical antisolvent, to produce inhalable particles, was reported. The best breathable fraction for naringin particles is obtained for particles with a d50~7 μm manufactured at 35 °C-150 bar and 60 °C-130 bar, corresponding to 32.6% and 36.7%, respectively. NuLi-1 cell line of immortalized bronchial epithelial cells adopted to evaluate powder cytotoxicity indicated after 24 h absence of toxicity at a concentration of 25 μM. These particles exhibit promising potential for incorporation into the anti-inflammatory formulation, serving as a supportive element for various disease treatments, including those associated with COVID-19 syndrome (ADAMI et al., 2022).

Li et al. (2017) realized microcrystalline cellulose to coat naringin to improve the release of the active compound through the fluidized bed operated at elevated pressure in which API particles are precipitated from a supercritical antisolvent process (SAS). It was observed that the coated particles resulting from the process have a higher load of active compound that provides higher release rates than particles produced using the conventional fluidized bed coating process. These particles are promising for application in agrochemistry, cosmetics, and food (LI et al., 2017).

Ma et al. (2023) carried out a fluidized bed coating process with supercritical antisolvent (SAS), a technique to manufacture dry powder inhalers (DPI) in which active ingredients such as micronized naringin for pulmonary distribution are incorporated. *In vitro* dissolution studies

using simulated lung fluid revealed that the NAR nanoparticles coated on the products were released immediately upon contact with the solution, with a cumulative dissolution greater than 90% in the first minute. Compared to oral crude NAR, the optimized DPI formulation demonstrated higher *in vivo* plasma and lung AUC0→∞ by 51.33-fold and 104.07-fold, respectively, in a Sprague-Dawley rat model (MA et al., 2023).

Only the work developed by Miao et al. (2018) for micronization of naringenin was reported in the literature. These authors performed the micronization of naringenin (NRG) using the SEDS technique. The process was carried out using a mixed solution of acetone/dichloromethane and CO_2 as solvent and antisolvent, respectively. The ideal process conditions were as follows: temperature of 35°C, pressure of 12 MPa, concentration of 15 mg/mL, solution flow rate of 1 mL/min, and the percentage of dichloromethane used in the process was 45%. As a result, the average particle size was approximately 611 nm. XRD and FTIR analyses showed that micronized (SEDS) and unprocessed NRG exhibited the same crystalline and chemical structure, and similar DSC thermograms. The *in vitro* dissolution test showed that micronization significantly increased the dissolution of NRG. The collaborators highlight that due to the large number of factors that affect the process, studies are needed to optimize the substance micronization process, drug release kinetic studies, and *in vivo* studies (MIAO et al., 2018).

The naringenin cocrystallization studies in the literature will be described here using conventional cocrystallization techniques. Jiang et al. (2020), in preliminary studies, found that naringenin, when in a high dose (100 mg/kg), had a prominent inhibitory effect on non-alcoholic fatty liver disease (NAFDL) in mice. After these findings, they carried out the cocrystallization of naringenin-isonicotinamide using solvent evaporation, to increase the naringenin solubility and dissolution rate. The results observed that in comparison with an equal dose (50 mg/kg) of the crude drug, the cocrystal significantly increased the in vitro release rate, as well as gastrointestinal absorption of naringenin, considerably alleviating the hepatic deposition of triglycerides in mice, therefore being a promising application for the treatment of NAFDL (JIANG et al., 2020).

Xu et al. (2020) conducted a study on the formation of naringenin-nicotinamide cocrystal (NRG-NIC), using the slow solvent evaporation and performed *in vivo* analysis. The study revealed a remarkable increase in the bioavailability of naringenin-nicotinamide by 175.09%, with a maximum concentration reaching 8.43 and 2.06 times that of NRG and NRG+NIC, respectively. Plasma concentration and pharmacokinetic analysis indicated rapid

absorption and slow elimination, as evidenced by an increase in half-life from 5.37 to 8.24 hours for NRG+NIC and NRG-NIC, respectively. Stability testing of NRG-NIC, conducted at 60°C and 90% relative humidity under light for 10 days, showed no change in appearance and DRX after 6 months. The findings provide important insights for future applications and research on naringenin (XU et al., 2020).

In the work of Cui et al. (2019), the formation of the naringenin cocrystal (NRG) and the coformers nicotinamide (NIC), isonicotinamide (INM), caffeine (CAF), betaine (BTN), and L-proline (LPROL) were studied. The method used to form the cocrystals was solution crystallization. Furthermore, antihyperlipidemic effects were evaluated in male Sprague-Dawley rats. The results showed that the NRG: INM and NRG: NIC cocrystal presented a maximum plasma concentration (Cmax) that increased by 6.65 and 5.71 times, respectively, compared to pure NRG. NRG: LPROL and NRG: BTN Cmax were 2 and 3.35 times higher, respectively, compared to pure NRG. The NRG: BTN cocrystal showed drug distribution in five internal organs, increasing oral absorption and antihyperlipidemic effect, and drug distribution in the liver after oral administration was significantly increased compared to pure NRG. Therefore, the NRG: BTN cocrystal showed the best antihyperlipidemic effects in studies in transgenic mice. Thus, the authors conclude that the formation of cocrystals is a promising way of delivering drugs with neutral pH and low aqueous solubility (CUI et al., 2019).

Luo et al. (2018) studied the cocrystallization of naringenin and the coformers isonicotinamide (INM) and picolinic acid (PCA) using the slurry technique. And two NRG-betaine (BTN) modifications using the liquid diffusion and slurry method (form A and B, respectively). The results obtained show that all cocrystals developed showed an improvement in solubility. The intrinsic dissolution rate of NRG-INM, NRG-PCA, NRG-BTN form A and B increased by 1.5, 3.03, 1.78, and 1.93 times, respectively, compared to pure NRG. For the first time, BTN was used to form cocrystals together with flavonoids by interacting with a carboxyl and hydroxyl functional group. The authors, therefore, encourage cocrystallization trials with BTN and other flavonoid compounds (LUO et al., 2018).

Lee et al. (2019) studied cocrystal formation using a natural flavonoid to improve the potential commercialization of API-containing cocrystals. The flavonoid used in this work was naringenin (NRG) and the API was carbamazepine (CBZ). The authors highlight that most studies design cocrystals based on intermolecular interactions and not on their health benefits. Therefore, they developed a CBZ:NRG (1:1) cocrystal using drowning-out crystallization. The results show that the cocrystal formed improved thermal stability and hydration resistance in

30 days at 93% relative humidity. The improvement in structural stability is due to the hydrogen bonds of the resorcinol functional group of NRG and the urea functional group of CBZ. In conclusion, using natural polyphenols with resorcinol to form cocrystals can provide new possibilities in research and development to improve the properties of APIs that can be explored (LEE et al., 2019).

Zhou et al. (2019) conducted an *in vitro/vivo* study of the carbamezepine:naringenin cocrystal (CBZ:NRG, 1:1) using the slow solvent evaporation technique. The results showed that the maximum concentration of the CBZ:NRG cocrystal (Cmax= 491.3 ng/mL) decreases with the longer elimination half-life of ($t_{1/2}$=8.5 h) compared to pure CBZ (Cmax =5258.1 ng/mL, $t_{1/2}$=0.7h). Compared with CBZ (97.2 µg/mL) in water the solubility of CBZ-NRG cocrystal decrease to 7.2 µg/mL, the same trends in pH 1.2 and 6.8 buffer solution. Therefore, it is concluded that the CBZ-NRG cocrystal presents different *in vitro/in vivo* performance compared to pure CBZ, which needs to be explored (ZHOU et al., 2019).

Khandavilli et al. (2018) studied the cocrystallization of naringenin with 27 coformers, in which new solid forms such as salt and cocrystal formed. The cocrystals were formed by the grinding technique, in which they were successful with the following flavone coformers, 4-hydroxypyridine, anthranilamide, and 4-4'-bipyridine. After structural characterization, it was observed that the hydrogen bond formed between the head-tail and the dimer is maintained only in the cocrystal, where flavonone is the coformer. The remaining neutral cocrystals maintain the S(6)O-H...O=C intramolecular hydrogen bond observed in naringenin with this bifurcated carbonyl oxygen atom. Solubility studies indicated that salt formation significantly improved the solubility of naringenin, and the piperazine salt improved solubility more than 3000 times compared to the same component in neutral form. Therefore, these solid forms require future studies to be further explored (KHANDAVILLI et al., 2018a).

Yin et al. (2020) studied the drug-drug cocrystal oxaliplatin (OXI), baicalein (BAI), and naringenin as coformers prepared using the slow evaporation and milling-evaporation technique. Cytotoxicity/anticancer effect tests were also carried out, and the results showed that OXA-NRG has very low toxicity in GES-1 cells. OXI-BAI showed more positive effects on inhibiting cancer cell lines SGC7901 than pure OXA. In the study comparing the cocrystal with the physical mixture, it was observed that they showed slight differences in *in vitro* tests; in the dissolution study, it exhibited slow release and delayed hydrolysis compared to the physical mixture. Cocrystals and coformers have supramolecular homosynthons that can be replaced by new heterosynthons that modify physicochemical properties such as solubility, dissolution and

stability. The study concludes that these findings contribute to the applications of cocrystals in the pharmaceutical industry (YIN et al., 2020) .

Zhang et al. (2022) studied naringenin-isonicotinamide (NGN-INT) cocrystallization and improving effects of polyvinyl pyrrolidone (PVP) and hydroxypropyl methylcellulose (HPMC) on precipitation rate, supersaturation, and bioavailability of naringenin. The results demonstrate that NGN-INT formulation, compared to the NGN crude drug, enhanced the dissolution rate of NGN and significantly increased Cmax and AUC (0–∞) of NGN by 18 times and 1.97 times, respectively. The addition of PVP or HPMC in NGN-INT cocrystal further increased the bioavailability of NGN in NGN-INT. The *in vivo* pharmacodynamic study showed that NGN-INT with HPMC significantly improved the inhibitory effects of NGN against abdominal aortic aneurysms (ZHANG et al., 2022).

A single study has been reported in the literature in which naringin (NAR) is used as a coformer forming cocrystals. Laxmi et al. (2019) studied the formation of doxorubicin HCl cocrystal (BCS III) with flavonoids (quercetin and naringin), DOX: NAR (1:1) and DOX: QUE (1:1, 1:2, 2:1) using the methodology of slow solvent evaporation. As a result, they obtained the solubility (pH 6.8 and 37°C) of the pure drug (DOX) was 20.72 µg/mL and of the cocrystal DOX: NAR (1:1) DOX: QUE (1:1, 1 :2, 2:1) the solubility was 191, 21 µg/mL, 8.52 µg/mL, 10.31 µg/mL, 8.18 µg/mL, respectively. As a result, it was observed that DOX: NAR presented an increase in solubility of 9.2 times compared to the pure drug and the cocrystal DOX: QUE. Therefore, cocrystal formation by slow solvent evaporation is a valuable strategy to increase the therapeutic potential of doxorubicin HCl (LAXMI et al., 2019).

Therefore, considering the work reported in the literature, it is possible to conclude that there were no cocrystals of naringin and naringenin formed in a supercritical environment until now, which is a promising technology in the formation of cocrystals (MÜLLERS; PAISANA; WAHL, 2015; PADRELA et al., 2015; PESSOA et al., 2019; TIAGO et al., 2013; TJANDRAWINATA; HIENDRAWAN; VERIANSYAH, 2019) that needs to be explored. The micronized forms of naringenin and naringin have already been discussed in the literature, but there are still gaps regarding changes in process parameters using FSC and applying these particles.

It should be added that works that present *in vitro* and *in vivo* tests are still need to be explored. However, the micronized and cocrystal forms are promising, showing several signs of improvement in dissolution rates, solubility, and bioavailability and, therefore, the

therapeutic potential of these particles needs to be studied to be used in the pharmaceutical industry, helping to treat diseases, among other areas.

2.10. SCHIZOPHRENIA

Schizophrenia is one of the most severe psychiatric illnesses. It is estimated that approximately 24 million people, or 1 in 300 people (0.32%) worldwide, suffers from this condition, according to data from the World Health Organization (WORLD HEALTH ORGANIZATION, 2022). It is a psychiatric disorder that presents positive symptoms, such as hallucinations and disorganized speech; negative symptoms, such as anhedonia; cognitive symptoms, such as language incoherence, difficulty associating, and neologisms; and aggressive; and hostile symptoms, which include self-destructive behaviour, such as suicide and symptoms of depression and anxiety (ASSOCIAÇÃO PSIQUIÁTRICA AMERICANA, 2013; EGERTON et al., 2021; ELKIS et al., 2008; STAHL, 2014).

This disease often begins in adolescence or young adulthood and may follow a course of relapses or become chronic and progressive, particularly in cases where the onset is late (BOYCHUK et al., 2018). There are more than 20 different antipsychotic drugs in clinical use, but the differences between them are small. Antipsychotics are divided into typical or first-generation, a more recent name, whose leading representatives are chlorpromazine and haloperidol, and atypical or second-generation, such as clozapine, risperidone, and aripiprazole. The distinction between the typical and atypical groups depends on the affinity profile for different receptors, the incidence of extrapyramidal effects (EPS) (lower in the atypical group), the efficacy (especially of clozapine) in the group of patients “refractory to treatment” and the efficacy against negative symptoms (higher in the atypical group) (ELKIS; MELTZER, 2007; SHI et al., 2007; STAHL, 2014; VINET; ZHEDANOV, 2011). Although atypical antipsychotics are less likely to cause movement disorders, such as EPS, they are associated with weight gain, elevated prolactin and glucose (metabolic syndromes), sedation and neuroleptic malignant syndrome (ELKIS et al., 2008).

Typical antipsychotics act primarily as dopaminergic D_2 receptor inverse agonists (HALL; STRANGE, 1997). The positive symptoms of schizophrenia are well resolved with the use of these drugs, but the negative symptoms tend to worsen with these drugs, in addition to the extrapyramidal symptoms, which appear with therapeutic doses (STAHL, 2014; VINET; ZHEDANOV, 2011).

Atypical antipsychotics, a class with a low tendency to cause extrapyramidal effects, are potent antagonists of multiple receptor subtypes, including dopamine and serotonin receptors. However, a significant proportion of patients remain refractory to treatment. Furthermore, this class induces adverse serious effects, such as agranulocytosis (mainly reported for the use of clozapine) and other effects, such as weight gain (STAHL, 2014; VINET; ZHEDANOV, 2011). A study by the National Institutes of Health in the United States demonstrated that 74% of patients discontinue use after 18 months of therapy due to low tolerability or incomplete efficacy, indicating the need for new treatments (SNYDER; MURPHY, 2008).

Clozapine, for example, is a BCS class II medication with low aqueous solubility and low bioavailability (< 27%) due to first-pass hepatic metabolism (VENKATESWARLU; MANJUNATH, 2004; ZENG et al., 2013). Treatment of refractory schizophrenia with clozapine can often be difficult for some patients who cannot tolerate the adverse effects (CLARK et al., 2018). The most common adverse effects are sedation, hypertension, weight gain, convulsions, hypersalivation or sialorrhea, benign fever, hypotension, nausea, nocturnal enuresis, gastroesophageal reflux, constipation, tachycardia, dizziness, blurred vision, dysarthria, blood dyscrasias, such as leukopenia/neutropenia/eosinophilia. Side effects classified as uncommon are agranulocytosis, diabetes mellitus/hyperglycemia, metabolic syndrome, delirium, liver enzyme abnormalities, interstitial nephritis, stuttering, thrombocytopenia, dysphonia, neuroleptic malignant syndrome (CLARK et al., 2018). Due to poor patient adherence to treatment for resistant schizophrenia, the risk of psychotic relapse can increase, which can lead to impairments in social and cognitive functioning, psychiatric hospitalizations, and increased treatment costs. Therefore, adverse effects are one of the common reasons for stopping this treatment (DE BERARDIS et al., 2018).

Recently, George et al. (2020) demonstrated that treatment with naringin and/or clozapine significantly attenuated ketamine-induced symptoms of schizophrenia, as well as central oxidative lesions caused by ketamine administration in rodents. Furthermore, ketamine provoked neuronal apoptosis by increasing Bax/Bcl2 expression, caspase-3 activity, and Cytochrome C and Akt protein expression, whereas naringin/clozapine treatment significantly inhibited this apoptotic effect. Furthermore, naringin activates neurodevelopment through the wnt/β-catenin signaling pathway, evidenced by increased pGSK-3β expression and reduced pβ-catenin expression (GEORGE et al., 2021).

These findings are particularly interesting since current data demonstrate a tendency for new antipsychotics to act on glutamatergic neurotransmission (EGERTON et al., 2021). In

recent years, within the pathophysiological hypothesis of schizophrenia, disturbances in cerebral glutamatergic neurotransmission and, in particular, of N-methyl-D-aspartate (NMDA) receptors have been demonstrated. This hypothesis is based on the observation that compounds that block NMDA receptors can cause psychotic behaviors in humans. Systemic administration of non-competitive NMDA antagonists such as phencyclidine or ketamine induces positive and negative symptoms as well as cognitive impairments in healthy individuals and exacerbates the same symptoms in schizophrenic patients (AALTO et al., 2005; EGERTON et al., 2021; PIETRASZEK, 2003; TSAI; COYLE, 2002). Thus, since naringin shows promising effects in an animal model that induces psychotic symptoms through the hypofunction of NMDA receptors, it is possible to infer that this molecule may represent an antipsychotic candidate with a different mechanism of action.

Additionally, naringin was effective in reducing adverse effects when added to treatment with the antipsychotic clozapine. Naringin, showing protective effects in the model of schizophrenia symptoms induced by ketamine in Wistar rats, increased the animals' total leukocyte count, preventing agranulocytosis when administered alone or in combination with clozapine. Also, naringin treatment reduced serum levels of total cholesterol and triglycerides. Naringin prevented weight gain caused by clozapine and reduced serum glucose levels, preventing hyperglycemia associated with treatment with the antipsychotic. These findings may suggest that naringin has a potential benefit when used as an add-on therapy (along with clozapine) in the treatment of schizophrenia (GEORGE et al., 2021).

It should be added that recent studies address the formation of multicomponent drug-nutraceutical or drug-drug cocrystals, which has numerous advantages, such as the combination of drugs showing a better effect than the sum of their individual effects, in addition to improving physicochemical properties of both constituents, possibility of synchronous release of the constituents, favoring unique pharmacokinetic interactions and synergistic effects in terms of clinical efficacy, in addition to reducing the number of prescriptions, reducing side effects, being a viable alternative to traditional drugs (ALMANSA et al., 2019; BOLLA; NANGIA, 2016; THAKURIA; SARMA, 2018). In addition, the growing demand to facilitate the reduction of drug manufacturing costs is one of the main reasons for the increasing trends in treat complex disorders such as HIV, AIDS, cancer and diabetes, and psychiatric disorders, among others (KARIMI-JAFARI et al., 2018; SARMAH et al., 2020).

Sarmah et al. (2020) reported the drug-nutraceutical cocrystallization of the antipsychotic olanzapine, a drug used to treat schizophrenia and bipolar disorder. The coformers

(nutraceuticals) used for cocrystallization were 2,4,6-trihydroxybenzoic acid (246 THBA), gallic acid (GA), and sinapic acid (SPA); they also performed the drug-drug cocrystallization of olanzapine and the nateglinide molecules (NAT), pyrazinoic acid (PZO), using liquid-assisted milling and grinding methodology. Solubility analysis showed a trend of OLN – PZO > OLN – SPA > OLN – GA > OLN – 246THBA > OLN with solubility improved by up to 219 times for OLN – PZO compared to that of pure OLN drug, which correlated well with the solubility of the coformer. Furthermore, the formation of a co-amorphous salt of OLN-NAT presented the potential for development as a combination drug to suppress or increase blood sugar, a common side effect observed during monotherapy of psychiatric patients. using OLN. The equilibrium solubility study shows a substantial increase in the solubility of olanzapine pyrazinoate compared to the pure base. The authors believe that developing new drug formulations through drug combinations will open a new avenue for treating specific diseases or multiple diseases simultaneously with reduced cost and lower dosage (SARMAH et al., 2020).

3.MICRONIZATION OF NARINGENIN

The results of this section were published in the paper “Micronization of naringenin in supercritical fluid medium: in vitro and *in vivo* assays” in the “Journal of Drug Delivery Science and Technology” (DE OLIVEIRA et al., 2023).

ABSTRACT

Naringenin is a citrus flavonoid that shows relevant biological actions. However, naringenin presents low solubility in water and poor oral bioavailability. These characteristics are a limiting factor for its biomedical applications. The micronization process can reduce particle size and improve properties such as dissolution rate, potentially improving the bioavailability of the compounds. Thus, this study aimed to obtain microparticles of naringenin by gas antisolvent (GAS) technique. After, the application of micronized naringenin was tested *in vivo* in a mice model predictive of positive symptoms of schizophrenia, the ketamine-induced hyperlocomotion model in mice. Naringenin microparticles were successfully obtained by the GAS technique. *In vitro* dissolution rate assays confirmed that micronized NAR exhibited a significantly higher dissolution rate than raw NAR. Our *in vivo* data suggest the antipsychotic

potential of micronized naringenin, which is probably related to its increased solubility and, consequently, increased bioavailability.

Keywords: GAS; Supercritical CO_2; Naringenin; Microparticles; Schizophrenia

3.1. INTRODUCTION

Naringenin ($C_{15}H_{12}O_5$, 4',5,7-Trihydroxyflavanone, molecular weight 272.25 $g \cdot mol^{-1}$) (NAR) is a metabolite of naringin and belongs to the class of flavonoids (flavanones) (HSIU et al., 2002). It is naturally found in citrus fruits, such as oranges, lemons, grapes, beans, cherries, cocoa, and oregano (PASAM et al., 2017; YUSOF; GHAZALI; KING, 1990; ZAIDUN; THENT; LATIFF, 2018).

NAR has relevant biological actions, such as antioxidant (CAVIA-SAIZ et al., 2010; HEO et al., 2004), anti-inflammatory (LIN; LIN, 2011; SPAGNUOLO; MOCCIA; RUSSO, 2018; TSAI et al., 2012), neuroprotective (EMRAN et al., 2023; SUGUMAR; SEVANAN; SEKAR, 2019), and antiapoptotic (WANG et al., 2017). Additionally, it can readily cross the blood-brain barrier (MUSCATELLO; ZOCCALI; BRUNO, 2018) and improves cognition (YANG et al., 2014). Therefore, this flavonoid is considered a multi-targeted agent with multi-therapeutic potential (GROSSO et al., 2013).

However, the biomedical application of NAR is hindered by its low solubility in water (46 $\mu g \cdot mL^{-1}$) and, consequently, poor oral bioavailability (5.81%). Thus, these characteristics are a limiting factor for medicinal applications of this flavonoid, making it necessary to develop alternative delivery systems and/or formulations.

The micronization process decreases the particle size and can change the structural and physicochemical properties of the substances. In this sense, the drug dissolution are improved by this approach due to an increase in the particles surface area and reduced particle size (Rasenack e Müller, 2004). Consequently, the bioavailability of poorly water-soluble drugs is potentially increased after the micronization process (CEREA et al., 2016; CHEN et al., 2018; RASENACK; MÜLLER, 2004). The increase in the bioavailability and dissolution rate commonly allows a reduction in the dose of drugs without affecting their efficacy, also triggering a reduction in the side effects (RASENACK E MÜLLER, 2004; YORK, KOMPELLA E SHEKUNOV, 2004).

Micronization by conventional methods such as spray-drying, freeze-drying, and mechanical techniques has several disadvantages, such as relatively large particle size, wide size

distribution, and the presence of organic solvent residue in the final product (FAHIM et al., 2014). On the other hand, micronization using supercritical fluids highlights the reduction of thermal and mechanical stress; use of moderate temperatures and an inert atmosphere that avoids the degradation of the products; elimination and/or reduction in the use of organic solvents compared to traditional methods (PANDO; CABAÑAS; CUADRA, 2016). In addition, the use of supercritical fluids considered "green solvents for the future" has been getting more attention, and the most used is supercritical carbon dioxide ($scCO_2$) due to its mild critical conditions (Tc = 31.1 °C and Pc = 73.9 bar). Moreover, $scCO_2$ has the advantages of being non-toxic, non-flammable, thermodynamically stable, and presenting relatively low cost (KNEZ et al., 2019; LOZOWSKI, 2010).

Micronization of NAR was already reported in the literature by Miao et al., using the SEDS (solution-enhanced dispersion by supercritical CO_2) technique to improve the absorption rate and oral-intestinal bioavailability of this compound. The authors point out that due to the large number of factors that affect the process, studies are needed to optimize the substance micronization process, drug release kinetics, and *in vivo* assays (MIAO et al., 2018).

Schizophrenia is a psychiatric disorder that affects 24 million people worldwide (“WHO”, 2021). Schizophrenia symptoms are classified as positive symptoms (hallucinations, disorganized speech); negative symptoms (anhedonia, social isolation); cognitive symptoms (language incoherence, memory impairment, neologisms), and aggressive and hostile symptoms (self-destructive behavior, such as suicide) (EGERTON et al., 2021; ELKIS et al., 2008; STAHL, 2014). There are over 20 different antipsychotic drugs for clinical use.

Antipsychotics are divided into typical (chlorpromazine and haloperidol), and atypical (clozapine, risperidone, and aripiprazole) drugs. The distinction between typical and atypical groups depends on the profile of affinity for different receptors, the incidence of extrapyramidal effects (EPS) (lower in the atypical group), the efficacy in treating refractory patients, and the efficacy against negative symptoms (higher in the atypical group) (ELKIS; MELTZER, 2007; SHI et al., 2007; STAHL, 2014; VINET; ZHEDANOV, 2011). Although atypical antipsychotics are less likely to cause movement disorders such as EPS, they are associated with weight gain, elevated prolactin, glucose (metabolic syndromes), and sedation (STAHL, 2014; VINET; ZHEDANOV, 2011). Approximately 69% of schizophrenic patients present a moderate adherence to pharmacological treatment, while ~27% have low adherence to pharmacotherapy, mainly due to the side effects (KALKAN; BUDAK, 2020). In this sense, searching for new drug candidates with antipsychotic action is a current need (DE FILIPPIS et

al., 2021). Within this context, there is growing interest in using natural products as therapeutic agents.

Interestingly, naringin (the flavonoid precursor of NAR), has already been investigated regarding its antipsychotic effect in preclinical trials. George et al. (2020) demonstrated that treatment with naringin and/or clozapine significantly attenuated ketamine-induced hyperlocomotion and central oxidative damage caused by ketamine administration in rodents (GEORGE et al., 2020). Additionally, George et al., (2021) showed that naringin could effectively reduce adverse effects when added to treatment with the antipsychotic clozapine. These findings suggest that naringin has a potential benefit when used as add-on therapy (along with clozapine) in treating of schizophrenia (GEORGE et al., 2021). However, there is no literature data about the antipsychotic effects of NAR.

In view of the above-illustrated scenario, this study aimed to obtain microparticles of naringenin (micro NAR) by gas antisolvent (GAS) technique. The particles were characterized using several methods. Considering that there is a lack of studies on NAR antipsychotic potential, the first application of NAR micro was demonstrated against positive symptoms of schizophrenia using the ketamine-induced hyperlocomotion model in mice.

3.2.MATERIALS AND METHODS

3.2.1. Materials

Naringenin ≥ 95% (Sigma-Aldrich) was used to perform the precipitation. Ethanol (EtOH 99.5%) purchased by Êxodo Científico and CO_2 (99.9% in liquid phase) was provided by White Martins S.A. Ketamine-D4 hydrochloride, 100 $\mu g \cdot mL^{-1}$ (Sigma-Aldrich) was used *in vivo* assays.

3.2.2. GAS (Gas antisolvent)

The experimental procedure of GAS (gas antisolvent) used to prepare naringenin (NAR) microparticles is based on the methodology described by Pessoa et al. (2019) and Sakata et al. (2021). The experimental procedure consisted of preparing a solution containing 17.5 $mg \cdot mL^{-1}$ of NAR dissolved in ethanol and placed in an ultrasonic bath to form a homogeneous solution. Afterward, the solution was injected using a syringe coupled to a 0.45 μm, PTFE

(polytetrafluoroethylene) filter. This solution was placed in the chamber (600 mL with an inner diameter of 8 cm and a height of 12 cm) and CO_2 was fed to a syringe pump at a rate of 10 $mL \cdot min^{-1}$ until reaching the desired operating pressure of 8 MPa, under a constant temperature of 35 °C (using a thermostatic bath). The pressure and temperature were chosen based on previous studies (SACHETT et al., 2022; SANTOS et al., 2022). When the pressure was reached, the antisolvent flow was stopped, and the chamber continued to agitate using magnetic stirring at 300 rpm for 10 min. After the washing stage began with the antisolvent flow at 10 $mL \cdot min^{-1}$, and the pressure was isobaric for 60 min. Finally, micronized NAR was collected for *in vitro* characterization assays and the application *in vivo*.

3.2.3. Morphology and determination of particle size

The morphology of the raw NAR and micro NAR was performed by Scanning Electron Microscopy (SEM - JEOL JSM6390LV, United States). The images obtained by SEM were analyzed by ImageJ software (SCHNEIDER; RASBAND; ELICEIRI, 2012). The average length of the diagonal line of approximately 300 particles was measured (SCAPINELLO et al., 2018).

3.2.4. X-ray powder diffraction (XRD)

To analyse the structure of the raw and micronized naringenin, the data was performed using a diffractometer Bruker D2 Phaser, using θ–θ geometry, and equipped with a detector LynxEye. The equipment is operated by a Cu Kα source (1.5418 Å) at 30 kV and 10 mA, using a scintillation counter 1-dimensional. The scan parameters were 5- 40° 2θ (RIBAS et al., 2019b).

3.2.5. Differential scanning calorimetry (DSC)

Thermograms were obtained using Perkin Elmer equipment. (Jade-DSC) using hermetically sealed aluminum crucibles, single heating cycles were performed in the range of 20 to 300 °C, under the dynamic atmosphere of nitrogen (20 $mL \cdot min^{-1}$) and heating rate of 10 $°C \cdot min^{-1}$ (DAL MAGRO et al., 2017).

3.2.6. Fourier- transform infrared (FTIR) spectroscopy

The raw NAR and micro NAR were analyzed in KBr pellets. The spectra were obtained using a spectrometer (Shimadzu, model IRPrestige-21, Japan) over a wave number range of 500-4500 cm^{-1} at a resolution of 4 cm^{-1} (TADE; NANGARE; PATIL, 2020).

3.2.7. Dissolution rate

To determine the rate of dissolution of raw NAR and micro NAR, the methodology was adapted from Cheng et al. (CHENG et al., 2016). Samples (10 mg) were added to 100 mL of distilled water; 0.1 M HCl solution and phosphate buffer solution (PBS, pH 6.8), and maintained under constant stirring (100 rpm) at 37 °C. At selected periods of 5, 10, 15, 20, 30, 40, 50, 60, 90, 120 e 180 min, 2 mL were collected from the solution, which was immediately replenished with pure media to maintain the constant volume. Then, the samples were filtered using a syringe attached to a membrane filter 0.45 µm, PTFE and concentrations were measured employing the UV–vis Spectrophotometer (Model T90+, PG Instruments) at 288 nm.

3.2.8. Specific surface area

The surface areas of raw NAR and micro NAR were measured using Brunauer–Emmett–Teller (BET) method based on N_2 adsorption-desorption using Autosorb-1 equipment from Quantachrome Instruments (JOHNSON et al., 2020). The samples were outgassed for 15 h at 140 °C under N_2 flow, before the determination of the specific surface area.

3.2.9. Residual solvent

The identification of residual solvent in micro NAR the particles produced was made by gas chromatography-flame ionization detector (GC-FID) from Agilent Technologies - GC 7890A. The methodology was adapted from Santos et al. (2022) and Aguiar et al. (2016). The GC analysis was performed on the instrument Agilent GC 7890A. The column, HP-5MS (Agilent) fused silica capillary column (30 m length x 250 µm i.d. x 0.25 µm film thickness composed of 5% phenylmethylpolysiloxane) was connected to a Flame ionization detector (FID). Helium was used as the carrier gas at a flow rate of 0.8 $mL \cdot min^{-1}$. The injector (splitless mode) and

detector temperatures were 220 ºC and 250 ºC, respectively. The injection volume was 250 µL with auto sampler Agilent GC Sampler 80. The oven temperature program consisted of ramping up from 45 ºC for 3 min, then 20 °C.min^{-1} to 90 °C for 1 min, then 30 °C.min^{-1} to 140 °C for 2 min. Total run time: 9.92 min. The headspace conditions: Incubation temperature (88 °C), incubation time (60 s), syringe temperature (105 °C), Agitator Speed (250 rpm), flush Time (300 s), injection speed (500 µL·s^{-1}).

3.2.10. Molecular Docking

Molecular docking was accomplished to evaluate the potential of naringenin for the treatment of schizophrenia-like symptoms. The receptors selected were 5-HT$_{2A}$ (serotonin receptor) and D$_2$R (dopamine receptor). Second-generation antipsychotics target these receptors (mainly 5-HT$_{2A}$) (KIMURA et al., 2019; WANG et al., 2018b). Therefore, a molecular docking study of the interaction between NAR and dopaminergic D$_2$R and serotonergic 5-HT$_{2A}$ receptors was performed. The structure of naringenin (CID: 439246) was obtained by PubChem (https://pubchem.ncbi.nlm. nih.gov/) and optimized using Avogadro software (HANWELL et al., 2012; RAPPÉ et al., 1992). The structure of the receptors was obtained from the Protein Data Bank, D$_2$R (PDB ID:6CM4) and 5-HT$_{2A}$ (PDB ID:6A93) (KIMURA et al., 2019; WANG et al., 2018b). Crystallographic validation of the protein was performed using the Ramachandran plot (http://molprobity.biochem.duke.edu/) (WILLIAMS et al., 2018).The details of the box simulation are the cartesian coordinates for the NAR (X= 25 Å, Y= 25 Å, Z= 25 Å), and the grid box-center cartesian coordinates for D$_2$R were X= 8.60 Å, Y= 4.40 Å, Z= -10.90 Å and for 5-HT$_{2A}$ were X= 14.70 Å, Y= 4.80 Å, Z= 15.90 Å was realized using ezCADD tool (TAO et al., 2019) . The software's AMDock version 1.5.2 (VALDÉS-TRESANCO et al., 2020) and Autodock Vina 1.2.1 (TROTT et al., 2009) was used to perform the molecular docking, following the methodology (MORGAN et al., 2021). The results were visualized using the PyMOL and Lig-Plot$^+$ programs [61].

3.2.11 *In vivo* assays

3.2.11.1. Animals

The experiments were performed with Male Swiss mice (*Mus musculus*) (25-35 g), provided by the Centro de Bioterismo (CBi) of Unochapecó, Chapecó, State of Santa Catarina, Brazil.

The animals were placed in polypropylene cages (17 x 33.5 x 40.5 cm) containing a maximum of 6 animals per cage. Mice were maintained under a 12-hour light / dark cycle (lights on at 6:00 am), with minimal noise, controlled temperature (22 ± 1 °C) and humidity (40 – 60%) and had free access to standard laboratory feed (NUVITAL-Nuvilab®) and water *ad libitum*. All *in vivo* procedures were approved by the Animal Care Local Ethical Committee (CEUA UNOCHAPECÓ; protocol 003/2021, Annex I). Animal care and experiments were conducted in accordance with Brazilian (CONCEA, 2018; PRESIDÊNCIA DA REPÚBLICA, CASA CIVIL, 2008), and EU Directive 2010/63/EU for animal experiments (EUROPEAN PARLIAMENT AND COUNCIL, 2010).

3.2.11.2. Treatments

Mice were orally (p.o.) and intraperitoneally (i.p.) treated with volumes of 10 $mg \cdot kg^{-1}$, according to their weight. The drugs used in the *in vivo* assays were dissolved in saline solution + 1% polysorbate 80 (Vehicle), except micro NAR. Raw NAR and micro NAR dose (200 $mg \cdot kg^{-1}$, p.o.) was selected based on previously published studies (CHUNG et al., 2019; DI CARLO et al., 1993; GANAPATHY et al., 2008; LV et al., 2013; SUGUMAR; SEVANAN; SEKAR, 2019). Ketamine was administered at 10 $mg \cdot kg^{-1}$ (i.p.) (BETTI et al., 2017). The animals were weighted 24 h before the behavioral assays. The sample size was calculated using the online calculator from the University of São Paulo (FOB - USP), available at http://estatistica.bauru.usp.br/calculoamostral/index.php, considering an alpha value of 0.05, test power of 0.8. Mice were fasted 1 h before the oral administration (food, but not water, was withheld). Solutions were prepared on the day of the experiment. The tests were conducted in 4 rounds, using different sets of animals. Outcome assessors were blinded to treatment conditions. The animals were assigned to the experimental groups following block randomization procedures to counterbalance for the cage as well as litter.

3.2.11.3. Ketamine-induced hyperlocomotion

The effects of raw NAR and micro NAR on ketamine-induced hyperlocomotion, an animal model predictive of positive symptoms of schizophrenia (COYLE et al., 2012; JAVITT, 2012) were evaluated according to Betti et al. (2017) , with minor modifications. For this purpose, the animals (n = 8 / group) were orally treated with vehicle (10 $mg \cdot kg^{-1}$, Sham and Ketamine

groups), raw NAR (200 mg·kg^{-1}) or micro NAR (200 mg·kg^{-1}) and allowed to spontaneously explore the open field arena (waterproofed MDF box; 40 × 30 × 30 cm). Afterward, ketamine (10 mg·kg^{-1}) (Ketamine, raw NAR, and micro NAR groups) or Saline (Sham group) were administered (i.p.) to the animals. The locomotor activity was videotaped for 20 min and the following parameters were analyzed: distance (m), speed (m·s^{-1}), number of rearing, grooming, and fecal bolus expelled during the session. The software ANY-Maze (Stoelting Co., Wood Dale, IL, USA) was used to analyze the videos. The apparatus was cleaned with 10% ethanol after each mice exposition. At the end of the trials, animals were individually euthanized by anesthetic overdose (sodium thiopental at 150 mg·kg^{-1} (i.p.) preceded by lidocaine at 10 mg·kg^{-1}, s.c.) (CONCEA, 2018). To verify the effects of raw NAR or micro NAR on the basal locomotor activity of mice, independent groups of animals were orally treated only with Vehicle (10 mg·kg^{-1}), raw NAR or micro NAR (200 mg·kg^{-1}) and observed in the open field arena following the same procedure described above.

3.2.11.4. Statistical analysis

The statistical analysis of results from the *in vivo* assays was performed by One-way analysis of variance (ANOVA) followed by Tukey's test. The normality of data was evaluated by Bartlett´s test. No outliers (mean ± 2 standard deviations) were detected in the tests. $p < 0.05$ was considered significant.

3.3. RESULTS AND DISCUSSION

3.3.1. Morphology and determination of particle size results

Figure 12 presents the morphology of raw NAR and micro NAR by the gas antisolvent technique**.** Raw NAR presents morphology with irregular granular crystals with variable lengths and widths. Microparticles NAR are significantly smaller than raw NAR, showing an irregular needle-like shape. The results found here agree with the study of Miao et al. in which the authors performed the micronization of NAR using SEDS technique, which is based on the use of supercritical antisolvent and obtained particles with needle-shaped morphology after processing (CONCEA, 2018). The mean diagonal size of the particles was 65.78 ± 4.05 µm for

raw NAR and 24.48 ± 1.28 µm for micro NAR, indicating a reduction in the size of particles. The yield of naringenin after processing by the GAS technique is approximately 30 %.

Figure 12-SEM of naringenin (NAR) particles. (a) raw NAR x500 (b) raw NAR x1000 (c) micro NAR x500 (d) micro NAR x1000.

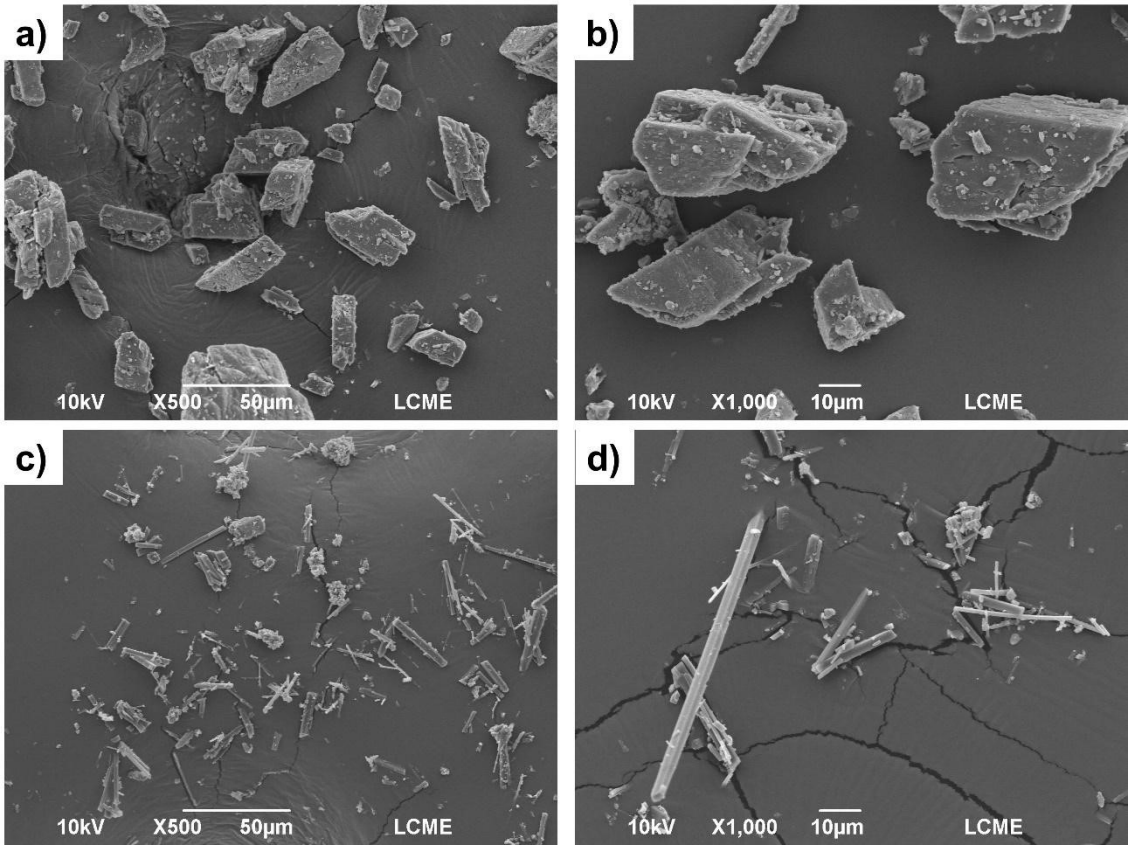

Source:Author (2024)

3.3.2. X-ray powder diffraction (XRD) results

The raw and micronized NAR particles were characterized by X-ray powder diffraction to evaluate changes in the crystalline structure of the compounds. Figure 13 illustrates the results obtained. The XRD of unprocessed NAR has diffraction angles (2Θ) 10.97°, 11.65°, 15.95°, 18.26°, 20.57°, 22.45°, 25.51°, and 27°, 86°. The profiles of the diffractograms from unprocessed NAR and micro NAR are similar, indicating that the crystal lattices are identical for both. However, it was observed that the intensities for micro NAR are smaller due to the reduction of the particle size (AMANI; SAADATI ARDESTANI; MAJD, 2021; MIAO et al., 2018).

Figure 13-XRD analysis of (a) micro NAR and (b) raw NAR.

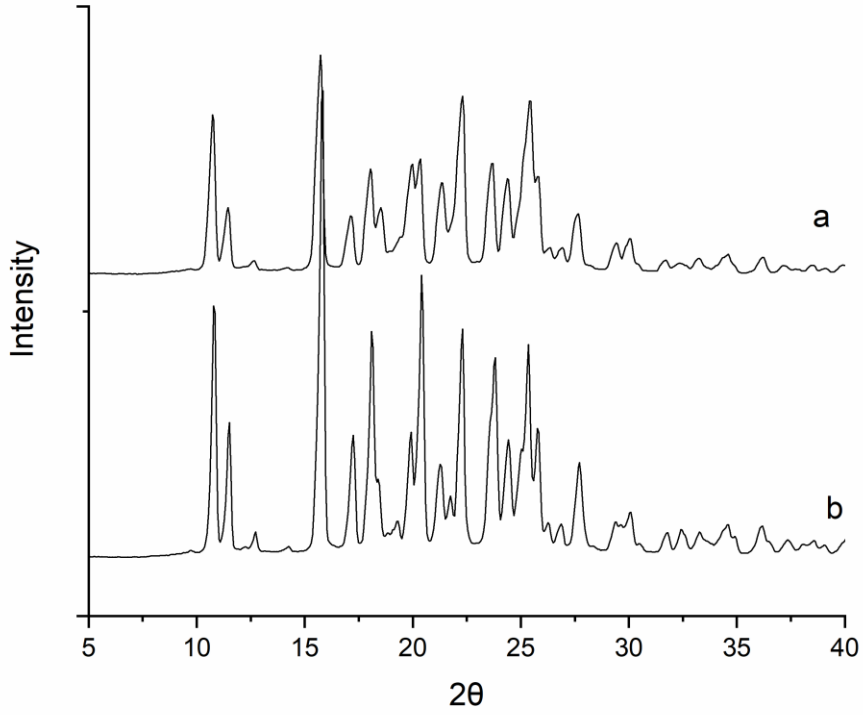

Source: Author (2024)

3.3.3. Differential scanning calorimetry (DSC) results

Thermograms of raw and micronized NAR are shown in Figure 14. Raw NAR shows an endothermic event at 254.98 °C (ΔH = 168.61 $J \cdot g^{-1}$). These values agree with the literature (MORAIS et al., 2020). Micro NAR exhibits an endothermic event at 252.97 °C (ΔH = 169.95 $J \cdot g^{-1}$). The thermograms of raw and micronized NAR samples are similar and both have similar melting points. These findings agree with literature data (MIAO et al., 2018).

Figure 14-DSC analysis of (a) micro NAR and (b) raw NAR.

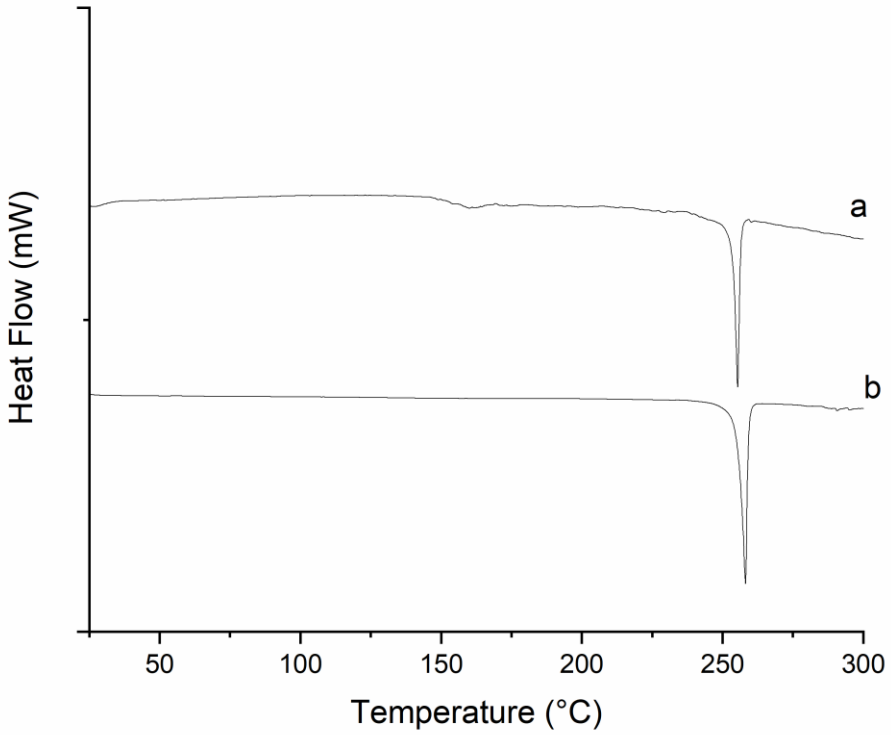

Source: Author (2024)

3.3.4. Fourier- transform infrared (FTIR) spectroscopy results

The raw and micronized NAR particles were evaluated by FTIR to verify possible changes in their structure caused by the processing in anti-solvent gas. The results are shown in Figure 15. Raw NAR shows characteristic stretches in 3294.41; 3118.89; 3037.88; 1639.46; 1604.77; 1496.76; 1460.11 cm^{-1}, which are in agreement with the literature (SEMALTY et al., 2010). The stretches 3282.84, 3118 cm^{-1} (-OH, hydroxyl group), 1641.42; 1498.10 cm^{-1} (-C=O carbonyl group), 1421.53; 1643 cm^{-1} (C=C), 1064-1159 cm^{-1} (C-O) (JI et al., 2016; KHAN et al., 2015; KUMAR et al., 2015; MAITY et al., 2017). The vibration bands of the absorption spectrum are not significantly different between the raw and micronized NAR, indicating that the chemical structure of NAR does not change after the micronization GAS procedure (LIU et al., 2017).

Figure 15-FTIR analysis of (a) micro NAR and (b) raw NAR.

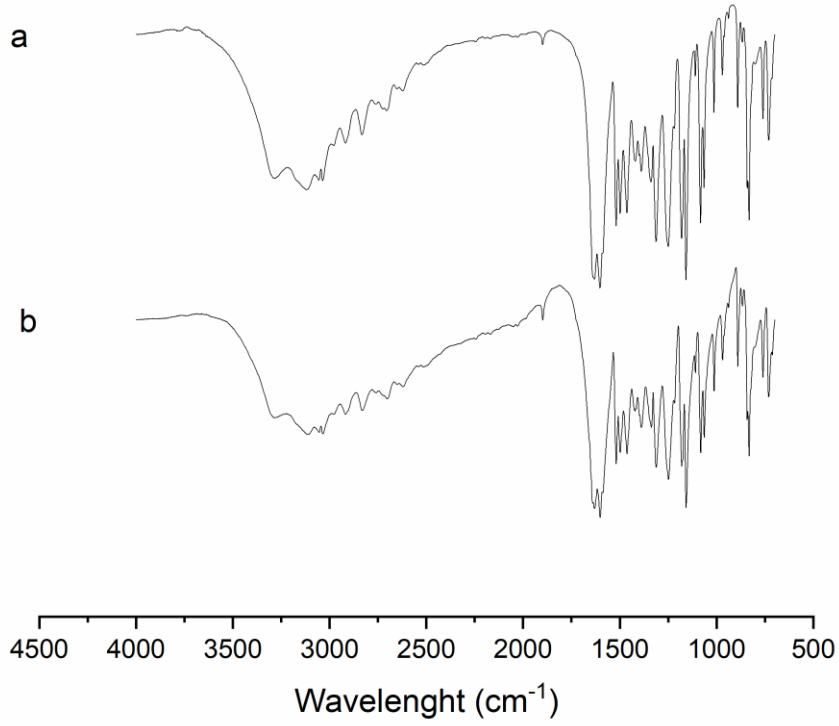

Source: Author (2024)

3.3.5. Dissolution rate analysis results

Figure 16 shows the dissolution profiles of raw and micro NAR in different media. In distilled water, approximately 180 min 100% of micro NAR is released. In contrast, raw NAR presented a slower dissolution rate, only approximately 67% was released at the end of the experiment (180 min).

All dissolution media studied here demonstrate that the dissolution rate of micro NAR was increased when compared to raw NAR. The dissolution profile of micro NAR in phosphate buffer solution (PBS, pH 6.8) was 50% in 40 min, and after 180 min, 76% of micro NAR was released. The raw NAR had a slower dissolution rate: after 40 min, 17% of raw NAR was released and after 180 min, 59% of raw NAR was released.

For micro NAR, in 0.1 M HCl solution, the results show that after 40 min, 46% of micro NAR was released and at the end of the experiment (180 min), 74% of NAR was released. On the other hand, after 180 min, only 13% of raw NAR was released.

The increase in dissolution rate for the microparticles occurs because due to the smaller particle size of material, the energy required to break the crystal lattice and proceed with the dissolution is lower (SODEIFIAN; SAJADIAN; DERAKHSHESHPOUR, 2022).

It was demonstrated that micronization results in a faster dissolution rate due to the increased surface area and reduced particle size of these drugs (CSICSÁK et al., 2023). Of course, micronization does not change the equilibrium solubility of a drug because solubility does not depend on particle size or other kinetic factors and accordingly, given enough time, even large particles will eventually dissolve (SAVJANI; GAJJAR; SAVJANI, 2012).

Figure 16-*In vitro* release profile of micronized naringenin (micro NAR) and raw naringenin (raw NAR) in different media.

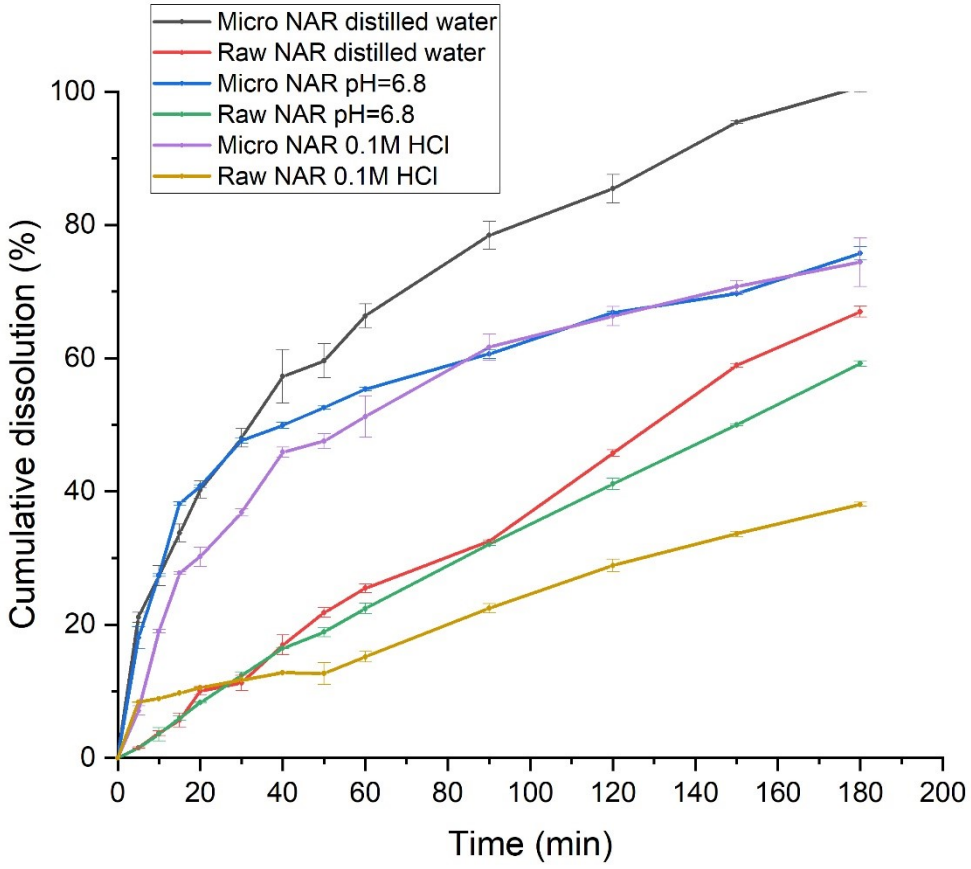

Source: Author (2024)

3.3.6. Specific surface area results

Micro NAR presented a specific surface area of 7.478 $m^2 \cdot g^{-1}$, while the specific surface area of raw NAR was 0.6954 $m^2 \cdot g^{-1}$. In other words, GAS-processed NAR increased the specific surface area by 11 times compared to raw NAR. The dissolution results are probably related to a reduction in particle size, resulting in an increase of the compound´s surface area, which consequently increased the dissolution velocity, as described by the Noyes–Whitney equation (CEREA et al., 2016; CHEN et al., 2018; NOYES; WHITNEY, 1897; RASENACK; MÜLLER, 2004).

3.3.7. Residual solvent results

Gas chromatography determined the residual amount of ethanol in micro NAR. For ethanol, the concentration (x) versus peak area (y) were established. The residual ethanol content is below the limit of quantification of 40 ppm, which was calculated based on the relationship based on the relationship ($y = 36277.825x-911639.1428$, $R^2 = 0.9907$, calibration curve with $n = 7$). The value is below the International Conference on Harmonization (ICH) requirements (EtOH < 5000 ppm), suitable for pharmaceutical use (INTERNATIONAL CONFERENCE ON HARMONISATION (ICH), 2021). Therefore, micro NAR obtained by the GAS technique would be suitable for pharmaceutical use with lower levels of organic solvent residues.

3.3.8. Molecular docking results

The molecular docking (Figure 17) demonstrated that NAR can fit into the cavity of dopaminergic D_2R and serotonergic 5-HT_{2A} receptors for the best docking pose. To determine the relevant intermolecular interactions between dopaminergic receptor and serotonergic and ligand (NAR) the corresponding Lig-Plot interaction diagrams analysis was performed (Figure 18).

Figure 17-Naringenin into the cavity of a) D_2R and b) 5-HT_{2A} receptors. The region of naringenin interaction with the residues in the cavity of the receptors is highlighted (yellow dashed lines represent hydrogen bond).

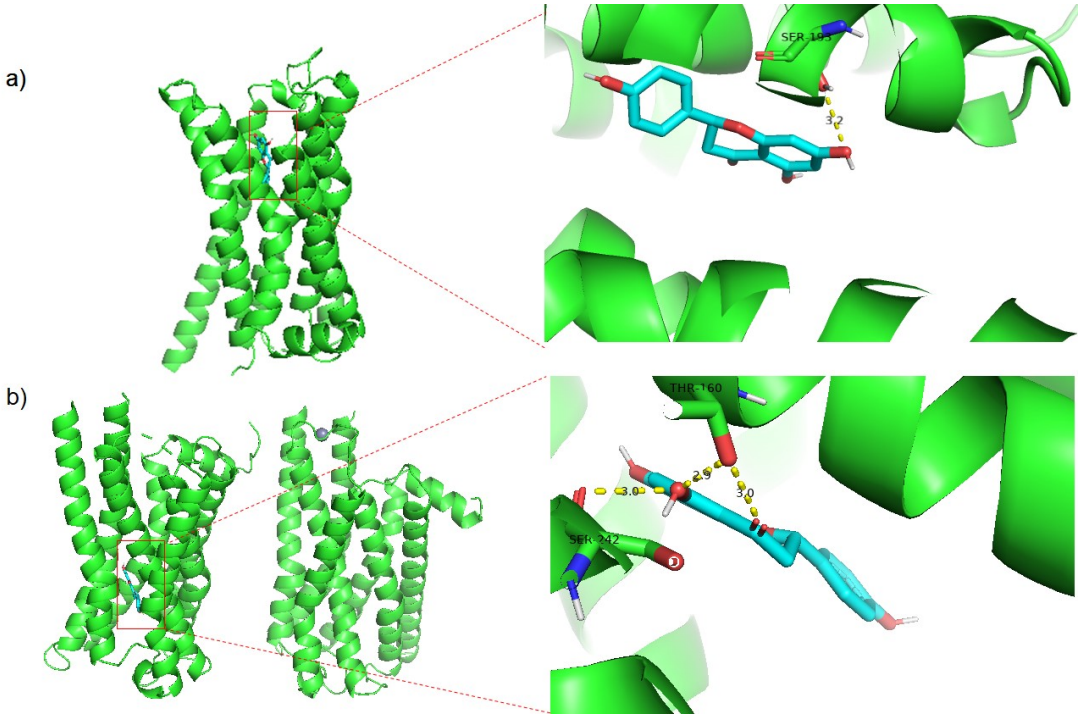

Source: Author (2024)

For complex dopaminergic receptors, D_2R and NAR were stabilized via the hydrogen-bonding interactions with binding residue Ser193 (3.24 Å) between the oxygen atoms from the residue and naringenin, respectively. In addition, was identified the presence of hydrophobic interaction involving the D_2R residues (Ala 122, Ser 197, Cys 118, Phe 382, Phe 198, Val 190, Phe 189, His 393, Asp 114, Phe 389, Tyr 416 and Trp 386) with NAR for the stabilization of the docking complex (D_2R -naringenin).

For serotonergic receptor 5-$HT_{2A,}$ NAR was stabilized via one hydrogen-bonding interaction with binding residue Ser242 (2.99 Å) between the oxygen atom from the residue and oxygen from the naringenin, and for two hydrogen-bonding interactions with binding residue Thr160 (3.01 and 2.7 Å) between the oxygen's atoms from the residue and oxygen from NAR, respectively. Also, there is a hydrophobic interaction involving the serotonergic receptor 5-HT_{2A} (Phe 339, Asp 155, Val 56 Phe 340, Phe 332, Phe 243, Ser 159, Trp 336 and Val 366) with NAR. The hydrogen bond interaction between ligands and residues within the hydrophobic binding pocket plays a significant role in stabilizing the docking complex.

Figure 18-Representation of the 2D-Lig-Plot diagram of interactions of critical residues. a) D_2R and b) 5-HT_{2A} receptors with naringenin for the best docking poses. Non-covalent interaction-like (hydrophobic and hydrogen-bond interaction) are represented.

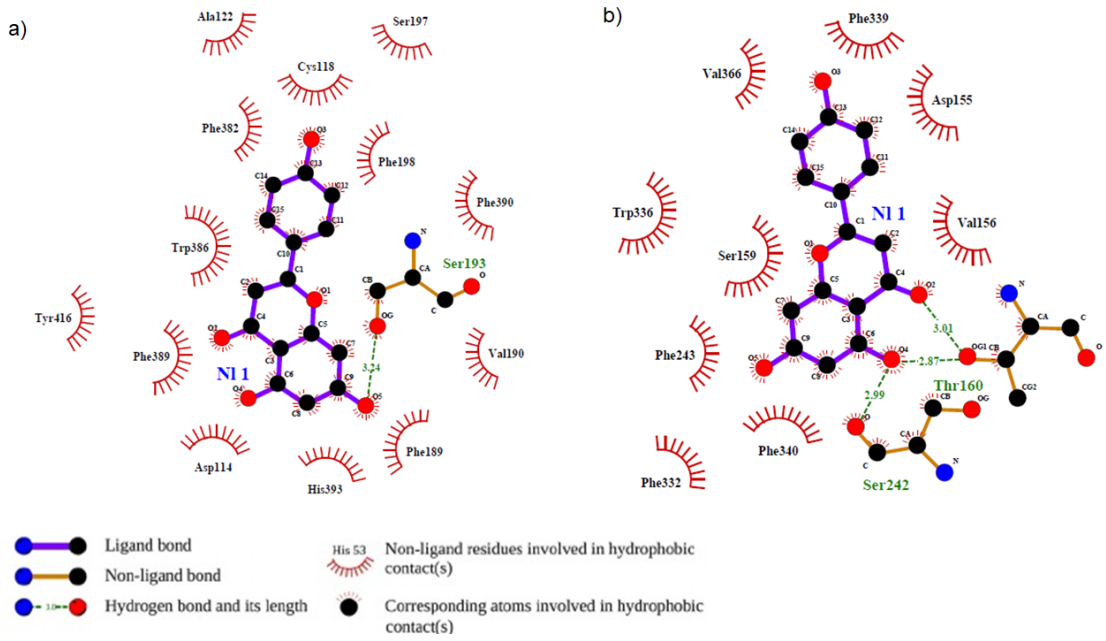

Source: Author (2024)

The free energy of binding (affinity) of docking NAR and D_2R complex was F.E.B = -9.3 Kcal/mol, and the estimated inhibition constant was Ki = 108.76 nM, while to the complex naringenin and 5-HT_{2A} the F.E.B = -9.1 Kcal/mol, Ki = 213.63 nM. The R.M.S.D < 2 Å for all systems studied, this value can be considered as a spontaneous thermodynamic process based on the obtained negative FEB value (TROTT et al., 2009). NAR shows expressive spontaneity to inhibit the receptors studied. The inhibition constant (Ki) of NAR is similar to quetiapine, an atypical antipsychotic, which acts as an antagonist of D_2R (Ki = 180 nM) and 5-HT_{2A} (Ki = 220 nM) receptors (ABLORDEPPEY et al., 2008). These findings are particularly interesting, since it represents a mechanism of action similar to antipsychotic drugs (BRUNTON et al., 2016).

The results of the Ramachandran plot confirm the crystallographic quality of the proteins, shown in the absence of the false positives docking interactions, because allowed torsion values for Ψ (Psi) vs. Φ(Phi) were verified. Additional information can be found in the supporting information (Appendix A).

3.3.9. In vivo assays results

3.3.9.1. Ketamine-induced hyperlocomotion in mice results

NMDA (N-methyl-D-aspartate receptors) antagonists, such as ketamine, have been used to induce behavioral alterations in animal models of schizophrenia, including hyperlocomotion, predictive of positive symptoms (JONES; WATSON; FONE, 2011). Stereotypic behaviors induced by ketamine are attributed to the blockade of NMDA receptors located on inhibitory GABAergic neurons in mesolimbic brain regions, which results in disinhibition and the consequent increase in neuronal excitation (COYLE, 2006; LEWIS et al., 1999). Atypical and typical antipsychotics are able to prevent the NMDA antagonist-induced hyperactivity, but the typical ones just prevent the hyperlocomotion at doses that hinder animals´ locomotion (GEYER; ELLENBROEK, 2003).

The findings of molecular docking are in accordance with the *in vivo* assays, which are displayed in Figure 19. One-way ANOVA revealed that the injection of ketamine induced a significant increase in the distance (m) traveled [$F(3,28) = 6.627$, $p = 0.0016$], speed ($m \cdot s^{-1}$) [$F(3,28) = 7.039$, $p = 0.0011$] and number of rearings [$F(3,28) = 9.901$, $p = 0.0001$] in the open field. These results are in accordance with previous studies that associate the hyperlocomotion induced by ketamine to the positive symptoms of schizophrenia (POWELL; GEYER, 2007) and indicate that the animal model employed by us was successfully accomplished. No effects of ketamine injection were detected on the number of groomings [$F(3,28) = 0.5611$, $p = 0.6452$] and fecal bolus expelled during the open field session [$F(3,28) = 1.294$, $p = 0.2960$]. Interestingly, raw NAR was not able to prevent the behavioral abnormalities induced by ketamine, but micro NAR, administered at the same dose of the raw NAR, was effective in preventing the increase in the distance traveled (m), speed ($m \cdot s^{-1}$), and a number of groomings induced by ketamine.

Gu et al. (GU et al., 2017) reported that some synthetic antipsychotic agents that contain an arylpiperazine (piperidine) group, characteristic of flavanones, antagonize the D_2R. Additionally, the authors investigated the preliminary antipsychotic effects of the compounds on neuroinflammation *in vitro*, and on hyperactive behavior in mouse models of schizophrenia (induced by MK -801 and by apomorphine) *in vivo*. The results show that the novel flavanone derivatives inhibit the overproduction of nitric oxide stimulated by lipopolysaccharide/interferon-γ in BV-2 microglial cells. Also, the intragastric administration of the newly synthesized compound reversed the MK-80-induced hyperlocomotion and decreased the apomorphine-induced climbing behavior. Similar results are shown by Ishola et

al. (ISHOLA et al., 2021) who used the flavonoid hesperidin to prevent and reverse ketamine-induced hyperlocomotion in rodents. Hesperidin prevented and reversed ketamine-induced schizophrenia-like behavior by inhibiting oxidative/nitrergic stress and acetylcholinesterase activity in mice brains (ISHOLA et al., 2021). In line with these observations, it has been shown that Morin, a naturally occurring flavonoid with antioxidant (SREEDHARAN; VENKATACHALAM; NAMASIVAYAM, 2009) and anti-inflammatory effects (FANG et al., 2003), presents antipsychotic-like properties devoid of extrapyramidal side effects, a pharmacological profile similar to atypical antipsychotics. These findings are consonant to ours (regarding micro NAR) and might point to the micronized flavanone NAR as a promising antipsychotic agent.

The results of molecular docking suggest that the mechanism of action of NAR is similar to the atypical antipsychotics, which act as antagonists of D_2R and 5-HT_{2A} (ABLORDEPPEY et al., 2008). The atypical antipsychotic drugs show higher affinity for 5-HT_{2A} than for D_2R receptors, and the blockade of these receptors is a pharmacodynamic mechanism that differentiates conventional from atypical antipsychotics. The blockade of 5-HT_{2A} receptors is responsible for the normalization of pyramidal cell activity, which leads to the therapeutic effect of atypical antipsychotics. Additionally, this mechanism may explain the reduced risk of extrapyramidal syndrome elicited by atypical antipsychotics when compared to the typical ones (HORACEK et al., 2006).

Our results show that the dose of micro NAR that prevented ketamine-induced hyperlocomotion did not impair the spontaneous locomotor activity of mice, since the animals treated only with raw NAR and micro NAR (*per se* groups) did not present differences in the parameters evaluated in the open field test when compared to the Vehicle-treated (Sham) group (Appendix B), which may indicate a pharmacological profile similar to atypical drugs. Nevertheless, this hypothesis deserves further investigation.

Herein was demonstrated for the first time the antipsychotic potential of micro NAR in the ketamine-induced hyperlocomotion assay in mice. It is known that raw NAR is poorly soluble in water (46 ± 6 $\mu g \cdot mL^{-1}$) and, consequently, presents poor oral bioavailability (5.81%) (KANAZE et al., 2006; KHAN et al., 2015). In this sense, our results point to an advance in the study of the biological properties of micro NAR, including the antipsychotic effect, since the particle size reduction and increased surface area of NAR particles after the micronization process, probably increased its bioavailability and allowed the successful application of micro NAR in biological assays.

Figure 19-Effects of micronized naringenin (micro NAR) on ketamine-induced hyperlocomotion in mice. The animals (n = 8 / group) were orally treated with Vehicle (saline solution + 1% polysorbate 80) (Sham and Ketamine groups), raw naringenin (raw NAR) or micronized naringenin (micro NAR) at 200 mg·kg^{-1}, 1 h before the injection of Saline solution (Sham group) or ketamine (10 mg·kg^{-1}, ketamine, raw NAR and micro NAR groups). Graphs display (A) the total distance traveled (m), (B) speed (m·s^{-1}), the number of (C) rearings, (D) groomings and (E) fecal bolus expelled during 20 min of observation in the open field arena. One-way ANOVA followed by Tukey's test. Data are presented as mean ± standard deviation. *p < 0.05; ** p < 0.01; *** p < 0.001 in comparison to the Sham group. #p < 0.05; ## p < 0.01 in comparison to the ketamine group.

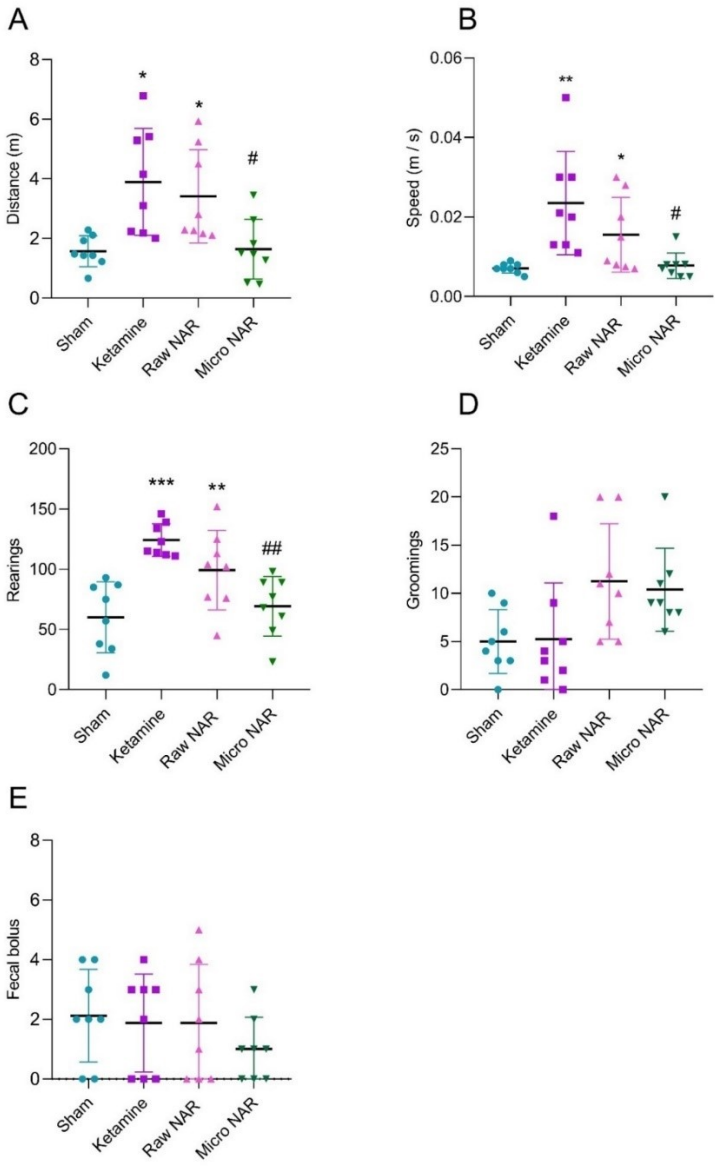

Source: Author (2024)

3.4. CONCLUSIONS

Naringenin microparticles were successfully obtained by the GAS technique. FTIR, DSC, XRD analysis indicate that no significant changes occur in the chemical structure of the naringenin crystal during processing. *In vitro* dissolution rate assays confirmed that micronized naringenin exhibited a significantly higher dissolution rate compared to raw naringenin in all media studied (distilled water; 0.1 M HCl solution and phosphate buffer solution - PBS, pH 6.8). The better dissolution rate is due to the reduction of particle size (approximately 2.6 times) and increased surface area (11 times) of micronized naringenin compared to unprocessed (raw) naringenin. Our *in vivo* data suggest the antipsychotic potential of micronized naringenin, which is related to its increased dissolution rate and, probably, increased bioavailability. The micronization of naringenin by the GAS technique is a promising approach for the biomedical application of this compound.

4.MICRONIZATION OF NARINGIN

The results of this section were published in the paper "Naringin processing using GAS antisolvent technique and *in vivo* applications" in the "Journal of Supercritical Fluids".

ABSTRACT

Naringin is a flavanone glycoside with various pharmacological activities, including neuroprotective and antipsychotic-like effects. However, it has poor solubility in water and oral bioavailability. This study aims to investigate the influence of gas antisolvent operational parameters (pressure, temperature, antisolvent flow rate, and initial concentration of solute) on particle diameter using a 2^4 Central Composite Design. Naringin particles produced were analyzed for dissolution rate and then applied to ketamine-induced hyperlocomotion in mice. Results for run with C= 5 $mg \cdot mL^{-1}$, P= 12 MPa, T= 308 K, CO_2 flow rate= 15 $mL.min^{-1}$ showed amorphous particles while run with C= 10 $mg.mL^{-1}$, P= 8 MPa, T= 318 K, CO_2 flow rate= 15 $mL.min^{-1}$ kept the crystalline structure of naringin. *In vivo* assays showed promising results for run with crystalline particles, probably due to the increased bioavailability, and amorphous particles had similar effects to commercial naringin because of the recrystallization when in contact with the aqueous medium.

Keywords: Naringin; GAS technique; schizophrenia; bioactive compound.

4.1. INTRODUCTION

Naringin is a natural flavanone glycoside that is found in Chinese herbal medicines and citrus fruits (YUSOF; GHAZALI; KING, 1990). Naringin modulates signaling pathways and interacts with molecules and thus has a wide range of pharmacological activities such as antioxidant (RAJADURAI; STANELY MAINZEN PRINCE, 2006), anti-inflammatory (INÊS AMARO et al., 2009), antihyperlipidemic (ROTIMI et al., 2018), anticancer (RAMESH; ALSHATWI, 2013), antidepressant, anti-apoptotic, neuroprotective, antidiabetic (ALAM et al., 2014) metabolic syndrome, oxidative stress, genetic damage, and central nervous system (CNS) diseases (CHEN et al., 2016). In addition, some studies show the therapeutic effects of naringin and/or clozapine/naringin combination on ketamine-induced psychotic-like symptoms (GEORGE et al., 2020) and reduces the main adverse effects of clozapine in rats (GEORGE et al., 2021).

Schizophrenia is a psychiatric disorder that affects 24 million people worldwide ("WHO, Schizophrenia.", 2022). Typical antipsychotics available in the market are frequently effective in treating positive symptoms in detriment of negative symptoms. Furthermore, extrapyramidal symptoms are related to typical antipsychotic therapeutic doses (STAHL, 2014; VINET; ZHEDANOV, 2011). However, many patients with positive symptoms are resistant to the drugs already on the market (CONLEY; BUCHANAN, 1997). Hence, there is an urgent need for the development of mechanistically innovative molecules with pharmacological action that act on different biological targets and could be effective against the multiple symptom dimensions of schizophrenia. Additionally, more potent, safe, and better-tolerated antipsychotic drugs are necessary.

In this context, there is growing interest in using natural products as therapeutic agents. Evidence has shown that citrus polyphenols can prevent and reverse neurodegeneration by protecting neural cells from radical-induced oxidative damage and neuroinflammation, which are known to play a crucial role in mental disorders (MUSCATELLO; ZOCCALI; BRUNO, 2018). Moreover, their neuroprotective effect extends to the interaction with intracellular targets involved in prosurvival signaling pathways and the induction of proteins that promote cognition (MUSCATELLO; ZOCCALI; BRUNO, 2018). In line with these observations, some studies using naringin, or similar polyphenols show that these compounds present significant antipsychotic-like action (BISHNOI; CHOPRA; KULKARNI, 2007; BRUNO et al., 2017;

CHTOUROU et al., 2016; MUSCATELLO; ZOCCALI; BRUNO, 2018; OKUYAMA et al., 2013).

Despite its promising biological properties, naringin has low solubility in water (0.6502 $mg \cdot mL^{-1}$), low oral bioavailability, and an undesirable bitter taste (LEE et al., 1999). It has been reported that modification of the bioactive compounds in terms of particle size and morphology can improve properties like bioavailability and dissolution rate (KUMAR et al., 2022). The relations of Noyes-Whitney and Ostwald-Freundlich confirm that solid solubility is directly proportional to its surface area and increases by decreasing the size of solid particles (AMANI; SAADATI ARDESTANI; MAJD, 2021).

The widespread use of techniques that employ supercritical fluids and supercritical carbon dioxide ($scCO_2$) has attracted considerable attention over the last years. $scCO_2$ can be used as a solvent or antisolvent due to its well-known properties: low viscosity, non-toxicity, mild critical conditions, easy accessibility, relatively low price, environmentally-friendly and the possibility to eliminate or reduce the use of organic solvents (KNEZ et al., 2019; LOZOWSKI, 2010; PANDO; CABAÑAS; CUADRA, 2016). The gas antisolvent (GAS) technique is efficient for micronization of low soluble pharmaceuticals or bioactive compounds using $scCO_2$ (AMANI; SAADATI ARDESTANI; MAJD, 2021; ESFANDIARI; SAJADIAN, 2022; MACEACHERN; KERMANSHAHI-POUR; MIRMEHRABI, 2020; SANTOS et al., 2022). In the GAS precipitation, $scCO_2$ acts as an antisolvent for the solute. In the GAS process, high pressure CO_2 is injected into the liquid phase solution, leading to large volume expansion of the liquid solvent, and significantly reduced solute solubility in the expanded liquid phase. In the supersaturation state, nucleation is initiated, and precipitation of the dissolved compound occurs. After obtaining fine particles with a narrow size distribution, the residual solvent is removed by further flow of $scCO_2$, and a dry precipitate is obtained after depressurization (AMANI; SAADATI ARDESTANI; MAJD, 2021; DODDS; WOOD; CHARPENTIER, 2007). The variation of the operational parameters, e.g., pressure, temperature, initial solute concentration, or antisolvent flow rate, can change the particle size, size distribution, and morphology of precipitated particles in the GAS process (AMANI; SAADATI ARDESTANI; MAJD, 2021; DODDS; WOOD; CHARPENTIER, 2007).

Micronization of naringin was already reported in the literature by Adami et al. (2022), who carried out the processing of naringin by supercritical antisolvent technique to obtain very highly breathable microparticles. As a result, particles with a permeability of 3.6 fold than raw naringin, due to a reduction in particle size and amorphization. The particles produced are

suitable for anti-inflammatory formulations supporting several types of disease treatments, including the COVID-19 syndrome (ADAMI et al., 2022). Li et al. (2017) produced amorphous nanoparticles of naringin through a supercritical anti-solvent process using excipient particles of microcrystalline cellulose fluidized under pressure to provide higher release rates (LI et al., 2017).

In this context, this work aims to investigate the influence of gas antisolvent operational parameters (pressure, temperature, antisolvent flow rate and initial concentration of solute) on the particle diameter, using a 2^4 Central Composite Design with 3 central points. The naringin particles produced were characterized and tested *in vitro dissolution rate*, molecular docking and *in vivo tests* (using ketamine-induced hyperlocomotion test in mice).

4.2. MATERIALS AND METHODS

4.2.1. Materials

Naringin dihydrate Sigma-Aldrich (Steinheim, Germany), ≥ 95% ($C_{27}H_{32}O_{14,}$ molecular weight 580.5 $g.gmol^{-1}$) was used to perform the precipitation. Acetone (99.5%, Êxodo Científico, Sumaré, São Paulo, Brazil), CO_2 (99.9% in liquid phase, White Martins S.A. São Paulo, Brazil). Ketamine-D4 hydrochloride, 100 $\mu g \cdot mL^{-1}$ (Sigma-Aldrich, Darmstadt, Germany), sodium thiopental (Sigma-Aldrich, St Louis, USA), lidocaine (Sigma Aldrich, Steinheim, Germany), polysorbate 80 Merck (Darmstadt, Germany) was used in the *in vivo* assays.

4.2.2. GAS (gas antisolvent) technique

The GAS methodology used to produce naringin particles was based on the research described by Pessoa et al. (2019) and Sakata et al. (2021). Firstly, a solution containing naringin and acetone was prepared at the desired concentration (5, 7.5, and 10 $mg \cdot mL^{-1}$) and then placed in the ultrasonic bath to form a homogeneous solution. Afterwards, the solution (35 mL) was injected using a syringe coupled to a filter of PTFE (polytetrafluoroethylene) 0.45 μm (Filtrilo, Paraná, Brazil), in the precipitation chamber with a capacity of 600 mL. After that, CO_2 was injected into the precipitation chamber through a set of syringe pumps (Teledyne Isco, model 500D, Lincoln, USA) at the pre-established flow rate (5, 10, and 15 $mL.min^{-1}$) until reaching the planned operating pressure (8, 10, and 12 MPa), under a constant desired temperature (308,

313, or 318 K) using a thermostatic bath (Nova Etica, Model 521/2D, Vargem Grande do Sul, Brazil). When the pressure was reached, the antisolvent flow was stopped, and the chamber was kept under agitation using a magnetic stirring at 300 rpm for 10 min. In the washing stage, approximately 600 mL of CO_2 is passed, with the same condition established in the experimental planning pressure (8, 10 or 12 MPa), temperature (308, 313, or 318 K) and CO_2 flow (5.10 or 15 $mg \cdot mL^{-1}$), during which the drying of the particles takes place. Finally, the chamber was depressurized, and the depressurization rate was controlled using a micrometric valve (HOKE, model 1315G2Y, Spartanburg SC, US) depressurization is carried out approximately every 5 $bar \cdot min^{-1}$. After, solid naringin particles were collected, characterized, and directed to *in vitro* and *in vivo* tests.

4.2.3. Statistical analysis

This work, evaluated the influence of pressure, temperature, antisolvent flow rate, and initial concentration of the solution by a 2^4 design central composite (DCC) with three central points, as presented in Table 1, comprising 19 experimental conditions. The process variable ranges were based on previous works (AGUIAR *et al.*, 2016, 2017; AMANI, SAADATI ARDESTANI e MAJD, 2021; DIAS *et al.*, 2022; SANTOS *et al.*, 2022). To evaluate the response variable particle size, data were submitted to analysis using Statistica 13.5 software (TIBCO Software Inc., Palo Alto, CA, USA) using the Pareto graph. The differences were considered significant for $p < 0.05$.

Table 1-Real and coded values of variables studied in the GAS antisolvent processing of naringin.

Variables	Coded Level		
	(-1) Low	(0) Medium	(+1) High
Concentration ($mg \cdot mL^{1}$)	5	7.5	10
Pressure (MPa)	8	10	12
Temperature (K)	308	313	318
CO_2 flow rate ($mL \cdot min^{-1}$)	5	10	15

Source: Author (2024)

4.2.4. Morphology and particle size determination

The morphology of commercial and processed naringin by GAS was performed by Scanning Electron Microscopy (SEM, Hitachi TM3030, Japan) at the accelerating voltage of 15 kV. Powders were dispersed on metal stubs with double-sided carbon adhesive tape and coated with gold under vacuum (EM SCD 500, Leica, Germany). The obtained SEM images were analyzed by ImageJ software to determine the morphology and measure the average length of the diagonal line of approximately 200-300 particles (SAKATA et al., 2021; SCAPINELLO et al., 2018; SCHNEIDER; RASBAND; ELICEIRI, 2012).

4.2.5. Power-X-ray diffraction (XRD)

Crystallographic analysis of the particles was performed using a MiniFlex600 X-Ray Diffractometer (Rigaku, Tokyo, Japan) (3 ~ 140º– 0.01 ~ 100º/min). Measurements were taken utilizing a copper X-ray source powered at 40 kV and 15 mA (Kα1 1.54059 Å) in θ-2θ scan mode. Scans were measured between 5° and 35° with a step size of 0.02° and with a scan rate of 6° min^{-1} (AMANI; SAADATI ARDESTANI; MAJD, 2021).

4.2.6. Differential scanning calorimetry (DSC)

Thermograms were accomplished in Jade-DSC (Perkin Elmer, Shelton, USA) equipment using hermetically sealed aluminum crucibles. For the dehydration cycle measurements, the sample was heated up to 130° C with a heating rate of 20 °C·min^{-1} and temperature was maintained at 130° C for 15 min to remove the residual solvent. Afterwards, samples were cooled at 25 °C and heated up to 350 °C with a heating rate of 10 °C·min^{-1} (SANSONE et al., 2009).

4.2.7. Fourier-transform infrared (FTIR) spectroscopy

Commercial and processed naringin were analyzed in Agilent Technologies (Cary 600 Series FTIR Spectrometer, Santa Clara, CA, USA) equipped with attenuated total reflectance (ATR) accessory with ZnSe crystal, with the resolution of 2 cm^{-1} and absorption spectra in the infrared region were obtained in the range of 4000 cm^{-1} to 500 cm^{-1} (PESSOA et al., 2019).

4.2.8. Dissolution rate

To determine the dissolution rate of commercial and processed naringin by GAS technique, the methodology from Cheng et al. (CHENG et al., 2016) was adapted. The dissolution experiments were carried out under non-sink conditions to evaluate the maximum solution concentration generated from an amorphous solid (SUN; WEN; TAYLOR, 2016). The amount of solid added was in excess of the amount required to achieve the equilibrium solubility of naringin. Samples of 100 mg were added to 50 mL of distilled water and maintained under constant stirring (100 rpm) at 37 ± 0.5 °C in a Dubnoff-type shaker (Marconi, Piracicaba, Sao Paulo, Brazil). At selected periods of 5, 10, 15, 20, 30, 40, 50, 60, 90, 120, and 180 min, samples of 2 mL were withdrawn, with flasks immediately replenished with distilled water at the same temperature to keep constant volume. Then, samples were filtered through a syringe attached to a membrane PTFE filter 0.45 μm, and concentrations were measured employing the UV–vis Spectrophotometer (Model T90+, PG Instruments, Leicestershire, United Kingdom) at 282 nm. Experiments were accomplished in duplicate, and results were expressed as naringin concentration over time. After dissolution rate assays, the residual solids were subjected to XRD analysis to check the phase changes.

4.2.9.Ultra-performance liquid chromatography coupled with mass spectrometry UPLC-MS

The UPLC-MS analysis was performed in an Acquity UPLC equipped with a single-quadrupole mass spectrometer ZQ-2000 (Waters, Manchester, UK). Chromatographic separation was carried out using a BHE C18 column (50 mm × 2.1 mm i.d. 1.8 μm) from Waters (Waters, Milford, USA), and the injection volume was 10μL for analysis. The mobile phase consisted of water with 0.1% formic acid (solvent A) and acetonitrile with 0.1% formic acid (Solvent B). An 8 min gradient elution at 0.3 $mL.min^{-1}$ was performed as follows: from 100% solvent A to 80% solvent A over 4 min, from 80% A to 20% A over 2 min, and from 20% A to 0% A over 2 min. Mass spectrometric detection was performed using an electrospray interface (ESI) operated in positive ionization mode for the naringin analyte. Nitrogen was used as a desolvation gas at a 600 $L.h^{-1}$ flow rate with the desolvation temperature set at 300 °C and the source temperature set at 120 °C. The capillary voltage was set at 3.5 kV, and the cone voltage was set at 20V.

4.2.10. Specific surface area

The surface area of commercial and GAS-processed naringin were measured using Brunauer–Emmett–Teller (BET) method based on N_2 adsorption-desorption using Autosorb-1 equipment from Anton Paar Quantachrome Instruments (Boynton Beach, FL, USA) (JOHNSON et al., 2020). The samples were outgassed for 18 h at 140 °C under N_2 flow before determining the specific surface area.

4.2.11. Molecular Docking

Molecular docking was performed using AMDock version 1.5.2 (VALDÉS-TRESANCO et al., 2020) and Autodock Vina 1.2.1 (TROTT et al., 2009) softwares. The receptors selected were 5-HT_{2A} (serotonin receptor) and D_2R (dopamine receptor) because the second-generation antipsychotics target these receptors (KIMURA et al., 2019; WANG et al., 2018b). The crystal structure of D_2R (PDB ID:6CM4) and 5-HT_{2A} (PDB ID:6A93) (KIMURA et al., 2019; WANG et al., 2018b) was obtained from Protein Data Bank (https://www.rcsb.org/).

After the crystal structure was refined, all solvent molecules and cocrystallized ligands were removed. The 3D structure of the compound naringin (CID: 442428) was obtained by PubChem (https://pubchem.ncbi.nlm. nih.gov/) and optimized using Avogadro software (HANWELL et al., 2012; RAPPÉ et al., 1992). The grid box size was set to 25, 25, and 25Å (x, y, and z), and grid box-center cartesian coordinates for D_2R were 8.60, 4.40, and -10.90 Å (x, y, and z), and for 5-HT_{2A} were 14.70, 4.80 and 15.90 Å (x, y, and z), which were performed using the ezCADD tool (TAO et al., 2019). After the simulations were completed, the docked structures were analyzed, and the interactions were visualized using the programs PyMOL, and Lig-Plot$^+$ [61].

4.2.12. *In vivo* assays

4.2.12.1. Animals

Experimental *in vivo* procedures were approved by the Animal Care Local Ethical Committee (CEUA-UNOCHAPECÓ; protocol #003/2021), performed according to Brazilian

law (CONCEA, 2018; PRESIDÊNCIA DA REPÚBLICA, CASA CIVIL, 2008), EU Directive 2010/63/EU for animal experimentation (EUROPEAN PARLIAMENT AND COUNCIL, 2010), and approved by the Animal Care Local Ethical Committee (CEUA-UNOCHAPECÓ; protocol 003/2021, Annex I). Male Swiss mice (*Mus musculus*) weighing 25-40 g were bred at the Animal Facility of Unochapecó (Chapecó, Santa Catarina, Brazil). The animals were housed in polypropylene cages (17 x 33.5 x 40.5 cm) with a maximum of 6 animals per cage. Mice were maintained in an appropriate room with minimal noise, controlled temperature (22 ± 1 °C) and humidity (40-60%) and at 12 h light-dark cycle (lights on at 6 am). Mice had free access to standard laboratory chow (NUVITAL-Nuvilab®, Colombo, Paraná, Brazil) and water *ad libitum*.

4.2.12.2. Treatments

Mice were orally (p.o.) and intraperitoneally (i.p.) treated with volumes of 10 $mL \cdot kg^{-1}$, according to their weight. Before oral administration, commercial naringin was dissolved in saline solution + 1% polysorbate 80 (vehicle), except runs 11 and 14 of naringin, were dissolved in saline solution only. Ketamine was dissolved in saline before the intraperitoneal (i.p.) injection. The doses of commercial naringin and run 11 and 14 of naringin (50 and 200 $mg \cdot kg^{-1}$, p.o.) were selected based on previous reports (CHUNG et al., 2019; CONLEY; BUCHANAN, 1997; DI CARLO et al., 1993; GANAPATHY et al., 2008; LV et al., 2013; SUGUMAR; SEVANAN; SEKAR, 2019). Ketamine was administered at 10 $mg \cdot kg^{-1}$ (i.p.) (BETTI et al., 2017). The animals were weighed 24 h before the behavioral assays. The sample size was calculated using the online calculator from the University of São Paulo (FOB - USP), available at http://estatistica.bauru.usp.br/calculoamostral/index.php (alpha value = 0.05, test power = 0.8). Mice were fasted 1 h before the oral administration (food, but not water, was withheld). Solutions were freshly prepared (on the day of the experiment). The tests were conducted in 4 rounds, using different sets of animals. Outcome assessors were blinded to treatment conditions. The animals were assigned to the experimental groups following block randomization procedures to counterbalance the cage as well as litter.

4.2.12.3. Ketamine-induced hyperlocomotion

Ketamine is a NMDA (N-methyl-D-aspartate receptors) antagonist that has been widely used to induce alterations related to schizophrenia-like behavior in rodents, including hyperlocomotion, predictive of positive symptoms (POWELL; GEYER, 2007). The antagonism of NMDA receptors located on inhibitory GABAergic neurons in mesolimbic brain regions, elicits neuronal excitation due to the disinhibition (POWELL; GEYER, 2007; RAZOUX; GARCIA; LÉNA, 2007). These effects result in stereotypic behaviors and hyperlocomotion induced by ketamine, which mimics the positive symptoms of schizophrenia (COYLE, 2006; LEWIS et al., 1999). Antipsychotics (atypical and typical) prevent the NMDA antagonist-induced hyperlocomotion, but the typical ones just prevent the hyperlocomotion at doses that impair the locomotion of animals (RAZOUX; GARCIA; LÉNA, 2007). The effects of commercial naringin, as well as run 11 and 14 of naringin on ketamine-induced hyperlocomotion, were tested in an animal model predictive of positive symptoms of schizophrenia (COYLE et al., 2012; JAVITT, 2012) according to Betti et al. (BETTI et al., 2017), with minor modifications adapted by our research group (DE OLIVEIRA et al., 2023). For this purpose, the animals (n = 8 / group) were orally treated with vehicle (saline solution at 10 mL.kg^{-1}, Sham and Ketamine groups), commercial naringin (50 and 200 mg·kg^{-1}) or naringin run 11 and 14 (50 and 200 mg·kg^{-1}) and allowed to spontaneously explore the open field arena for 30 min (waterproofed MDF box; 40 × 30 × 30 cm). Afterwards, ketamine (10 mg·kg^{-1}) (Ketamine, commercial naringin, run 11 and 14 of naringin groups) or saline (Sham group) were administered (i.p.) to the animals.

Thirty minutes after the ketamine administration (i.p.), animals were gently placed in the open field arena, and the locomotor activity [total distance traveled (m), number of rearings, groomings, and fecal bolus expelled during the session] was evaluated for 20 minutes. The sessions were video recorded, and the parameters were analyzed using the software ANY-Maze (Stoelting Co., Wood Dale, IL, USA). To verify the effects of commercial naringin or run 14 of naringin on the basal locomotor activity of mice, independent groups of animals were orally treated only with vehicle (10 mg·kg^{-1}), commercial naringin or run 14 (50 and 200 mg·kg^{-1}) and observed in the open field arena following the same procedure described above. The apparatus was cleaned with 10% ethanol between the sessions. At the end of the experiments, the animals were immediately euthanized with sodium thiopental 120 mg·kg^{-1} (i.p.) preceded by lidocaine injection (10 mg·kg^{-1}, s.c.) (CONCEA, 2018).

4.2.12.4. Statistical analysis

Data from the *in vivo* assays were analyzed by One-way analysis of variance (ANOVA) followed by Tukey's test. Normality of the data was assessed by Bartlett's test. No outliers (mean ± 2 standard deviations) were found in the results. $p < 0.05$ was considered significant.

4.3. RESULTS AND DISCUSSION

4.3.1.Effect of operating conditions on particle diameter from naringin GAS-processing

Results from the 2^4 CCD design are shown in Table 2, evaluating the effects of processing variables on the particle diameter. As can be seen from the Pareto chart depicted in Figure 20, within 95% confidence level.

Table 2-Results of 2^4 CCD experimental design for naringin by GAS antisolvent technique.

Run	Concentration ($mg \cdot mL^{-1}$)	Pressure (MPa)	Temperature (K)	CO_2 flow rate ($mL \cdot min^{-1}$)	Dp± SD (μm)
1	5	8	308	5.0	0.914 ±1.636
2	10	8	308	5.0	1.622±1.312
3	5	12	308	5.0	1.018±1.018
4	10	12	308	5.0	1.444±1.323
5	5	8	318	5.0	1.251±1.167
6	10	8	318	5.0	2.280±1.301
7	5	12	318	5.0	1.298±1.560
8	10	12	318	5.0	2.573±2.165
9	5	8	308	15.0	1.662±2.585
10	10	8	308	15.0	1.513±1.849
11	5	12	308	15.0	0.835± 1.252
12	10	12	308	15.0	1.443± 1.309
13	5	8	318	15.0	5.596±1.995
14	10	8	318	15.0	8.997±2.771
15	5	12	318	15.0	1.008±1.278
16	10	12	318	15.0	1.878±1.338
17	7.5	10	313	10.0	1.159±1.324
18	7.5	10	313	10.0	1.266±1.325
19	7.5	10	313	10.0	1.571±1.461

Legend: Dp= Particle diameter and SD=Standard deviation
Source: Author (2024)

Next, the effects of the process parameters temperature, pressure, CO_2 flow, and concentration and how they affect particle size will be described:

I)Temperature effect- temperature (308, 313, and 318K) had a positive effect on particle diameter, so an increase in this parameter led to an undesirable increase in particle diameter. This effect was observed in literature; the effect of temperature on particle size may be described by nucleation and growth mechanisms (THANH; MACLEAN; MAHIDDINE,

2014). Reduction of solute solubility due to $scCO_2$ dissolution in the solvent is the basis of solid precipitation in GAS process. While a raise in temperature increases the solubility of solute molecules in the solvent, there is, on the other hand, a decrease in CO_2 solubility, which makes particle precipitation from the solution more difficult. Achieving sufficient volume expansion to reach supersaturation at high temperatures takes a long time. Thus, the nucleation rate and the number of nuclei formed reduce at high temperatures, and growth becomes the predominant mechanism. Consequently, crystal agglomerates and larger particles are obtained at higher temperatures (Aguiar *et al.*, 2016; Amani, Saadati Ardestani e Majd, 2021; Zhang, J. *et al.*, 2019). The same effect was observed in the work of Amani, Ardestani et al.(AMANI; SAADATI ARDESTANI; MAJD, 2021) and Kim et al (KIM et al., 2011) by GAS.

II) Pressure by CO_2 flow rate effect- the pressure-CO_2 flow rate interaction effect negatively influenced on particle diameter; in other words, it caused a reduction in particle diameter. In literature, it is observed that increasing the CO_2 flow rate, CO_2 mole fraction, and operational pressure decreases aggregates formation, reducing the particle size (ADAMI et al., 2022). Also, a higher amount of $scCO_2$, and consequently a higher CO_2 fraction, increases the supersaturation. At high supersaturations, typical for antisolvent precipitation, primary nucleation is the most crucial mechanism affecting the particle size. In addition, The nucleation in the GAS process is faster, and it is impossible to achieve high saturation levels (BRISTOW et al., 2001).

III) Pressure effect- increasing the operational pressure (8, 10, and 12 MPa) had a negative effect, i.e., a pressure increase led to a reduction in particle diameter. This phenomenon is also observed in literature with increasing pressure, the particle length becomes short, and its thickness thinner. Also, higher pressure values favor nucleation, which creates many nuclei; thus, smaller size crystals are observed (CHEN et al., 2005). The same effect was observed by Rantakylä (RANTAKYLÄ et al., 2002); increasing pressure at constant temperature produces particles with reduced size.

IV) CO_2 flow rate effect-increasing CO_2 flow rate (5, 10, and 15 $ml.min^{-1}$) also promoted a positive effect; undesirably increased particle diameter. This phenomenon is also observed in literature higher CO_2 flow rate resulted in a higher capillary number, which exhibits the relationship between force and surface tension, thus leading to the breakage of smaller droplets when using the dilute solution, but results in larger particles when the concentrated solution was used (FUSARO; MAZZOTTI; MUHRER, 2004; KRÖBER; TEIPEL, 2002). In the present study, when the initial solute concentration is low, we get smaller particles when

the CO_2 flow rate is higher. Furthermore, the same effect can be observed; for example, from run 11, the CO_2 flow rate of 15 $mL.min^{-1}$ (highest value) and concentration of 5 $mg.mL^{-1}$ (lowest value) produced the smallest particle diameter of approximately 0.835 µm. This previously mentioned effect was also reported in the literature by Chen et al (2005) dealing with *Ginkgo ginkgolides* precipitation by gas antisolvent technique (CHEN et al., 2005).

V) Pressure by temperature effect- the pressure - temperature interaction effect showed a negative impact on particle diameter, such as reduction in particle size. Amani et al. (2021), observed that processing of capecitabine using a gas antisolvent process, increasing the pressure and decreasing temperature, reduces particle size (AMANI; SAADATI ARDESTANI; MAJD, 2021).

This phenomenon observed in the literature is explained by the fastest solubilization at higher densities and higher amount of particles formed during the expansion (MARTELLO et al., 2019). The interfacial tension between the organic solution and the supercritical antisolvent determines the size of the droplets. However, increased pressure at a constant temperature leads to increased CO_2 density and, correspondingly, to better dispersion of the solution in the antisolvent, which reduces the droplet size. Mass transfer is then improved by increasing the diffusion coefficient of supercritical CO_2, which results in better removal of the solvent from the solution and precipitation of the compound (Aguiar *et al.*, 2016; Chen *et al.*, 2007; Franceschi *et al.*, 2008).

VI) Temperature by CO2 flow effect- the temperature-CO_2 flow rate interaction showed a positive effect, increasing particle diameter. Kim et al. (KIM et al., 2011) also observed the effect of temperature and CO_2 addition rate, which can be explained because lower temperatures and higher CO_2 flow led to smaller particle size. This effect can be explained using nucleation and precipitation growth mechanisms. It has been observed that the pressure required to expand the solution sufficiently to precipitate the solutes is low at lower temperatures. This means that sufficient volume expansion to reach supersaturation was achieved in a short time at low temperatures. At a high degree of supersaturation, the nucleation rate was rapid, and the formation of small particles was favorable. In addition, at low temperatures, the solubility of CO_2 in the solvent increased due to the high density of CO_2. While the volume of the solution expanded, the solvent power was reduced easily with only a small change in pressure. This led to a higher nucleation rate and thus to forming small particle sizes (MOCHIZUKI et al., 2010).

VII) Concentration effect- the increase in concentration variable (5, 7.5, and 10 mg·mL^{-1}) also had a positive effect, increasing the particle diameter. This phenomenon is explained by the literature; at higher concentrations, the supersaturation profile tends to be closer to the saturation line, and nucleation begins in the lower volume expansions. In this way, the first nuclei formed have more time to grow. Therefore, the growth mechanism dominates nucleation, resulting in agglomeration and formation of larger particles with a wide particle size distribution. However, at lower concentrations, precipitation starts later, and nucleation becomes the predominant mechanism, leading to precipitation of fine crystals (AMANI; SAADATI ARDESTANI; MAJD, 2021). Amani, Ardestani et al. (AMANI; SAADATI ARDESTANI; MAJD, 2021); Dodds et al. (DODDS; WOOD; CHARPENTIER, 2007), and Bakhbakhi et al. (BAKHBAKHI; CHARPENTIER; ROHANI, 2006) observed the same effect; the precipitation occurs at lower volume expansion by increasing the initial solute concentration, leading to the produced larger particles. This feature can be observed in this work, for example, in run 14, for which the concentration of 10 mg·mL^{-1} provided the greatest particle diameter, as high as 8.996 µm.

VII) Concentration by temperature effect- the concentration- temperature interaction showed a positive effect on particle diameter, in other words, an increase in the particle diameter. This effect was observed in the literature that an increase in temperature changes the shape of the precipitated particles. The volume expansion decreases by decreasing the solubility and supersaturation, increasing the size of the produced particles. The precipitation will occur at lower volume expansion by increasing the initial solute concentration, resulting in longer periods of crystal growth, ultimately forming larger particles. For higher solute concentrations, the supersaturated profile will rapidly approach the saturation line, causing an increase of the initial nucleation, which may superimpose the secondary nucleation, resulting in large particle formation. Similar results on their subject were reported by Aguiar et al. (2016), Amani, Ardestani et al. (AMANI; SAADATI ARDESTANI; MAJD, 2021), more diluted solutions and lower temperatures and high pressures in the GAS process have precipitation of smaller particles. The interaction effects of concentration - pressure and concentration - antisolvent flow rate were not statistically.

Figure 20-Pareto chart showing the effect of temperature, pressure, concentration, flow CO_2 in gas antisolvent process in diameter of particle (Dp) of naringin. The bars crossing the reference line correspond to statistically significant eff effects ($p < 0.05$).

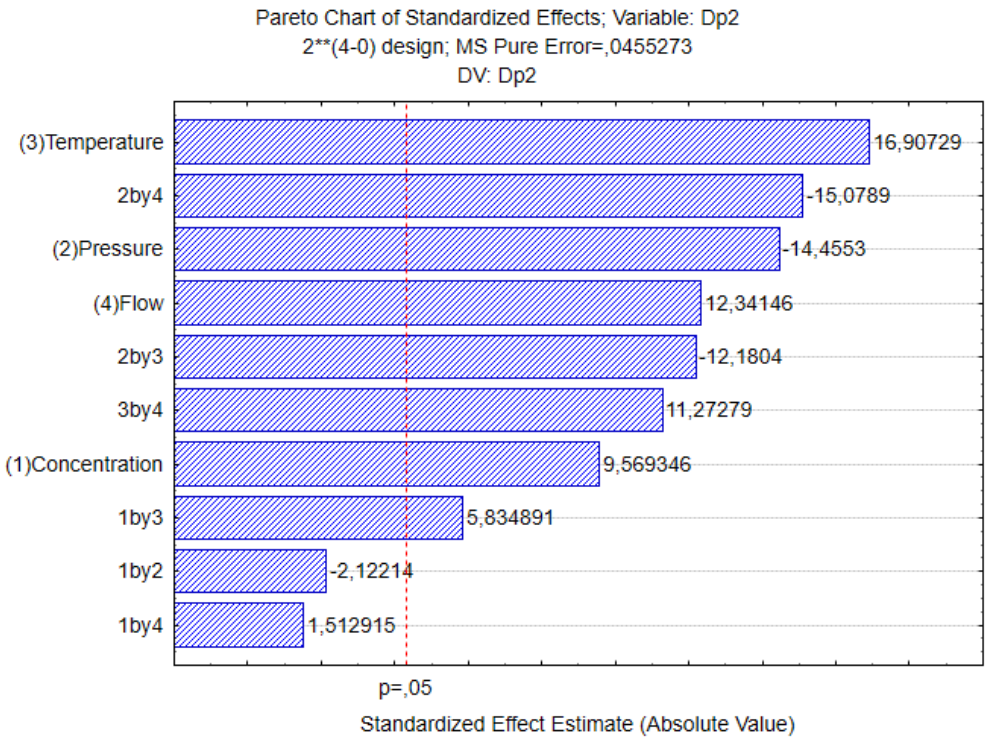

Source: Author (2024)

4.3.2. Morphology and determination of particle size results

Figure 21 presents the morphology of commercial and processed naringin by GAS technique. Two runs were selected from the experimental design to be investigated in more detail, runs 11 and 14, affording the smaller and the biggest particle diameters, respectively. Micrographs in such figure show the shape of raw and processed naringin for runs 11 and 14, and it can be seen that commercial naringin has a rectangular needle-like characteristic, while run 11 afforded a spherical morphology and run 14 led to a morphology similar to thin rectangular needles. Spherical morphology probably provides a higher dissolution rate compared to large and irregular particles. This fact may be explained in terms of the Prandtl boundary layer equation, in which the change in the average thickness of the hydrodynamic boundary layer leads to a change in the distance over which diffusion dominates, causing a difference in the diffusion rate (MOSHARRAF; NYSTRÖM, 1995). The mean diagonal size of the particles was 15.741 ± 1.565 µm for commercial naringin and 0.835 ± 1.252 and 8.997 ± 2.771 µm for processed naringin, runs 11 and 14, respectively.

Figure 21- Scanning Electron Microscopy (SEM) of naringin commercial, run 11 (C= 5 mg·mL^{-1}, P= 12 MPa, T= 308K, CO_2 flow rate= 15 mL.min^{-1}), and run 14 (C= 10 mg.mL^{-1}, P= 8 MPa, T= 318K, CO_2 flow rate= 15 mL.min^{-1}).

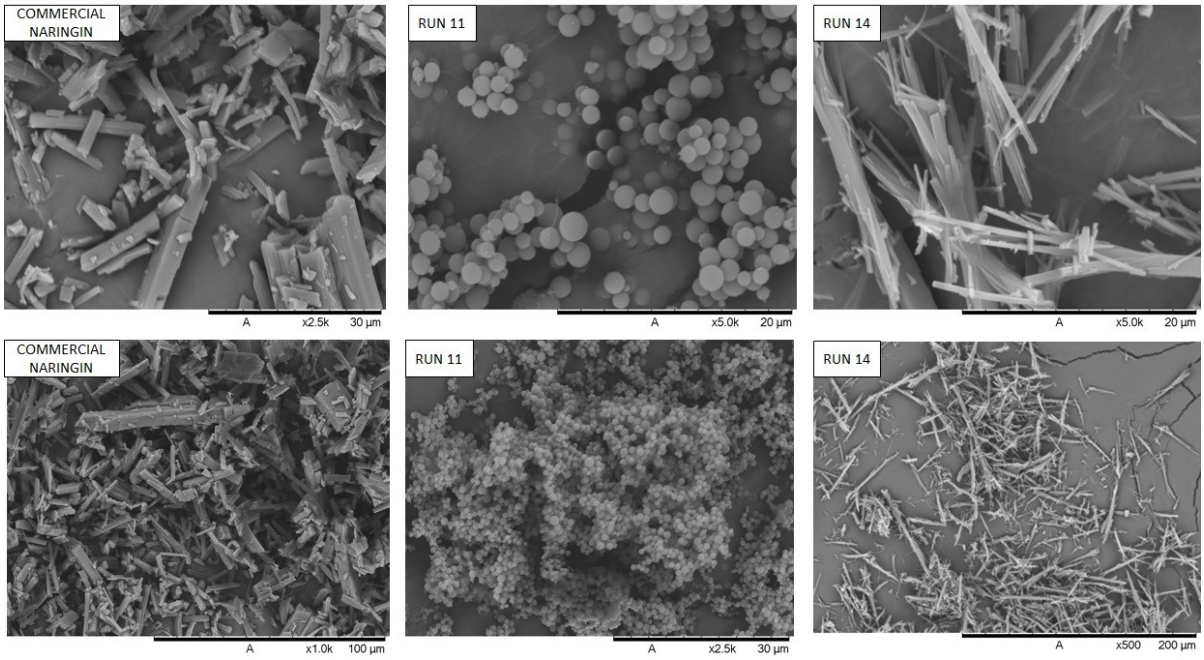

Source: Author (2024)

After GAS technique naringin changed the morphology, there was a reduction in particle size capable of leading to changes in produced particles structural, physical-chemical, and functional properties. Properties such as water absorption, reaction rate, and release are improved at the microscale due to the increased surface area, thus enhancing the bioavailability of poorly water-soluble compounds (CEREA et al., 2016; CHEN et al., 2018; RASENACK; MÜLLER, 2004). In addition, these characteristics make it possible to reduce the dosage of ingested medication, reduce side effects, promote a controlled release of active ingredients, and increase drug circulation time in the body (YORK; KOMPELLA; SHEKUNOV, 2004).

Appendix C, presents the morphology of commercial and processed naringin by GAS technique, and Table 2 shows the diameter particles for all runs. Notably, runs 1, 2, 3, 4, 6, 7, 11, 12, 15, 16, 17, and 18 particles showed spherical morphology and different ranges for particle diameter 0.835 ± 1.252 to 2.280 ± 1.301 µm. Runs 5, 8, 9, 10, and 19 showed a morphology mix of spherical in a more significant proportion, some with needle-like characteristics, and the particle diameter range 1.662 ± 2.258 to 2.573 ± 2.165 µm. Runs 13 and 14 showed needle-like features, and the particle diameter 5.596 ± 1.995 µm and 8.997 ± 2.771 µm, respectively.

Dalvi, Mukhopadhyay (DALVI; MUKHOPADHYAY, 2009) explain that the morphology of the particles changes with decreasing pressure from needle-shaped to near-spherical particles. The higher the initial pressure, the greater the instantaneous temperature drop, drastically reducing the equilibrium solubility of solids in the solution and creating a high supersaturation. This high supersaturation leads to such a high crystal growth rate that the heat of crystallization released cannot be dissipated immediately to the solution. The depletion of solutes from the solution near the crystal surface (due to high growth rates) also makes further growth of a crystal surface in this direction impossible. This leads to very rapid growth along the other dimension and an increase in surface area to dissipate the heat of crystallization, resulting in needle-shaped particles (TIWARY, 2001). Reverchon et al (REVERCHON et al., 2008) obtained spherical microparticles that were usually amorphous, but in some cases, crystals of different morphologies were obtained with supercritical CO_2. Spherical microparticles can be successfully obtained under near-critical pressure conditions up to fully developed supercritical conditions (REVERCHON et al., 2008).

4.3.3. Power-X-ray diffraction (XRD) results

Commercial and processed naringin particles were characterized by X-ray powder diffraction to evaluate changes in the crystalline structure of the compounds. As can be seen in Figure 22, XRD analysis of commercial naringin has diffraction angles (2Θ) 9.87°, 11.64°, 13.22°, 14. 62°, 15.72°, 16.63°, 17.60°, 18.76° and 28.11°, which are in agreement with literature (MOHAMED et al., 2018). Note that for run 11, processed naringin lost all characteristic peaks, changing from crystalline structure to amorphous during processing. In addition, a halo formation is typical of amorphous material (CULLITY, BERNARD DENNIS; STOCK, 2014). According to the literature, naringin amorphization may be due to a probable break in the glycosidic bond present in the naringin molecule (YU; WU, 2010). Cavallini and Franco (CAVALLINI; FRANCO, 2010), who carried out the micronization of substances with the aid of a ball mill, showed that the breaking of hydrogen bonds within the granules causes an increase in amorphous areas and a reduction in crystalline parts (CAVALLINI; FRANCO, 2010). Also, in the particle formation mechanism in supercritical or near-critical conditions, the surface tension of the system CO_2-solvent is close to zero, leading to very fast nucleation and growth during particle formation, resulting in a disordered molecular organization (ADAMI et al., 2022). The profiles of the diffractograms from commercial and GAS-processed technique

naringin from run 14 exhibit both crystalline structures; however, they are not identical, probably due to the formation of a polymorph material. Appendix D, shows XRD for all runs studied in this work; it is possible to observe the presence of amorphous and crystalline characteristics or just amorphous depending on the processing conditions. Runs 1 to 4, 6, 9, 11, 17, and 18 are majority amorphous. For the other rums, they presented both amorphous and crystalline characteristics.

Figure 22- Power-X-ray diffraction (XRD) analysis of commercial and processed naringin from runs 11 (C= 5 mg·mL^{-1}, P= 12 MPa, T= 308K, CO_2 flow rate= 15 mL.min^{-1}), and 14 C= 10 mg.mL^{-1}, P= 8 MPa, T= 318K, CO_2 flow rate= 15 mL.min^{-1}).

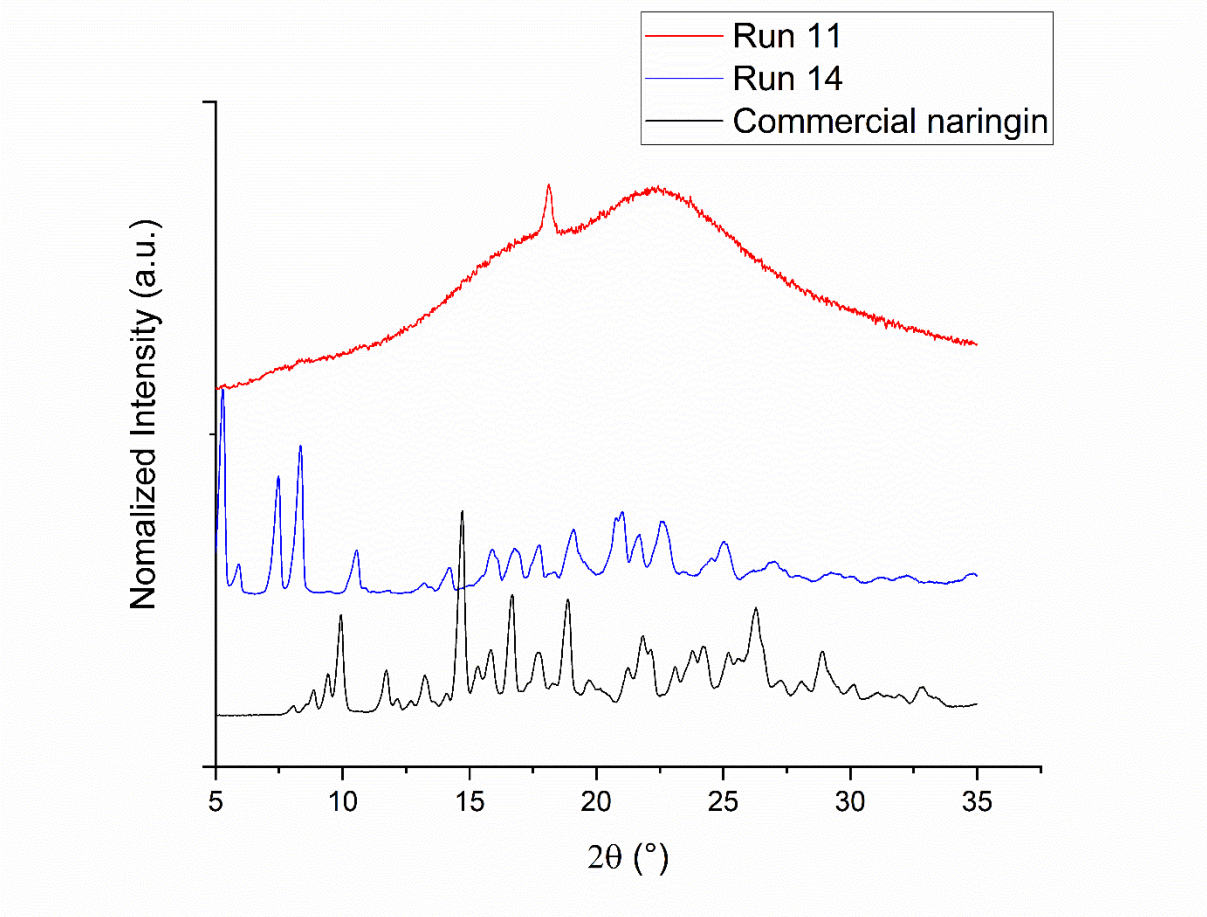

Source: Author (2024)

4.3.4. Differential scanning calorimetry (DSC) results

Thermograms of commercial and processed naringin from runs 11 and 14 are shown in Fig. 23. It can be seen that commercial naringin shows the phase transition at 157.29 °C,

related to the molecular rearrangement, and the endothermic event of melting at 238.71°C whose sharpness confirmed that the bioactive compound was in a crystalline form. The peaks at over 260.0 °C are due to the decomposition of naringin, which agrees with the literature (LAURO et al., 2007; SANSONE et al., 2009). Sample from run 11 shows one phase transition at 153.92 °C, and an endotherm small peak, probably because the residual crystallinity reflected by the peak at ~17 degrees in the XRD result, corresponding to the crystal melting point may be interpreted as a consequence of amorphization (SANSONE et al., 2009).

Figure 23- Differential scanning calorimetry (DSC) analysis of commercial and processed naringin from runs 11 (C= 5 mg·mL^{-1}, P= 12 MPa, T= 308K, CO_2 flow rate= 15 mL.min^{-1}) and 14 (C= 10 mg.mL^{-1}, P= 8 MPa, T= 318K, CO_2 flow rate= 15 mL.min^{-1}).

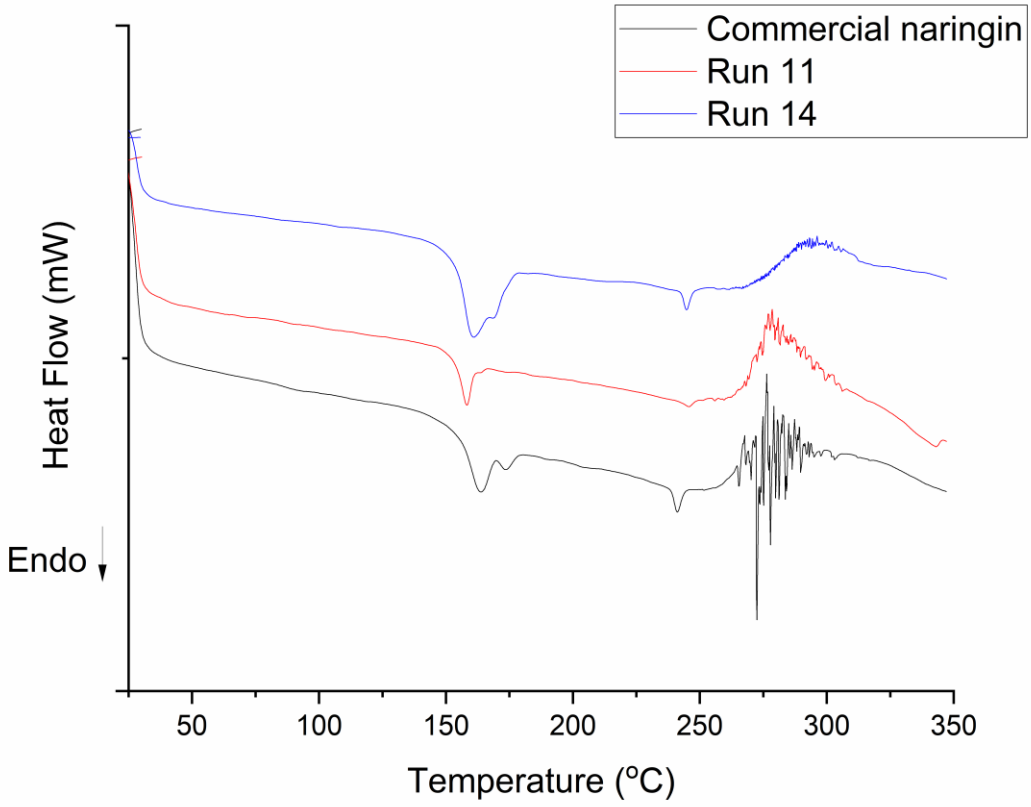

Source: Author (2024)

For run 14, the phase transition was determined at 154.21°C and melting point at 242.63 °C, confirming the crystalline form of naringin after GAS processing. The peak that occurs at 157.29 °C, 153.92 °C, and 154.21 °C is the rearrangement of the structure. This

phenomenon is confirmed in the literature by Hurtta et al. (HURTTA; PITKÄNEN; KNUUTINEN, 2004) and Lee. (LEE; THOMAS; SCHMIDT, 2011) for compounds that have a similar structure to naringin. A phase transition is a thermal event, and a large endothermic peak event is when the crystalline material absorbs energy (heat) and breaks intermolecular bonds, loss of the crystalline structure, and results in a phase transition to the liquid phase (HURTTA; PITKÄNEN; KNUUTINEN, 2004; LEE; THOMAS; SCHMIDT, 2011). This phenomenon is described by Lee (LEE; THOMAS; SCHMIDT, 2011) as "apparent melting" and describes the transition from the crystalline to the amorphous phase, a transition caused by a kinetic process in DSC analyses. The endothermic event around 240-252°C is the melting of the aglycone portion of the molecule, naringenin (KHANDAVILLI et al., 2018b).

4.3.5. Fourier-transform infrared (FTIR) spectroscopy results

FTIR evaluated the commercial and processed naringin particles to verify possible changes in their structure caused by GAS processing, as presented in Figure 24. Commercial naringin shows characteristic stretching in 3416.65; 2923.60, 1643.33; 1515.63; 1449.48 cm^{-1}, which agrees with the literature (GHOSAL; GHOSH; DAS, 2018). The stretches 3425 cm^{-1} and 2924.0 cm^{-1} correspond to O-H and C-H bonding, respectively. The stretching 1645.0 and 1043.0 cm^{-1} refer to functional groups C=O and C-O-, respectively, in agreement with the literature (HUSSAIN et al., 2022). It is highlighted that in certain bands in the region around 1150 cm^{-1}, glycosidic linkage (C-O-C) characteristics for runs 11 and 14 decrease the intensity of the peaks if compared to commercial naringin. As demonstrated in the literature by Islam et al. (ISLAM et al., 2019), the presence of weak bands associated with the C-O-C bridges was regarded as the partial breakdown of the glycosidic bond at the surface level (ISLAM et al., 2019).

Figure 24- Fourier-transform infrared (FTIR) spectrum analysis of commercial naringin, runs 11 (C= 5 mg·mL^{-1}, P= 12 MPa, T= 308K, CO_2 flow rate= 15 mL.min^{-1}) and 14 (C= 10 mg.mL^{-1}, P= 8 MPa, T= 318K, CO_2 flow rate= 15 mL.min^{-1}).

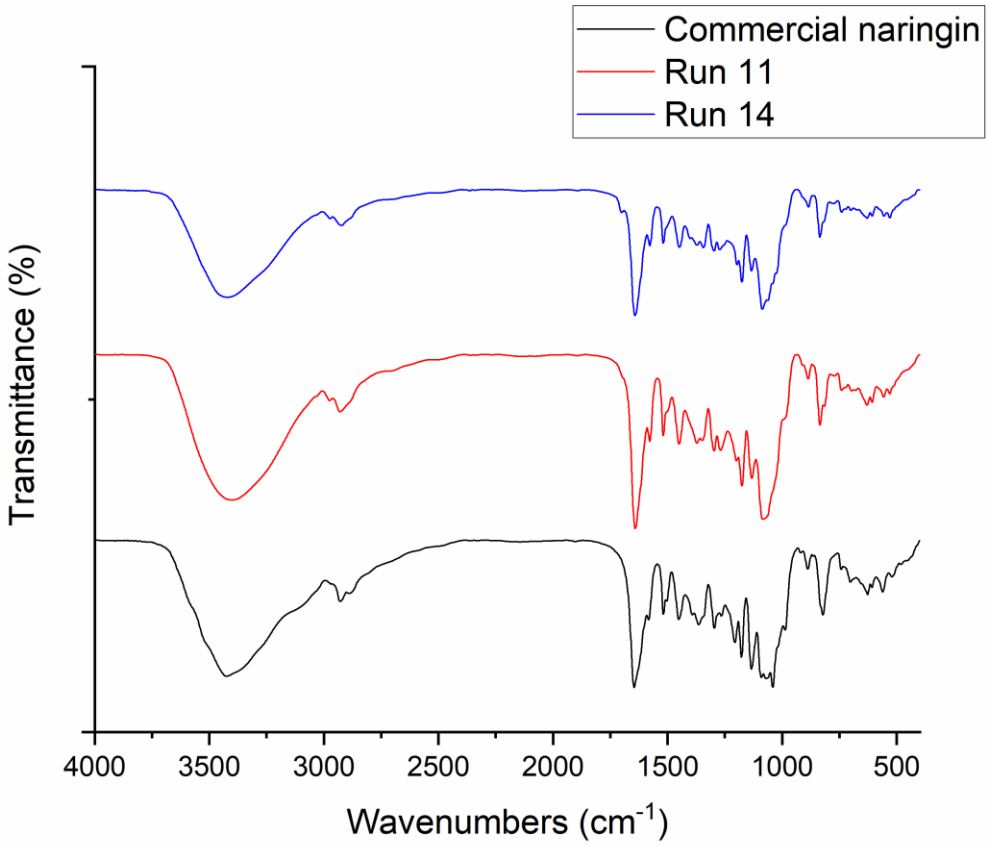

Source: Author (2024)

4.3.6. Dissolution rate analysis results

Figure 25 shows the dissolution profiles of commercial naringin and GAS processed naringin from runs 11 and 14, all of them in distilled water. The results show that runs 11 and 14 solubilization approximately 3.76 and 3.96 fold compared to commercial naringin at 180 min, the end of the experiment. Comparing amorphous and crystalline forms, runs 11 and 14, respectively, it can be seen that the solubility of run 11 at 180 min have similar values, reaching nearly the value of run 14, due to the crystallization of the amorphous powder (SANSONE et al., 2009). The XRD (Appendix E) of solid material collected after the dissolution study is clearly different in terms of peak positions and intensity compared to the spectrum of commercial naringin, suggesting that another naringin polymorph had been formed.

Also, the results confirmed that the solid material of naringin run 11 recrystallized on contact with the dissolution medium over 180 min or thought of the supersaturation of the solution (ALONZO et al., 2010). The amorphous is metastable, with phase transformations occurring over 180 min during dissolution (ALONZO et al., 2010). In amorphous forms, it is widely observed that fine particles tend to dissolve and recrystallize onto larger ones, producing a shift in particle size distribution until an equilibrium solubility is reached ("Ostwald ripening") (ALONZO et al., 2010; PERRUT; JUNG; LEBOEUF, 2005). Also, reducing particle size promotes recrystallization by increasing the available surface areas during exposure to the dissolution medium. That is because, on the free surface, amorphous solids have molecules with high mobility, which is favorable for crystal growth (ZHENG et al., 2019). A strategy to inhibit supersaturation crystallization is adding polymers capable of delaying the crystallization of supersaturated solutions (ALONZO et al., 2010).

Figure 25- *In vitro* release profile of commercial and processed naringin from runs 11 (C= 5 mg·mL^{-1}, P= 12 MPa, T= 308K, CO_2 flow rate= 15 mL.min^{-1}) and 14 (C= 10 mg.mL^{-1}, P= 8 MPa, T= 318K, CO_2 flow rate= 15 mL.min^{-1}) in distilled water. Data are reported as the mean ± SD of two independent experiments.

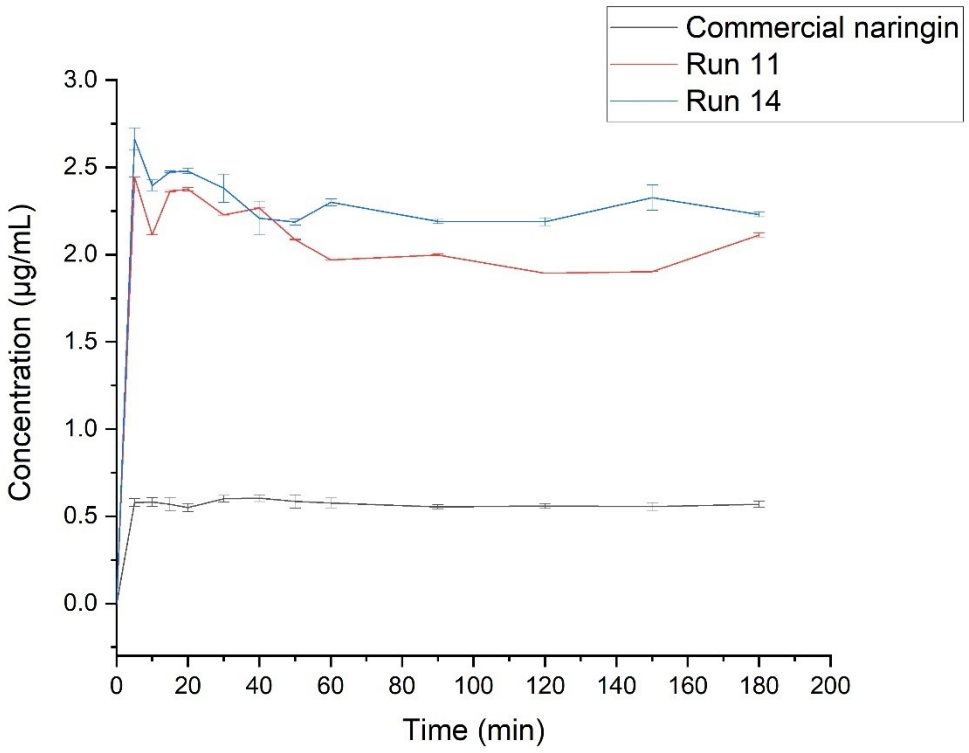

Source: Author (2024).

4.3.7. Ultra-performance liquid chromatography coupled with mass spectrometry UPLC-MS results

UPLC-MS analysis was performed to identify naringin after processing using gas antisolvent technique and after dissolution study using distilled water. The results it can be seen that Appendix F-K show that naringin m/z $[M+H]^+$ 581 ionizes and cleave the conjugation bond when subjected to ESI mass ionization, resulting in aglycone proved to be naringenin m/z $[M+H]^+$273. But it is observed that in commercial naringin, run 11 and run 14 after processing and after dissolution assays, the UPLC-MS presents the same profile confirming that it is naringin. Other fragmentation mass peaks have been identified in the mass spectra, and the corresponding speculated structures are described in the Figure 26 legend and Appendix L.

Figure 26- UPLC-MS naringin run 14.

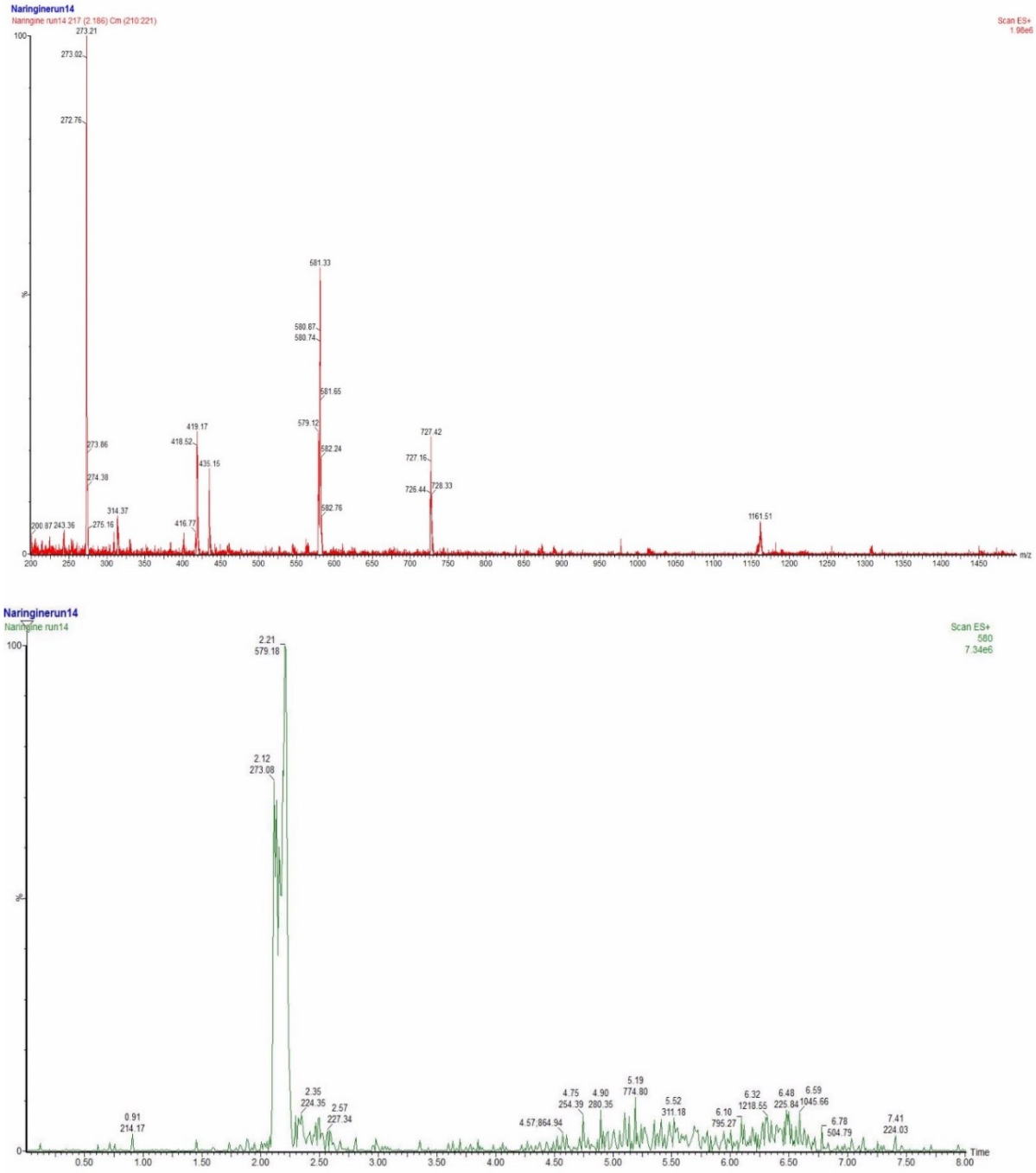

Legend: Rt=2.21 min. Fragmentation mass peak suggests: $[M+H]^+$314: naringenin and residual of acetonitrile, $[M+H]^+$418: is the naringenin and one sugar unit only, $[M+H]^+$435 : the high voltages due to loss of the one sugar resulting from a proton transfer and cleavage between two sugar units, $[M+H]^+$727: impurity of naringin probably kaempferol-3-lathyroside-7-rhamnoside and $[M+H]^+$1161: dimers of naringin.

4.3.8. Specific surface area results

Commercial naringin presented a specific surface area of 2.39 $m^2 \cdot g^{-1}$, while the specific surface area of naringin from runs 11 and 14 was 11.62 $m^2 \cdot g^{-1}$ and 4.65 $m^2 \cdot g^{-1}$, respectively. In other words, GAS processed naringin samples from runs 11 and 14 increased the specific surface area approximately 5 and 2 times, respectively, as compared to commercial naringin. In addition, the amorphous form shows an increase in the surface area, probably due to the reduction in particle size compared to the commercial form (HA et al., 2015; KIM et al., 2008).

4.3.9. Molecular docking results

The free energy of binding (affinity) of the docking naringin and D_2R complex was F.E.B = -9.4 kcal/mol, and the estimated inhibition constant was Ki = 128.75 nM, whereas for the complex naringin and 5-HT_{2A}, we found F.E.B = -9.8 Kcal/mol, Ki = 65.55 nM. The R.M.S.D was < 2 Å for all studied systems, and this value can be considered as a spontaneous thermodynamic process based on the obtained negative FEB value (TROTT et al., 2009).

Naringin shows expressive spontaneity to inhibit the studied receptors. The inhibition constant (ki) of naringin is similar to that of clozapine for D_2R (ki = 130 nM) (SIKAZWE et al., 2003) and clozapine for 5-HT_{2A} (ki = 25.12 nM) (KNIGHT et al., 2004). Also, naringin shows superior Ki for these receptors than the atypical antipsychotic olanzapine (D_2R ki = 11 nM and 5-HT_{2A} ki = 4 nM) and risperidone (D_2R ki = 3 nM and 5-HT_{2A} ki = 0.6 nM) (BYMASTER et al., 1996). These results are particularly interesting, since they suggest that naringin presents a similar mechanism of action to second generation antipsychotics, which are D_2R and 5-$HT2_A$ antagonists (BRUNTON et al., 2016).

The Figure 27 shows that naringin can fit into the cavity of the dopaminergic D_2R and 5-HT_{2A} receptors in the best docking position. Figure 28 shows the Lig-Plot relevant intermolecular interaction between the complex (naringin-receptors).

Figure 27-Naringin into the cavity of a) 5-HT_{2A} and b) D_2R receptors. The region of naringin interaction with the residues in the cavity of the receptors is highlighted and yellow dashed lines represent hydrogen bonds.

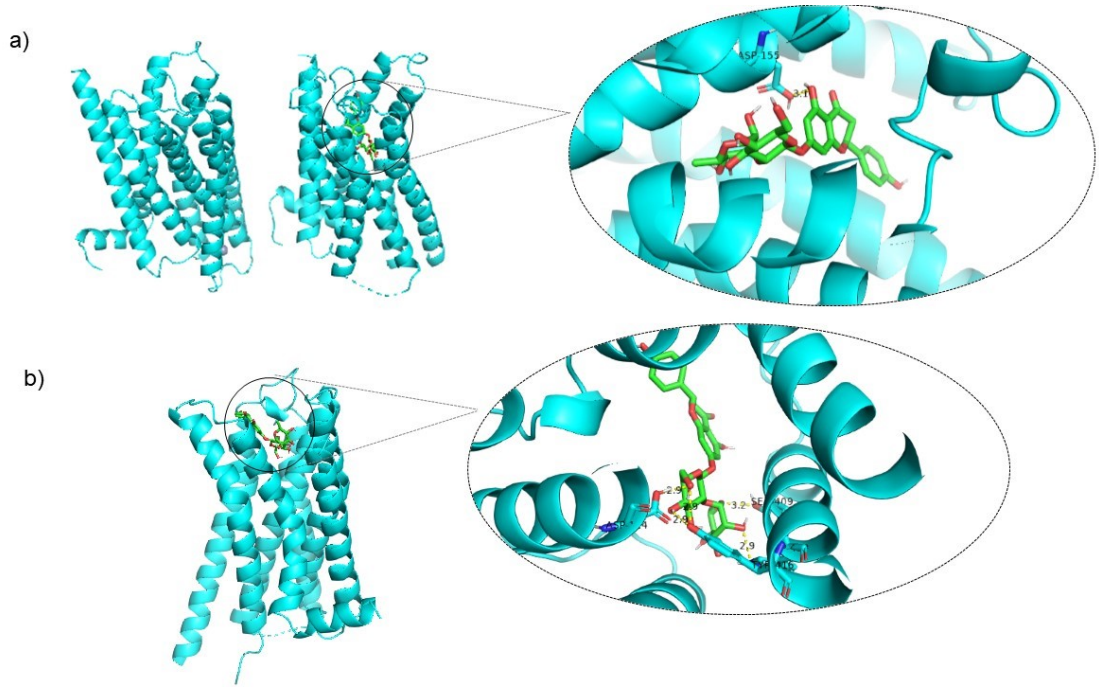

Source: Author (2024)

Figure 28-Representation of the 2D-Lig-Plot diagram of interactions of critical residues. a) 5-HT_{2A} and b) D_2R receptors with naringin for the best docking poses. Hydrogen-bond interactions are represented.

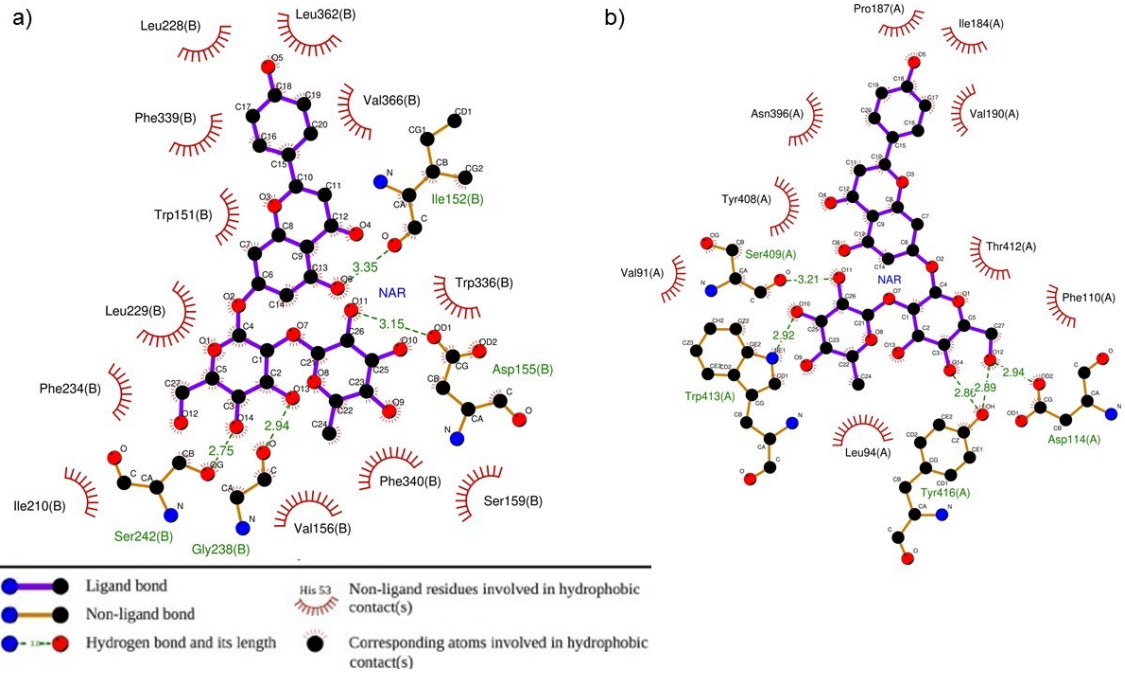

Source: Author (2024)

Regarding the 5-HT_{2A} receptor, naringin was stabilized by hydrogen bond interaction with binding residues Ile 152, Asp 155, Gly 238, and Ser 242 with lengths of 3.35; 3.15; 2.94; and 2.75 Å. There was also a hydrophobic interaction involving the serotonergic receptor 5-HT_{2A} (chain B) with naringin: Trp 336, Val 366, Leu 362, Leu 228, Phe 339, Trp 151, Leu 229, Phe 234, Ile 210, Val 156, Phe 340 and Ser 159.The hydrogen bonding interaction between ligands and residues within the hydrophobic binding pocket plays an important role in stabilizing the docking complex.

For the complex of D_2R and naringin, the hydrogen bond interactions occurred with amino acids residues Ser 409 (3.21 Å), Trp 413 (2.92 Å), Tyr 416 (2.82 and 2.89 Å) and Asp 144 (2.94 Å) (chain A). In addition, the presence of a hydrophobic interaction between the D_2R residues (Leu 94, Phe 110, Thr 412, Val 190, Ile 184, Pro 187, Asn 396, Tyr 408 and Val 91) with naringin is important for the stabilization of the docking complex (D_2R - naringin).

4.3.10. *In vivo* experiments

The results of hyperlocomotion induced by ketamine in mice are depicted in Figure 29. As expected, the injection of ketamine induced a significant increase in the total distance traveled (m) [$F(7,56) = 8.785$, $p < 0.001$] and in the number of rearings [$F(7,56) = 14.34$, $p < 0.0001$] of mice. In addition, there were no effects of ketamine injection on the number of groomings [$F(7,56) = 1.520$, $p = 0.1794$] and fecal bolus expelled by mice during the open field session [$F(7,56) = 2.246$, $p = 0.0634$].Several studies show that ketamine induces disruptive effects on motor behavior of rodents (POWELL; GEYER, 2007; RAZOUX; GARCIA; LÉNA, 2007). These alterations have been associated with psychotic-like effects and might be the result of potentiated synaptic transmission between the prefrontal cortex and the nucleus accumbens, mediated by increased glutamate levels observed in the nucleus accumbens after ketamine administration (RAZOUX; GARCIA; LÉNA, 2007). In this sense, our results suggest that the animal model used here was successfully accomplished.

On the one hand, the oral administration of commercial naringin at 50 $mg.kg^{-1}$ was not able to significantly prevent the ketamine-induced hyperlocomotion in mice, which is mainly evidenced by similarity of the total distance (m) traveled in the open field arena and the number of rearings between the ketamine group and commercial naringin-pretreated (50 $mg.kg^{-1}$) group. On the other hand, we may suggest a partial effect of commercial naringin at 200 $mg.kg^{-1}$ in the ketamine-induced hyperlocomotion, considering that the total distance (m) traveled by the

commercial naringin-pretreated group at 200 mg.kg^{-1} was not different from the total distance traveled (m) of sham and ketamine groups. Additionally, the number of rearings of the group pretreated with commercial naringin at the highest dose was significantly smaller than the number of rearings from the ketamine group.

Figure 29- Effects of run 11 and run 14 of naringin on ketamine-induced hyperlocomotion in mice. The animals (n = 8 / group) were orally pretreated with Vehicle (saline solution + 1% polysorbate 80) (Sham and Ketamine groups), commercial naringin, run 11 or run 14 of naringin at 50 or 200 mg·kg^{-1} (p.o.) 1 h before the injection of Saline solution (Sham group) or ketamine (10 mg·kg^{-1}, ketamine, commercial naringin and run 11 and run 14 of naringin at 50 and 200 mg.kg^{-1} groups). Graphs display the total distance (m) traveled, the number of rearings, groomings and fecal bolus expelled during 20 min of observation in the open field arena. One-way ANOVA followed by Tukey's test. Data are presented as mean ± standard deviation. (*** $p < 0.001$; **** $p < 0.0001$ in comparison to the Sham group. ##$p < 0.01$; #### $p < 0.0001$ in comparison to the ketamine group. ++ $p < 0.01$ in comparison to the commercial naringin-treated group at 50 mg.kg^{-1}; §§ $p < 0.01$ in comparison to the run 11 of naringin-treated group at 50 mg.kg^{-1}).

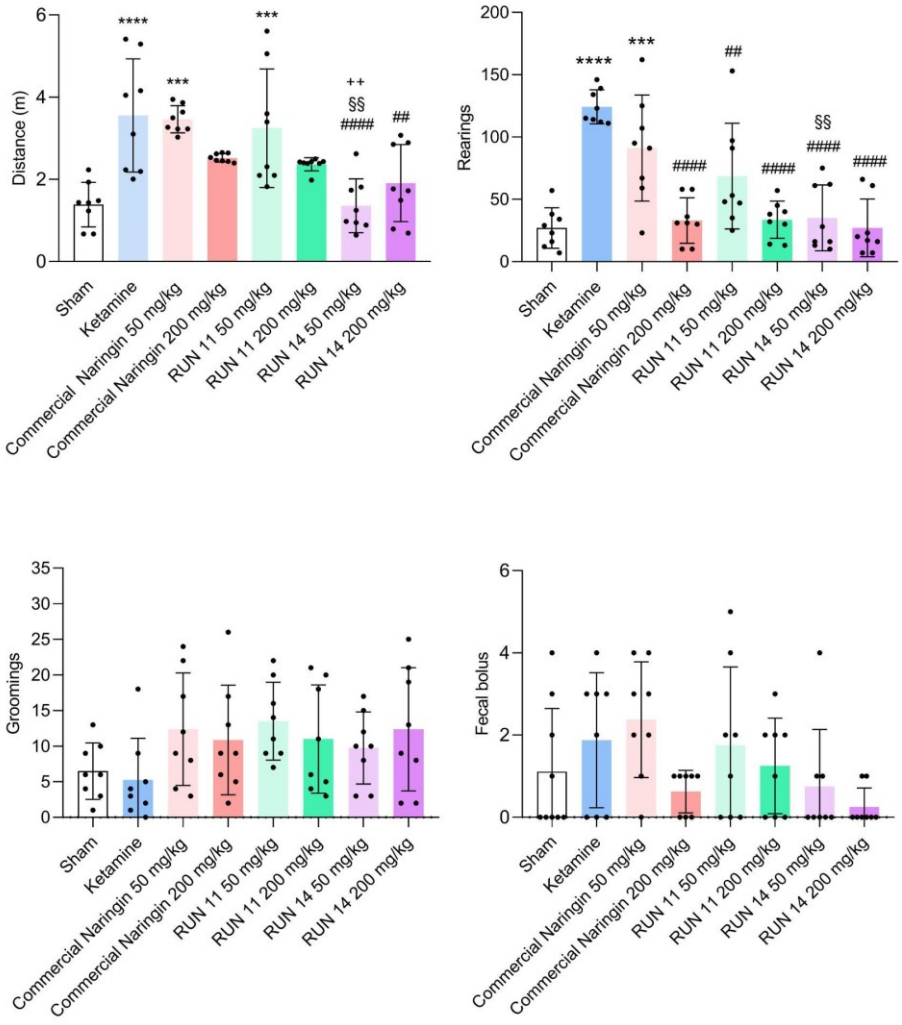

Source: Author (2024)

Indeed, naringin (at 100 mg.kg^{-1}, p.o.) prevents ketamine-induced schizophrenia-like deficits in rats (GEORGE et al., 2020), and this agrees with our findings (at least for the group treated with commercial naringin at 200 mg.kg^{-1}). The effects of commercial naringin in this animal model are mediated by wnt/β-catenin and Akt/GSK-3β pathways regulation, as well as its antioxidant and antiapoptotic activities (GEORGE et al., 2020). Additionally, George et al. (GEORGE et al., 2021) demonstrated that naringin presents beneficial outcomes when added to clozapine in the treatment of ketamine-induced schizophrenia-like effects in rats, since its combination with clozapine reduces several side effects of the antipsychotic (GEORGE et al., 2021).

The run 11 of naringin at both tested doses (50 and 200 mg.kg^{-1}, p.o.) was not able to prevent the increase in the total distance (m) traveled in the open field arena induced by ketamine. Nevertheless, the run 11 of naringin at both tested doses (50 and 200 mg.kg^{-1}, p.o.) prevented the ketamine-induced increase in the number of rearings. These results are similar to the ones of the commercial naringin-treated groups at the same doses. Noteworthy, the pretreatment of animals with run 14 of naringin at both tested doses (50 and 200 mg.kg^{-1}, p.o.) were effective in preventing the disruption in the motor activity induced by ketamine.

The run 11 of naringin has the same effect as naringin in commercial form probably because, as shown in section *4.3.7*, after dissolution in aqueous medium, naringin run 11 recrystallizes in contact with aqueous medium after 180 minutes. The formation of amorphous solids may not necessarily increase the bioavailability of a drug proportionally to their solubility (DEBNATH; PREDECKI; SURYANARAYANAN, 2004; GRECO; BOGNER, 2010). This was not observed for run 14 of naringin, which presented crystalline characteristics that remained after the dissolution in an aqueous medium. Therefore, GAS processed naringin run 14 showed a significant biological effect probably due to increased bioavailability.

The results show that the dose of GAS processed naringin that prevented ketamine-induced hyperlocomotion did not impair the spontaneous locomotor activity of mice since the animals treated only with commercial naringin and naringin run 11 and 14 (*per se* groups) did not present differences in the total distance (m) traveled in the open field arena when compared to the Vehicle-treated (Sham) group at the highest doses (Appendix M). We only found a reduction in the number of groomings elicited by run 11 and run 14 of naringin. These results may indicate a pharmacological profile similar to atypical drugs. Nevertheless, this hypothesis deserves further investigation.

4.4. CONCLUSION

The gas antisolvent technique conferred naringin better characteristics *in vitro* and *in vivo* assays. It is observed that the dissolution rate of naringin GAS increases compared to commercial naringin (runs 11 and 14), which is due to the increase of the surface area and the decrease of the average size of the particles. The results of *in vivo* assays for treating ketamine-induced hyperlocomotion test in mice were promising for run 14, probably due to the increased bioavailability of the processed GAS compound. For run 11, the *in vivo* results are similar to commercial naringin, because of the recrystallization of the amorphous form when in contact with the aqueous/biological medium. Therefore, the application of these particles produced here opens the possibility of expanding the application of naringin in the pharmaceutical field.

5.COCRYSTAL NARINGENIN: BETAINE AND PERMEATION STUDIES

The results of this section were submitted in the paper "Synthesis of naringenin-betaine cocrystal by gas antisolvent technique and cell models for *in vitro* permeation studies" in the "Journal of Drug Delivery Science and Technology".

ABSTRACT

Naringenin (NRG) is a flavanone characterized by potential neuroprotective properties, even if low water solubility and poor oral bioavailability limit the ability of this compound to target the central nervous system. As an attempt to overcome these limitations, it is here described the synthesis and characterization of a cocrystal obtained with NRG and betaine (BTN) using gas antisolvent (GAS) technique. The ability of NRG, its cocrystal and the parent physical mixture to permeate across the intestinal and the blood-brain (BBB) barriers was simulated *in vitro* by using monolayers obtained by IEC-6 cells and a model established by ECV 304, respectively. It is evidenced that the NRG: BTN cocrystal improves both the solubility and dissolution rate of NRG, potentially allowing to enhance its oral bioavailability. Moreover, the results of viability studies performed on IEC-6 cells suggest that low doses of cocrystal frequently administered are required for absorption to be efficient and safe. The study also suggests a synergistic effect of NRG and BTN for the cocrystal and physical mixture in

enhancing NRG permeation through the BBB. These results indicate that the NRG:BTN cocrystal is potentially useful for the brain targeting of NRG, following its oral administration.
Keywords: cocrystallization; permeability; dissolution; gas antisolvent; IEC-6 cell; ECV304 cell

5.1.INTRODUCTION

Naringenin (NRG, $C_{15}H_{12}O_5$, 4′,5,7- trihydroxyflavanone, molecular weight 272.25 g/mol, Figure 30) is a naturally occurring flavonoid classified as flavonones present in citrus fruits, grapes, beans, cherries, cocoa, oregano and tomatoes (GÜRSUL et al., 2016; HSIU et al., 2002; YUSOF; GHAZALI; KING, 1990). NRG presents important properties: antioxidant (CAVIA-SAIZ et al., 2010; HEO et al., 2004), anticancer (JIN et al., 2011; KRISHNAKUMAR et al., 2011), anti-inflammatory (LIN; LIN, 2011; SPAGNUOLO; MOCCIA; RUSSO, 2018; TSAI et al., 2012), antiviral (GOLDWASSER et al., 2011), antidiabetic (AHMED et al., 2017), antimutagenic (LEE; YOON; MOON, 2004), antibacterial (AGUS; ACHMADI; MUBARIK, 2017; WANG et al., 2018a), neuroprotective (HEGAZY; ALI; SABRY, 2016), and anti-apoptotic (WANG et al., 2017), among others.

NRG is characterized by poor aqueous solubility in water (46 $\mu g \cdot mL^{-1}$) (KANAZE et al., 2006), which seems to contribute to its low oral bioavailability (5.81%) (KANAZE et al., 2006; KHAN et al., 2015) requiring therefore high doses for pharmaceutical uses of this compound. New strategies allowing to increase the water solubility of NRG are needed in order to enhance its therapeutic activity. The general strategy utilized for limited solubility drugs is the generation of novel solid phases, such as amorphous, polymorphs, hydrates, solvates, salts, and cocrystals (GUPTA et al., 2018; HEALY et al., 2017; SINGH et al., 2023; SOKAL; PINDELSKA, 2017; XU et al., 2023). Recently, cocrystallization has received increasing attention because of its significant ability to regulate physicochemical properties like dissolution rates, bioavailability, stability, manufacturability (flow, compactness, and processability), and the hygroscopicity of substances that suffer from poor solubility (GADADE; PEKAMWAR, 2016; KAVANAGH et al., 2019; LI; MATZGER, 2016; PESSOA et al., 2019; RIBAS et al., 2019a, 2019b; SHAIKH et al., 2018; SOKAL; PINDELSKA, 2017).

Cocrystallization is based on the interaction between two or more chemically different molecules, generally in stoichiometric ratio (AITIPAMULA et al., 2012; DUNITZ, 2003; FRIŠČIČ; JONES, 2009). Pharmaceutical cocrystal, can be obtained by a target molecule or API (active pharmaceutical ingredient) and a coformer or guest molecule, normally included in

the list of GRAS substances (Generally Recognized as Safe) (GADADE; PEKAMWAR, 2016; SHAIKH et al., 2018).

The use of conventional methods of cocrystallization, such as solvent evaporation, solid grinding, liquid-assisted grinding, slurring, and extrusion (twin screw extrusion**,** hot melt crystallization) in the cocrystal preparation presents several drawbacks, such as scaling-up difficulties or the presence of homocrystals in the final product and often require post purification steps to eliminate solvents (CUADRA et al., 2020; MUNDHE, 2013). That said, the use of supercritical fluid (FSC) presents a new and interesting pathway for the formation of cocrystals, since it avoids most of the drawbacks of traditional methods while having as main advantages: high purity of products, versatile approach to produce cocrystals with different morphologies and particle sizes, the possibility of thermolabile molecule processing, single step process, as well as being an environmentally acceptable technology reducing the use of organic solvent and minimizing the residual amount of solvent in the cocrystal when compared to some conventional techniques (FAGES *et al.*, 2004; PANDO, CABAÑAS E CUADRA, 2016). In this work, we applied GAS (gas antisolvent) technique, which involves adding compressed CO_2 to a solution containing the target molecule and coformer solutes until the desired pressure is reached. After that, CO_2 is incorporated into the liquid solvent, expanding it and decreasing the solvent power, leading to the precipitation of solutes (PANDO, CABAÑAS E CUADRA, 2016).

There are published studies involving the cocrystallization of NRG which involves the use of conventional techniques (JIANG et al., 2020; KHANDAVILLI et al., 2018a; LEE et al., 2019; XU et al., 2020; YIN et al., 2020; ZHOU et al., 2019). Recently, some works made use of betaine (BTN, Figure 30) as coformer to cocrystallize NRG. To date, the fabrication of cocrystals consisting of NRG: BTN via the GAS technique or using FSC has not been found.

The formation of the NRG: BTN cocrystal is justified by the fact that NRG has two competitive hydrogen bonding sites that can act as donors and acceptors (4′,5,7-hydroxyl, and a carbonyl group), which makes it a good candidate for cocrystal formation. Also, NRG is a neutral compound with pKa = 7.05, so it is unsuitable for salt formation (CUI et al., 2019; ZHANG et al., 2015). BTN, also known as trimethylglycine ($C_5H_{11}NO_2$, molecular weight: 117.148 g/mol), is a natural sweetener found in microorganisms, plants, and animals (ZHANG et al., 2019b). It has gained significant attention in pharmaceutical formulations as a coformer due to its ability to form hydrogen bonds with molecule targets (HASKINS et al., 2023; PUTRA et al., 2018; ZHANG et al., 2019b).

Recent work indicates that cocrystallization can change the permeability properties of drugs (EMAMI et al., 2018; PANDEY; GHOSH, 2022). Some studies investigating the permeability of cocrystals, physical mixtures, and pure drugs through intestinal monolayer cells evidenced that cocrystals can induce significant differences in influencing the integrity of intestinal cell monolayers compared to the pure drugs and the physical mixtures (DALPIAZ et al., 2018; FERRETTI et al., 2015; SEGALINA et al., 2022). Other studies did not have evidence effects on permeability by coformers or cocrystals on cell monolayers (REGGANE et al., 2018).

The efficacy of most drugs depends critically on their ability to cross cellular barriers and this aspect appears crucial for drugs targeting the central nervous system (CNS). Ideally, drugs intended for the blood-brain barrier (BBB) crossing should be reasonably lipid soluble, easily permeable, and metabolically stable to reach their target (YUAN et al., 2016). Flavonoids such as NRG are known to be able to cross the BBB (YOUDIM et al., 2004), even if this property requires to be improved. Very recently it has been demonstrated that neuroactive drugs, such as ketoprofen-gabapentin can synergistically and mutually increase BBB crossing, and that their cocrystal further enhances these effects, possibly leading to higher CNS permeation and central effects of these compounds (ARAMINI et al., 2023).

This study aims to perform the cocrystalization between NRG and BTN using the GAS technique and the characterization. Also, *in vitro* assays investigated the permeability of NRG as raw drug, physical mixture with betaine (NRG-BTN Mix), and cocrystal naringenin: betaine (1:1) (NRG:BTN Coc) across cell monolayers of IEC-6 and a BBB model, which was established by ECV 304.

Figure 30- Molecular structure of (a) naringenin and (b) betaine.

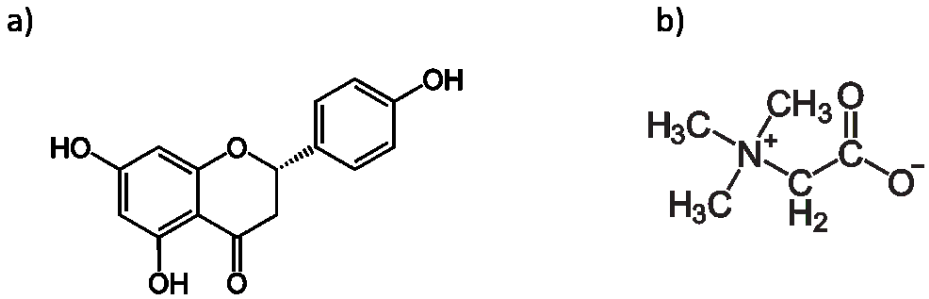

Source: Author (2024)

5.2. MATERIALS AND METHODS

5.2.1. Materials

Naringenin (≥ 95%, Sigma-Aldrich), betaine (anidra ≥ 98%, Suzhou Vitajoy Bio Tech), ethanol (99.5%, Êxodo Científico), CO_2 (99.9%, White Martins S.A) were obtained from certified suppliers. Methanol and water were of high-performance liquid chromatography (HPLC) grade from Sigma-Aldrich. Dulbecco's modified Eagle's medium (DMEM) + Glutamax, fetal bovine serum (FBS), penicillin, streptomycin, Dulbecco's phosphate buffered saline (DPBS), and trypsin−EDTA were obtained from ThermoFisher Scientific-Life Technologies (Monza, Italy) and Microtech (Naples, Italy). The IEC-6 cell line was obtained from Sigma-Aldrich, following terms and conditions of the supply of products from the Culture Collections of Public Health England (Culture Collections) comprising the European Collection of Authenticated Cell Cultures (ECACC). The 12-well cellQART inserts were obtained from Sabeu GmbH (Northeim, Deutschland). All other reagents and solvents were of analytical grade (Sigma-Aldrich).

5.2.2. GAS (Gas antisolvent) for preparation of cocrystal naringenin-betaine (1:1)

The experimental procedure of GAS (gas antisolvent) used to prepare cocrystal naringenin and betaine, was based on the methodology described by Pessoa and Sakata et al. (PESSOA et al., 2019; SAKATA et al., 2021). The experimental procedure consisted of preparing equimolar amounts of naringenin (0.272 g, 0.1 mmol) and betaine (0.116 g, 0.1 mmol) dissolved in 30 mL of ethanol and placing them in an ultrasonic bath (Ultronique Q3.0/37 A, Ecosonics, Indaiatuba, SP, Brazil). The conditions for forming the cocrystal were based on the previous works (IMCHALEE; CHAROENCHAITRAKOOL, 2015; LUO et al., 2018; PESSOA et al., 2019; WICHIANPHONG; CHAROENCHAITRAKOOL, 2018). The solution was then injected using a syringe coupled with a 0.45 μm, PTFE (polytetrafluoroethylene) filter. This solution was added to the chamber (stainless steel vessel with an internal volume of 600 cm^3, and inner diameter of 8 cm), and CO_2 was fed to a syringe pump (ISCO, Model 500D, USA) at a flow rate of 10 $mL \cdot min^{-1}$ until the desired operating pressure of 9 MPa, was reached at a constant temperature of 318K using a thermostatic bath (Nova Etica, Model 521/2D). When the pressure was reached, the antisolvent flow was stopped, and the chamber continued to agitate the

solution at 300 rpm for 10 min. After the washing stage began with the antisolvent flow at 10 $mL \cdot min^{-1}$, and the pressure was isobaric for approximately 60 min. Finally, the vessel was depressurized, and the samples were collected for characterization after the application *in vivo/in vitro*.

5.2.3. Preparation of physical mixture

Naringenin-betaine (1:1; 0.272 g: 0.116 g) is mixed with vortex mixer Fisatan (Model 772, 30 W, 60 Hz) at the maximum speed for 1 min. The final mixture was characterized.

5.2.4. Characterization methods

5.2.4.1. Morphology and determination of particle size

Scanning Electron Microscopy (SEM - JEOL JSM6390LV, United States) was used to examine the morphology of the cocrystal, physical mixture, and raw compounds. ImageJ® software was used to investigate the SEM-obtained images (SCHNEIDER; RASBAND; ELICEIRI, 2012). To obtain the average length of the particle diameter, approximately 250-300 particles were measured (SAKATA et al., 2021; SCAPINELLO et al., 2018).

5.2.4.2. Power-X-ray diffraction (XRD)

The particles were subjected to crystallographic analysis using a Rigaku MiniFlex600 X-Ray Diffractometer (3 ~ 140º – 0.01 ~ 100º/min). A copper X-ray source powered at 40 kV and 15 mA (Kα1 1.54059 Å) operating in θ-2θ scan mode. Scans were measured between 5°-35° with a scan rate of 6° min^{-1} and step size of 0.02° (AMANI; SAADATI ARDESTANI; MAJD, 2021; DIAS et al., 2022).

5.2.4.3. Differential scanning calorimetry (DSC)

A thermogram was obtained using Perkin Elmer equipment (Jade-DSC). Single heating cycles were carried out in the range of 20 to 350 °C using hermetically sealed aluminum

crucibles with a dynamic nitrogen environment (20 mL·min^{-1}) and heating rate of 10 °C·min^{-1} (PESSOA et al., 2019).

5.2.4.4. Fourier- transform infrared (FTIR) spectroscopy

The particles commercial and processed by GAS technique were analyzed using Agilent Technologies (Cary 600 Series FTIR Spectrometer) with an attenuated total reflectance accessory with ZnSe Crystal. The instrument had a resolution of 2 cm^{-1}, and the range of absorption spectra in the infrared region was 4000 cm^{-1} to 500 cm^{-1} (DAL MAGRO et al., 2017).

5.2.4.5. Specific surface area

Using Autosorb-1 equipment from Quantachrome Instruments, the surface areas of cocrystal and physical mixture naringenin-betaine were evaluated using the Brunauer–Emmett–Teller (BET) method based on N_2 adsorption-desorption (JOHNSON et al., 2020). The samples were outgassed for 18 hours at 130 °C under N_2 flow.

5.2.5. High-performance liquid chromatography (HPLC) analyses

NRG was quantified through HPLC, using a chromatographic apparatus made of a modular system (LC-10 AD VD model pump and SPD-10A VP model variable wavelength UV-vis detector; Shimadzu, Kyoto, Japan) and completed with an injection valve provided of a 10 µL sample loop (model 7725; Rheodyne, IDEX, Torrance, CA, USA). The separation was conducted at room temperature on a Force Biphenyl column (150 mm, 5 µm) with a precolumn filled with the same separation phase (Restek, Milan, Italy). Data were acquired and processed through CLASS-VP Software, version 7.2.1 (Shimadzu Italia, Milan, Italy), installed on a personal computer. The mobile phase comprised a methanol-water mixture 72:28 (v/v) ratio, and the flow rate was set at 0.8 mL·min^{-1}. The UV detector was set up at 288 nm. The retention time of NRG under these conditions was 4.9 min. The chromatographic precision for NRG was evaluated by repeated analysis (n = 6) of the same sample (50 µM – 13.62 µg·mL^{-1}) of NRG dissolved in 10 mM DPBS; the relative standard deviation (RSD) value was 0.82%. The calibration curves of peak areas versus concentration of NRG were obtained

in a range from 1 μM (0.27 μg·mL^{-1}) to 100 μM (27.22 μg·mL^{-1}) in DPBS and was linear (n = 5, r = 0.998; P < 0.0001). A preliminary analysis performed with 50 μM solutions showed that BTN did not interfere with the retention time of NRG.

5.2.6. Dissolution studies

All the samples were micronized and then sieved through stainless steel standard-mesh sieves with a mesh. size of 106 μm. In each experiment, the solid powders were poured into 12 mL of 10 mM DPBS (pH 7.4) at 37 °C and incubated in a water bath under gentle shaking (100 rpm). The quantity of sieved powders used was 10.0 mg of NRG; 14.3 mg of cocrystal NRG: BTN; 10.0 mg of NRG mixed with 4.30 mg of BTN for the physical mixtures NRG-BNT. Aliquots (200 μL) were withdrawn from the suspensions at predefined time intervals, filtered through regenerated cellulose filters (0.45 μm), and diluted 1:10 in DPBS. Ten microliters of the treated sample were injected into the HPLC system to quantify the NRG concentrations. The obtained values were the mean of three independent experiments.

5.2.7. IEC-6 cell culture and differentiation of IEC-6 cells to polarized monolayers

The rat normal small intestine epithelial IEC-6 cell line was grown in DMEM + Glutamax supplemented with 10% fetal bovine serum (FBS), 100 U/mL penicillin/streptomycin at 37 °C in a humidified atmosphere of 95%, with 5% of CO_2. After two passages in culture, confluent cells were seeded in 12-well cellQART inserts consisting of 1.0 μm pore size polyethylene terephthalate (PET) filter membranes, whose surface was 1.12 cm^2. In particular, filters were pre-soaked for 24 h with fresh culture medium; then, 400 μL of the diluted cells (2 × 10^5 cells/mL) were added to the upper compartment (apical, A), whereas 2 mL of the medium in the absence of cells was put in the lower compartment (basolateral, B). The exhausted growth medium was replaced with fresh medium both in the apical and basolateral compartments every second day until the cell monolayer was fully confluent. The day before starting the experiment the medium was replaced on both apical and basolateral compartment by the medium containing low serum (1% FBS). The integrity of the cell monolayers was monitored after 24 h by measuring the transepithelial electrical resistance (TEER, Ω·cm^2) by means of a voltmeter (Millicell-ERS; Millipore, Milan, Italy). The TEER values of cell monolayers, obtained by deducing the background resistance of blank inserts not plated with cells, reached at confluence

a stable value of 50 Ω·cm^2. The homogeneity and integrity of the cell monolayer were also monitored by phase contrast microscopy before permeation studies.

5.2.8. Permeation studies across cell monolayers

Inserts were washed three times with prewarmed DPBS buffer in the apical (A, 400 µL) and basolateral (B, 2 mL) compartments; DPBS buffer containing 0.9 mM calcium, 0.5 mM magnesium and 5.3 mM glucose at 37 °C was then added to both compartments. In this phase, the TEER values of the monolayers were measured. The sieved powders were then added to the apical compartments of inserts both in the presence and in the absence of cell monolayer in the following amounts: 0.33 mg of NRG; 0.48 mg of cocrystal made of NRG and BTN; 0.33 mg of NRG mixed with 0.14 mg of BTN for the parent physical mixture. During permeation experiments, cellQART inserts loaded with the powders were continuously swirled on an orbital shaker (100 rpm; model 711/CT, ASAL, Cernusco, Milan, Italy) at 37 °C. At programmed time points, the inserts were removed and transferred into the subsequent well containing fresh DPBS; then basolateral DPBS was harvested, filtered through regenerated cellulose filters (0.45 µm), and injected (10 µL) into the HPLC system for NRG detection and quantification. At the end of incubation, the apical slurries were withdrawn, filtered, and injected into the HPLC system (10 µL). After the withdrawal of apical samples, 400 µL of DPBS was added in the apical compartments that were inserted in the original basolateral compartments of cellQART plates filled with 2 mL of DPBS, in order to perform TEER measurements. Permeation experiments were also conducted using cell-free inserts in the same conditions. The values obtained were the mean of three independent experiments. Apparent permeability coefficients (P_{app}) of NRG were calculated according to equation 1 (ARTURSSON; KARLSSON, 1991; PAL; UDATA; MITRA, 2000; RAJE et al., 2003).

$$P = \frac{\frac{dc}{dt} \cdot V_r}{S_A \cdot C} \quad (1)$$

where P_{app} is the apparent permeability coefficient in cm/min; dc/dt is the flux of drug across the filters, calculated as the linearly regressed slope through linear data; V_r is the volume in the receiving compartment (basolateral = 2 mL); S_A is the diffusion area (1.12 cm^2); and C is the compound concentration in the donor chamber (apical) detected at 60 min and chosen as the approximate apical concentration. The permeabilities were determined for the filters alone (P_f) and for the filters covered by cells (P_t). The apparent permeability

coefficients P_E referred to the cellular monolayer were then calculated as follows equation 2 (PAL; UDATA; MITRA, 2000; YEE, 1997)

$$\frac{1}{P_E} = \frac{1}{P_t} - \frac{1}{P_f} \quad (2)$$

5.2.9. Statistical analysis about permeation studies

Statistical comparisons between apparent permeability coefficients of NRG were performed by one-way ANOVA followed by Dunnett's post-test; statistical comparisons between the transepithelial electrical resistance before and after incubation with the sieved samples were performed using t-test. $P < 0.05$ was considered statistically significant. All the calculations were performed by using the computer program Graph Pad Prism (GraphPad Software Incorporated, San Diego, CA, USA), which was also used for the linear regression of the cumulative amounts of the compounds in the basolateral compartments of the cellQART systems. The fit quality was determined by evaluating the correlation coefficients (r) and P values.

5.2.10. MTT (3-(4,5-dimethylthiazol-2-yl)-2,5-diphenyltetrazolium bromide) assay for toxicity evaluation in IEC-6 cells

IEC-6 cells were seeded in 96-well plates at a density of 30000 cells/well and reached the confluence in 24 hours. The cells were washed three times with Dulbecco's phosphate buffer saline (DPBS), without calcium and magnesium, supplemented with 0.9 mM calcium, 0.5 mM magnesium and, 5.3 mM glucose. Then, they were incubated for 1 h at 37 °C in a 95% humidified atmosphere with 5% CO_2 with NRG, the mixture and its cocrystal at the same conditions of dissolution and permeation experiments (0.833 mg of NRG alone, 0.833 mg of NRG mixed with 0.36 mg of BTN for the parent physical mixture, and 1.19 mg of cocrystal per 1 mL of DPBS supplemented with calcium, magnesium and glucose) and their dilutions 1:10 and 1:100. After 1 h of incubation of 0.2 mL of the suspensions, the cells were assayed with the 3-(4,5-dimethylthiazol-2-yl)-2,5-diphenyltetrazolium (MTT) test for their viability: the incubation buffer was withdrawn, and 0.2 mL of MTT solution (0.5 $mg \cdot mL^{-1}$) in DPBS were added to each well (4 h; 37 °C and 5% CO_2). After the conversion of the substrate to a chromogenic product by metabolically active cells, the MTT solution was removed, and the purple MTT formazan crystals were solubilized with 0.1 mL/well of DMSO for 30 min at 37 °C in an orbital shaker incubator. Finally, the absorbance of each well was measured at 570 nm

using a microtiter plate reader (Sunrise® Microplate Reader, Tecan Trading AG, Switzerland). The values were expressed as cell vitality percentages with respect to control in the absence of compounds. Each reported value represents the mean of four independent incubation experiments. Cell viability data were statistically analyzed by one-way ANOVA followed by Dunnett's multiple comparisons test. $P < 0.05$ was considered statistically significant.

5.2.11. ECV304 cell culture

ECV304 cells (obtained from American Type Culture Collection; ATCC CRL-1998) are maintained at 37°C in a humidified atmosphere of 5% CO_2. Cells were grown in DMEM supplemented with 10% fetal bovine serum (FBS, Lonza Biosciences, Switzerland), L-glutamine (2 mM; Sigma-Aldrich) and 1% Penicillin-Streptomycin (Sigma-Aldrich). Medium was exchanged every 02 days. ECV304 has been described as an appropriate monoculture model to assess the blood-brain barrier, permeability, demonstrating tighter barrier function than other endothelial cell lines. Combined with chromatography-mass spectroscopy analysis, it is a fast and successful technique to screen bioactive compounds crossing the BBB (YANG; JIN; ZHAO, 2018).

5.2.12. MTT (3-(4,5-dimethylthiazol-2-yl)-2,5-diphenyltetrazolium bromide) assay for toxicity evaluation in ECV304 cells

In this assay, we evaluate the cell viability of ECV304 cells exposed to different concentrations of naringenin, a physical mixture, and a cocrystal of naringenin: betaine. Cells were seeded in 96-well culture plates at a density of approximately 10,000 cells/well and cultured incubated (37°C, 5% CO_2) overnight. After, the cells ECV304 were exposed to different concentrations of NRG, NRG-BTN Mix, and cocrystal NRG:BTN Coc (200, 20, 2, and 0.2 µM) and maintained overnight, concentrations are based on other similar studies (CUI et al., 2019; YOUDIM et al., 2004). After 24 h of treatment, the cell viability was analyzed using MTT Cell Proliferation Kit I (MTT, 11465007001, Roche Life Science). After changing the medium with substance-free one, 10µL/well of MTT (3-(4,5-dimethylthiazol, 2-yl)-2,5-diphenyltetrazolium bromide) reagent was added and incubated for 4 hours protected from light at 37°C, 5% CO_2. This assay is based on the cleavage of yellow tetrazolium salt MTT (3-(4,5-dimethylthiazol-2-yl)-2,5- diphenyl tetrazolium bromide labeling reagent) to purple formazan

crystals by metabolic active cells. Then, 100 µL of solubilization solution was added to each well. Cells were incubated overnight to dissolve the formazan crystal, and the absorbance 570 nm was measured using a microplate reader (Thermo Fisher Scientific). Cell culture treated with Triton X-100 (Sigma-Aldrich) served as a negative control, while untreated cells were considered as 100% viability.

5.2.13. Permeation studies across endothelial cells

Permeability assays were performed using Tissue Culture (TC) Inserts containing polyethylene terephthalate (PET) membrane with 3µm pores (Sarstedt, Nümbrect, Germany). This assay is designed to assess the permeability of compounds (raw NRG, physical mixture NRG-BTN Mix, and cocrystal NRG: BTN Coc), an *in vitro* model that simulates the blood-brain barrier. A total of 150 000 cells/well were plated on TC Inserts, with proliferation medium added in the upper (apical) and bottom (basal) compartments. The cells were then maintained overnight (37 °C, 5% CO_2) to allow the cells to form a confluent monolayer. After incubation, the culture medium was carefully removed from both apical and basal compartments. In the basal compartment, 1500 µL of fresh proliferation medium was added. A volume of 500 µL containing the treatment compounds was added to apical compartment. The treatments were NRG, NRG: BTN Coc and NRG-BTN Mix with concentrations of 2 µM and 0.2 µM and incubated (37 °C, 5% CO_2). After 2 hours of incubation, the sample aliquots from both apical and basal compartments were collected to quantify naringenin using Ultra-High Performace Liquid Chromatography- MS/MS (UPLC-MS/MS).

For calculation, apparent permeability (Papp) was used in the following equation (3):

$$\text{Papp} = \frac{V_{acc}}{\text{Aera x Time}} \times \frac{c_{acc}}{C_{initial,d}} \quad (3)$$

Where: V_{acc}: volume of transport buffer in acceptor well; Area: surface area of the insert (1.31 cm^2); Time: time of the assay (7200 s); C_{acc}: concentration of test compound in acceptor well; $C_{initial, d}$: initial concentration of test compound in a donor well.

For calculation, apparent % recovery was used the following equation (4) (CHEN et al., 2023; HANDA et al., 2023; LAURANZANO et al., 2019):

$$\% \text{ Recovery} = \frac{(c_{acc} \times V_{acc}) + (C_d \times V_d)}{C_{initial,d} \times V_d} \times 100 \quad (4)$$

Where: V_{acc}: volume of compound solution in acceptor well (cm^3); V_d: volume of compound solution in donor well (cm^3); C_{acc}: concentration of test compound in acceptor well; $C_{initial,d}$: initial concentration of test compound in a donor well.

5.2.14. UPLC-MS/MS methodology

To perform UPLC-MS/MS analyses, an Acquity High Class with ESI TQD Xevo Waters Company was employed to quantify naringenin in TC-Insert in endothelial cells. A Luna Omega 1.6 µm, Polar C18 (50 mm x 2.1 µm) column was used to separate the target analytes maintained at 40°C. The flow rate was 0.4 mL/min, and the mobile phases comprised of water containing 0.1% formic acid (A) and ACN 0.1% formic acid (B) was the following gradient elution program: Initial (95% A, 5% B), 4 min (5% A and 95% B), 5 min (5% A and 95% B), 5.10 min (95% A and 5% B). The injection volume was 1µL. The detection was operated in positive ESI ion mode with optimum MS parameter setting as follows: Parent ion: 273.1642, quantification Fragment: 153.013 (cone voltage: 44 V; collision energy: 22 V) and Parent ion: 273.1642 Qualification Fragment: 146.971 (cone voltage: 44 V; collision energy: 20 V).

For the preparation of samples of naringenin in a culture medium they were centrifuged at 14000 rpm for 30 minutes at 4°C. The UPLC-MS/MS precision for naringenin was evaluated by repeated analyses (n=6) of the samples 5 to 200 total ng (ng in 50 µL of matrix).

5.3. RESULTS AND DISCUSSION

5. 3.1. Characterization of particles results

5.3.1.1. Morphology and determination of particle size results

Figure 31 reports the SEM images evidencing the morphology of raw naringenin, betaine; cocrystal naringenin: betaine, and physical mixture. Raw NRG and BTN present morphology with multi-shaped particles of various sizes and rounded, respectively. Cocrystal NRG:BTN shows that morphology differs from that of raw compounds, small plate-like crystals covered with smaller flakes, which are different from those of raw components. Physical mixture NRG-BTN shows morphology similar to raw compounds with larger particles. The mean particle diameter of the particles was 65.78 µm for raw naringenin and 76.65 µm for raw

betaine. For the cocrystal and physical mixture (naringenin-betaine) the mean particle diameter was 9.05 and 110.93 µm, respectively.

Figure 31-SEM (a) raw naringenin (NRG), (b) raw betaine (BTN), (c) cocrystal naringenin-betaine (NRG: BTN Coc), and (d) the parent physical mixture (NRG-BTN Mix).

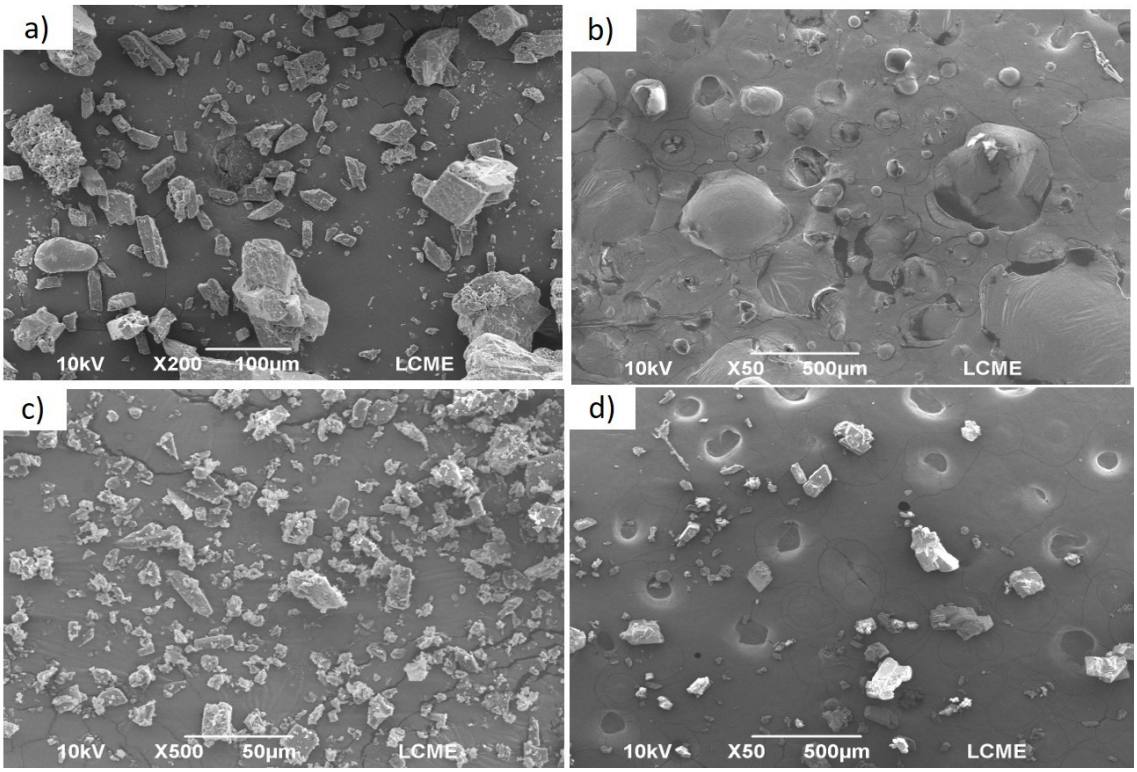

Source: Author (2024)

5.3.1.2. Power-X-ray diffraction (XRD) results

X-ray powder diffraction characterized the raw and cocrystallized physical mixture of naringin-betaine particles. Figure 32 illustrates the results obtained. The XRD raw naringenin has diffraction angles (2Θ) 10.97°, 11.65°, 15.95°, 18.26°, 20.57°, 22.45°, 25.51°, and 27°, 86° (AMANI; SAADATI ARDESTANI; MAJD, 2021; MIAO et al., 2018). For raw betaine the main peaks (2Θ) were 12.2°; 15.51°;16.56°; 17.78°; 19.47°; 20.40°; 22.67°; 24,41°, and 28.84° (CUI et al., 2019). The reflections of the cocrystal NRG:BTN processed using gas antisolvent technique was 6.44°, 8.08°, 10.14°, 10.44°, 12.96°, 13.34°, 14.86°, 15.52°, 17.82°, 18.76°, 19.4°, 20.5°, 21.68°, 25.2°, 25.74°, 25.56°, 26.62°, and 27.42°. It is observed that new reflections appear after the formation of the cocrystal, as well as the disappearance of some of the main reflections of the raw compounds NRG and BTN, evidencing the formation of the

cocrystal NRG:BTN (CUI et al., 2019; LUO et al., 2018). Naringenin:betaine GAS cocrystal exhibited new peaks at (2Θ) 6.49°, 8.12°, 14.87° and 18.77°, indicating the formation of a new solid form. In addition to shifts and/or displacements of naringenin peaks 10.74°, 11.49°, 15.80°, 17.26°, 19.93°, 20.46°, 22.26°, 23.78, 27.73° and for betaine 12.20°, 13.65° and 22.26°. Furthermore, the structure of this cocrystal is already cataloged in the literature in the Cambridge Structural Database (CSD), under CCDC number:1820098, and the database identified: LEYFIH, presents the peaks with the same profile as the cocrystal produced by the GAS technique (LUO et al., 2018). It is added that the main peaks of the NRG-BTN Mix are 10.8°, 11.44°, 13.3°, 15.75°, 16.38°, 18.01°, 19.35°, 20.05°, 21.21°, 22.38°, 23.54°, 24.30°, 25.17°, and 27.68°, in which they present a different profile of reflections compared to the cocrystal.

Figure 32- XRD analysis of raw naringenin (NRG) and betaine (BTN), cocrystal (NRG: BTN Coc), and the parent physical mixture (NRG-BTN Mix), and reference CCDC n°1820098.

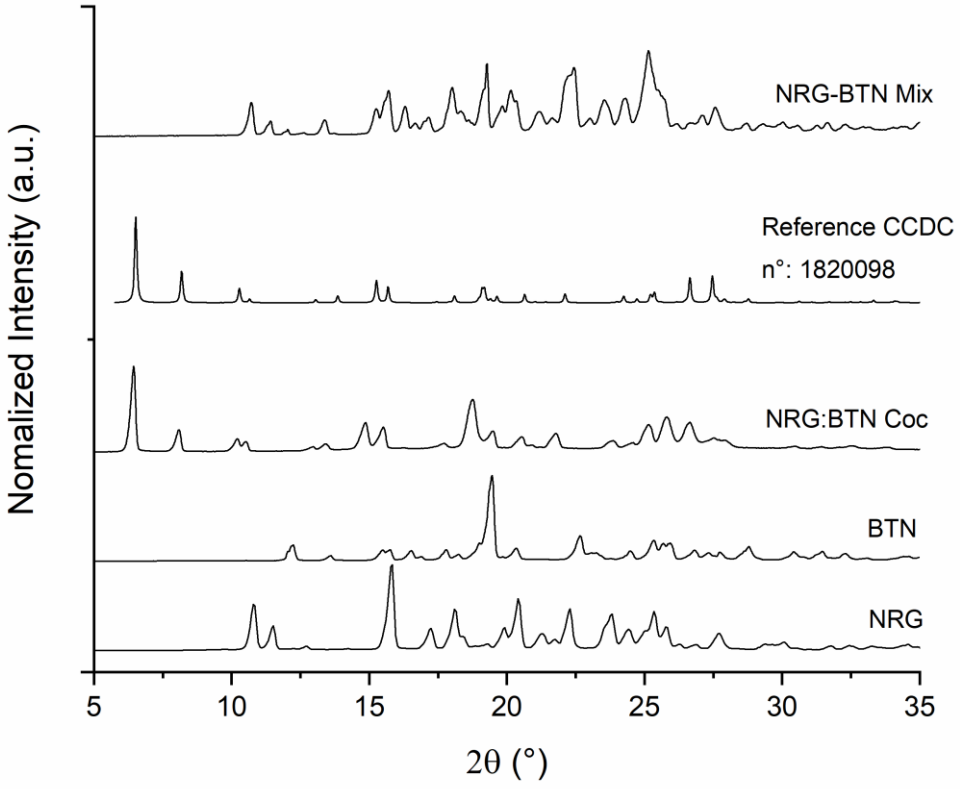

Source: Author (2024)

5.3.1.3. Differential scanning calorimetry (DSC) results

Thermograms of raw NRG and BTN, cocrystal (NRG:BTN) and physical mixture (NRG-BTN) were shown in Figure 33. Raw naringenin and betaine shows an endothermic event at 246 °C (ΔH=168. 61 $J \cdot g^{-1}$), and 293.78°C (ΔH =673.2015 $J \cdot g^{-1}$), respectively. Cocrystal NRG:BTN shows a new melting temperature at 199.81°C (ΔH=84.5719 $J \cdot g^{-1}$), agreeing with the literature (LUO et al., 2018); generally, the point cocrystal melting is between or below the coformer and target molecule (CUI et al., 2019). The physical mixture NRG-BTN had a melting point of 250.27°C (ΔH=5.9147 $J \cdot g^{-1}$), different from the cocrystal.

Figure 33- DSC analysis of raw naringenin (NRG) and betaine (BTN), cocrystal (NRG: BTN Coc) and the parent physical mixture (NRG-BTN Mix).

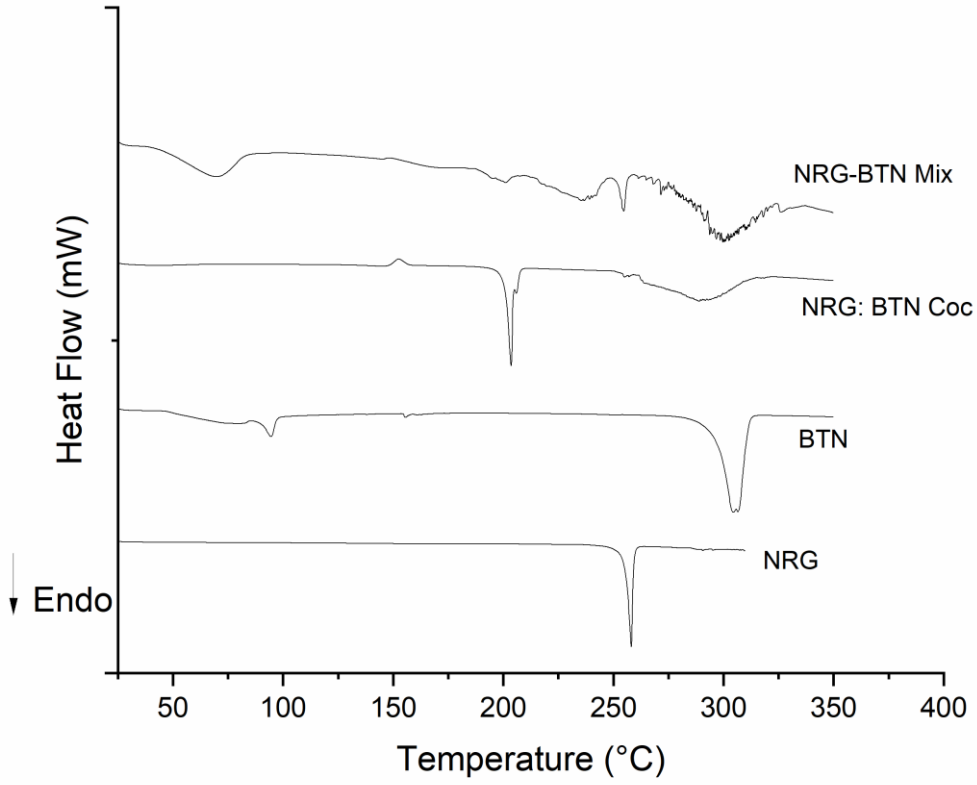

Source: Author (2024)

5.3.1.4. Fourier- transform infrared (FTIR) spectroscopy results

The FTIR spectrum (Figure 34) NRG shows feature absorption peaks at 3299 and 1641 cm^{-1}, corresponding to the -OH and C=O, stretching, respectively, in accordance with previous studies (JI et al., 2016; KHAN et al., 2015; KUMAR et al., 2015; MAITY et al., 2017). For BTN, the characteristics peak at 3386.34, 1641.10, and 1346 cm^{-1}, denoting the vibrations of -OH, C=O, and C-N, respectively (CUI et al., 2019; LUO et al., 2018).In the NRG:BTN cocrystal the most obvious peak difference between raw materials and cocrystal is in hydroxyl and carbonyl vibration, 3367.98 and 1621.97 cm^{-1}, respectively. These findings agree with the literature; these hydroxyl···carbonyl intermolecular interaction (supramolecular synthon) observed in NRG: BTN cocrystals, indicated the formation of hydrogen bonds between the molecules (CUI et al., 2019; LUO et al., 2018; ZHANG et al., 2019b). In the physical mixture NRG-BTN, there was no indicated hydrogen bonding formed between the target molecule and coformer.

Figure 34- FTIR analysis of raw naringenin (NRG) and betaine (BTN), cocrystal (NRG:BTN Coc), and the parent physical mixture (NRG-BTN Mix).

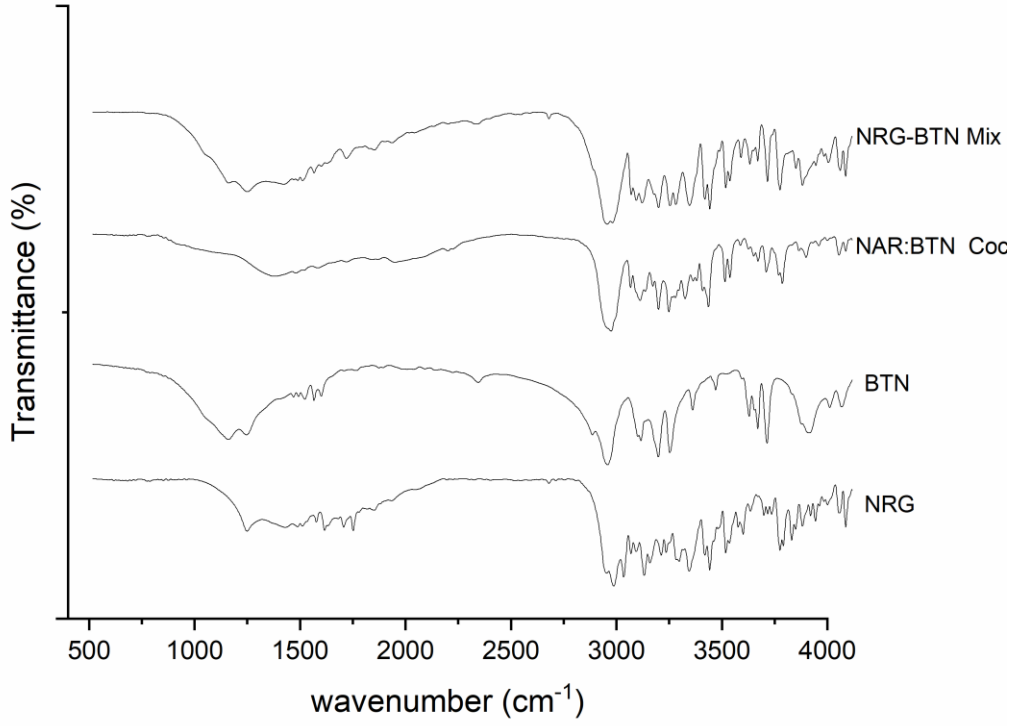

Source: Author (2024)

5.3.1.5. Specific surface area results

Cocrystal NRG:BTN presented a specific surface area of 7.04 $m^2 \cdot g^{-1}$, while the specific surface area of the physical mixture NRG-BTN was 1.04 $m^2 \cdot g^{-1}$. Also, the compound bioactive naringenin shows a specific surface area of 0.6954 $m^2 \cdot g^{-1}$. In other words, the GAS-processed cocrystal increased the specific surface area by 6 times compared to the physical mixture and 10 times compared to raw naringenin.

This fact can be explained because when the particle size is decreased, the larger surface area of the drug allows the increase in the surface area to volume ratio, thus increasing the surface area available for solvation. Consequently, particle size reduction technologies are routinely used to improve the bioavailability of poorly soluble drugs (NOYES; WHITNEY, 1897; WILLIAMS et al., 2013).

5.3.2. Dissolution studies

The dissolution profiles within 180 min in 10 mM DPBS at 37 °C of NRG as a free drug, cocrystallized with BTN, or mixed in the parent mixture are reported in Figure 35. The saturation concentration of free NRG was reached within 15 min of its incubation in the buffer, showing a value of about 60 μg/mL which was maintained during the remaining incubation time. This dissolution profile did not appear significantly altered when NRG was mixed with BTN. On the other hand, the cocrystal NRG:BTN was associated with both an increase of NRG concentration and dissolution rate. Indeed, the NRG concentration values were about 80 μg/mL at 15 min of incubation and further increased to about 100 μg/mL at 30 min of incubation, then slightly decreased, showing a value of about 80 μg/mL at 180 min of incubation. These data appear in good agreement with those obtained by previous dissolution studies of NRG:BTN cocrystals. In particular, Luo et al. also performed the cocrystallization by slurry technique and got cocrystal NRG: BTN by two forms (A and B), which showed better solubility and the intrinsic dissolution rate of NRG:BTN forms A and B, respectively increased 1.78 and 1.93 times compared to pure NRG (LUO et al., 2018).

The formation of cocrystals can influence the enhancement of the dissolution rate. The lattice energy of cocrystal decreases during the cocrystalization step. This lower lattice energy of the cocrystal facilitates the disruption of the structure, increasing the dissolution rate (BRITTAIN, 2013). The low melting point of the cocrystal may be the basis for the decreased crystal energy

that causes the enhanced dissolution rate (SEO et al., 2017). The decrease in particle size, widely known, is related to the increase in surface area and decrease in the diffusion layer thickness, which causes an enhancement in the dissolution rate (JAIN; PATEL; LIN, 2015; SEO et al., 2017).

Figure 35- Solubility and dissolution profiles in DPBS 10 mM at 37 °C for naringenin as free drug (NRG), or cocrystallized with betaine (NRG:BTN Coc), or mixed in the parent mixture (NRG-BTN Mix).

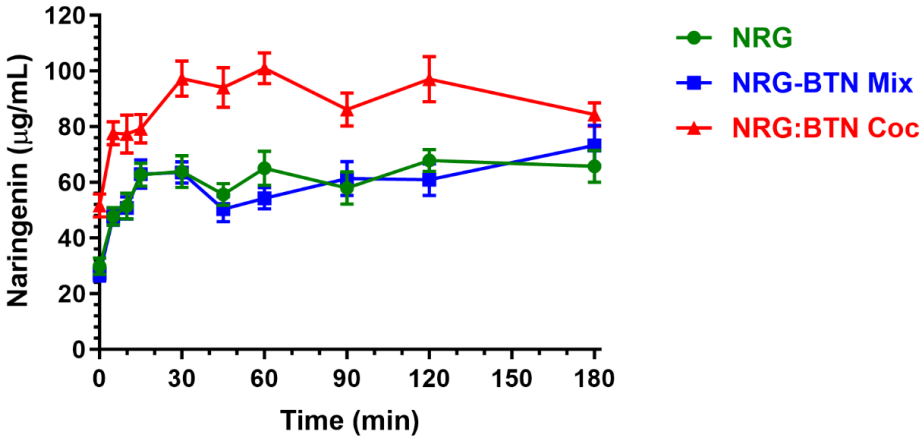

Source: Author (2024)

5.3.3. Permeation studies

The permeation studies of NRG across the *in vitro* model of the small intestinal wall, constituted by IEC-6 cells, were performed using glucose-enriched DPBS as an incubation medium. In order to simulate an oral administration, the sieved powders of NRG, its cocrystal with BTN, or the parent mixture were added in the apical compartment of the "cellQART" systems with the same ratio between solid powders and the same incubation medium used for dissolution studies. For permeation studies, the analysis time was 60 min for all samples. The cumulative amounts of NRG in the basolateral receiving compartments were linear within 60 min ($n = 4$, $r \geq 0.966$, $P < 0.0001$), as reported in Figure 36, indicating constant permeation conditions within this range of time, both in the presence and absence of cell monolayers coating the polyethylene terephthalate (PET) filter membranes.

Figure 36- Permeation kinetics of naringenin after introduction in the "cellQART" apical compartments of powders constituted by free naringenin (NRG), its cocrystal (NRG:BTN Coc), or the parent mixture (NRG-BTN Mix). The permeations were analysed across both cellQART filters alone (filters) and coated by monolayers obtained by IEC-6 cells (cells). The cumulative amounts in the basolateral receiving compartments were linear within 60 min ($n = 4$, $r \geq 0.966$, $P < 0.0001$). All data are reported as mean ± SD of three independent experiments.

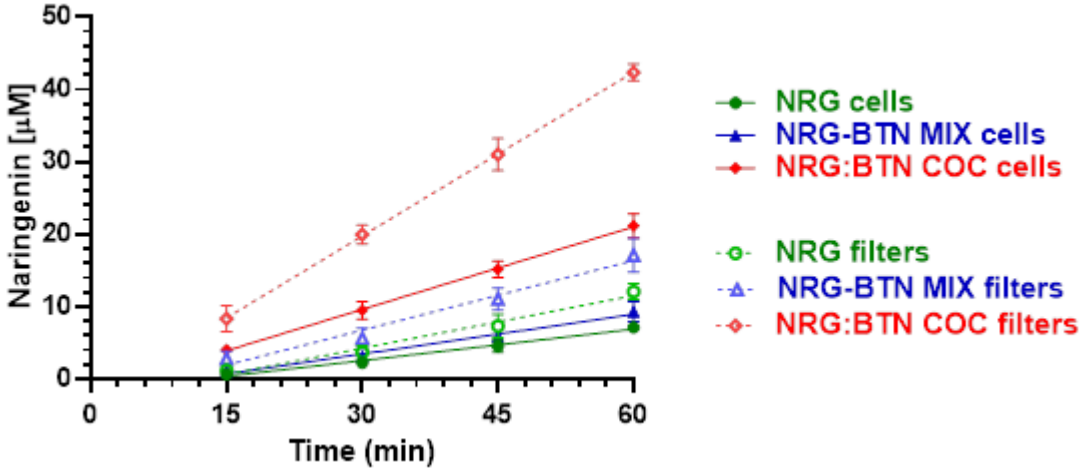

Source: Author (2024)

A comparison between the patterns obtained in the presence or in the absence of IEC-6 monolayers for each type of powder incubated (Figure 36) indicated a lower permeation of the drug in the presence of cells than in their absence, confirming the ability of the cell monolayers to behave as a physiologic barrier. Accordingly, the TEER values measured at confluence for the IEC-6 monolayers were about 50 $\Omega \cdot cm^2$ as reported in Figure 37 (TEER values at 0 min), as expected for this type of cell line (GILDEA; ROBERTS; BUSH, 2017).

Figure 37- Transepithelial electrical resistance (TEER) values of IEC-6 monolayers obtained when cell cultures reached the confluence (0 min) and at the end (60 min) of incubation with naringenin (NRG), its cocrystal with betaine (NRG: BTN Coc), and the parent physical mixture (NRG-BTN Mix). The data are reported as the mean ± SD of three independent experiments. *P < 0.05 versus 0 min; **P < 0.01 versus 0 min.

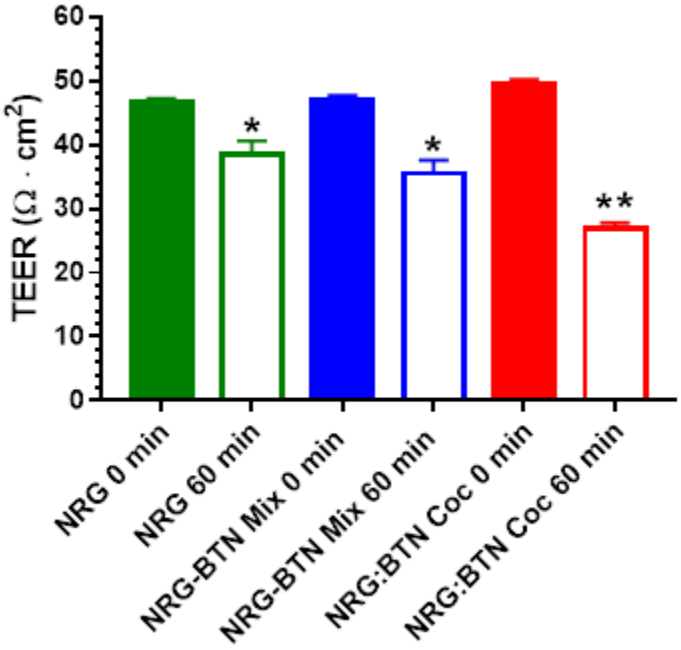

Source: Author (2024)

The resulting slopes of the linear fits reported in Figure 36 allowed us to calculate the apparent permeability coefficients (P_E) of NRG (Figure 38) according to equations 1 and 2. For equation 1 application, the drug concentrations detected in the apical compartments after 1 h of incubation of the powders were used as approximate apical concentrations.

Figure 38- Permeability coefficients (P_E) of naringenin across IEC-6 monolayers after an introduction in the "cellQART" apical compartments of powders constituted by free naringenin (NRG), its cocrystal with betaine (NRG: BTN Coc), or the parent mixture (NRG-BTN Mix). All data are reported as the mean ± SD of three independent experiments.

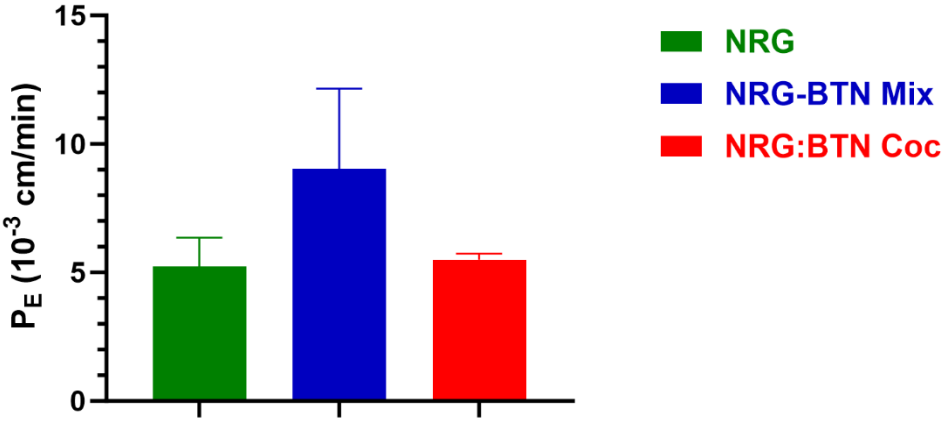

Source: Author (2024

The P_E value of pure NRG across IEC-6 monolayers was 5.23 ± 1.13 · 10^{-3} cm/min and did not appear significantly altered ($P > 0.05$) by the presence of BTN in the physical mixture (P_E = 9.03 ± 3.13 · 10^{-3} cm/min) or the cocrystal (P_E = 5.49 ± 0.24 · 10^{-3} cm/min). These results indicate that the more efficient permeation pattern reported in Figure 36 of NRG as cocrystal in comparison to the pure or mixed drug cannot be attributed to an increase of its permeability coefficient across the cell monolayers, but solely to its improved dissolution in DPBS. The P_E values evidence that NRG itself is characterized by a high aptitude to permeate across the IEC-6 monolayers, a phenomenon that can be related to the ability of the drug to significantly decrease the TEER value of the monolayer during its incubation (as reported in Figure 37), hence suggesting the capacity of NRG to open the tight junctions of the IEC-6 cells. In this case, the mixture or cocrystallization of NRG with BTN did not appear suitable to modify this aptitude of the drug. This behaviour is different in comparison to that evidenced by carbamazepine (CBZ) cocrystals, where cocrystallization allows both to restore the TEER values, which are reduced by the drug incubation, and to modify the permeability coefficient of CBZ (DALPIAZ et al., 2018). Similarly, the cocrystallization of nitrofurantoin (NITRO) with isoniazide allows to increase its permeability coefficient (SEGALINA et al., 2022). Again, some cocrystals of indomethacin appear able to sensibly modulate the TEER values of intestinal

cell monolayers, whereas other does not induce any effects (FERRETTI et al., 2015), as evidenced in this case for the NRG: BTN cocrystal.

The cocrystal NRG:BTN can be however considered suitable to increase the oral bioavailability of NRG, taking into account its ability to increase the solubility and dissolution rate of this compound. Accordingly, Reggane et al, despite the inability of the cocrystal imatinib-synergic acid to alter the drug permeability across the artificial membranes, suggested that this cocrystal may induce improved oral bioavailability through higher kinetic solubility at the biological barriers (REGGANE et al., 2018). Similarly, other studies evidence the ability of cocrystals to modify the drug permeability across artificial membranes by changes in solubility of the drugs (DAI et al., 2016; EEDARA et al., 2019; PALANISAMY et al., 2021; SAIKIA et al., 2015; SANPHUI et al., 2015).

These considerations appear confirmed by the *in vivo* behaviour of an NRG:BTN cocrystal obtained by the cocrystallization technique of the solution. In particular, the oral bioavailability of cocrystal in rats was greater than that of pure naringenin. The cocrystal was allowed to induce an NRG maximum plasma concentration (Cmax) increased 3.35 times and AUC 4.91 fold, higher than pure naringenin (CUI et al., 2019).

5.3.4. IEC-6 cell viability

Taking into account the NRG effects on TEER values of intestinal cell monolayers, the potential toxicities toward IEC-6 cells of this drug, its cocrystal and physical mixture were evaluated. In particular, IEC-6 were exposed for 1h at 37°C to NRG, its cocrystal with BTN and its physical mixture firstly at the same conditions of dissolution and permeation experiments (saturation conditions), then after dilution 1:10 and 1:100, to investigate their potential cytotoxic effect on the intestinal barrier when orally administered; after the incubation with the compounds as different formulations and amounts, the cells were incubated with MTT solution in DPBS for 4 h. As reported in Figure 39, the viability assessment indicated that all the suspensions at saturation conditions and diluted 1:10 induce a significant decrease of the cell viability compared to control ($P < 0.01$), with values ranging from 40 and 65%. On the contrary, the dilutions 1:100 (with NRG concentration estimated 30 μM, or 8.3 μg/mL) of raw NRG, parent physical mixture and cocrystal did not affect the viability of the intestinal cells. Interestingly, no differences in cell viability assessment were found among the three different

formulations, indicating that only the concentration of NRG, and not the cocrystallization technique, influence the cytotoxicity of the parent drug on the intestinal barrier.

Figure 39- Cell viability of IEC-6 cells incubated with different suspensions made of naringenin alone (NRG), naringenin and betaine as physical mixture (NRG-BTN Mix), and cocrystal of naringenin and betaine (NRG:BTN Coc). Data of MTT assay are presented as cell viability percentage (%) normalized to control (in the absence of compounds) for IEC-6 cells incubated with naringenin, the mixture and its cocrystal at the same conditions of dissolution and permeation experiments and diluted 1:10 and 1:100. Data are expressed as mean ± S.E.M. of four independent experiments. Data were statistically analyzed by one-way ANOVA followed by Dunnett's multiple comparisons test. *P<0.01 vs Control.

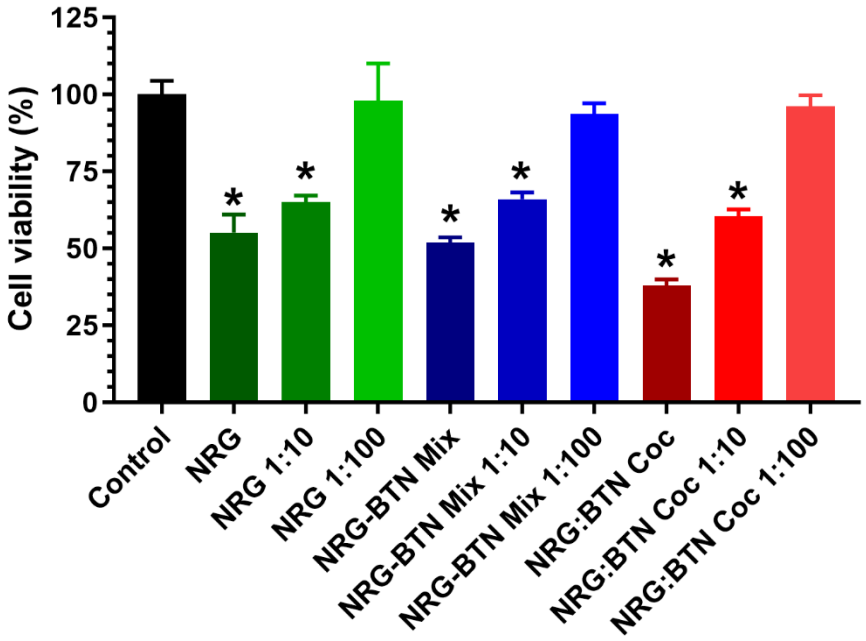

Source: Author (2024)

5.3.5. ECV304 cell viability

The cell viability shown in Figure 40, these concentrations 2 and 0.2 µM were used for permeability tests in the BBB, as they do not present toxic effects to the cell for the cocrystal and physical mixing. The 2 µM concentration showed cytotoxicity for commercial naringenin, moreover, the 200 and 20 µM concentrations showed cytotoxicity effects for all molecules due to the higher concentration of solvent DMSO. The cell viability in all these studied

concentrations shows that NRG, NRG-BTN Mix, and NRG:BTN Coc displayed dose-dependent toxicity.

Figure 40-Cell viability of naringenin (NRG), physical mixture (NRG-BTN Mix) and cocrystal (NRG: BTN Coc) after 24 hours treatment in ECV304. Data are reported as the mean ± SD of three independent experiments.

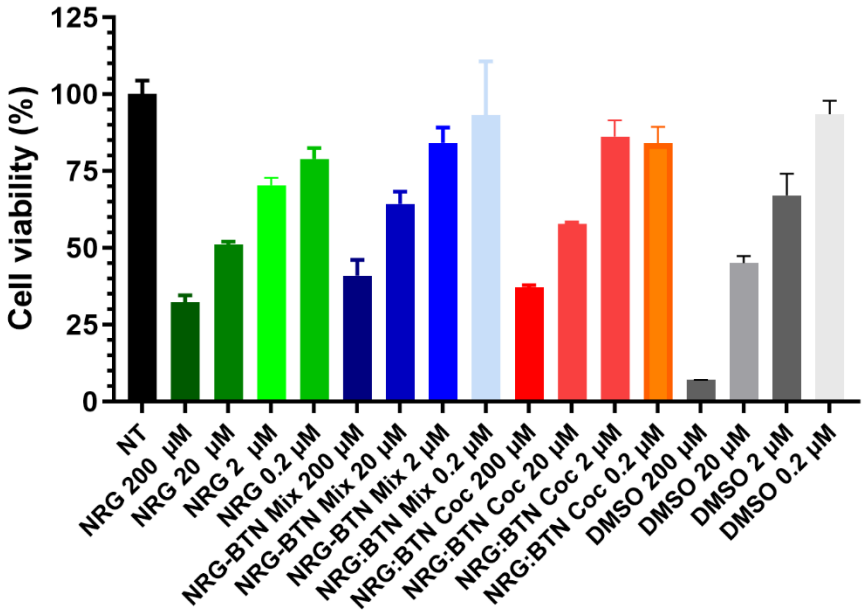

Source: Author (2024)

5.3.6. Permeation studies in endothelial cells

In Table 3, it was observed that for commercial naringenin, physical mixture, and cocrystal at 2 µM apparent permeability (Papp) and % recovery was higher for naringenin; however, this may be caused by more significant toxicity of naringenin at this concentration; as seen in the MTT assay. Next, the Papp and % recovery in concentration 2 µM physical mixture and cocrystal showed similar values, probably because the cocrystal, when in solution, presents a dissociation between the molecules, target, and coformer, and is no longer in the form of a cocrystal. In some cases, the presence of a coformer influences the permeation of the target molecule. This behavior is expected and was observed in literature by Do Amaral et al. (DO AMARAL et al., 2018). Also, the percentage recoveries of flavonoids not found to cross the

monolayer ranged between 70-90%, suggesting in some cases, significant membrane retention (YOUDIM et al., 2003).

In this study, it was observed that for both the cocrystal and physical mixture (concentrations 2 μM), there was better naringenin permeability if relatively compared when present alone in the solution. Thus, in some way, the presence of coformer, in this case, betaine, can influence the permeation of cocrystal and the physical mixture (DO AMARAL et al., 2018). This phenomenon can be explained by the betaine synergic effect on the absorption amount of naringenin. This effect can be observed in the literature on cocrystal baicalein and caffeine in pharmacokinetic studies (ZHU et al., 2017). Also, the data of this work agrees with the study of Cui et al. who synthesized NRG: BTN cocrystals with betaine using the solution crystallization technique. They evaluated the anti-hyperlipidemia effects in male Sprague-Dawley rats. The results showed that cocrystal NRG:BTN has C_{max} 3.35 times higher than pure NRG. Also, the NRG:BTN cocrystal showed drug distribution in five internal organs, increasing oral absorption and antihyperlipidemic effect, and drug distribution in the liver after oral administration was significantly increased compared to pure NRG (CUI et al., 2019). However, future studies were necessary to understand better and elucidate the compounds' permeation mechanism in the blood-brain barrier.

Table 3-Behavior of commercial naringenin, physical mixture (NRG-BTN) and cocrystal (NRG:BTN) *in vitro* model of the blood-brain barrier formed by ECV304 cells.

Compounds	Concentration (μM)	Papp x 10^{-6} (cm/s)	Recovery (%)
Naringenin	2*	70.35	100.85
Naringenin	0.2	7.60	27.79
NAR-BTN Mix	2	47.98	80.07
NAR:BTN Coc	2	49.32	80.22

Legend: *2 μM concentration is cytotoxic, what was observed by cell viability assay. Thus, these values might have a bias due to the possible damage of the barrier integrity.

Source: Author (2024)

5.4.CONCLUSION

In this study, cocrystals of NRG:BTN (1:1) were successfully synthesized using the gas antisolvent technique and characterized. The data obtained by dissolution, permeation, and viability studies suggest that the ability of the NRG:BTN cocrystal to increase the solubility of naringenin can be potentially useful to enhance the oral bioavailability of this drug; this cocrystal should be, however administered frequently with relatively low doses, in order to optimize the absorption in the bloodstream and safety of naringenin. The data indicate that both the cocrystal and the physical mixture present similar behavior in the permeation of the blood-brain barrier. However, it is important to highlight that the presence of betaine, regardless of whether it is in the form of a physical mixture or cocrystal, synergistically contributes to increasing the permeability of naringenin in the BBB, due to its synergistic effect when combined with naringenin. However, future studies were necessary to better understand and elucidate the compounds' permeation mechanism in the blood-brain barrier.

6. FINAL CONCLUSIONS

This work presents micronization and cocrystallization using the GAS technique as interesting strategies to improve the dissolution and solubility of naringin and naringenin and, consequently, improve bioavailability. Furthermore, the micronized forms of naringin and naringenin, when tested *in vivo*, showed antipsychotic potential against positive symptoms of schizophrenia using the ketamine-induced hyperlocomotion model in mice. The cocrystal naringenin:betaine and *in vitro* permeation across intestinal cells (IEC-6) and BBB cells (ECV 304). The results suggest a synergistic effect of NRG and BTN for the cocrystal and physical mixture in enhancing NRG permeation through the BBB. These results indicate that the NRG:BTN cocrystal is potentially helpful, following its oral administration with low doses of cocrystal, and frequently administered doses are required for safe intestinal absorption. Therefore, this work opens a potential for the application of micronized naringenin, naringin, and the cocrystal NRG:BTN for the treatment of another disease. Furthermore, it opens avenues for the evaluation of their peripheral effects.

REFERENCES

AAKERÖY, C. B.; FASULO, M. E.; DESPER, J. Cocrystal or salt: Does it really matter? **Molecular Pharmaceutics**, v. 4, n. 3, p. 317–322, maio 2007.

AALTO, S. et al. Frontal and temporal dopamine release during working memory and attention tasks in healthy humans: A positron emission tomography study using the high-affinity dopamine D2 receptor ligand [11C]FLB 457. **Journal of Neuroscience**, v. 25, n. 10, p. 2471–2477, 9 mar. 2005.

ABLORDEPPEY, S. Y. et al. Identification of a butyrophenone analog as a potential atypical antipsychotic agent: 4-[4-(4-Chlorophenyl)-1,4-diazepan-1-yl]-1-(4-fluorophenyl)butan-1-one. **Bioorganic & Medicinal Chemistry**, v. 16, n. 15, p. 7291–7301, 1 ago. 2008.

ADAMI, R. et al. Supercritical antisolvent technique for the production of breathable naringin powder. **Pharmaceutics**, v. 14, n. 8, p. 1623, 3 ago. 2022.

AGUBATA, C. Self-Emulsifying Formulations: A Pharmaceutical Review. **Journal of Drug Delivery and Therapeutics**, v. 10, n. 3, p. 231–240, 15 maio 2020.

AGUIAR, G. P. S. et al. Trans-resveratrol micronization by SEDS technique. **Industrial Crops and Products**, v. 89, p. 350–355, 30 out. 2016.

AGUIAR, G. P. S. et al. Micronization of N-acetylcysteine by supercritical fluid: evaluation of in vitro and in vivo biological activity. **Journal of Supercritical Fluids**, v. 130, p. 282–291, 1 dez. 2017.

AGUIAR, G. P. S. et al. Micronization of trans-resveratrol by supercritical fluid: Dissolution, solubility and in vitro antioxidant activity. **Industrial Crops and Products**, v. 112, p. 1–5, 1 fev. 2018.

AGUS, S.; ACHMADI, S. S.; MUBARIK, N. R. Antibacterial activity of naringenin-rich fraction of pigeon pea leaves toward Salmonella thypi. **Asian Pacific Journal of Tropical Biomedicine**, v. 7, n. 8, p. 725–728, 1 ago. 2017.

AHMED, O. M. et al. Navel orange peel hydroethanolic extract, naringin and naringenin have anti-diabetic potentials in type 2 diabetic rats. **Biomedicine and Pharmacotherapy**, v. 94, p. 197–205, 1 out. 2017.

AINOUZ, A. et al. Modeling and prediction of cocrystal phase diagrams. **International Journal of Pharmaceutics**, v. 374, n. 1–2, p. 82–89, 2009.

AITIPAMULA, S. et al. Polymorphs, salts, and cocrystals: What's in a name? **Crystal Growth and Design**, v. 12, n. 5, p. 2147–2152, 2 maio 2012.

ALAM, M. A. et al. Effect of citrus flavonoids, naringin and naringenin, on metabolic syndrome and their mechanisms of action. **Advances in Nutrition**, v. 5, n. 4, p. 404–417, 1 jul. 2014.

ALMANSA, C. et al. Co-crystals as a new approach to multimodal analgesia and the treatment of pain. **Journal of Pain Research**, v. 12, p. 2679–2689, 2019.

ALMARSSON, Ö.; ZAWOROTKO, M. J. Crystal engineering of the composition of pharmaceutical phases. Do pharmaceutical co-crystals represent a new path to improved medicines? **Chemical Communications**, n. 17, p. 1889–1896, 2004.

ALMEIDA E SOUSA, L. et al. Supersaturation Potential of Salt, Co-Crystal, and Amorphous Forms of a Model Weak Base. **Crystal Growth and Design**, v. 16, n. 2, p. 737–748, 2016.

ALONZO, D. E. et al. Understanding the behavior of amorphous pharmaceutical systems during dissolution. **Pharmaceutical Research**, v. 27, n. 4, p. 608–618, 2010.

AMANI, M.; SAADATI ARDESTANI, N.; MAJD, N. Y. Utilization of supercritical CO2gas antisolvent (GAS) for production of Capecitabine nanoparticles as anti-cancer drug: Analysis and optimization of the process conditions. **Journal of CO2 Utilization**, v. 46, p. 101465, 1 abr. 2021.

AMIDON, G. L. et al. A Theoretical Basis for a Biopharmaceutic Drug Classification: The Correlation of in Vitro Drug Product Dissolution and in Vivo Bioavailability. **Pharmaceutical Research: An Official Journal of the American Association of Pharmaceutical Scientists**, v. 12, n. 3, p. 413–420, 1995.

ARAMINI, A. et al. Ketoprofen, lysine and gabapentin co-crystal magnifies synergistic efficacy and tolerability of the constituent drugs: Pre-clinical evidences towards an innovative therapeutic approach for neuroinflammatory pain. **Biomedicine and Pharmacotherapy**, v. 163, p. 114845, 2023.

ARTURSSON, P.; KARLSSON, J. Correlation between oral drug absorption in humans and apparent drug permeability coefficients in human intestinal epithelial (Caco-2) cells. **Biochemical and Biophysical Research Communications**, v. 175, n. 3, p. 880–885, 29 mar. 1991.

ASSOCIAÇÃO PSIQUIÁTRICA AMERICANA. **Manual de Transtornos Mentais DSM-5**. [s.l: s.n.]. v. 1

ATOKI, A. V. et al. Naringenin: its chemistry and roles in neuroprotection. **Nutritional Neuroscience**, 4 ago. 2023.

BAKHBAKHI, Y.; CHARPENTIER, P. A.; ROHANI, S. Experimental study of the GAS process for producing microparticles of beclomethasone-17,21-dipropionate suitable for pulmonary delivery. **International Journal of Pharmaceutics**, v. 309, n. 1–2, p. 71–80, 17 fev. 2006.

BELL, R. G.; KOTT, L.; BELL, R. G. Regulatory considerations in dissolution and drug release of BCS class II and IV compounds. **Nutrients and Foods in Aids**, p. 573–602, 2017.

BEN-AZU, B. et al. Possible neuroprotective mechanisms of action involved in the neurobehavioral property of naringin in mice. **Biomedicine and Pharmacotherapy**, v. 109, p. 536–546, 1 jan. 2019.

BERNAL, J. L.; MARTÍN, M. T.; TORIBIO, L. Supercritical fluid chromatography in food analysis. **Journal of Chromatography A**, v. 1313, p. 24–36, 2013.

BETTI, A. H. et al. LASSBio-1422: A new molecular scaffold with efficacy in animal models of schizophrenia and disorders of attention and cognition. **Behavioural Pharmacology**, v. 28, n. 1, p. 48–62, 1 fev. 2017.

BHANDARI, R.; PALIWAL, J. K.; KUHAD, A. Naringenin and its nanocarriers as potential phytotherapy for autism spectrum disorders. **Journal of Functional Foods**, v. 47, p. 361–375, 1 ago. 2018.

BISHNOI, M.; CHOPRA, K.; KULKARNI, S. K. Protective effect of rutin, a polyphenolic flavonoid against haloperidol-induced orofacial dyskinesia and associated behavioural, biochemical and neurochemical changes. **Fundamental and Clinical Pharmacology**, v. 21, n. 5, p. 521–529, 2007.

BLAGDEN, N. et al. Current directions in co-crystal growth. **New Journal of Chemistry**, v. 32, n. 10, p. 1659–1672, 16 out. 2008.

BOLLA, G.; NANGIA, A. Pharmaceutical cocrystals: Walking the talk. **Chemical Communications**, v. 52, n. 54, p. 8342–8360, 28 jun. 2016.

BOND, A. D. Chapter 2. Fundamental Aspects of Salts and Co-crystals. In: **Pharmaceutical Salts and Co-crystals. Cambridge**. [s.l.] The Royal Society of Chemistry, 2011. p. 9–28.

BOYCHUK, C. et al. Career decision-making processes of young adults with first-episode psychosis. **journals.sagepub.com**, v. 28, n. 6, p. 1016–1031, 1 maio 2018.

BRISTOW, S. et al. Analysis of the supersaturation and precipitation process with supercritical CO2. **The Journal of Supercritical Fluids**, v. 21, n. 3, p. 257–271, 1 nov. 2001.

BRITTAIN, H. G. Pharmaceutical cocrystals: The coming wave of new drug substances. **Journal of Pharmaceutical Sciences**, v. 102, n. 2, p. 311–317, 2013.

BRODOWSKA, K.; BRODOWSKA, K. M. Natural flavonoids: classification, potential role, and application of flavonoid analogues. **European Journal of Biological Research**, v. 7, n. 2, p. 108–123, 30 jun. 2017.

BROWN, R. J. C. F. C.; BROWN, R. J. C. F. C. Melting Point and Molecular Symmetry. **Journal of Chemical Education**, v. 77, n. 6, p. 724–731, 2000.

BRUNER, G. **Gas Extraction: An Introduction to Fundamentals of Supercritical Fluids**. [s.l.] Springer Science & Business Media, 1994. v. 4

BRUNNER, G. Supercritical fluids: Technology and application to food processing. **Journal of Food Engineering**, v. 67, n. 1–2, p. 21–33, 1 mar. 2005.

BRUNO, A. et al. Bergamot polyphenolic fraction supplementation improves cognitive functioning in schizophrenia. **Journal of Clinical Psychopharmacology**, v. 37, n. 4, p. 468–471, 1 ago. 2017.

BRUNTON, L. et al. **Goodman & Gilman: As bases farmacológicas da terapêutica**. [s.l: s.n.].

BYMASTER, F. P. et al. Radioreceptor binding profile of the atypical antipsychotic olanzapine. **Neuropsychopharmacology : official publication of the American College of Neuropsychopharmacology**, v. 14, n. 2, p. 87–96, 1996.

CASTRO, K. C. DE; COSTA, J. M.; CAMPOS, M. G. N. Drug-loaded polymeric nanoparticles: a review. **International Journal of Polymeric Materials and Polymeric Biomaterials**, p. 1–13, 2020.

CAVALLINI, C. M.; FRANCO, C. M. L. Effect of acid-ethanol treatment followed by ball milling on structural and physicochemical characteristics of cassava starch. **Starch/Staerke**, v. 62, n. 5, p. 236–245, maio 2010.

CAVIA-SAIZ, M. et al. Antioxidant properties, radical scavenging activity and biomolecule protection capacity of flavonoid naringenin and its glycoside naringin: A comparative study. **Journal of the Science of Food and Agriculture**, v. 90, n. 7, p. 1238–1244, 1 maio 2010.

CEREA, M. et al. Preparation of multiparticulate systems for oral delivery of a micronized or nanosized poorly soluble drug. v. 42, n. 9, p. 1466–1475, 1 set. 2016.

CERREIA VIOGLIO, P.; CHIEROTTI, M. R.; GOBETTO, R. Pharmaceutical aspects of salt and cocrystal forms of APIs and characterization challenges. **Advanced Drug Delivery Reviews**, v. 117, p. 86–110, 1 ago. 2017.

CHAFIDZ, A. ET AL. Formation of fine particles using supercritical fluid (SCF) process: Short review. **Communications in Science and Technology**, v. 3, n. 2, p. 57–63, 2018.

CHARBIT, G.; BADENS, E.; BOUTIN, O. Methods of particle production. **Supercritical Fluid Technology for Drug Product Development**, p. 159–212, 2004.

CHAVAN, R. B. et al. Continuous manufacturing of co-crystals: challenges and prospects. **Drug Delivery and Translational Research**, v. 8, n. 6, p. 1726–1739, 15 dez. 2018.

CHEN, A. Z. et al. Study of poly(L-lactide) microparticles based on supercritical CO 2. **Journal of Materials Science: Materials in Medicine**, v. 18, n. 12, p. 2339–2345, dez. 2007.

CHEN, H. et al. Design and characterization of a heterobifunctional degrader of KEAP1. **Redox Biology**, v. 59, p. 102552, 2023.

CHEN, K. et al. Gas antisolvent precipitation of Ginkgo ginkgolides with supercritical CO2. **Powder Technology**, v. 152, n. 1–3, p. 127–132, 2005.

CHEN, R. et al. Therapeutic potential of naringin: an overview. **Pharmaceutical Biology**, v. 54, n. 12, p. 3203–3210, 26 dez. 2016.

CHEN, T. et al. Micronization and nanosizing of particles for an enhanced quality of

food: A review. **Critical Reviews in Food Science and Nutrition**, v. 58, n. 6, p. 993–1001, 13 abr. 2018.

CHENG, Y. et al. Micronization of etoposide using solution-enhanced dispersion by supercritical CO2. **Journal of Supercritical Fluids**, v. 115, p. 10–16, 1 set. 2016.

CHIENG, N.; RADES, T.; AALTONEN, J. An overview of recent studies on the analysis of pharmaceutical polymorphs. **Journal of Pharmaceutical and Biomedical Analysis**, v. 55, n. 4, p. 618–644, 2011.

CHIOU, W. L. The rate and extent of oral bioavailability versus the rate and extent of oral absorption: Clarification and recommendation of terminology. **Journal of Pharmacokinetics and Pharmacodynamics**, v. 28, n. 1, p. 3–6, 2001.

CHTOUROU, Y. et al. Anti-apoptotic and anti-inflammatory effects of naringin on cisplatin-induced renal injury in the rat. **Chemico-Biological Interactions**, v. 243, p. 1–9, 5 jan. 2016.

CHUNG, T. W. et al. Antinociceptive and anti-inflammatory effects of the citrus flavanone naringenin. **Tzu Chi Medical Journal**, v. 31, n. 2, p. 81–85, 2019.

CLARK, S. R. et al. Elevated clozapine levels associated with infection: A systematic review. **Schizophrenia Research**, v. 192, p. 50–56, 1 fev. 2018.

COCERO, M.; MARTIN, A. Precipitation Processes with Supercritical Fluids: Patents Review. **Recent Patents on Engineering**, v. 2, n. 1, p. 9–20, 2008.

CONCEA. **Diretriz da prática de eutanásia do concea**. Disponível em: <https://ceua.ufop.br/sites/default/files/ceua/files/resolucao-normativa-n-37-diretriz-da-pratica-de-eutanasia_site-concea.pdf?m=1534249510>. Acesso em: 6 mar. 2021.

CONLEY, R. R.; BUCHANAN, R. W. Evaluation of treatment-resistant schizophrenia. **Schizophrenia Bulletin**, v. 23, n. 4, p. 663–674, 1 jan. 1997.

COYLE, J. T. Glutamate and schizophrenia: beyond the dopamine hypothesis. **Cellular and molecular neurobiology**, v. 26, n. 4–6, p. 365–384, 2006.

COYLE, J. T. et al. Glutamatergic synaptic dysregulation in schizophrenia: Therapeutic implications. **Handbook of Experimental Pharmacology**, v. 213, p. 267–295, 2012.

CSICSÁK, D. et al. The Effect of the Particle Size Reduction on the Biorelevant Solubility and Dissolution of Poorly Soluble Drugs with Different Acid-Base Character. **Pharmaceutics**, v. 15, n. 1, 2023.

CUADRA, I. A. et al. Cocrystallization of the anticancer drug 5-fluorouracil and coformers urea, thiourea or pyrazinamide using supercritical CO2 as an antisolvent (SAS) and as a solvent (CSS). **Journal of Supercritical Fluids**, v. 160, p. 104813, 2020.

CUI, W. et al. Naringenin Cocrystals Prepared by Solution Crystallization Method for Improving Bioavailability and Anti-hyperlipidemia Effects. **AAPS PharmSciTech**, v. 20, n. 3,

p. 1–12, 1 abr. 2019.

CULLITY, BERNARD DENNIS; STOCK, S. R. **Elements of X-ray Diffraction**. [s.l.] Pearson India Education Services, 2014.

DA SILVA, R. P. F. F.; ROCHA-SANTOS, T. A. P.; DUARTE, A. C. Supercritical fluid extraction of bioactive compounds. **TrAC - Trends in Analytical Chemistry**, v. 76, p. 40–51, 1 fev. 2016.

DAI, X. L. et al. Improving the Membrane Permeability of 5-Fluorouracil via Cocrystallization. **Crystal Growth and Design**, v. 16, n. 8, p. 4430–4438, 3 ago. 2016.

DAL MAGRO, C. et al. Co-precipitation of trans-resveratrol in PHBV using Solution Enhanced Dispersion by Supercritical Fluids technique. **Journal of Supercritical Fluids**, v. 127, p. 182–190, 1 set. 2017.

DALPIAZ, A. et al. From Physical Mixtures to Co-Crystals: How the Coformers Can Modify Solubility and Biological Activity of Carbamazepine. **Molecular Pharmaceutics**, v. 15, n. 1, p. 268–278, 2 jan. 2018.

DALVI, S. V.; MUKHOPADHYAY, M. A novel process for precipitation of ultra-fine particles using sub-critical CO2. **Powder Technology**, v. 195, n. 3, p. 190–195, 2009.

DE BERARDIS, D. et al. Safety of antipsychotics for the treatment of schizophrenia: a focus on the adverse effects of clozapine. **Therapeutic Advances in Drug Safety**, v. 9, n. 5, p. 237–256, maio 2018.

DE FILIPPIS, R. et al. Current and emerging long-acting antipsychotics for the treatment of schizophrenia. **Expert Opinion on Drug Safety**, v. 20, n. 7, p. 771–790, 2021.

DE OLIVEIRA, P. V. et al. Micronization of naringenin in supercritical fluid medium: In vitro and in vivo assays. **Journal of Drug Delivery Science and Technology**, v. 82, p. 104382, 1 abr. 2023.

DEBENEDETTI, P. G. et al. Rapid expansion of supercritical solutions (ress): fundamentals and applications. **Fluid Phase Equilibria**, v. 82, n. C, p. 311–321, 1993.

DEBNATH, S.; PREDECKI, P.; SURYANARAYANAN, R. Use of glancing angle X-ray powder diffractometry to depth-profile phase transformations during dissolution of indomethacin and theophylline tablets. **Pharmaceutical Research**, v. 21, n. 1, p. 149–159, jan. 2004.

DECUI, L. et al. Micronized resveratrol shows promising effects in a seizure model in zebrafish and signalizes an important advance in epilepsy treatment. **Epilepsy Research**, v. 159, p. 106243, 1 jan. 2020.

DEHGHANI, F.; FOSTER, N. R. Dense gas anti-solvent processes for pharmaceutical formulation. **Current Opinion in Solid State and Materials Science**, v. 7, n. 4–5, p. 363–369, 2003.

DESIRAJU, G. R. Crystal engineering: A holistic view. **Angewandte Chemie -**

International Edition, v. 46, n. 44, p. 8342–8356, 2007.

DI CARLO, G. et al. Inhibition of intestinal motility and secretion by flavonoids in mice and rats: structure-activity relationships. **Journal of Pharmacy and Pharmacology**, v. 45, n. 12, p. 1054–1059, 1993.

DIAS, J. L. et al. Production of quercetin-nicotinamide cocrystals by gas antisolvent (GAS) process. **Journal of Supercritical Fluids**, v. 188, p. 105670, 1 set. 2022.

DO AMARAL, L. H. et al. Development and Characterization of Dapsone Cocrystal Prepared by Scalable Production Methods. **AAPS PharmSciTech**, v. 19, n. 6, p. 2687–2699, 2 ago. 2018.

DODDS, S.; WOOD, J. A.; CHARPENTIER, P. A. Modeling of the Gas-Antisolvent (GAS) process for crystallization of beclomethasone dipropionate using carbon dioxide. **Industrial and Engineering Chemistry Research**, v. 46, n. 24, p. 8009–8017, 2007.

DOS SANTOS LIMA, B. et al. Inclusion complex with cyclodextrins enhances the bioavailability of flavonoid compounds: a systematic review. **Phytochemistry Reviews**, v. 18, n. 5, p. 1337–1359, 1 out. 2019.

DOUROUMIS, D.; ROSS, S. A.; NOKHODCHI, A. Advanced methodologies for cocrystal synthesis. **Advanced Drug Delivery Reviews**, v. 117, p. 178–195, 2017.

DRESSMAN, J. B.; REPPAS, C. In vitro-in vivo correlations for lipophilic, poorly water-soluble drugs. **European Journal of Pharmaceutical Sciences**, v. 11, n. SUPPL. 2, p. S73–S80, 2000.

DUNITZ, J. D. Crystal and co-crystal: A second opinion. **CrystEngComm**, v. 5, p. 506, 2003.

EEDARA, B. B. et al. Crystalline adduct of moxifloxacin with trans-cinnamic acid to reduce the aqueous solubility and dissolution rate for improved residence time in the lungs. **European Journal of Pharmaceutical Sciences**, v. 136, p. 104961, 1 ago. 2019.

EGERTON, A. et al. Dopamine and Glutamate in Antipsychotic-Responsive Compared with Antipsychotic-Nonresponsive Psychosis: A Multicenter Positron Emission Tomography and Magnetic Resonance Spectroscopy Study (STRATA). **Schizophrenia Bulletin**, v. 47, n. 2, p. 505–516, 10 set. 2021.

ELDER, D. P.; HOLM, R.; DE DIEGO, H. L. Use of pharmaceutical salts and cocrystals to address the issue of poor solubility. **International Journal of Pharmaceutics**, v. 453, n. 1, p. 88–100, 2013.

ELKIS, H. et al. Consenso Brasileiro sobre antipsicóticos de segunda geração e distúrbios metabólicos. **Revista Brasileira de Psiquiatria**, v. 30, n. 1, p. 77–85, mar. 2008.

ELKIS, H.; MELTZER, H. Y. Refractory schizophrenia. **Revista Brasileira de Psiquiatria**, v. 29, n. SUPPL. 2, 2007.

EMAMI, S. et al. Recent advances in improving oral drug bioavailability by cocrystals.

BioImpacts, v. 8, n. 4, p. 305–320, 2018.

EMRAN, T. BIN et al. Naringin and Naringenin Polyphenols in Neurological Diseases: Understandings from a Therapeutic Viewpoint. **Life 2023, Vol. 13, Page 99**, v. 13, n. 1, p. 99, 29 dez. 2022.

EMRAN, T. BIN et al. Naringin and naringenin polyphenols in neurological diseases: understandings from a therapeutic viewpoint. **Life**, v. 13, n. 1, p. 99, 2023.

ESFANDIARI, N. Production of micro and nano particles of pharmaceutical by supercritical carbon dioxide. **Journal of Supercritical Fluids**, v. 100, p. 129–141, 2015.

ESFANDIARI, N.; SAJADIAN, S. A. CO2 utilization as gas antisolvent for the pharmaceutical micro and nanoparticle production: A review. **Arabian Journal of Chemistry**, v. 15, n. 10, p. 104164, 2022.

ETTER, M. C.; REUTZEL, S. M. Hydrogen Bond Directed Cocrystallization and Molecular Recognition Properties of Acyclic Imides. **Journal of the American Chemical Society**, v. 113, n. 7, p. 2586–2598, 1991.

ETZL, E. E.; WINTER, G.; ENGERT, J. Toward intradermal vaccination: Preparation of powder formulations by collapse freeze-drying. **Pharmaceutical Development and Technology**, v. 19, n. 2, p. 213–222, 2014.

EUROPEAN MEDICINES AGENCY. Reflection paper on the use of cocrystals of active substances in medicinal products. p. 1–10, 2014.

EUROPEAN PARLIAMENT AND COUNCIL. Directive 2010/63/EU of the European parliament and of the council of 22 September 2010 on the protection of animals used for scientific purposes (Text with EEA relevance). **Official Journal of the European Union**, v. 276, p. 33–79, 2010.

FAGES, J. et al. Particle generation for pharmaceutical applications using supercritical fluid technology. **Powder Technology**, v. 141, n. 3, p. 219–226, 2004.

FAHIM, T. K. et al. Particle formation and micronization using non-conventional techniques- review. **Chemical Engineering and Processing: Process Intensification**, v. 86, p. 47–52, 1 dez. 2014.

FANG, S. H. et al. Morin sulfates/glucuronides exert anti-inflammatory activity on activated macrophages and decreased the incidence of septic shock. **Life Sciences**, v. 74, n. 6, p. 743–756, 2003.

FDA. **Guidance for Industry Regulatory Classification of Pharmaceutical Co-Crystals Guidance for Industry Regulatory Classification of Pharmaceutical Co-Crystals**. Disponível em: <http://www.fda.gov/downloads/Drugs/Guidances/UCM281764.pdf>. Acesso em: 23 jul. 2020.

FERRETTI, V. et al. Indomethacin co-crystals and their parent mixtures: Does the intestinal barrier recognize them differently? **Molecular Pharmaceutics**, v. 12, n. 5, p. 1501–

1511, 4 maio 2015.

FLEISCHMAN, S. G. et al. Crystal Engineering of the Composition of Pharmaceutical Phases: Multiple-Component Crystalline Solids Involving Carbamazepine. **Crystal Growth and Design**, v. 3, n. 6, p. 909–919, nov. 2003.

FRANCESCHI, E. et al. Precipitation of β-carotene and PHBV and co-precipitation from SEDS technique using supercritical CO2. **The Journal of Supercritical Fluids**, v. 47, n. 2, p. 259–269, 1 dez. 2008.

FRIIĆ, T. et al. The role of solvent in mechanochemical and sonochemical cocrystal formation: A solubility-based approach for predicting cocrystallisation outcome. **CrystEngComm**, v. 11, n. 3, p. 418–426, 23 fev. 2009.

FRIŠČIČ, T.; JONES, W. Recent advances in understanding the mechanism of cocrystal formation via grinding. **Crystal Growth and Design**, v. 9, n. 3, p. 1621–1637, 2009.

FUSARO, F.; MAZZOTTI, M.; MUHRER, G. Gas antisolvent recrystallization of paracetamol from acetone using compressed carbon dioxide as antisolvent. **Crystal Growth and Design**, v. 4, n. 5, p. 881–889, set. 2004.

GADADE, D. D.; PEKAMWAR, S. S. Pharmaceutical cocrystals: Regulatory and strategic aspects, design and development. **Advanced Pharmaceutical Bulletin**, v. 6, n. 4, p. 479–494, 2016.

GAJDA, M. et al. Continuous, one-step synthesis of pharmaceutical cocrystals via hot melt extrusion from neat to matrix-assisted processing – State of the art. **International Journal of Pharmaceutics**, v. 558, p. 426–440, 10 mar. 2019.

GALLAGHER, P. M. et al. Gas Antisolvent Recrystallization: New Process To Recrystallize Compounds Insoluble in Supercritical Fluids. In: ACS Public ed. [s.l: s.n.]. p. 334–354, 1989.

GANAPATHY, E. et al. Modulatory effect of naringenin on N-methyl-N′-nitro-N-nitrosoguanidine- and saturated sodium chloride-induced gastric carcinogenesis in male wistar rats. **Clinical and Experimental Pharmacology and Physiology**, v. 35, n. 10, p. 1190–1196, out. 2008.

GAO, Z. et al. Recent Developments in the Crystallization Process: Toward the Pharmaceutical Industry. **Engineering**, v. 3, n. 3, p. 343–353, 2017.

GATTUSO, G. et al. Flavonoid composition of citrus juices. **Molecules**, v. 12, n. 8, p. 1641–1673, 3 ago. 2007.

GEORGE, M. Y. et al. Potential therapeutic antipsychotic effects of naringin against ketamine-induced deficits in rats: involvement of Akt/GSK-3β and Wnt/β-catenin signaling pathways. **Life Sciences**, v. 249, p. 117535, 15 maio 2020.

GEORGE, M. Y. et al. Naringin treatment improved main clozapine-induced adverse effects in rats; emphasis on weight gain, metabolic abnormalities, and agranulocytosis. **Drug Development Research**, v. 82, n. 7, p. 21800, 1 fev. 2021.

GEYER, M. A.; ELLENBROEK, B. Animal behavior models of the mechanisms underlying antipsychotic atypicality. **Progress in Neuro-Psychopharmacology and Biological Psychiatry**, v. 27, n. 7, p. 1071–1079, 2003.

GHOSAL, K.; GHOSH, D.; DAS, S. K. Preparation and evaluation of naringin-loaded polycaprolactone microspheres based oral suspension using Box-Behnken design. **Journal of Molecular Liquids**, v. 256, p. 49–57, 15 abr. 2018.

GIL-RAMÍREZ, A.; RODRIGUEZ-MEIZOSO, I. Purification of Natural Products by Selective Precipitation Using Supercritical/Gas Antisolvent Techniques (SAS/GAS). **Separation and Purification Reviews**, v. 50, n. 1, p. 32–52, 21 maio 2021.

GILDEA, J. J.; ROBERTS, D. A.; BUSH, Z. Protective Effects of Lignite Extract Supplement on Intestinal Barrier Function in Glyphosate-Mediated Tight Junction Injury. **Journal of Clinical Nutrition & Dietetics**, v. 03, n. 01, p. 1, 2017.

GIROTRA, P.; SINGH, S. K.; NAGPAL, K. Supercritical fluid technology: A promising approach in pharmaceutical research. **Pharmaceutical Development and Technology**, v. 18, n. 1, p. 22–38, fev. 2013.

GOLDWASSER, J. et al. Naringenin inhibits the assembly and long-term production of infectious hepatitis C virus particles through a PPAR-mediated mechanism. **Journal of Hepatology**, v. 55, n. 5, p. 963–971, 1 nov. 2011.

GRECO, K.; BOGNER, R. Crystallization of amorphous indomethacin during dissolution: effect of processing and annealing. **Molecular Pharmaceutics**, v. 7, n. 5, p. 1406–1418, 4 out. 2010.

GROOM, C. R. et al. The Cambridge structural database. **Acta Crystallographica Section B: Structural Science, Crystal Engineering and Materials**, v. 72, n. 2, p. 171–179, 2016.

GROSSO, C. et al. The Use of Flavonoids in Central Nervous System Disorders. **Current Medicinal Chemistry**, v. 20, n. 37, p. 4694–4719, 2013.

GU, H. S. et al. Synthesis and biological evaluation of novel flavanone derivatives as potential antipsychotic agents. **Chemical Biology & Drug Design**, v. 89, n. 3, p. 353–364, 1 mar. 2017.

GUPTA, D. et al. Salts of Therapeutic Agents: Chemical, Physicochemical, and Biological Considerations. **Molecules**, v. 23, n. 7, p. 1719, 14 jul. 2018.

GÜRSUL, C. et al. Protective effect of Naringin on experimental hindlimb ischemia/reperfusion injury in rats. **Journal of Enzyme Inhibition and Medicinal Chemistry**, v. 31, p. 56–61, 2016.

HA, E. S. et al. Enhancement of dissolution and bioavailability of ezetimibe by amorphous solid dispersion nanoparticles fabricated using supercritical antisolvent process. **Journal of Pharmaceutical Investigation**, v. 45, n. 7, p. 641–649, 1 dez. 2015.

HAKUTA, Y.; HAYASHI, H.; ARAI, K. Fine particle formation using supercritical fluids. **Current Opinion in Solid State and Materials Science**, v. 7, n. 4–5, p. 341–351, 2003.

HALL, D. A.; STRANGE, P. G. Evidence that antipsychotic drugs are inverse agonists at D2 dopamine receptors. **British Journal of Pharmacology**, v. 121, n. 4, p. 731–736, 1 jun. 1997.

HANDA, K. et al. Prediction of Compound Plasma Concentration-Time Profiles in Mice Using Random Forest. **Molecular Pharmaceutics**, v. 20, n. 6, p. 3060–3072, 5 jun. 2023.

HANNA, M.; YORK, P. **Method and apparatus for the formation of particles.HANNA, Mazen; YORK, Peter. Method and apparatus for the formation of particles. U.S. Patent n. 6,063**. , 2000.

HANWELL, M. D. et al. Avogadro: An advanced semantic chemical editor, visualization, and analysis platform. **Journal of Cheminformatics**, v. 4, n. 8, p. 17, 13 ago. 2012.

HASKINS, M. M. et al. Tuning the Pharmacokinetic Performance of Quercetin by Cocrystallization. **Crystal Growth & Design**, v. 23, n. 8, p. 6059–6066, 2 ago. 2023.

HEALY, A. M. et al. Pharmaceutical solvates, hydrates and amorphous forms: A special emphasis on cocrystals. **Advanced Drug Delivery Reviews**, v. 117, p. 25–46, 1 ago. 2017.

HEGAZY, H. G.; ALI, E. H. A.; SABRY, H. A. The neuroprotective action of naringenin on oseltamivir (Tamiflu) treated male rats. **The Journal of Basic & Applied Zoology**, v. 77, p. 83–90, 1 out. 2016.

HENG, D. et al. What is a suitable dissolution method for drug nanoparticles? **Pharmaceutical Research**, v. 25, n. 7, p. 1696–1701, 2008.

HEO, H. J. et al. Effect of Antioxidant Flavanone, Naringenin, from Citrus junos on Neuroprotection. **Journal of Agricultural and Food Chemistry**, v. 52, n. 6, p. 1520–1525, 24 mar. 2004.

HIGUCHI, T.; CONNORS, K. A. Adv anal chem instrum. **Phase-solubility Techniques**, v. 4, p. 117–212, 1965.

HILDEBRAND, J. **Solubility**. 17. ed. [s.l.] Chemical Catalog Company, 1924.

HORACEK, J. et al. Mechanism of action of atypical antipsychotic drugs and the neurobiology of schizophrenia. **CNS Drugs**, v. 20, n. 5, p. 389–409, 2006.

HSIU, S. L. et al. Comparison of metabolic pharmacokinetics of naringin and naringenin in rabbits. **Life Sciences**, v. 70, n. 13, p. 1481–1489, 15 fev. 2002.

HURTTA, M.; PITKÄNEN, I.; KNUUTINEN, J. Melting behaviour of d-sucrose, d-glucose and d-fructose. **Carbohydrate Research**, v. 339, n. 13, p. 2267–2273, set. 2004.

HUSSAIN, K. et al. Enhanced antibacterial potential of naringin Loaded β

cyclodextrin nanoparticles. **Journal of Cluster Science**, v. 33, n. 1, p. 339–348, 2022.

HWANG, I.; KANG, C. Y.; PARK, J. B. Advances in hot-melt extrusion technology toward pharmaceutical objectives. **Journal of Pharmaceutical Investigation**, v. 47, n. 2, p. 123–132, 2017.

IMCHALEE, R.; CHAROENCHAITRAKOOL, M. Gas anti-solvent processing of a new sulfamethoxazole-l-malic acid cocrystal. **Journal of Industrial and Engineering Chemistry**, v. 25, p. 12–15, 2015.

INÊS AMARO, M. et al. Anti-inflammatory activity of naringin and the biosynthesised naringenin by naringinase immobilized in microstructured materials in a model of DSS-induced colitis in mice. **Food Research International**, v. 42, n. 8, p. 1010–1017, 1 out. 2009.

INTERNATIONAL CONFERENCE ON HARMONISATION (ICH). **Committee for Medicinal Products for Human Use ICH guideline Q3C (R8) on impurities: guideline for residual solventsICH Expert Working Group**. [s.l: s.n.]. Disponível em: <www.ema.europa.eu/contact>. Acesso em: 28 jun. 2022.

ISHOLA, I. O. et al. Prevention and reversal of ketamine-induced experimental psychosis in mice by the neuroactive flavonoid, hesperidin: The role of oxidative and cholinergic mechanisms. **Brain Research Bulletin**, v. 177, p. 239–251, 1 dez. 2021.

ISLAM, N. et al. In vitro enzymatic digestibility of glutaraldehyde-crosslinked chitosan nanoparticles in lysozyme solution and their applicability in pulmonary drug delivery. **Molecules**, v. 24, n. 7, p. 1271, 1 abr. 2019.

JAIN, A.; YANG, G.; YALKOWSKY, S. H. Estimation of melting points of organic compounds. **Industrial and Engineering Chemistry Research**, v. 43, n. 23, p. 7618–7621, 10 nov. 2004.

JAIN, H.; CHELLA, N. Methods to improve the solubility of therapeutical natural products: a review. **Environmental Chemistry Letters**, v. 19, n. 1, p. 111–121, 9 set. 2021.

JAIN, S.; PATEL, N.; LIN, S. Solubility and dissolution enhancement strategies: Current understanding and recent trends. **Drug Development and Industrial Pharmacy**, v. 41, n. 6, p. 875–887, 1 jun. 2015.

JAVITT, D. C. Twenty-five years of glutamate in schizophrenia: are we there yet? **Schizophrenia Bulletin**, v. 38, n. 5, p. 911–913, 1 set. 2012.

JI, P. et al. Naringenin-loaded solid lipid nanoparticles: Preparation, controlled delivery, cellular uptake, and pulmonary pharmacokinetics. **Drug Design, Development and Therapy**, v. 10, p. 911–925, 1 mar. 2016.

JIA, J. et al. Controlled morphology and size of curcumin using ultrasound in supercritical CO2 antisolvent. **Ultrasonics Sonochemistry**, v. 27, p. 389–394, 2015.

JIANG, J. et al. The isonicotinamide cocrystal promotes inhibitory effects of

naringenin on nonalcoholic fatty liver disease in mice. **Journal of Drug Delivery Science and Technology**, v. 59, p. 101874, 1 out. 2020.

JIN, C. Y. et al. Naringenin up-regulates the expression of death receptor 5 and enhances TRAIL-induced apoptosis in human lung cancer A549 cells. **Molecular Nutrition and Food Research**, v. 55, n. 2, p. 300–309, fev. 2011.

JOHNSON, K. ANNE et al. Drug-impregnated, pressurized gas expanded liquid-processed alginate hydrogel scaffolds for accelerated burn wound healing. **Acta Biomaterialia**, v. 112, p. 101–111, 1 ago. 2020.

JONES, C.; WATSON, D.; FONE, K. Animal models of schizophrenia. **British Journal of Pharmacology**, v. 164, n. 4, p. 1162–1194, out. 2011.

JOSHI, J. T. A Review on Micronization Techniques. **Journal of Pharmaceutical Science and Technology**, v. 3, n. 7, p. 651–681, 2011.

JUNG, J.; PERRUT, M. Particle design using supercritical fluids: Literature and patent survey. **Journal of Supercritical Fluids**, v. 20, n. 3, p. 179–219, 2001.

KALANI, M.; YUNUS, R. Application of supercritical antisolvent method in drug encapsulation: a review. **International journal of nanomedicine**, v. 6, p. 1429–1442, 2011.

KALE, D. P.; ZODE, S. S.; BANSAL, A. K. Challenges in Translational Development of Pharmaceutical Cocrystals. **Journal of Pharmaceutical Sciences**, v. 106, n. 2, p. 457–470, 1 fev. 2017.

KALKAN, E.; BUDAK, F. K. The effect of insights on medication adherence in patients with schizophrenia. **Perspectives in Psychiatric Care**, v. 56, n. 1, p. 222–228, 1 jan. 2020.

KANAZE, F. I. et al. Dissolution enhancement of flavonoids by solid dispersion in PVP and PEG matrixes: A comparative study. **Journal of Applied Polymer Science**, v. 102, n. 1, p. 460–471, 5 out. 2006.

KANAZE, F. I. et al. Pharmacokinetics of the citrus flavanone aglycones hesperetin and naringenin after single oral administration in human subjects. **European Journal of Clinical Nutrition**, v. 61, n. 4, p. 472–477, 2007.

KANDEMIR, F. M. et al. Therapeutic effects of silymarin and naringin on methotrexate-induced nephrotoxicity in rats: Biochemical evaluation of anti-inflammatory, antiapoptotic, and antiautophagic properties. **Journal of Food Biochemistry**, v. 41, n. 5, p. e12398, 1 out. 2017.

KARAGIANNI, A.; MALAMATARI, M.; KACHRIMANIS, K. Pharmaceutical cocrystals: New solid phase modification approaches for the formulation of APIs. **Pharmaceutics**, v. 10, n. 1, p. 18, 2018.

KARIMI-JAFARI, M. et al. Creating cocrystals: A review of pharmaceutical cocrystal preparation routes and applications. **Crystal Growth and Design**, v. 18, n. 10, p. 6370–6387, 3 out. 2018.

KATRITZKY, A. R. et al. Perspective on the Relationship between Melting Points and Chemical Structure. **Crystal Growth and Design**, v. 1, n. 4, p. 261–265, jul. 2001.

KAVANAGH, O. N. et al. Pharmaceutical cocrystals: from serendipity to design to application. **Drug Discovery Today**, v. 24, n. 3, p. 796–804, 2019.

KHADKA, P. et al. Pharmaceutical particle technologies: An approach to improve drug solubility, dissolution and bioavailability. **Asian Journal of Pharmaceutical Sciences**, v. 9, n. 6, p. 304–316, 1 dez. 2014.

KHAN, A. W. et al. Enhanced dissolution and bioavailability of grapefruit flavonoid Naringenin by solid dispersion utilizing fourth generation carrier. **Drug Development and Industrial Pharmacy**, v. 41, n. 5, p. 772–779, 1 maio 2015.

KHANDAVILLI, U. B. R. et al. Cocrystals and a Salt of the Bioactive Flavonoid: Naringenin. **Crystal Growth and Design**, v. 18, n. 8, p. 4571–4577, 1 ago. 2018a.

KHANDAVILLI, U. B. R. et al. Cocrystals and a salt of the bioactive flavonoid: naringenin. **Crystal Growth & Design**, v. 18, n. 8, p. 4571–4577, 1 ago. 2018b.

KIM, M. S. et al. Preparation, characterization and in vivo evaluation of amorphous atorvastatin calcium nanoparticles using supercritical antisolvent (SAS) process. **European Journal of Pharmaceutics and Biopharmaceutics**, v. 69, n. 2, p. 454–465, 1 jun. 2008.

KIM, S. J. et al. Recrystallization of cyclotetramethylenetetranitramine (HMX) using gas anti-solvent (GAS) process. **Journal of Supercritical Fluids**, v. 59, p. 108–116, 1 nov. 2011.

KIMURA, K. T. et al. Structures of the 5-HT 2A receptor in complex with the antipsychotics risperidone and zotepine. **Nature Structural and Molecular Biology**, v. 26, n. 2, p. 121–128, 2019.

KNEZ et al. Industrial applications of supercritical fluids: A review. **Energy**, v. 77, p. 235–243, 1 dez. 2014a.

KNEZ, Z. et al. Particle Formation Using Sub- and Supercritical Fluids. **Supercritical Fluid Technology for Energy and Environmental Applications**, p. 31–67, 2014b.

KNEZ, Ž. et al. Are supercritical fluids solvents for the future? **Chemical Engineering and Processing - Process Intensification**, v. 141, p. 107532, 1 jul. 2019.

KNEZ, Z.; WEIDNER, E. Particles formation and particle design using supercritical fluids. **Current Opinion in Solid State and Materials Science**, v. 7, n. 4–5, p. 353–361, 2003.

KNIGHT, A. R. et al. Pharmacological characterisation of the agonist radioligand binding site of 5-HT2A, 5-HT2B and 5-HT2C receptors. **Naunyn-Schmiedeberg's Archives of Pharmacology**, v. 370, n. 2, p. 114–123, ago. 2004.

KŐRÖSI, M. et al. Fast further purification of diastereomeric salts of a nonracemic acid by gas antisolvent fractionation. **Chirality**, v. 29, n. 10, p. 610–615, 2017.

KRISHNAKUMAR, N. et al. Enhanced anticancer activity of naringenin-loaded nanoparticles in human cervical (HeLa) cancer cells. **Biomedicine and Preventive Nutrition**, v. 1, n. 4, p. 223–231, 1 out. 2011.

KRÖBER, H.; TEIPEL, U. Materials processing with supercritical antisolvent precipitation: process parameters and morphology of tartaric acid. **The Journal of Supercritical Fluids**, v. 22, n. 3, p. 229–235, 1 abr. 2002.

KUMAR, A.; DOGRA, S.; PRAKASH, A. Protective effect of naringin, a citrus flavonoid, against colchicine-induced cognitive dysfunction and oxidative damage in rats. **Journal of Medicinal Food**, v. 13, n. 4, p. 976–984, 1 ago. 2010.

KUMAR, A.; KUMAR, S.; NANDA, A. A review about regulatory status and recent patents of pharmaceutical co-crystals. **Advanced Pharmaceutical Bulletin**, v. 8, n. 3, p. 355–363, 2018.

KUMAR, R. et al. Particle size reduction techniques of pharmaceutical compounds for the enhancement of their dissolution rate and bioavailability. **Journal of Pharmaceutical Innovation**, v. 17, n. 2, p. 333–352, 1 jun. 2022.

KUMAR, S. P. et al. Antioxidant studies of chitosan nanoparticles containing naringenin and their cytotoxicity effects in lung cancer cells. **International Journal of Biological Macromolecules**, v. 78, p. 87–95, 1 jul. 2015.

LASKOWSKI, R. A.; SWINDELLS, M. B. LigPlot+: Multiple ligand-protein interaction diagrams for drug discovery. **Journal of Chemical Information and Modeling**, v. 51, n. 10, p. 2778–2786, 24 out. 2011.

LAURANZANO, E. et al. A Microfluidic Human Model of Blood–Brain Barrier Employing Primary Human Astrocytes. **Advanced Biosystems**, v. 3, n. 7, p. 1800335, 1 jul. 2019.

LAURO, M. R. et al. Preparations and release characteristics of naringin and naringenin gastro-resistant microparticles by spray-drying. **Journal of Drug Delivery Science and Technology**, v. 17, n. 2, p. 119–124, 1 jan. 2007.

LAXMI, P. et al. Experimental data of fabricated co-crystals of doxorubicin HCl with flavonoids. **Indian Journal of Pharmaceutical Education and Research**, v. 53, n. 3, p. S225–S230, 2019.

LEE, C. et al. Cocrystal Formation via Resorcinol-Urea Interactions: Naringenin and Carbamazepine. **Crystal Growth and Design**, v. 19, n. 7, p. 3807–3814, 10 jun. 2019.

LEE, J. W.; THOMAS, L. C.; SCHMIDT, S. J. Investigation of the heating rate dependency associated with the loss of crystalline structure in sucrose, glucose, and fructose using a thermal analysis approach (Part I). **Journal of Agricultural and Food Chemistry**, v. 59, n. 2, p. 684–701, 26 jan. 2011.

LEE, K. S.; KIM, K. J.; ULRICH, J. Formation of Salicylic Acid/4,4′-Dipyridyl Cocrystals Based on the Ternary Phase Diagram. **Chemical Engineering and Technology**, v. 38, n. 6, p. 1073–1080, 1 jun. 2015.

LEE, M.-H.; YOON, S.; MOON, J.-O. The Flavonoid Naringenin Inhibits Dimethylnitrosamine-Induced Liver Damage in Rats. **Biological & Pharmaceutical Bulletin**, v. 27, n. 1, p. 72–76, jan. 2004.

LEE, S. J. S. Y. et al. Transglycosylation of naringin by Bacillus stearothermophilus maltogenic amylase to give glycosylated naringin. **Journal of Agricultural and Food Chemistry**, v. 47, n. 9, p. 3669–3674, set. 1999.

LEWIS, D. A. et al. Altered GABA neurotransmission and prefrontal cortical dysfunction in schizophrenia. **Biological Psychiatry**, v. 46, n. 5, p. 616–626, 1999.

LI, Q. et al. Supercritical fluid coating of API on excipient enhances drug release. **Chemical Engineering Journal**, v. 313, p. 317–327, 1 abr. 2017.

LI, S. et al. Mechanochemical synthesis of pharmaceutical cocrystal suspensions via hot melt extrusion: Feasibility studies and physicochemical characterization. **Molecular Pharmaceutics**, v. 13, n. 9, p. 3054–3068, 6 set. 2016.

LI, Z.; MATZGER, A. J. Influence of Coformer Stoichiometric Ratio on Pharmaceutical Cocrystal Dissolution: Three Cocrystals of Carbamazepine/4-Aminobenzoic Acid. **Molecular Pharmaceutics**, v. 13, n. 3, p. 990–995, 7 mar. 2016.

LIN, W.-C.; LIN, J.-Y. Five Bitter Compounds Display Different Anti-inflammatory Effects through Modulating Cytokine Secretion Using Mouse Primary Splenocytes in Vitro. **J. Agric. Food Chem**, v. 59, n. 1, p. 184–192, 12 jan. 2011.

LIU, G. et al. Tailoring the particle microstructures of gefitinib by supercritical CO2 anti-solvent process. **Journal of CO2 Utilization**, v. 20, p. 43–51, 1 jul. 2017.

LIU, J. et al. Co-Amorphous Drug Formulations in Numbers: Recent Advances in Co-Amorphous Drug Formulations with Focus on Co-Formability, Molar Ratio, Preparation Methods, Physical Stability, In Vitro and In Vivo Performance, and New Formulation Strategies. **Pharmaceutics 2021, Vol. 13, Page 389**, v. 13, n. 3, p. 389, 15 mar. 2021.

LONG, B. et al. Generation and physicochemical characterization of posaconazole cocrystals using Gas Antisolvent (GAS) and Supercritical Solvent (CSS) methods. **Journal of Supercritical Fluids**, v. 170, p. 105134, 2021.

LONG, B.; RYAN, K. M.; PADRELA, L. From batch to continuous — New opportunities for supercritical CO2 technology in pharmaceutical manufacturing. **European Journal of Pharmaceutical Sciences**, v. 137, p. 104971, 2019.

LOZOWSKI, D. Supercritical CO2: A green solvent. **Chemical Engineering**, v. 117, n. 2, p. 15–18, 2010.

LUO, C. et al. Pharmaceutical cocrystals of naringenin with improved dissolution performance. **CrystEngComm**, v. 20, n. 22, p. 3025–3033, 5 jun. 2018.

LV, Y. et al. Protective effect of naringenin against acetaminophen-induced acute liver injury in metallothionein (MT)-null mice. **Food and Function**, v. 4, n. 2, p. 297–302, 2013.

MA, Z. et al. Supercritical antisolvent-fluidized bed for the preparation of dry powder inhaler for pulmonary delivery of nanomedicine. **International Journal of Pharmaceutics**, v. 648, p. 123580, 15 dez. 2023.

MACEACHERN, L.; KERMANSHAHI-POUR, A.; MIRMEHRABI, M. Supercritical carbon dioxide for pharmaceutical co-crystal production. **Crystal Growth and Design**, v. 20, n. 9, p. 6226–6244, 2 set. 2020.

MAITY, S. et al. Alginate coated chitosan core-shell nanoparticles for efficient oral delivery of naringenin in diabetic animals—An in vitro and in vivo approach. **Carbohydrate Polymers**, v. 170, p. 124–132, 15 ago. 2017.

MALAMATARI, M. et al. Experimental cocrystal screening and solution based scale-up cocrystallization methods. **Advanced Drug Delivery Reviews**, v. 117, p. 162–177, 1 ago. 2017.

MANGIN, D.; PUEL, F.; VEESLER, S. ReViews Polymorphism in Processes of Crystallization in Solution: A Practical Review. **ACS Publications**, v. 13, n. 6, p. 1241–1253, 20 nov. 2009.

MARTELLO, R. H. et al. Micronization of thymol by RESS and its larvicidal activity against Aedes aegypti (Diptera, Culicidae). **Industrial Crops and Products**, v. 139, p. 111495, 1 nov. 2019.

MARTIN, A. Solubility and related properties. **Journal of Pharmaceutical Sciences**, v. 76, n. 2, p. 185–186, 1987.

MARTÍN, A.; COCERO, M. J. Micronization processes with supercritical fluids: Fundamentals and mechanisms. **Advanced Drug Delivery Reviews**, v. 60, n. 3, p. 339–350, 14 fev. 2008.

MATHUR, V. Biopharmaceutical perform-ance and stability of co-crystal. **International Journal of Pharmaceutical Frontier Research**, v. 1, n. 1, p. 135–145, 2011.

MATOS, R. L. et al. Dense CO2 technology: Overview of recent applications for drug processing/formulation/delivery. **Chemical Engineering and Processing - Process Intensification**, v. 140, p. 64–77, 1 jun. 2019.

MIAO, H. et al. Preparation and characterization of naringenin microparticles via a supercritical anti-Solvent process. **Journal of Supercritical Fluids**, v. 131, p. 19–25, 1 jan. 2018.

MISHIMA, K. Biodegradable particle formation for drug and gene delivery using supercritical fluid and dense gas. **Advanced Drug Delivery Reviews**, v. 60, n. 3, p. 411–432, 14 fev. 2008.

MOCHIZUKI, S. et al. Size-controlled recrystallization of fullerene by gas-antisolvent process. **Journal of Materials Science**, v. 45, n. 6, p. 1588–1594, mar. 2010.

MOGHADDAM, R. H. et al. Naringenin and naringin in cardiovascular disease prevention: A preclinical review. **European Journal of Pharmacology**, v. 887, p. 173535,

2020.

MOHAMED, E. A. et al. Polymeric micelles for potentiated antiulcer and anticancer activities of naringin. **International Journal of Nanomedicine**, v. 13, p. 1009–1027, 19 fev. 2018.

MOHAMMAD, M. A.; ALHALAWEH, A.; VELAGA, S. P. Hansen solubility parameter as a tool to predict cocrystal formation. **International Journal of Pharmaceutics**, v. 407, n. 1–2, p. 63–71, 4 abr. 2011.

MORAIS, R. P. et al. Naringenin-Functionalized Multi-Walled Carbon Nanotubes: A Potential Approach for Site-Specific Remote-Controlled Anticancer Delivery for the Treatment of Lung Cancer Cells. **International Journal of Molecular Sciences**, v. 21, n. 12, p. 4557, 26 jun. 2020.

MORGAN, L. V. et al. Investigation of the anti-inflammatory effects of stigmasterol in mice: insight into its mechanism of action. **Behavioural pharmacology**, v. 32, n. 8, p. 640–651, 1 dez. 2021.

MÖSCHWITZER, J. Nanotechnology: Particle size reduction technologies in the pharmaceutical development process. **American Pharmaceutical Review**, v. 13, n. 3, p. 54–59, 2010.

MOSHARRAF, M.; NYSTRÖM, C. The effect of particle size and shape on the surface specific dissolution rate of microsized practically insoluble drugs. **International Journal of Pharmaceutics**, v. 122, n. 1–2, p. 35–47, 1 ago. 1995.

MÜLLERS, K. C.; PAISANA, M.; WAHL, M. A. Simultaneous formation and micronization of pharmaceutical cocrystals by Rapid Expansion of Supercritical Solutions (RESS). **Pharmaceutical Research**, v. 32, n. 2, p. 702–713, 2015.

MUNDHE, A. V. COCRYSTALIZATION: AN ALTERNATIVE APPROACH FOR SOLID MODIFICATION. **Journal of Drug Delivery and Therapeutics**, v. 3, n. 4, p. 166, 15 jul. 2013.

MUSCATELLO, M. R. A.; ZOCCALI, R. A.; BRUNO, A. Citrus fruit polyphenols and flavonoids: Applications to psychiatric disorders. **Polyphenols: Mechanisms of Action in Human Health and Disease**, p. 119–131, 1 jan. 2018.

NAEEM, A. et al. The fate of flavonoids after oral administration: a comprehensive overview of its bioavailability. **Critical Reviews in Food Science and Nutrition**, p. 1–18, 2021.

NANGIA, A.; DESIRAJU, G. R. Supramolecular Synthons and Pattern Recognition. In: **Design of Organic Solids**. [s.l.] Design of Organic Solids, 1998. p. 57–95.

NIJVELDT, R. J. et al. Flavonoids: A review of probable mechanisms of action and potential applications. **American Journal of Clinical Nutrition**, v. 74, n. 4, p. 418–425, 2001.

NOYES, A. A.; WHITNEY, W. R. The rate of solution of solid substances in their

own solutions. **Journal of the American Chemical Society**, v. 19, n. 12, p. 930–934, 1 dez. 1897.

OKUYAMA, S. et al. Citrus flavonoid improves MK-801-induced locomotive hyperactivity: possible relevance to schizophrenia. **Journal of Functional Foods**, v. 5, n. 4, p. 2002–2006, 1 out. 2013.

PADRELA, L. et al. Formation of indomethacin-saccharin cocrystals using supercritical fluid technology. **European Journal of Pharmaceutical Sciences**, v. 38, n. 1, p. 9–17, 2009.

PADRELA, L. et al. Screening for pharmaceutical cocrystals using the supercritical fluid enhanced atomization process. **Journal of Supercritical Fluids**, v. 53, n. 1–3, p. 156–164, 1 jun. 2010.

PADRELA, L. et al. Insight into the Mechanisms of Cocrystallization of Pharmaceuticals in Supercritical Solvents. **Crystal Growth and Design**, v. 15, n. 7, p. 3175–3181, 1 jul. 2015.

PADRELA, L. et al. Supercritical carbon dioxide-based technologies for the production of drug nanoparticles/nanocrystals – A comprehensive review. **Advanced Drug Delivery Reviews**, v. 131, p. 22–78, 2018.

PAL, D.; UDATA, C.; MITRA, A. K. Transport of cosalane—A highly lipophilic novel anti-HIV agent—Across Caco-2 cell monolayers. **Journal of Pharmaceutical Sciences**, v. 89, n. 6, p. 826–833, jun. 2000.

PALANISAMY, V. et al. Tuning diffusion permeability of an anti-retroviral drug, emtricitabine, via multicomponent crystallizations. **ACS Publications**, v. 21, n. 3, p. 1548–1561, 3 mar. 2021.

PANCHE, A. N.; DIWAN, A. D.; CHANDRA, S. R. Flavonoids: An overview. **Journal of Nutritional Science**, v. 5, n. 47, p. 1–15, 8 jan. 2016.

PANDEY, N.; GHOSH, A. An outlook on permeability escalation through cocrystallization for developing pharmaceuticals with improved biopharmaceutical properties. **Journal of Drug Delivery Science and Technology**, v. 76, p. 103757, 1 out. 2022.

PANDO, C.; CABAÑAS, A.; CUADRA, I. A. Preparation of pharmaceutical co-crystals through sustainable processes using supercritical carbon dioxide: A review. **RSC Advances**, v. 6, n. 75, p. 71134–71150, 2016.

PARIKH, D. M. Handbook of pharmaceutical granulation technology. **Handbook of Pharmaceutical Granulation Technology**, p. 1–660, 2016.

PASAM, V. R. et al. Flavonoid : A review on Naringenin. **Journal of Pharmacognosy and Phytochemistry**, v. 6, n. 5, p. 2778–2783, 2017.

PATTNAIK, S.; ARUN, G.; SWAIN, K. **Supercritical Fluid Technologies: A Green Solvent Approach for Pharmaceutical Product Development**. [s.l.] Springer, Cham, 2020.

PERRUT, M.; JUNG, J.; LEBOEUF, F. Enhancement of dissolution rate of poorly-soluble active ingredients by supercritical fluid processes: part I: micronization of neat particles. **International Journal of Pharmaceutics**, v. 288, n. 1, p. 3–10, 6 jan. 2005.

PESSOA, A. S. et al. Precipitation of resveratrol-isoniazid and resveratrol-nicotinamide cocrystals by gas antisolvent. **The Journal of Supercritical Fluids**, v. 145, p. 93–102, 1 mar. 2019.

PIETRASZEK, M. Significance of dysfunctional glutamatergic transmission for the development of psychotic symptoms. **Polish Journal of Pharmacology**, v. 55, n. 2, p. 133–154, 2003.

PINDELSKA, E.; SOKAL, A.; KOLODZIEJSKI, W. Pharmaceutical cocrystals, salts and polymorphs: Advanced characterization techniques. **Advanced Drug Delivery Reviews**, v. 117, p. 111–146, 1 ago. 2017.

POOLE, R. M.; DUNGO, R. T. Ipragliflozin: First global approval. **Drugs**, v. 74, n. 5, p. 611–617, 2014.

POWELL, S. B.; GEYER, M. A. Overview of animal models of schizophrenia. **Current protocols in neuroscience / editorial board, Jacqueline N. Crawley ... [et al.]**, v. Chapter 9, n. 1, p. 9–24, abr. 2007.

PRESIDÊNCIA DA REPÚBLICA, CASA CIVIL, (SUBCHEFIA PARA ASSUNTOS JURÍDICOS). **LEI Nº 11.794, DE 8 DE OUTUBRO DE 2008 (Lei Arouca)**. **Diário Oficial da União - Seção 1 - 09/10/2008**, 2008. Disponível em: <https://scholar.google.com/scholar?hl=pt-BR&as_sdt=0%2C5&q=BRASIL%2C+LEI+Nº+11.794%2C+DE++8+DE+OUTUBRO+DE+2008.&btnG=>. Acesso em: 6 mar. 2021

PUTRA, O. D. et al. Simultaneous Improvement of Epalrestat Photostability and Solubility via Cocrystallization: A Case Study. **Crystal Growth & Design**, v. 18, n. 1, p. 373–379, 3 jan. 2018.

QIAO, N. et al. Pharmaceutical cocrystals: An overview. **International Journal of Pharmaceutics**, v. 419, n. 1–2, p. 1–11, 31 out. 2011.

RAJADURAI, M.; STANELY MAINZEN PRINCE, P. Preventive effect of naringin on lipid peroxides and antioxidants in isoproterenol-induced cardiotoxicity in wistar rats: biochemical and histopathological evidences. **Toxicology**, v. 228, n. 2–3, p. 259–268, 7 dez. 2006.

RAJE, S. et al. Evaluation of the Blood-Brain Barrier Transport, Population Pharmacokinetics, and Brain Distribution of Benztropine Analogs and Cocaine Using in Vitro and in Vivo Techniques. **Journal of Pharmacology and Experimental Therapeutics**, v. 307, n. 2, p. 801–808, nov. 2003.

RAMESH, E.; ALSHATWI, A. A. Naringin induces death receptor and mitochondria-mediated apoptosis in human cervical cancer (SiHa) cells. **Food and Chemical Toxicology**, v. 51, n. 1, p. 97–105, 1 jan. 2013.

RANTAKYLÄ, M. et al. The effect of initial drop size on particle size in the supercritical antisolvent precipitation (SAS) technique. **Journal of Supercritical Fluids**, v. 24, n. 3, p. 251–263, 2002.

RAPPÉ, A. K. et al. UFF, a full periodic table force field for molecular mechanics and molecular dynamics simulations. **Journal of the American Chemical Society**, v. 114, n. 25, p. 10024–10035, 1 dez. 1992.

RASENACK, N.; MÜLLER, B. W. Micron-Size Drug Particles: Common and Novel Micronization Techniques. **Pharmaceutical Development and Technology**, v. 9, n. 1, p. 1–13, 2004.

RAZA, S. S. et al. Neuroprotective effect of naringenin is mediated through suppression of NF-κB signaling pathway in experimental stroke. **Neuroscience**, v. 230, p. 157–171, 29 jan. 2013.

RAZOUX, F.; GARCIA, R.; LÉNA, I. Ketamine, at a dose that disrupts motor behavior and latent inhibition, enhances prefrontal cortex synaptic efficacy and glutamate release in the nucleus accumbens. **Neuropsychopharmacology**, v. 32, n. 3, p. 719–727, 8 mar. 2007.

RÉ, M. I. Drying Technology MICROENCAPSULATION BY SPRAY DRYING. **MICROENCAPSULATION BY SPRAY DRYING, Drying Technology**, v. 16, n. 6, p. 1195–1236, 1998.

REGGANE, M. et al. Bioinspired co-crystals of Imatinib providing enhanced kinetic solubility. **European Journal of Pharmaceutics and Biopharmaceutics**, v. 128, p. 290–299, 1 jul. 2018.

REVERCHON, E. et al. Spherical microparticles production by supercritical antisolvent precipitation: Interpretation of results. **Journal of Supercritical Fluids**, v. 47, n. 1, p. 70–84, 2008.

RIBAS, M. M. et al. Curcumin cocrystals using supercritical fluid technology. **Journal of Supercritical Fluids**, v. 152, p. 104564, 2019a.

RIBAS, M. M. et al. Curcumin-nicotinamide cocrystallization with supercritical solvent (CSS): Synthesis, characterization and in vivo antinociceptive and anti-inflammatory activities. **Industrial Crops and Products**, v. 139, p. 111537, 1 nov. 2019b.

RIBEIRO, M. H. Naringinases: Occurrence, characteristics, and applications. **Applied Microbiology and Biotechnology**, v. 90, n. 6, p. 1883–1895, 5 jun. 2011.

RODRIGUES, M. et al. Pharmaceutical cocrystallization techniques. Advances and challenges. **International Journal of Pharmaceutics**, v. 547, n. 1–2, p. 404–420, 25 ago. 2018.

RODRÍGUEZ-HORNEDO, N. **Cocrystal Solubility and Thermodynamic Stability: Pharmaceutical Implications**. ABSTRACTS OF PAPERS OF THE AMERICAN CHEMICAL SOCIETY. **Anais**...WASHINGTON, DC 20036 USA: AMER CHEMICAL SOC: 2012. Disponível em: <http://www2.ul.ie/pdf/6712759.pdf>. Acesso em: 23 jul. 2020

ROTIMI, S. O. et al. Naringin enhances reverse cholesterol transport in high fat/low streptozocin induced diabetic rats. **Biomedicine and Pharmacotherapy**, v. 101, p. 430–437, 1 maio 2018.

RUPASINGHE, H. P. V. Special Issue "Flavonoids and Their Disease Prevention and Treatment Potential": Recent Advances and Future Perspectives. **Molecules 2020, Vol. 25, Page 4746**, v. 25, n. 20, p. 4746, 16 out. 2020.

SACHETT, A. et al. Curcumin micronization by supercritical fluid: In vitro and in vivo biological relevance. **Industrial Crops and Products**, v. 177, p. 114501, 1 mar. 2022.

SAIKIA, B. et al. Hydrogen bond synthons in the interplay of solubility and membrane permeability/diffusion in variable stoichiometry drug cocrystals. **ACS Publications**, v. 15, n. 11, p. 5593–5603, 4 nov. 2015.

SAKATA, G. S. B. et al. Encapsulation of trans-resveratrol in poly(ε-caprolactone) by GAS antisolvent. **The Journal of Supercritical Fluids**, v. 171, p. 105164, 1 maio 2021.

SANPHUI, P. et al. Cocrystals of hydrochlorothiazide: Solubility and diffusion/permeability enhancements through drug-coformer interactions. **Molecular Pharmaceutics**, v. 12, n. 5, p. 1615–1622, 4 maio 2015.

SANSONE, F. et al. Physical characteristics and aerosol performance of naringin dry powders for pulmonary delivery prepared by spray-drying. **European Journal of Pharmaceutics and Biopharmaceutics**, v. 72, n. 1, p. 206–213, 2009.

SANTOS, A. E. DOS et al. Micronization of luteolin using supercritical carbon dioxide: Characterization of particles and biological activity in vitro. **Journal of Supercritical Fluids**, v. 181, p. 105471, 1 fev. 2022.

SARMAH, K. K. et al. Mechanochemical synthesis of drug-drug and drug-nutraceutical multicomponent solids of olanzapine. **CrystEngComm**, v. 22, n. 6, p. 1120–1130, 14 fev. 2020.

SATHISARAN, I.; DALVI, S. V. Engineering cocrystals of poorlywater-soluble drugs to enhance dissolution in aqueous medium. **Pharmaceutics**, v. 10, n. 3, 2018.

SAVJANI, J. Co-crystallization: An approach to improve the performance characteristics of active pharmaceutical ingredients. **Asian Journal of Pharmaceutics**, v. 9, n. 3, p. 147–151, 2015.

SAVJANI, K.; … A. G.-I. S.; 2012, UNDEFINED. Drug solubility: importance and enhancement techniques. **downloads.hindawi.com**, v. 2012, 1957.

SAVJANI, K. T.; GAJJAR, A. K.; SAVJANI, J. K. Drug Solubility: Importance and Enhancement Techniques. **ISRN Pharmaceutics**, v. 2012, p. 1–10, 2012.

SCAPINELLO, J. et al. Extraction of bioactive compounds from Philodendron bipinnatifidum schott ex endl and encapsulation in PHBV by SEDS technique. **Industrial Crops and Products**, v. 125, p. 65–71, 2018.

SCHNEIDER, C. A.; RASBAND, W. S.; ELICEIRI, K. W. NIH Image to ImageJ: 25 years of image analysis. **Nature Methods**, v. 9, n. 7, p. 671–675, 2012.

SCHULTHEISS, N.; NEWMAN, A. Pharmaceutical cocrystals and their physicochemical properties. **Crystal Growth and Design**, v. 9, n. 6, p. 2950–2967, 3 jun. 2009.

SEGALINA, A. et al. Cocrystals of Nitrofurantoin: How Coformers Can Modify Its Solubility and Permeability Across Intestinal Cell Monolayers. **Crystal Growth and Design**, v. 22, n. 5, p. 3090–3106, 4 maio 2022.

SEMALTY, A. et al. Preparation and characterization of phospholipid complexes of naringenin for effective drug delivery. **Journal of Inclusion Phenomena and Macrocyclic Chemistry**, v. 67, n. 3, p. 253–260, 2010.

SEO, J.-W. et al. Preparation and characterization of adefovir dipivoxil–stearic acid cocrystal with enhanced physicochemical properties. **Taylor & Francis**, v. 23, n. 9, p. 890–899, 21 out. 2017.

SERAJUDDIN, A. T. M. Salt formation to improve drug solubility. **Advanced Drug Delivery Reviews**, v. 59, n. 7, p. 603–616, 2007.

SHAIKH, R. et al. Pharmaceutical Cocrystal Drug Products: An Outlook on Product Development. **Trends in Pharmacological Sciences**, v. 39, n. 12, p. 1033–1048, 2018.

SHAN, N.; TODA, F.; JONES, W. Mechanochemistry and co-crystal formation: Effect of solvent on reaction kinetics. **Chemical Communications**, v. 2, n. 20, p. 2372–2373, 2002.

SHARMA, A.; BHARDWAJ, P.; ARYA, S. K. Naringin: A potential natural product in the field of biomedical applications. **Carbohydrate Polymer Technologies and Applications**, v. 2, p. 100068, 25 dez. 2021.

SHI, L. et al. Characteristics and use patterns of patients taking first-generation depot antipsychotics or oral antipsychotics for schizophrenia. **Psychiatric Services**, v. 58, n. 4, p. 482–488, abr. 2007.

SIKAZWE, D. M. N. et al. The acute EPS of haloperidol may be unrelated to its metabolic transformation to BCPP +. **Bioorganic & Medicinal Chemistry Letters**, v. 13, p. 3779–3782, 2003.

SIMÕES, C. M. O. et al. Do produto natural ao medicamento. **Journal of Experimental Psychology: General**, v. 1, p. 167–184, 2017.

SINGH, M. et al. Cocrystals by Design: A Rational Coformer Selection Approach for Tackling the API Problems. **Pharmaceutics**, v. 15, n. 4, p. 1161, 2023.

SMITH, R. D. **Supercritical fluid molecular spray film deposition and powder formation**. **U.S. Patent n. 4,582,731**, 1986. Disponível em: <https://patents.google.com/patent/US4582731A/en>. Acesso em: 24 jul. 2020

SNYDER, E. M.; MURPHY, M. R. Schizophrenia therapy: Beyond atypical

antipsychotics. **Nature Reviews Drug Discovery**, v. 7, n. 6, p. 471–472, 2008.

SODEIFIAN, G.; SAJADIAN, S. A.; DERAKHSHESHPOUR, R. CO2 utilization as a supercritical solvent and supercritical antisolvent in production of sertraline hydrochloride nanoparticles. **Journal of CO2 Utilization**, v. 55, 1 jan. 2022.

SOKAL, A.; PINDELSKA, E. Pharmaceutical Cocrystals as an Opportunity to Modify Drug Properties: From the Idea to Application: A Review. **Current Pharmaceutical Design**, v. 24, n. 13, p. 1357–1365, 2017.

SPAGNUOLO, C.; MOCCIA, S.; RUSSO, G. L. Anti-inflammatory effects of flavonoids in neurodegenerative disorders. **European Journal of Medicinal Chemistry**, v. 153, p. 105–115, 10 jun. 2018.

SREEDHARAN, V.; VENKATACHALAM, K. K.; NAMASIVAYAM, N. Effect of morin on tissue lipid peroxidation and antioxidant status in 1, 2-dimethylhydrazine induced experimental colon carcinogenesis. **Investigational New Drugs**, v. 27, n. 1, p. 21–30, fev. 2009.

SREENIVAS REDDY, L. et al. Cocrystals and salts of gabapentin: pH dependent cocrystal stability and solubility. **Crystal Growth and Design**, v. 9, n. 1, p. 378–385, jan. 2009.

STAHL, S. M. Long-acting injectable antipsychotics: shall the last be first? **CNS Spectrums**, v. 19, n. 1, p. 3–5, 2014.

STASIŁOWICZ-KRZEMIEŃ, A. et al. The Systems of Naringenin with Solubilizers Expand Its Capability to Prevent Neurodegenerative Diseases. **International Journal of Molecular Sciences**, v. 23, n. 2, p. 755, 1 jan. 2022.

STEED, J. W. The role of co-crystals in pharmaceutical design. **Trends in Pharmacological Sciences**, v. 34, n. 3, p. 185–193, 2013.

SUGUMAR, M.; SEVANAN, M.; SEKAR, S. Neuroprotective effect of naringenin against MPTP-induced oxidative stress. **International Journal of Neuroscience**, v. 129, n. 6, p. 534–539, 3 jun. 2019.

SUN, D. D.; WEN, H.; TAYLOR, L. S. Non-sink dissolution conditions for predicting product quality and in vivo performance of supersaturating drug delivery systems. **Journal of Pharmaceutical Sciences**, v. 105, n. 9, p. 2477–2488, 2016.

SUN, L. et al. Cocrystal Engineering: A Collaborative Strategy toward Functional Materials. **Advanced Materials**, v. 31, n. 39, 1 set. 2019.

SWAMY, R. S. et al. Neuroprotective effect by naringin against fluorosis-induced neurodegeneration in adult Wistar rats. **NeuroReport**, v. 34, n. 9, p. 449–456, 7 jun. 2023.

TABERNERO, A.; MARTÍN DEL VALLE, E. M.; GALÁN, M. A. Supercritical fluids for pharmaceutical particle engineering: Methods, basic fundamentals and modelling. **Chemical Engineering and Processing: Process Intensification**, v. 60, p. 9–25, 1 out. 2012.

TADE, R. S.; NANGARE, S. N.; PATIL, P. O. Agro-Industrial waste-mediated green

synthesis of silver nanoparticles and evaluation of its antibacterial activity. **Nano Biomedicine and Engineering**, v. 12, n. 1, p. 57–66, 2020.

TALACZYNSKA, A.; DZITKO, J.; CIELECKA-PIONTEK, J. Benefits and Limitations of Polymorphic and Amorphous Forms of Active Pharmaceutical Ingredients. **Current Pharmaceutical Design**, v. 22, n. 32, p. 4975–4980, 2016.

TAN, H. S.; BORSADIA, S. Particle formation using supercritical fluids: Pharmaceutical applications. **Expert Opinion on Therapeutic Patents**, v. 11, n. 5, p. 861–872, 2001.

TANG, X.; PIKAL, M. J. Design of Freeze-Drying Processes for Pharmaceuticals: Practical Advice. **Pharmaceutical Research**, v. 21, n. 2, p. 191–200, fev. 2004.

TAO, A. et al. EzCADD: a rapid 2D/3D visualization-enabled web modeling environment for democratizing computer-aided drug design. **Journal of Chemical Information and Modeling**, v. 59, n. 1, p. 18–24, 28 jan. 2019.

THAKURIA, R.; SARMA, B. Drug-drug and drug-nutraceutical cocrystal/salt as alternative medicine for combination therapy: A crystal engineering approach. **Crystals**, v. 8, n. 2, 2018.

THANH, N. T. K.; MACLEAN, N.; MAHIDDINE, S. Mechanisms of nucleation and growth of nanoparticles in solution. **Chemical Reviews**, v. 114, n. 15, p. 7610–7630, 2014.

THIERING, R.; DEHGHANI, F.; FOSTER, N. R. Current issues relating to anti-solvent micronisation techniques and their extension to industrial scales. **Journal of Supercritical Fluids**, v. 21, n. 2, p. 159–177, 2001.

TIAGO, J. M. et al. Single-step co-crystallization and lipid dispersion by supercritical enhanced atomization. **Crystal Growth and Design**, v. 13, n. 11, p. 4940–4947, 6 nov. 2013.

TIRUWA, R. A review on nanoparticles – preparation and evaluation parameters. **Indian Journal of Pharmaceutical and Biological Research**, v. 4, n. 2, p. 27–31, 30 jun. 2016.

TIWARY, A. K. Modification of crystal habit and its role in dosage form performance. **Drug Development and Industrial Pharmacy**, v. 27, n. 7, p. 699–709, 2001.

TJANDRAWINATA, R. R.; HIENDRAWAN, S.; VERIANSYAH, B. Processing paracetamol-5-nitroisophthalic acid cocrystal using supercritical CO2 as an anti-solvent. **International Journal of Applied Pharmaceutics**, v. 11, n. 5, p. 194–199, 2019.

TROTT, O. et al. AutoDock Vina: Improving the speed and accuracy of docking with a new scoring function, efficient optimization, and multithreading. **Journal of Computational Chemistry**, v. 31, n. 2, p. 455–461, 30 jan. 2009.

TSAI, G.; COYLE, J. T. Glutamatergic mechanisms in schizophrenia. **Annual Review of Pharmacology and Toxicology**, v. 42, p. 165–179, 2002.

TSAI, S. J. et al. Anti-inflammatory and antifibrotic effects of naringenin in diabetic

mice. **Journal of Agricultural and Food Chemistry**, v. 60, n. 1, p. 514–521, 11 jan. 2012.

TÜRK, M. Manufacture of submicron drug particles with enhanced dissolution behaviour by rapid expansion processes. **Journal of Supercritical Fluids**, v. 47, n. 3, p. 537–545, 2009.

VALDÉS-TRESANCO, M. S. et al. AMDock: a versatile graphical tool for assisting molecular docking with Autodock Vina and Autodock4. **Biology Direct**, v. 15, n. 1, p. 12, 16 set. 2020.

VAN DEN MOOTER, G. The use of amorphous solid dispersions: A formulation strategy to overcome poor solubility and dissolution rate. **Drug Discovery Today: Technologies**, v. 9, n. 2, p. 79–85, 1 jun. 2012.

VENKATESWARLU, V.; MANJUNATH, K. Preparation, characterization and in vitro release kinetics of clozapine solid lipid nanoparticles. **Journal of Controlled Release**, v. 95, n. 3, p. 627–638, 24 mar. 2004.

VINET, L.; ZHEDANOV, A. A "missing" family of classical orthogonal polynomials. **Journal of Physics A: Mathematical and Theoretical**, v. 44, n. 8, p. 543–550, 2011.

WANG, G. et al. Antidepressant-like effect of acute dose of Naringin involves suppression of NR1 and activation of protein kinase A/cyclic adenosine monophosphate response element-binding protein/brain-derived neurotrophic factor signaling in hippocampus. **Behavioural Pharmacology**, v. 34, n. 2–3, p. 101–111, 1 abr. 2023.

WANG, K. et al. Naringenin prevents ischaemic stroke damage via anti-apoptotic and anti-oxidant effects. **Clinical and Experimental Pharmacology and Physiology**, v. 44, n. 8, p. 862–871, 1 ago. 2017.

WANG, L. H. et al. Modification of membrane properties and fatty acids biosynthesis-related genes in Escherichia coli and Staphylococcus aureus: Implications for the antibacterial mechanism of naringenin. **Biochimica et Biophysica Acta - Biomembranes**, v. 1860, n. 2, p. 481–490, 1 fev. 2018a.

WANG, M. H. et al. Naringin Ameliorates Haloperidol-Induced Neurotoxicity and Orofacial Dyskinesia in a Rat Model of Human Tardive Dyskinesia. **Neurotoxicity Research**, v. 39, n. 3, p. 774–786, 1 jun. 2021.

WANG, S. et al. Structure of the D2 dopamine receptor bound to the atypical antipsychotic drug risperidone. **Nature**, v. 555, n. 7695, p. 269–273, 2018b.

WANG, T. YANG; LI, Q.; BI, K. SHUN. Bioactive flavonoids in medicinal plants: Structure, activity and biological fate. **Asian Journal of Pharmaceutical Sciences**, v. 13, n. 1, p. 12–23, 1 jan. 2018.

WANG, Y.; CHEN, S.; YU, O. Metabolic engineering of flavonoids in plants and microorganisms. **Applied Microbiology and Biotechnology**, v. 91, n. 4, p. 949–956, 6 ago. 2011.

WEST, C. Current trends in supercritical fluid chromatography. **Analytical and Bioanalytical Chemistry**, v. 410, n. 25, p. 6441–6457, 1 out. 2018.

WHO, Schizophrenia. Disponível em: <https://www.who.int/news-room/fact-sheets/detail/schizophrenia>. Acesso em: 14 mar. 2023.

WHO. Disponível em: <https://www.who.int/news-room/fact-sheets/detail/schizophrenia>. Acesso em: 14 jul. 2022.

WICHIANPHONG, N.; CHAROENCHAITRAKOOL, M. Statistical optimization for production of mefenamic acid–nicotinamide cocrystals using gas anti-solvent (GAS) process. **Journal of Industrial and Engineering Chemistry**, v. 62, p. 375–382, jun. 2018.

WILLIAMS, C. J. et al. MolProbity: More and better reference data for improved all-atom structure validation. **Protein Science**, v. 27, n. 1, p. 293–315, 1 jan. 2018.

WILLIAMS, H. D. et al. Strategies to Address Low Drug Solubility in Discovery and Development. **Pharmacological Reviews**, v. 65, n. 1, p. 315–499, 3 jan. 2013.

WOJDYŁO, A.; OSZMIAŃSKI, J.; CZEMERYS, R. Antioxidant activity and phenolic compounds in 32 selected herbs. **Food Chemistry**, v. 105, n. 3, p. 940–949, 1 jan. 2007.

WORLD HEALTH ORGANIZATION. **Schizophrenia**. Disponível em: <https://www.who.int/news-room/fact-sheets/detail/schizophrenia>. Acesso em: 3 mar. 2024.

XU, D. et al. Pharmacokinetic Comparisons of Naringenin and Naringenin-Nicotinamide Cocrystal in Rats by LC-MS/MS. **Journal of Analytical Methods in Chemistry**, v. 2020, p. 1–10, 2020.

XU, J. et al. Recent Advances in Pharmaceutical Cocrystals: A Focused Review of Flavonoid Cocrystals. **Molecules**, v. 28, n. 2, p. 613, 6 jan. 2023.

YAMAMOTO, K. et al. Physicochemical evaluation and developability assessment of co-amorphouses of low soluble drugs and comparison to the co-crystals. **Chemical and Pharmaceutical Bulletin**, v. 64, n. 12, p. 1739–1746, 2016.

YANG, S.; JIN, H.; ZHAO, Z. An ECV304 monoculture model for permeability assessment of blood–brain barrier. **Neurological Research**, v. 40, n. 2, p. 117–121, 1 fev. 2018.

YANG, W. et al. Effect of naringenin on brain insulin signaling and cognitive functions in ICV-STZ induced dementia model of rats. **Neurological Sciences**, v. 35, n. 5, p. 741–751, 2014.

YAO, L. H. et al. Flavonoids in food and their health benefits. **Plant Foods for Human Nutrition**, v. 59, n. 3, p. 113–122, 2004.

YEE, S. In vitro permeability across Caco-2 cells (colonic) can predict in vivo (small intestinal) absorption in man - Fact or myth. **Pharmaceutical Research**, v. 14, n. 6, p. 763–766, 1997.

YEO, S. DO; KIRAN, E. Formation of polymer particles with supercritical fluids: A review. **Journal of Supercritical Fluids**, v. 34, n. 3, p. 287–308, 1 jul. 2005.

YIN, H.-M. et al. Slow-Release Drug–Drug Cocrystals of Oxaliplatin with Flavonoids: Delaying Hydrolysis and Reducing Toxicity. **Crystal Growth & Design**, v. 21, n. 1, p. 75–85, 6 jan. 2020.

YORK, P. Strategies for particle design using supercritical fluid technologies. **Pharmaceutical Science and Technology Today**, v. 2, n. 11, p. 430–440, 1 nov. 1999.

YORK, P.; KOMPELLA, U. B.; SHEKUNOV, B. Y. Supercritical fluid technology for drug product development. **Supercritical Fluid Technology for Drug Product Development**, p. 1–670, 2004.

YOSHII, H. et al. Effects of protein on retention of ADH enzyme activity encapsulated in trehalose matrices by spray drying. **Journal of Food Engineering**, v. 87, n. 1, p. 34–39, 2008.

YOUDIM, K. A. et al. Interaction between flavonoids and the blood–brain barrier: in vitro studies. **Wiley Online LibraryKA Youdim, MS Dobbie, G Kuhnle, AR Proteggente, NJ Abbott, C Rice-EvansJournal of neurochemistry, 2003•Wiley Online Library**, v. 85, n. 1, p. 180–192, 2003.

YOUDIM, K. A. et al. Flavonoid permeability across an in situ model of the blood-brain barrier. **Free Radical Biology and Medicine**, v. 36, n. 5, p. 592–604, 2004.

YOUSEFI, M. et al. Supercritical fluid extraction of essential oils. **Trends in Analytical Chemistry**, v. 118, p. 182–193, 1 set. 2019.

YU, Y.; WU, H. Significant differences in the hydrolysis behavior of amorphous and crystalline portions within microcrystalline cellulose in hot-compressed water. **Industrial and Engineering Chemistry Research**, v. 49, n. 8, p. 3902–3909, 2010.

YUAN, G.; HUI, Z.; JIANJUN, Z. Pharmaceutical cocrystals. **Progress in Chemistry**, v. 22, n. 5, p. 829–836, 2010.

YUAN, J. F. et al. ECV304/C6 coculture model of the BBB coupled with LC–MS analysis for drug screening from Rhubarb extract. **Medicinal Chemistry Research**, v. 25, n. 9, p. 1935–1944, 1 set. 2016.

YUSOF, S.; GHAZALI, H. M.; KING, G. S. Naringin content in local citrus fruits. **Food Chemistry**, v. 37, n. 2, p. 113–121, 1 jan. 1990.

ZAIDUN, N. H.; THENT, Z. C.; LATIFF, A. A. Combating oxidative stress disorders with citrus flavonoid: Naringenin. **Life Sciences**, v. 208, p. 111–122, 1 set. 2018.

ZENG, F. et al. Formulation and in vivo evaluation of orally disintegrating tablets of clozapine/hydroxypropyl-β-cyclodextrin inclusion complexes. **AAPS PharmSciTech**, v. 14, n. 2, p. 854–860, 2013.

ZHANG, J. et al. Micronization of gefitinib using solution-enhanced dispersion by

supercritical CO2. **Chemical Engineering and Technology**, v. 42, n. 2, p. 388–396, 2019a.

ZHANG, L. et al. Solubilities of naringin and naringenin in different solvents and dissociation constants of naringenin. **ACS Publications**, v. 60, n. 3, p. 932–940, 12 mar. 2015.

ZHANG, L. et al. Naringenin and apigenin ameliorates corticosterone-induced depressive behaviors. **Heliyon**, v. 9, n. 5, 2023.

ZHANG, X. et al. HPMC improves protective effects of naringenin and isonicotinamide co-crystals against abdominal aortic aneurysm. **Cardiovascular Drugs and Therapy**, v. 36, n. 6, p. 1109–1119, 1 dez. 2022.

ZHANG, Z. et al. Cocrystals of Natural Products: Improving the Dissolution Performance of Flavonoids Using Betaine. **Crystal Growth and Design**, v. 19, n. 7, p. 3851–3859, 3 jul. 2019b.

ZHENG, K. et al. Effect of particle size and polymer loading on dissolution behavior of amorphous griseofulvin powder. **Journal of Pharmaceutical Sciences**, v. 108, n. 1, p. 234–242, 1 jan. 2019.

ZHOU, F. et al. Structure determination and in vitro/vivo study on carbamazepine-naringenin (1:1) cocrystal. **Journal of Drug Delivery Science and Technology**, v. 54, p. 101244, 1 dez. 2019.

ZHU, B. et al. Cocrystals of Baicalein with Higher Solubility and Enhanced Bioavailability. **Crystal Growth & Design**, v. 17, n. 4, p. 1893–1901, 5 abr. 2017.

APPENDIX A

Representation of Ramachandran diagrams obtained for all the residues composing a) D_2R (PDB ID:6CM4) and b) 5-HT_{2A} (PDB ID:6A93). The possible combinations of torsion dihedral angles Phi (φ) vs. Psi (Φ) are shown. Note the total absence of Ramachandran outlier residues for the three conditions evaluated (general and individual Ramachandran plot), usually, unfavored residues or torsion angles (Phi (φ) vs. Psi (Φ)) are located outside the Ramachandran colored-purple contour.

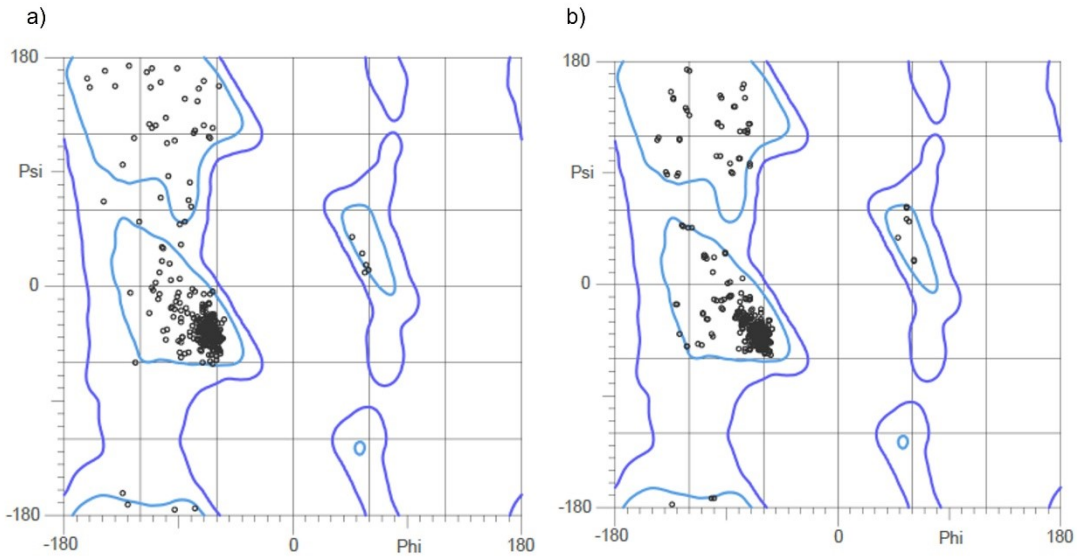

Source: Author (2024)

APPENDIX B

Effects of raw naringenin (NAR) and micronized naringenin (micro NAR) on mice locomotor activity assessed in the open field test. The animals were orally treated with Vehicle (saline solution + 1% polysorbate 80), raw NAR or micro NAR (200 mg·kg^{-1}) 1 h before being observed in the arena. Data were analyzed by One-Way ANOVA and are expressed as mean ± S.D.

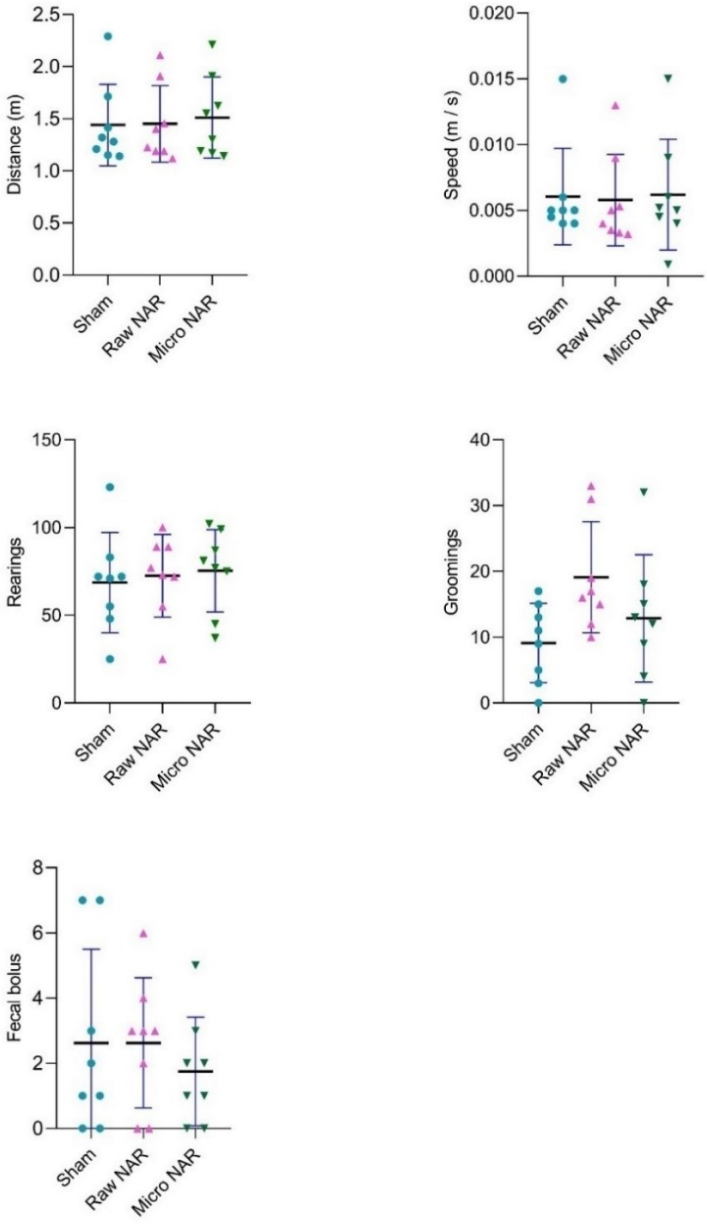

Source: Author (2024)

APPENDIX C

Scanning Electron Microscopy (SEM) of naringin commercial and runs 1-19

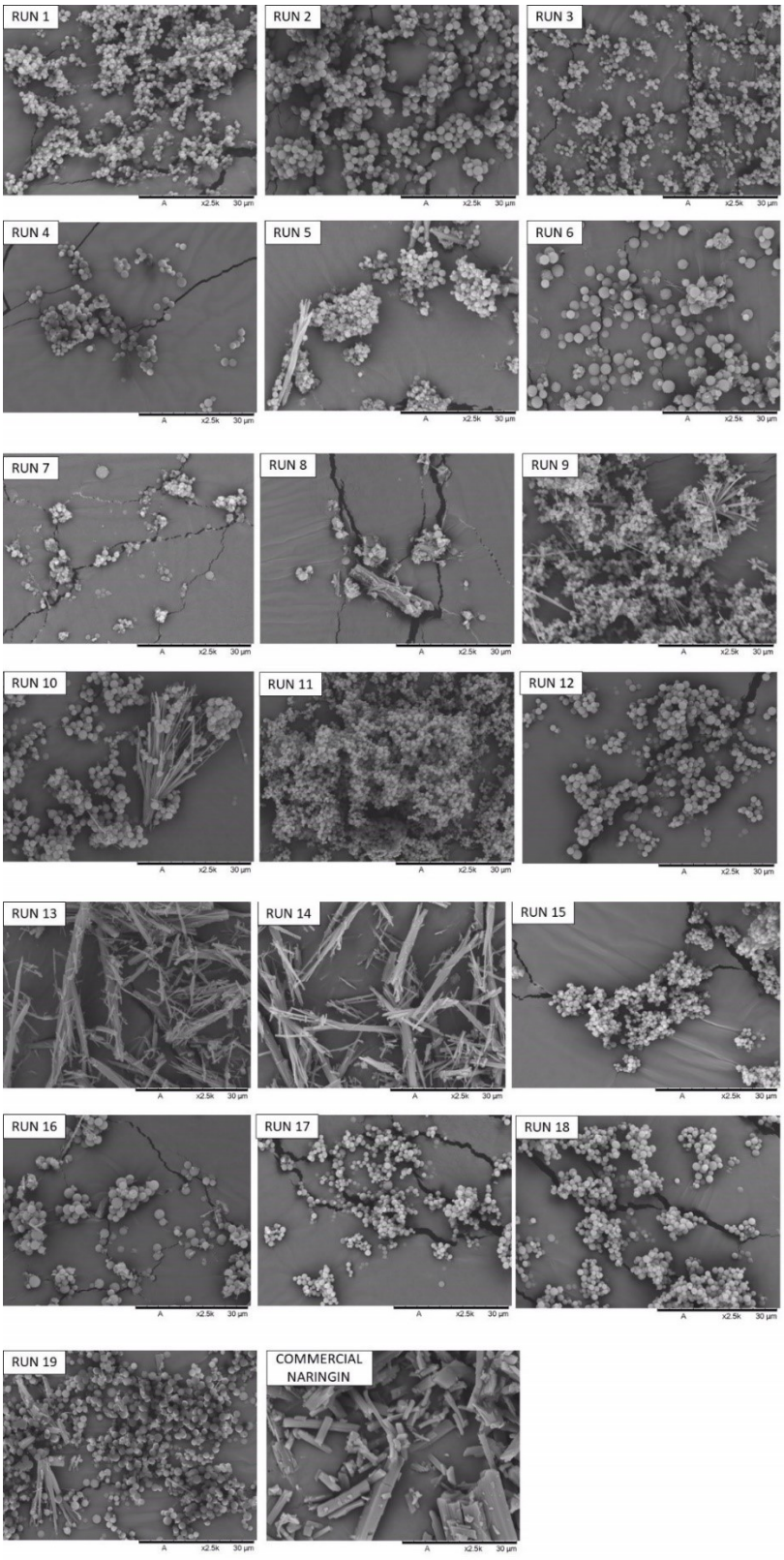

APPENDIX D

Power-X-ray diffraction (XRD) analysis of commercial and runs 1-19.

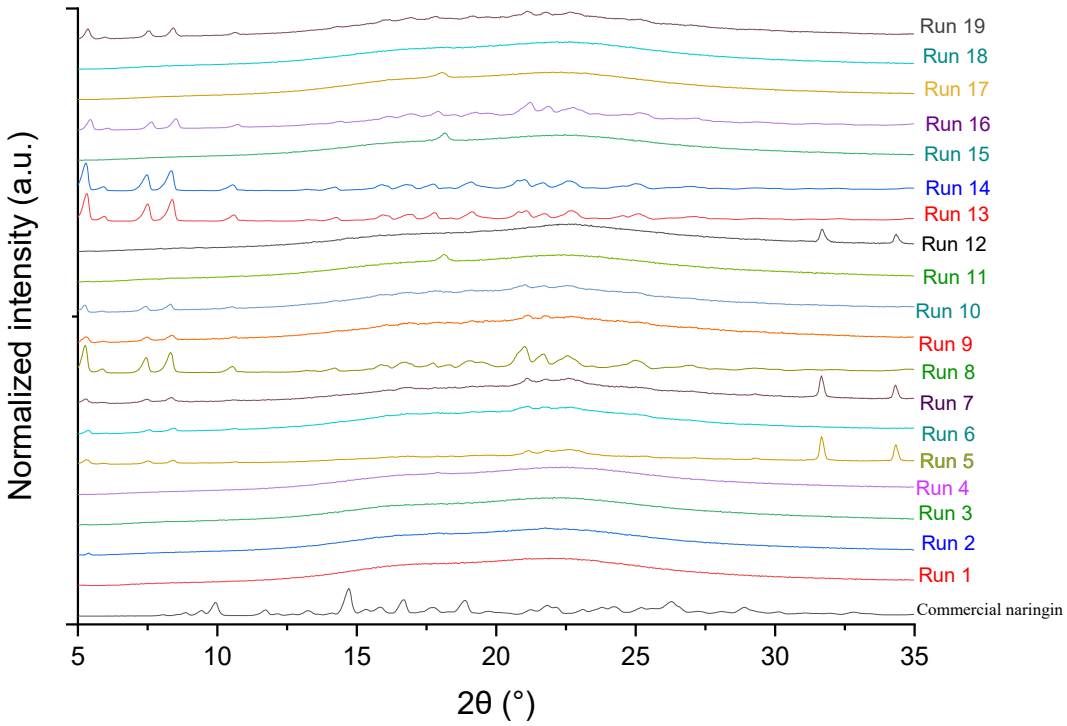

Source: Author (2024)

APPENDIX E

XRD analysis of commercial and processed naringin from runs 11 and 14, after dissolution rate assays.

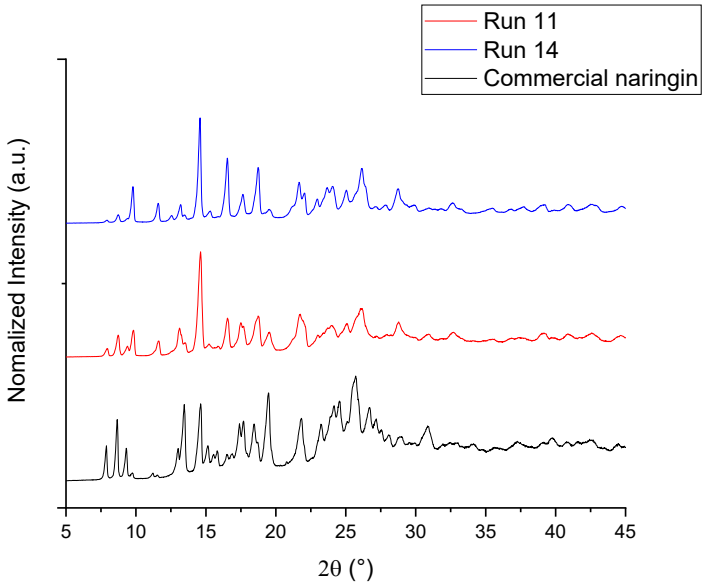

Source: Author (2024)

APPENDIX F

UPLC-MS naringin commercial.

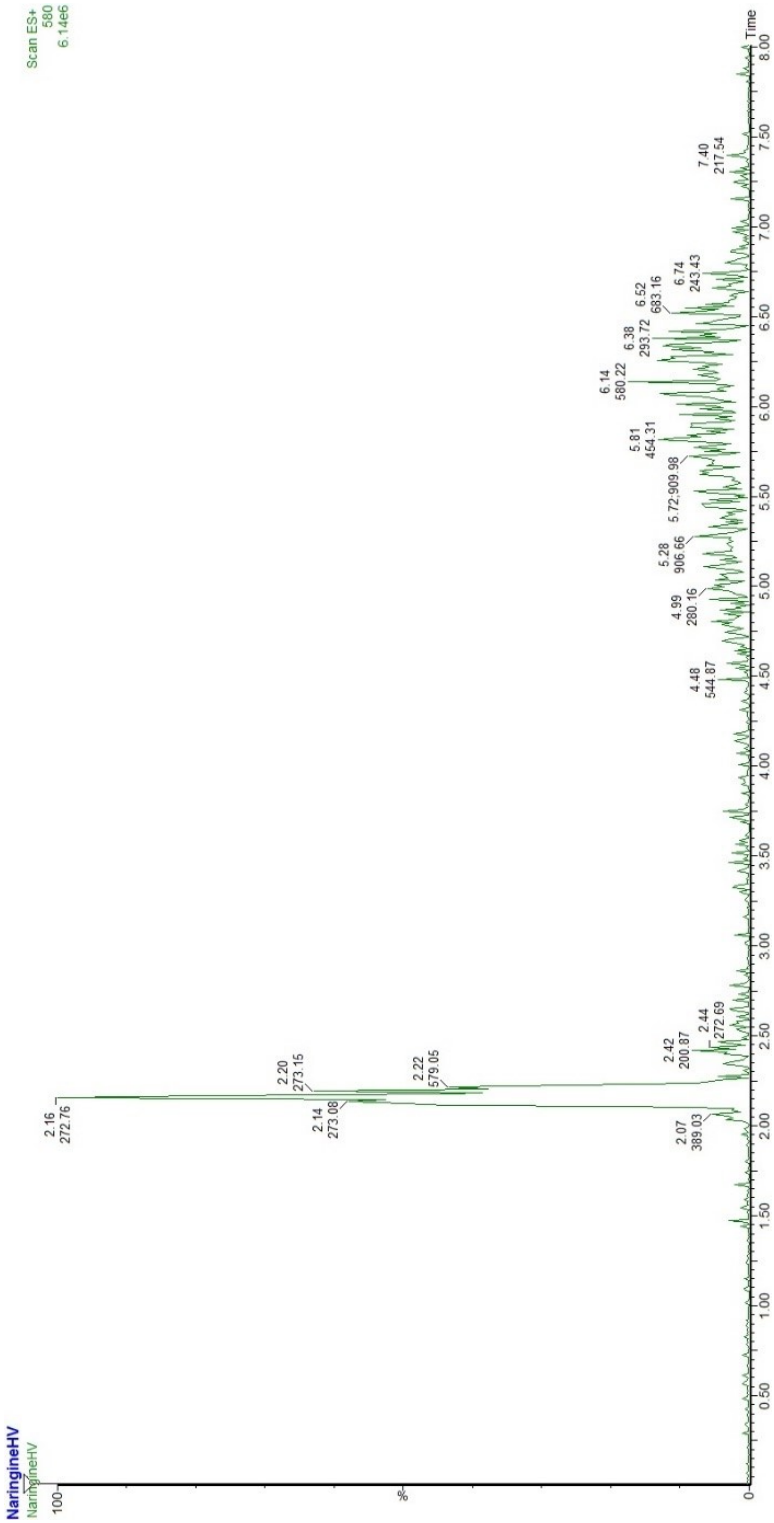

Appendix F (continued).

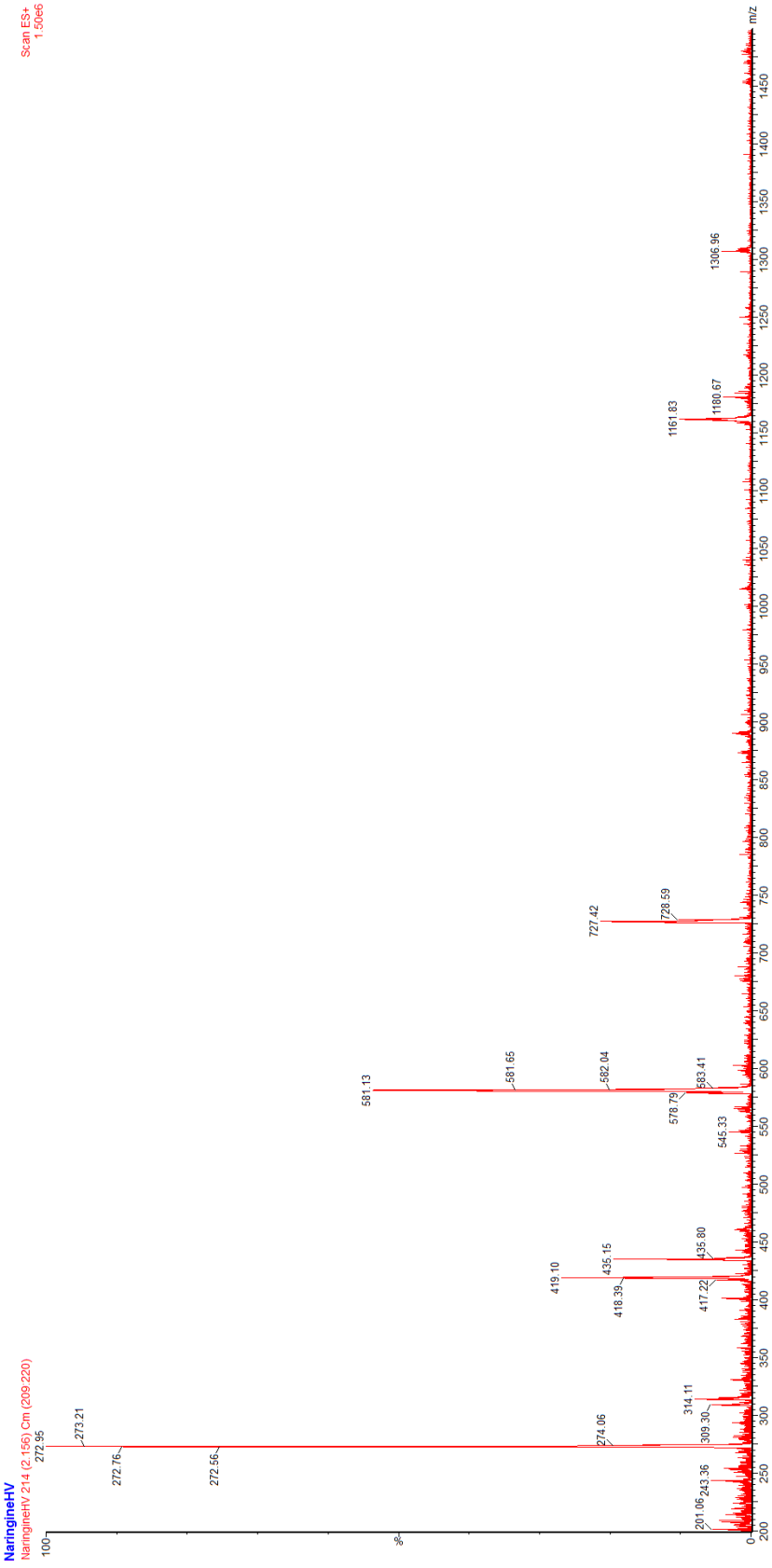

APPENDIX G

UPLC-MS naringin commercial after dissolution rate assays.

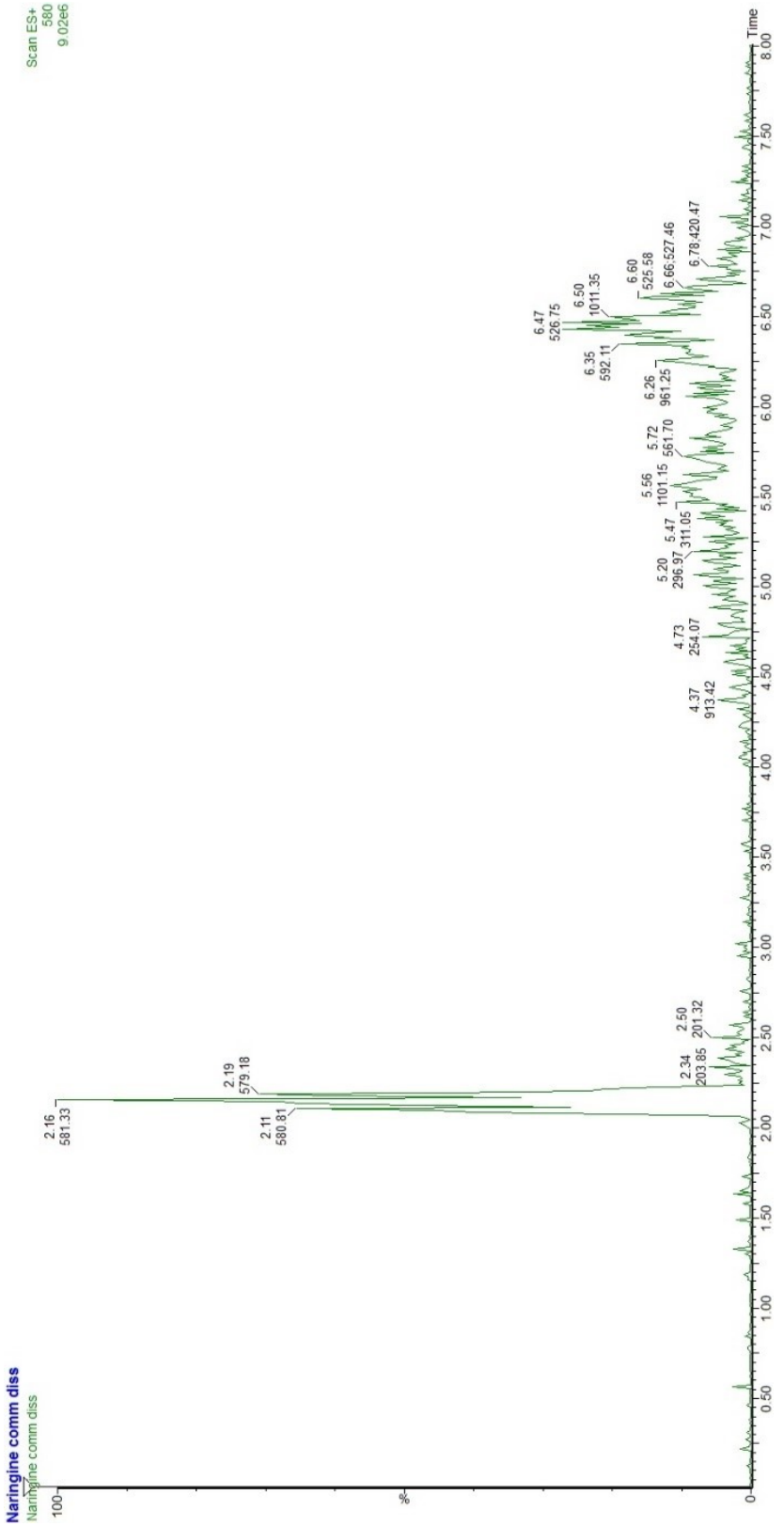

Appendix G (continued).

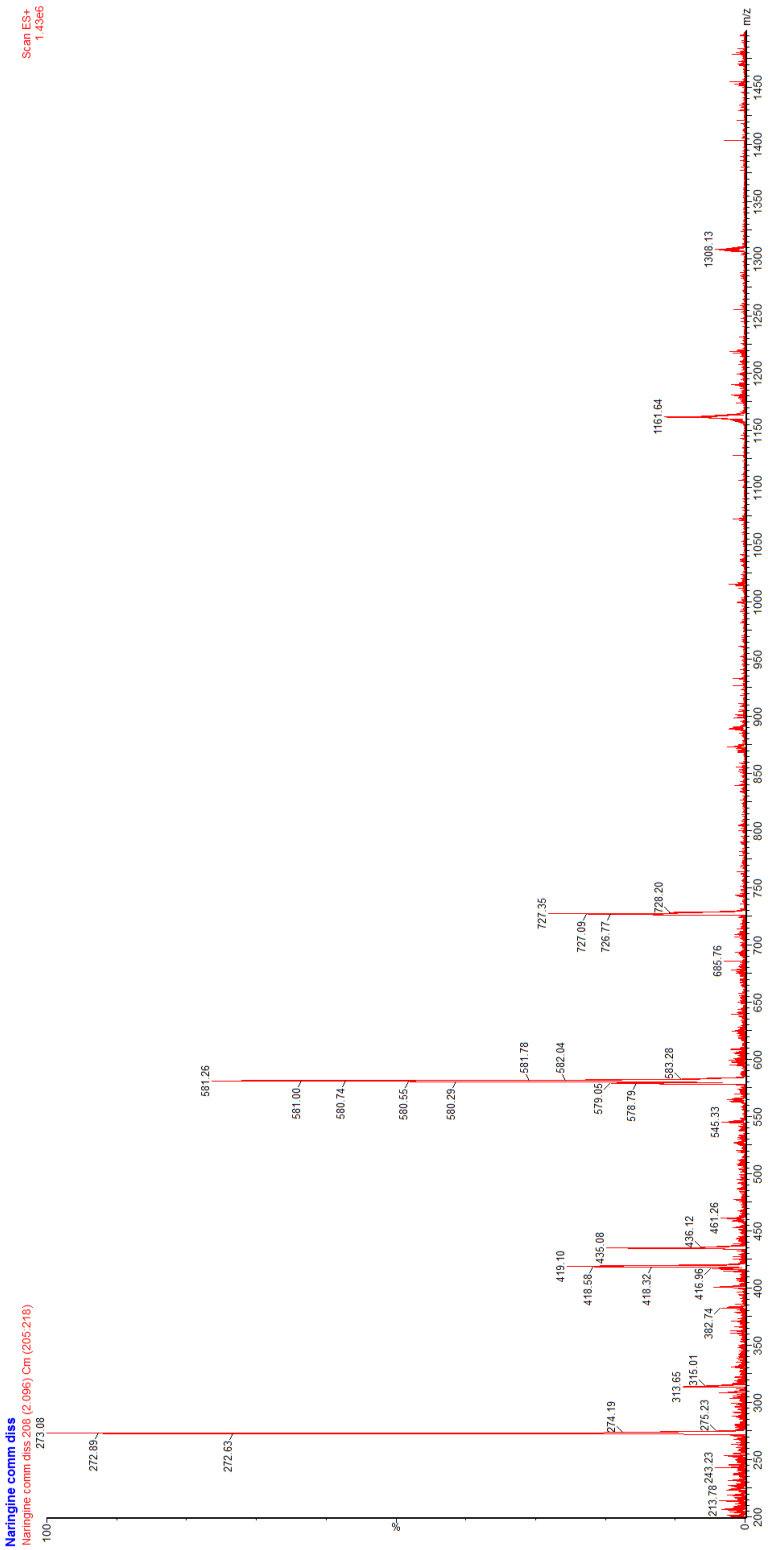

APPENDIX H

UPLC-MS naringin run 11 after gas antisolvent process

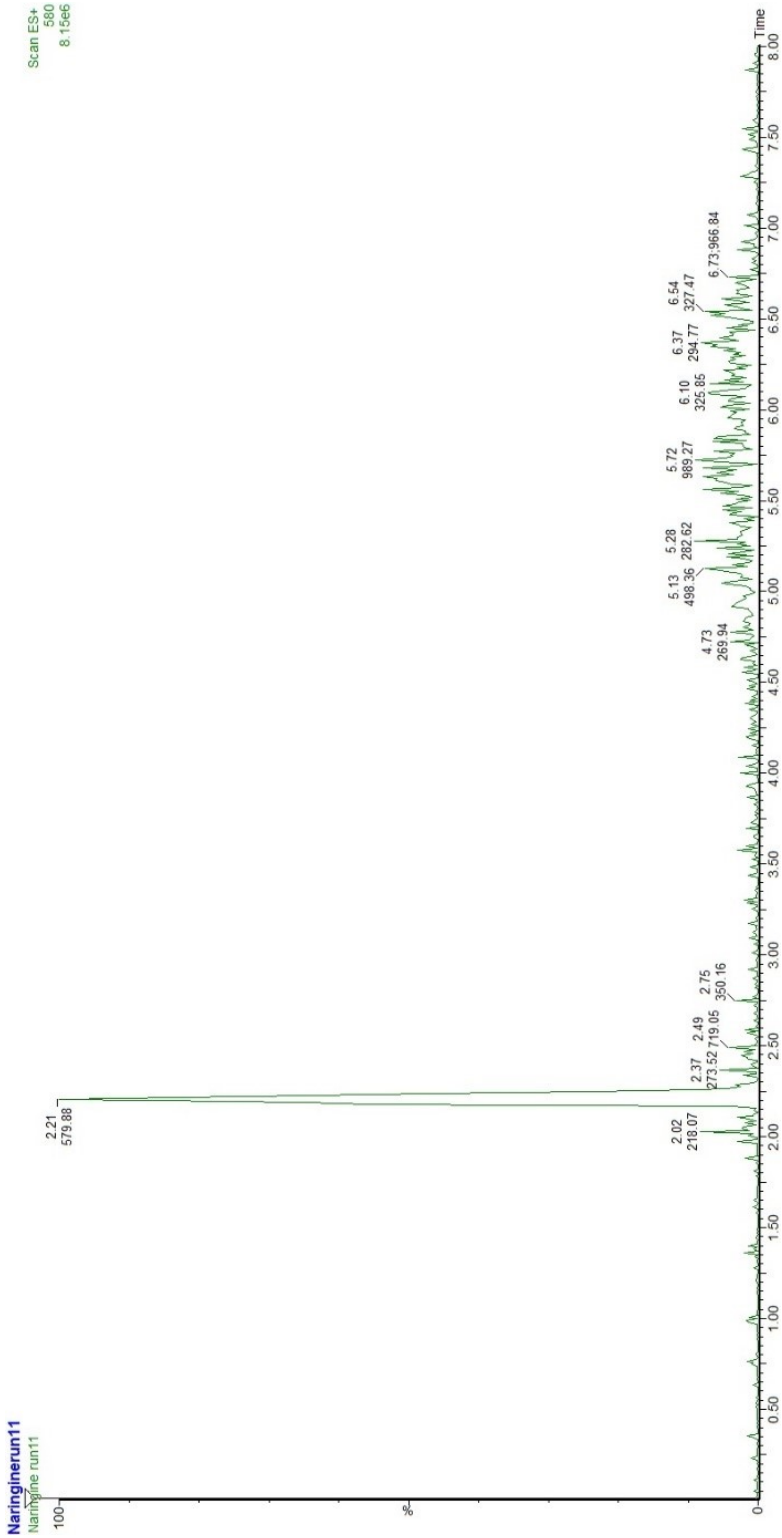

Appendix H (continued).

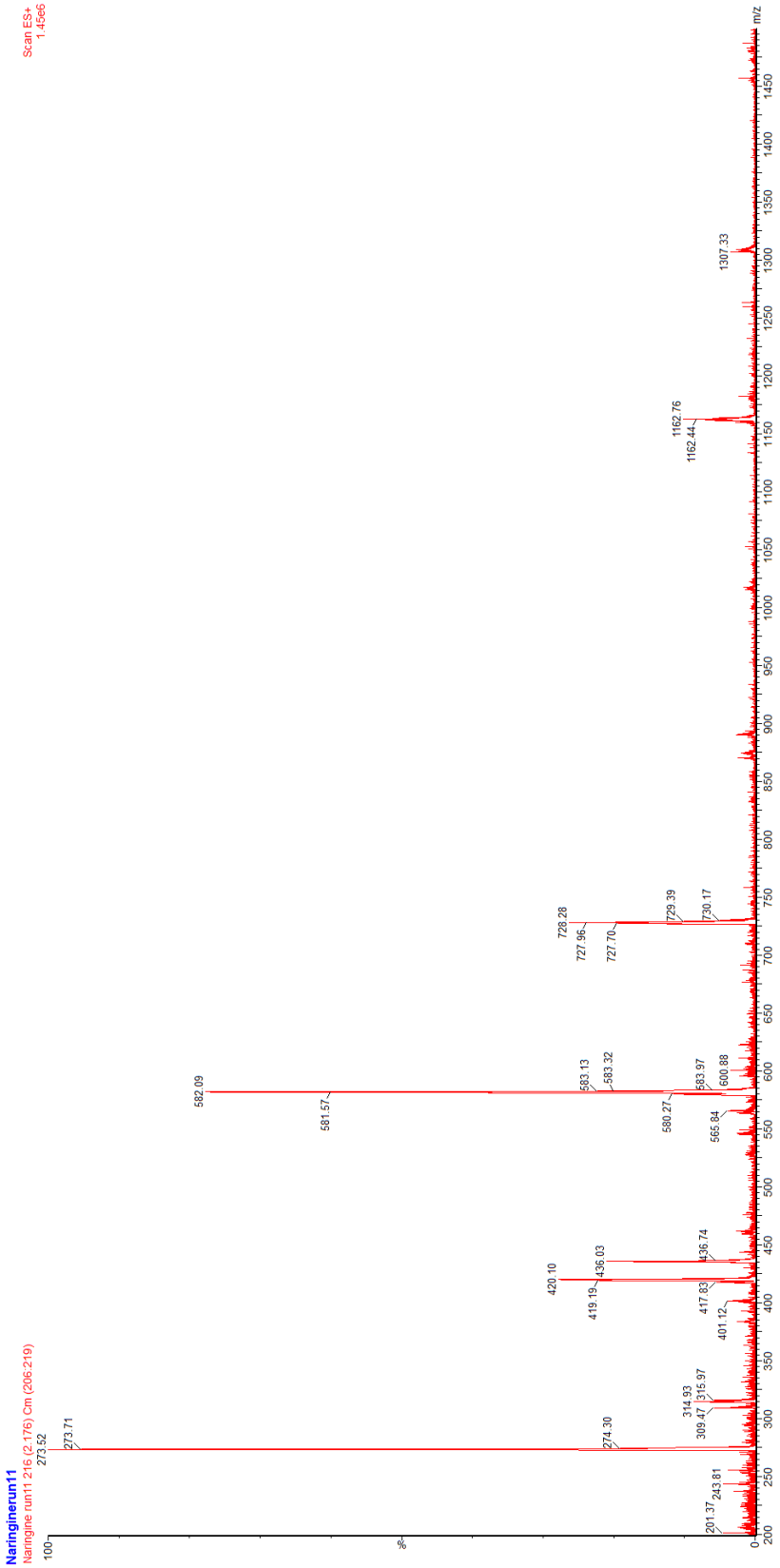

APPENDIX I

UPLC-MS naringin run 11 after dissolution rate assays.

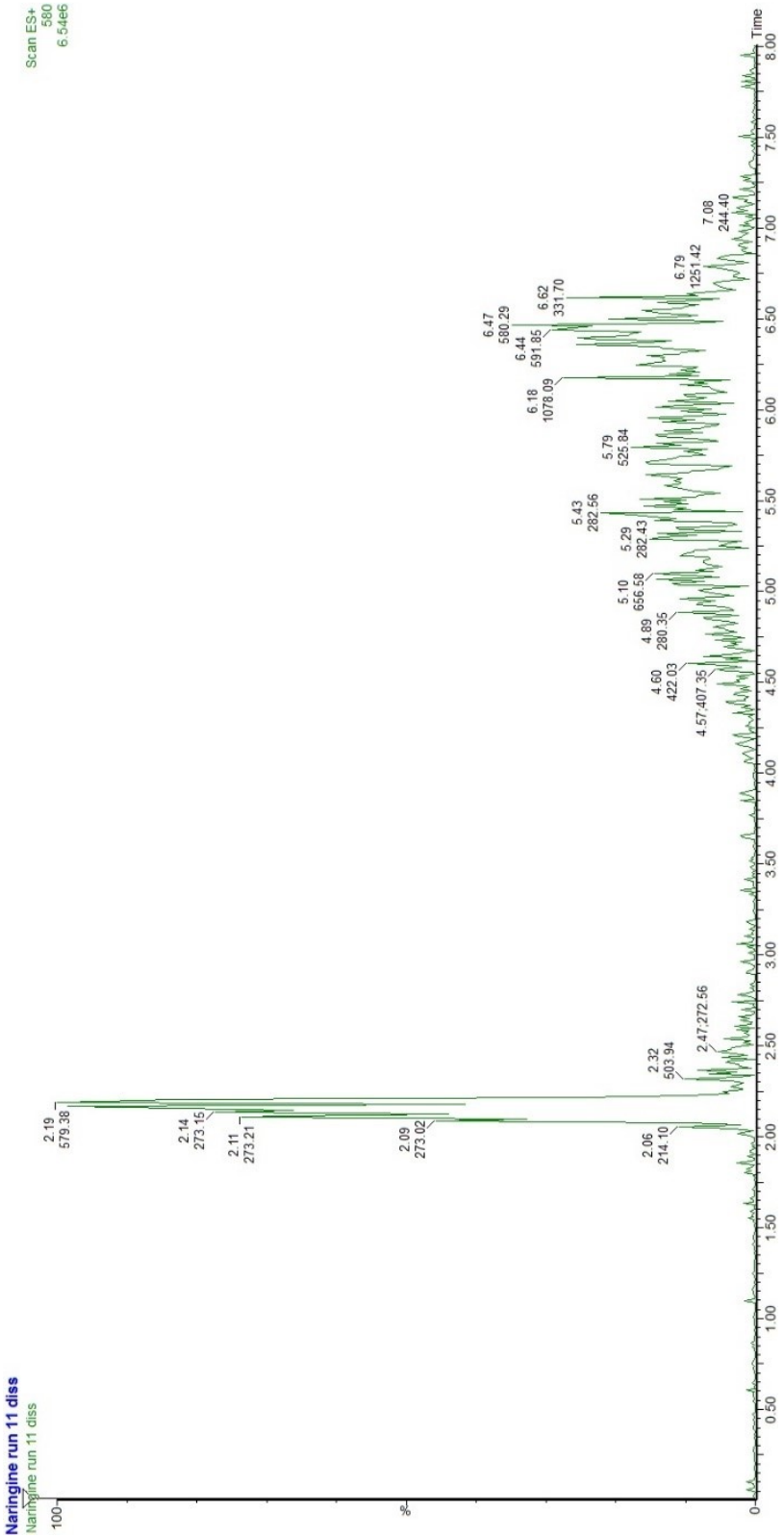

Appendix I (continued).

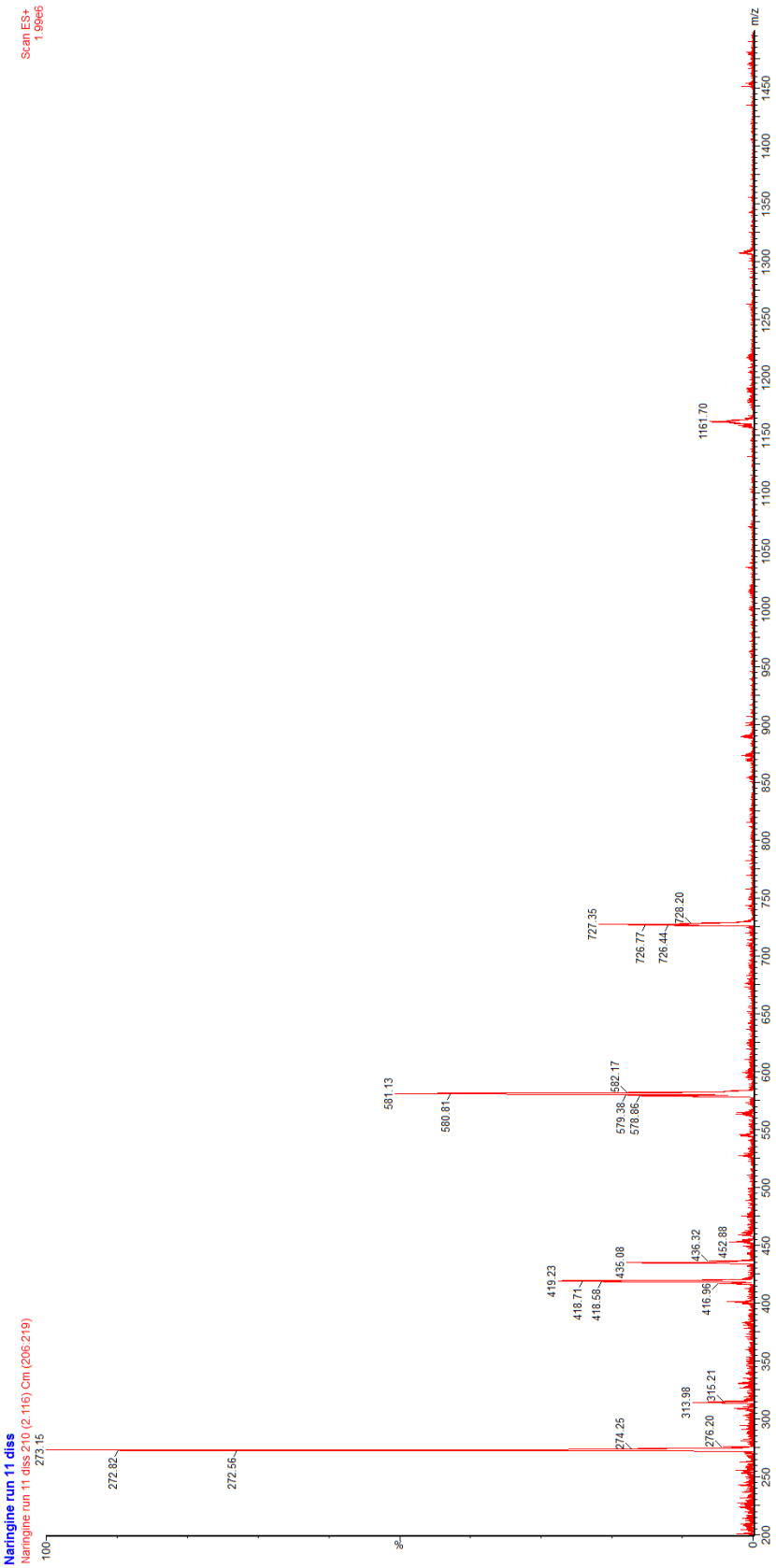

APPENDIX J

UPLC-MS naringin run 14 after gas antisolvent process.

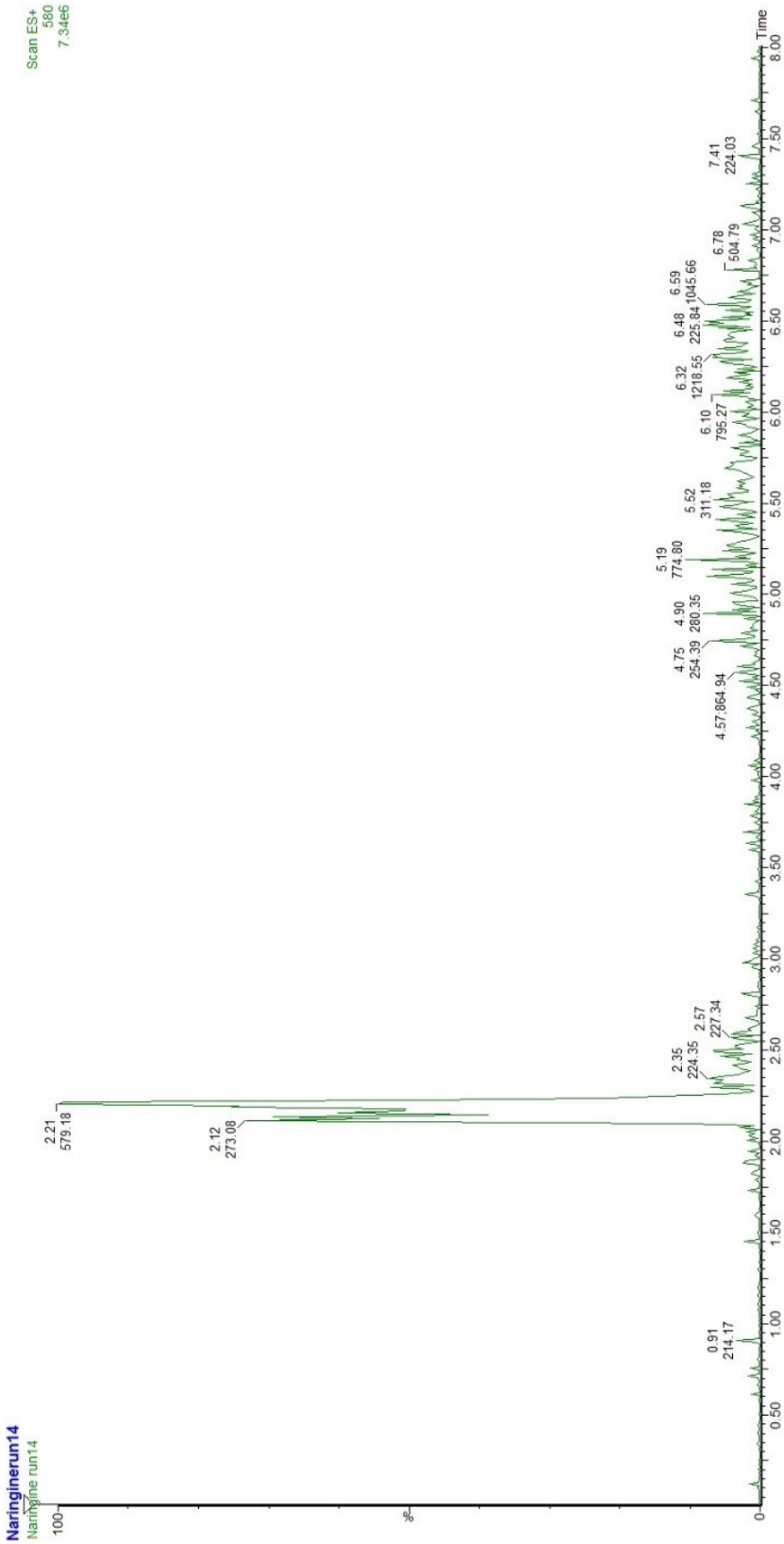

Appendix J (continued).

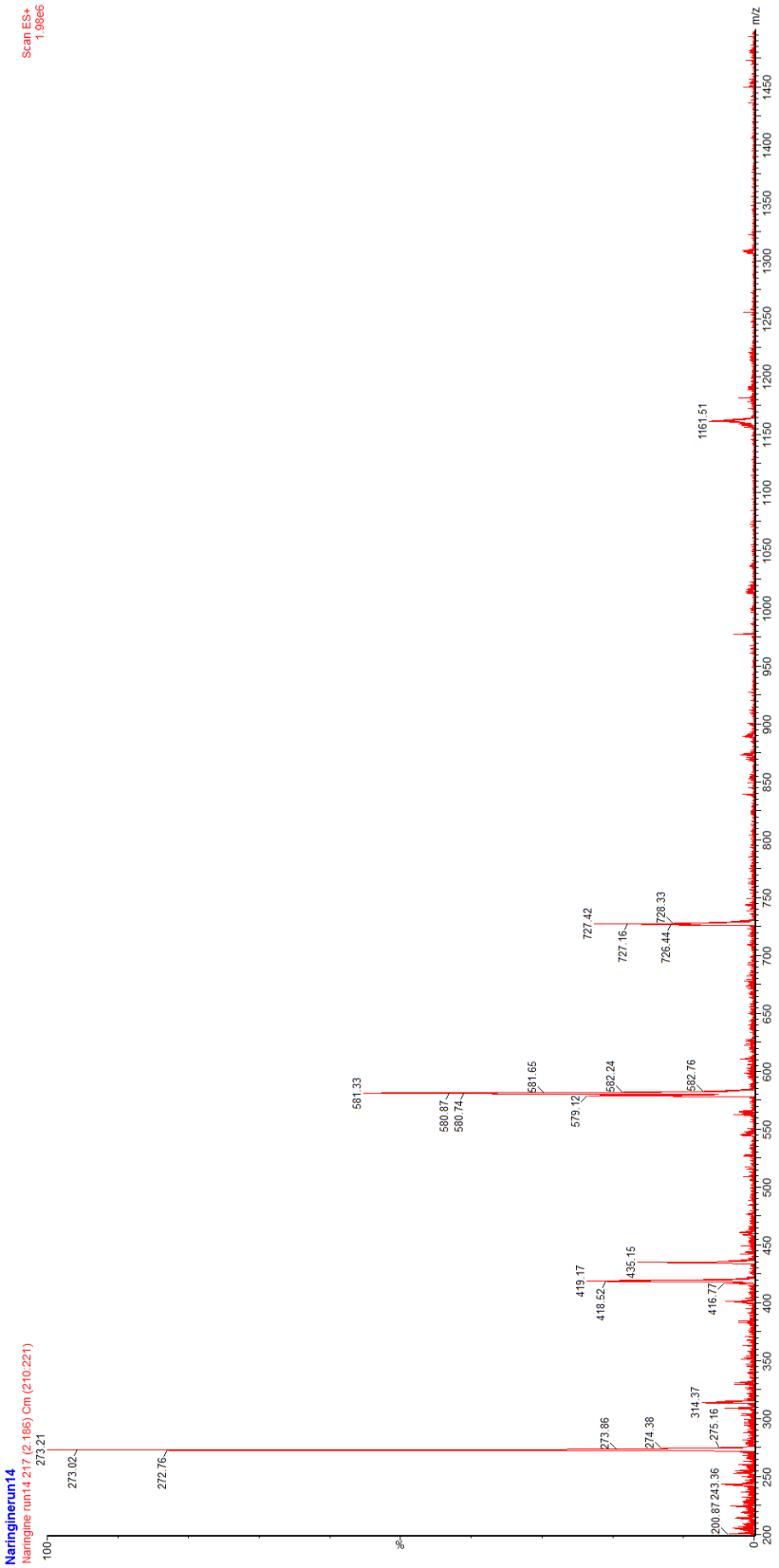

APPENDIX K

UPLC-MS naringin run 14 after dissolution rate assays.

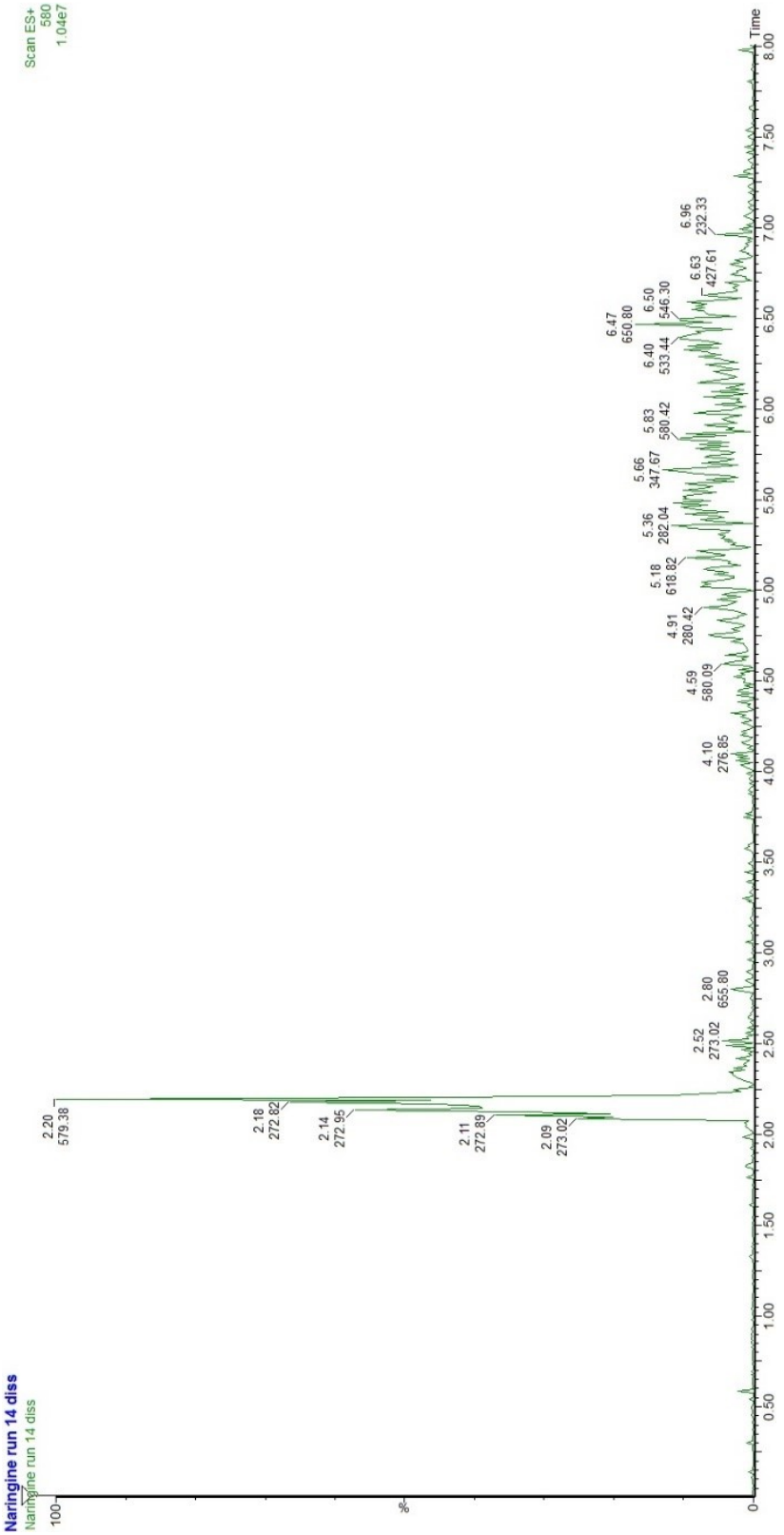

Appendix K (continued).

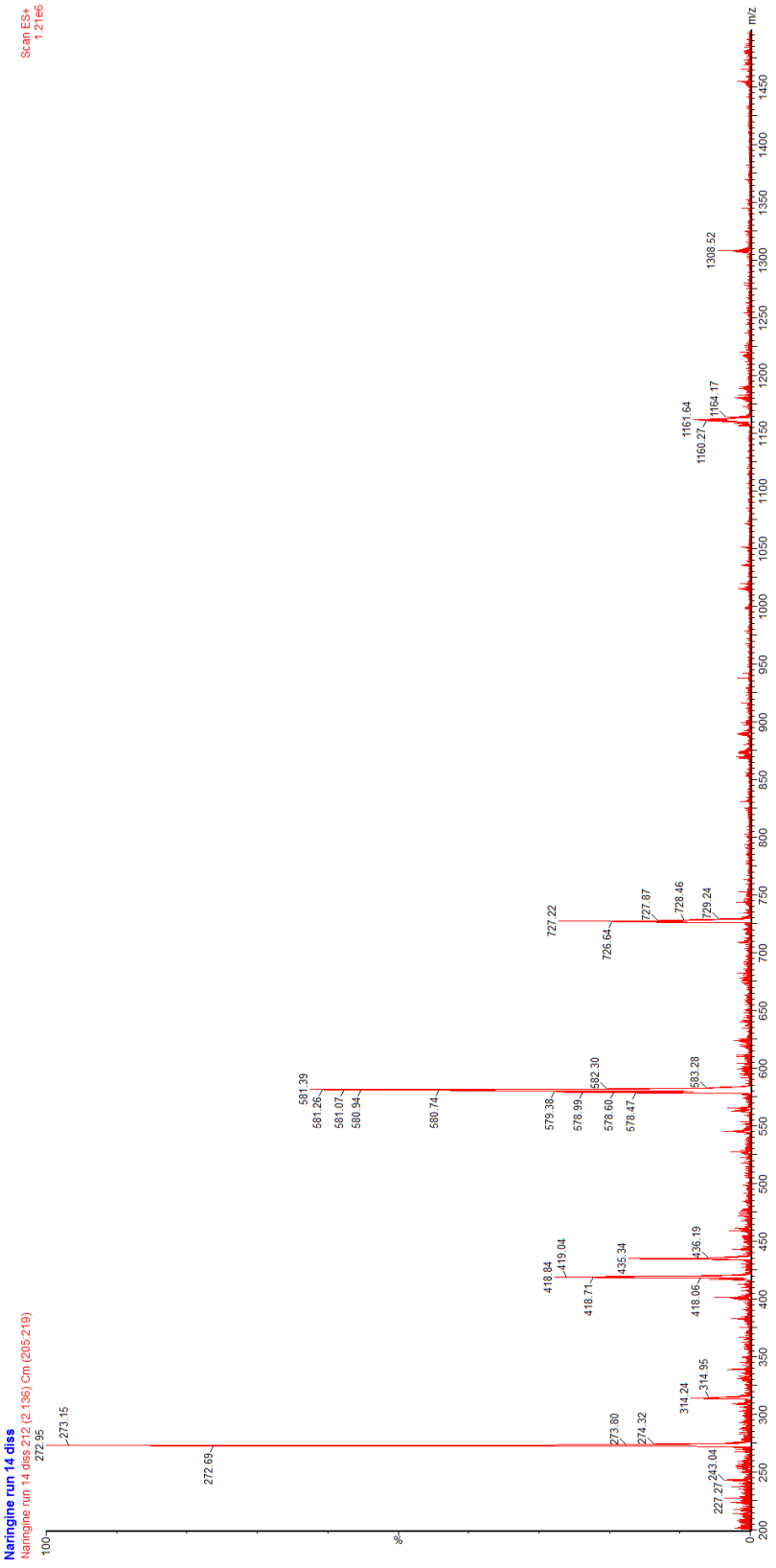

APPENDIX L

Proposed fragmentation of naringin.

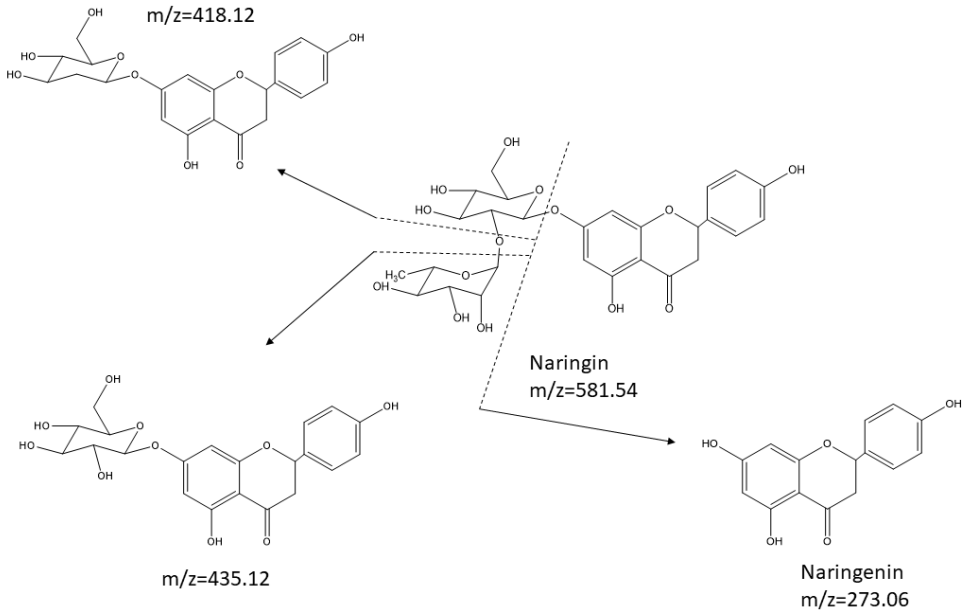

Source:Author (2024)

APPENDIX M

Effects of commercial naringin, run 11 and run 14 of naringin on locomotor activity in mice. The animals (n = 8 / group) were orally treated with Vehicle (saline solution + 1% polysorbate 80) (Sham group), commercial naringin, run 11 or run 14 of naringin at 50 $mg.kg^{-1}$ (p.o.) 1 h before being submitted to the open field test. Graphs display the total distance (m) traveled, the number of rearings, groomings and fecal bolus expelled during 20 min of observation in the arena. One-way ANOVA followed by Tukey's test. Data are presented as mean ± standard deviation. (*$p < 0.05$ in comparison to the Sham group).

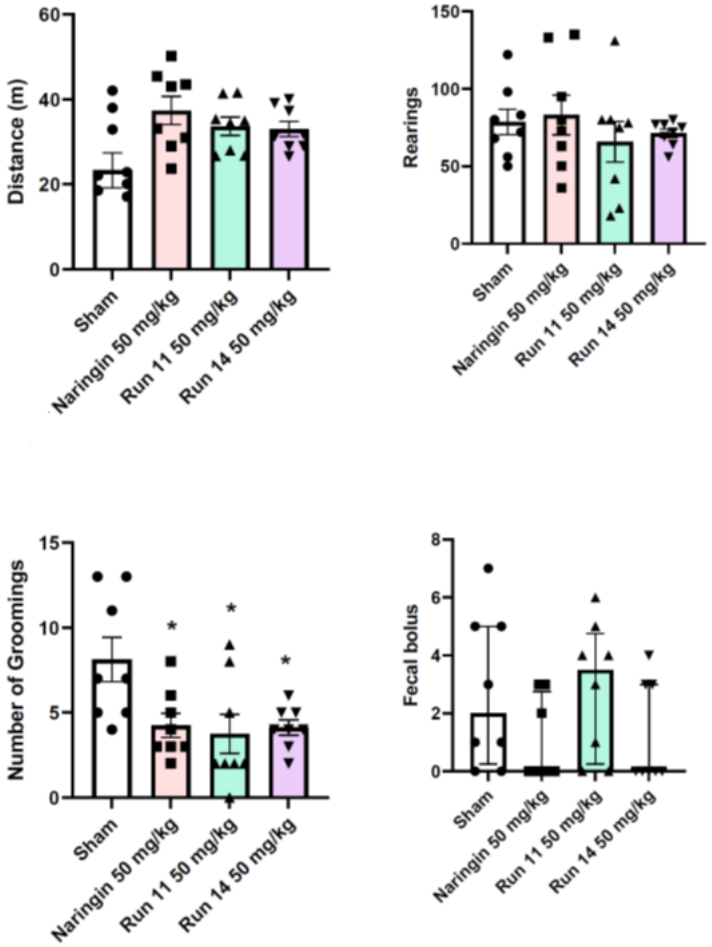

Source: Author (2024)

ANNEX A

Protocol n° 003/CEUA/2021

UNIVERSIDADE COMUNITÁRIA DA REGIÃO DE CHAPECÓ
PRÓ-REITORIA DE PESQUISA, INOVAÇÃO E PÓS GRADUAÇÃO
COMISSÃO DE ÉTICA NO USO DE ANIMAIS – CEUA

CERTIFICADO

Certificamos que o protocolo intitulado "AVALIAÇÃO PRÉ-CLÍNICA DA ATIVIDADE ANTIPSICÓTICA DE PARTÍCULAS DE NARINGINA E NARINGENINA PRODUZIDAS EM MEIO SUPERCRÍTICO", protocolo nº 003/CEUA/2021, sob a responsabilidade de LIZ GIRARDI MÜLLER, que envolve a produção/ manutenção e/ou utilização de animais pertencentes ao filo Chordata, subfilo vertebrada (exceto homem), para fins de ensino e pesquisa científica – encontra-se de acordo com os preceitos da Lei nº 11.794 de oito de outubro de 2008, do Decreto nº 6.899 de 15 de julho de 2009, e com as normas editadas pelo Conselho Nacional de Controle da Experimentação Animal (CONCEA), e foi **APROVADO** pela COMISSÃO DE ÉTICA NO USO DE ANIMAIS (CEUA) da Universidade Comunitária da Região de Chapecó (UNOCHAPECÓ), em 20/04/2021.

Finalidade	() Ensino (X) Pesquisa Científica
Vigência da Autorização	01/06/2021 à 30/12/2022
Espécie/Linhagem/Raça	Camundongos linhagem Swiss (Mus musculus); Peixes-zebra (*Danio rerio*) linhagem Wild-type;
Nº de animais	252 Camundongos; 280 Peixes;
Peso/Idade	25- 35 g/ 06 a 08, semanas Camundongos; 0,3 a 05g/ 03 meses, Peixes.
Sexo	42 Fêmeas, 210 machos camundongos; 280 indefinido.
Origem	**Camundongo** Centro de Bioterismo da Unochapecó (CBi) **Peixes-zebra** Animais adultos: Fornecedor especializado - Recanto dos Peixes (Passo Fundo, RS)

Lilian C. Bohnen

Prof.ª Lilian Caroline Bohnen

Coordenadora da CEUA-Unochapecó